Quantifying the impact of building design on the potential of structural storage for active demand response in residential buildings

Glenn REYNDERS

Examination committee:
Prof. dr. ir. Jean Berlamont, chair
Prof. dr. ir.-arch. Dirk Saelens, supervisor
Prof. dr. ir.-arch. Karen Allacker
Prof. dr. ir. Lieve Helsen
Prof. dr. ir. Peder Bacher
(Technical University of Denmark)
Prof. dr. ir. Dirk Müller
(RWTH Aachen University)
dr. ir. Michael Wetter
(Lawrence Berkeley National Laboratory)

Dissertation presented in partial
fulfillment of the requirements for
the degree of Doctor
in Engineering Science

September 2015

Woordje van dank

Alle wetenschap ter zijde zijn deze eerste pagina's van deze tekst voor mij persoonlijk de belangrijkste: de pagina's waarin ik iedereen die me in dit hele proces gesteund heeft kan bedanken. Het maken van dit doctoraat is voor mij een enorm boeiende, soms wat zware, maar vooral heel fijne rit geweest, die ik zonder jullie hulp, luisterend oor of opbeurend pintje nooit had uitgereden.

Allereerst wil ik Dirk bedanken, mijn promotor en de persoon die ervoor gezorgd heeft dat ik met fierheid *mijn boekje* kan voorleggen. Niet alleen omdat hij me 5 jaar geleden wist te overtuigen om aan dit avontuur te beginnen, maar vooral omdat hij zijn gedrevenheid en passie voor onderzoek op me wist over te dragen. Dirk, je leerde me dat *goed* niet goed genoeg is en slaagde er steeds in om me tot het uiterste te drijven. Bovendien wil ik je, vol bewondering, bedanken voor de grondigheid en kritische manier waarop je heel mijn werk hebt nagelezen en bijgestuurd, ook wanneer het weer eens op het laatste nippertje in je mailbox verscheen. Bedankt voor je ongezoute mening en vooral om in me te geloven.

Naast een promotor had ik het geluk om altijd te kunnen rekenen op de hulp en begeleiding vanuit VITO. Jan en Johan, bedankt dat ik altijd kon rekenen op jullie frisse kijk. Jullie hebben er steeds op toegezien dat er schot in de zaak bleef en dat publicaties en rapporten tijdig de deur uit gingen. Wanneer ik me weer eens iets te diep vastbeet in een zijtak, zorgden jullie er voor dat ik het grote verhaal niet uit het oog verloor. Jan, jouw deur stond altijd open voor vragen en bovendien wil ik je extra bedanken voor het geduld waarmee je alle hoofdstukken hebt gelezen en herlezen. Daarnaast uiteraard ook mijn hartelijke dank aan VITO om dit doctoraatsonderzoek mogelijk te maken. Bedankt voor jullie vertrouwen.

I would also like to sincerely thank my examination committee for their thorough review of the manuscript and the interesting and in-depth discussion during the defence. Special thanks to Prof. Peder Bacher, who introduced me to the wonderful world of grey-box modelling during

the IEA EBC Annex 58-project and the summer school. Peder, your enthusiasm was inspiring and I will always remember to solve problems by taking *tiny steps at a time*.

Het grote voordeel van een doctoraat binnen 2 onderzoeksinstellingen is dat je er 2 keer zoveel leuke collega's aan overhoudt. Aan elk van hen een overweldigende dankjewel voor alle hulp en pep-talk gedurende de laatste maanden, maar ook voor alle leuke en boeiende koffiepauzes, lunchtalks, kartingavonden... In het bijzonder wil ik ook Ruben bedanken voor alle keren dat ik aan zijn deur mocht komen kloppen met vragen en onverklaarbare *errors*, zelfs als we allebei aan onze eindspurt bezig waren. Ook mijn bureau-maatje An-Heleen verdient een speciale plaats voor alle grey-box-problemen die we samen oplosten en uiteraard voor haar kritische evaluatie van al mijn *barcharts* en *powerpoint tekeningen*.

Uiteraard verdienen ook mijn vrienden een belangrijk plaats in dit dankwoord voor al die avonden dat ze het gezeur over mijn doctoraat hebben doorstaan, maar uitaard ook voor alle keren dat ik op hen kon rekenen om even mijn gedachten te verzetten. In het bijzonder Jorrit en Thomas die zelfs de moed vonden om stukken tekst na te lezen en te verbeteren.

Ten slotte wil ik mijn familie, en in het bijzonder mijn ouders, graag dubbel bedanken. Niet enkel voor hun onvoorwaardelijke steun gedurende mijn doctoraat – en bij uitbreiding mijn hele schoolcarriere – maar ook omdat ze alle zondagen, verjaardags- en kerstfeesten dat ik (mentaal) niet aanwezig was, tollereerden.

En als allerlaatst, maar met de allergrootste dankbaarheid, mijn kersverse vrouw. Sacha, zonder jou zou dit nooit gelukt zijn. Bedankt voor alles, voor elke knuffel, elk steunend woord, elke keer dat je de afwas deed zonder mijn hulp te vragen, elke keer dat ik slechtgezind mocht zijn... Bedankt voor je eindeloze steun en liefde!

Glenn Reynders
14 September 2015

Abstract

The main goal of this work is a fundamental analysis of the impact of building design parameters on the potential of structural thermal energy storage (STES) for active demand response (ADR). The scope of the work is on residential buildings – both new and existing – in the heating dominated context of Belgium.

To evaluate the ADR potential, firstly a quantification method is developed based on 4 performance indicators: the available storage capacity, storage efficiency, power shifting capability and state of charge. This method not only enables an inter-building comparison, but also allows for a generic comparison of ADR technologies. An evaluation of the indicators shows that although they depend on dynamic boundary conditions, and are hence time-dependent, the available capacity and storage efficiency provide valuable input to f.i. building designers and grid operators in a design phase. Additionally, the power shifting capability and state of charge quantify the instantaneous flexibility in an operational phase.

Secondly, a grey-box modelling framework is established for the characterization of the thermal properties that govern the ADR potential and the dynamic thermal behaviour of dwellings using on-site measurements. The main added value of this work lays in the simulation-based approach used to examine the relation between the design of experiment, the proposed model structure and the performance of the obtained model.

Finally, both tools are combined to assess the ADR potential for the Belgian residential building stock, showing that intelligent use of STES can reduce the required peak power capacity associated with a wide-spread integration of heat pumps, while increasing the penetration of renewables and reducing CO_2-emissions. For Belgian dwellings, the available storage capacity – obtained for simplified boundary conditions, an ADR-event of 4 h and comfort range of 2 $^{\circ}\mathrm{C}$– is estimated between 12-30 kWh for the radiator heated buildings and 16-66 kWh for the floor heating. The corresponding efficiencies vary between 66-85 % for radiator heating and above 90 % for floor heated buildings and are mainly governed by the heat loss coefficient of the building.

Beknopte samenvatting

Het doel van dit onderzoek is om fundamenteel inzicht te krijgen in de relatie tussen thermische gebouwparameters en het potentieel van structurele thermische opslag voor vraagsturing. De focus van het werk ligt daarbij op residentiële gebouwen – zowel nieuwe als bestaande – in een verwarmingsgedomineerde Belgische context.

Om het potentieel voor thermische opslag te evalueren, is in een eerste luik een berekeningsmethode ontwikkeld gebaseerd op 4 indicatoren: de beschikbare opslagcapaciteit, de efficiëntie, de laadtoestand en de toelaatbare vermogensvariatie. De ontwikkelde methode laat daarbij niet enkel een onderlinge vergelijk van gebouwen toe, maar eveneens van opslagtechnologieën in het algemeen. Ondanks de tijdsafhankelijkheid van de indicatoren – ten gevolge van de invloed van dynamische randvoorwaarden – toont een parameterstudie dat de beschikbare opslagcapaciteit en de efficiëntie belangrijke informatie bevatten in een ontwerpstadium voor o.a. gebouwontwerpers of netwerkoperatoren. Aanvullend, geven de toelaatbare vermogensvariatie en laadtoestand informatie over de ogenblikkelijke flexibiliteit van een gebouw in een operationeel stadium.

In het tweede luik is een 'grey-box modelling' methode voorgesteld voor het karakteriseren van de dynamische eigenschappen van gebouwen die een impact hebben op het potentieel voor vraagsturing, alsook voor het identificeren van de dynamische response van bestaande gebouwen op basis van in-situ metingen. De belangrijkste bijdrage van dit werk ligt bij het gebruik van een simulatiegebaseerde methode om het verband tussen experiment, modelstructuur en performantie van het model te analyseren.

Ten slotte, zijn de ontwikkelde methodes gecombineerd om het potentieel van structurele thermische opslag in het Belgische gebouwbestand te bepalen. De resultaten tonen dat intelligent gebruik van thermische opslag toelaat om de bijkomende piekcapaciteit alsook de CO_2 uitstoot te reduceren en tegelijk het aandeel aan hernieuwbare energie te verhogen. Voor Belgische woningen varieert de geschatte, beschikbare opslagcapaciteit – op basis van vereenvoudigde randvoorwaarden, een duurtijd van 4 u en toelaatbare

temperatuurschommeling van 2 $^{\circ}\mathrm{C}$– tussen 12-30 kWh bij radiatoren en tussen 16-66 kWh bij vloerverwarming. De overeenkomstige efficiënties liggen tussen 66-85 % bij radiatoren en boven 90 % bij vloerverwarming. De variatie wordt daarbij hoofdzakelijk veroorzaakt door de totale warmteverlies coëfficient van het gebouw.

Contents

List of Symbols

$\dot{Q}$	Thermal power [W]
$\dot{Q}_\delta$	Power shift [W]
ϵ	Measurement noise
η	Efficiency $[-]$
η_{ADR}	Storage efficiency $[-]$
Ψ	Linear thermal transmittance $[\mathrm{W}/(\mathrm{mK})]$
θ	Model parameter
A	Surface area $[\mathrm{m}^2]$
A, B, C, D	State-space system matrices
c	Specific heat capacity [J/(kgK)]
C'	Effective thermal capacity $[\mathrm{J}/\mathrm{K}]$
C_a	Thermal capacity indoor air [J/K]
C_{ADR}	Available storage capacity for ADR [J]
d	Thickness [m]
dT_{comf}	Comfort range available for ADR [$^\circ\mathrm{C}$]
g	Solar transmittance $[\mathrm{W}/\mathrm{m}^2]$
H	Heat transfer coefficient [W/K]
h_c	Convective heat transfer coefficient $[\mathrm{W}/(\mathrm{m}^2\mathrm{K})]$
HLC	Total heat loss coefficient [W/K]
j	Dummy index
L	Length [m]
l_{ADR}	Duration of the ADR-event [s]
PSC	Power shifting capability [s]
Q	Thermal energy [J]
q	Heat flux $[\mathrm{W}/\mathrm{m}^2]$
R	Thermal resistance [K/W or $\mathrm{m}^2\mathrm{K}/\mathrm{W}$]

SOC	State of charge $[-]$
t	time $[\mathrm{s}]$
T_b	Boundary temperature $[^{\circ}\mathrm{C}]$
T_e	Outdoor air temperature $[^{\circ}\mathrm{C}]$
T_r	Star temperature $[^{\circ}\mathrm{C}]$
T_{air}	Indoor air temperature $[^{\circ}\mathrm{C}]$
T_{max}	Maximum comfort temperature $[^{\circ}\mathrm{C}]$
T_{min}	Minimum comfort temperature $[^{\circ}\mathrm{C}]$
T_{op}	Operative temperature $[^{\circ}\mathrm{C}]$
T_{set}	Set-point temperature $[^{\circ}\mathrm{C}]$
T_{sky}	Sky temperature $[^{\circ}\mathrm{C}]$
T_{sup}	Supply air temperature $[^{\circ}\mathrm{C}]$
T_s	Surface temperature $[^{\circ}\mathrm{C}]$
U	Heat transfer coefficient $[\,\mathrm{W}/(\mathrm{m}^2\mathrm{K})\,]$
U	Vector of input signals
V	Volume $[\mathrm{m}^3]$
X	State vector
Y	Vector of observation measurements

Subscripts

a	Air
ADR	Active demand response
c	Convective
e	Exterior
f	Floor
FH	Floor heating
fi	Interior floor
g	Internal gains
i	Interior / Dummy index
inf	Infiltration
lw	Long wave radiation
Nom	Nominal
r	Radiative
Rad	Radiator
rad	Radiator
Ref	Reference
sol	Solar (gains)
sw	Short wave radiation

sys	Heating system
$vent$	Ventilation
w	Exterior wall
wi	Interior wall

Chapter 1

Introduction

1.1 Background and problem statement

Large-scale integration of decentralized electricity production from renewable energy sources is often suggested as a key technology to counter fuel poverty and climate change. Statistics show how the potential production from renewable sources may outgrow the demand by far [1, 2]. However, an important bottleneck is, amongst others, the strong intermittency of electricity production from renewable sources such as solar or wind energy. Because of the stochastic nature of both the electricity demand and the renewable electricity production, a mismatch may occur between demand and supply [3, 4, 5]. Currently, the electricity grid is used as a virtual storage to overcome this mismatch between local electricity production and demand [6, 7]. With an increasing penetration of renewable energy sources this approach may in the current infrastructure no longer be sustainable, resulting in grid instability problems and decreasing efficiencies of large power plants [8, 9, 10].

In this context buildings play a significant role. Today, buildings in Europe represent 40% of the energy use, hence they account for an important share in the electricity demand (19.8 % of the annual electricity use in Belgium [11]) and CO_2-emission worldwide [12]. In residential buildings 54% of the energy end-use or 42% of the primary energy is used for space heating and domestic hot water production. In order to reduce this share, the European Commission imposes, in the “European Performance of Buildings Directive” (EPBD), that all new buildings should be nearly zero energy buildings (nZEB) by 2021 [13]. Thereby, an

nZEB combines the minimization of the energy demand by an adequate building envelope and efficient heating and ventilation systems, with the integration of local renewable energy sources. Whereas the annual net energy demand of nZEB's is to be nearly zero, research shows that as a consequence of the intermittent and stochastic nature of both demand and supply a significant mismatch exists between the instantaneous local demand and production [14, 3, 15]. Consequently, when no active measures are taken to match the energy demand and the production from renewable sources, a high penetration of nZEB's may result in grid stability problems and efficiency losses [9, 10, 3, 16].

To overcome the imbalance between demand and supply, guarantee the stability of the electricity network and optimize the use of renewable energy sources, a decentralization of the energy market with an increased participation of the consumer is often suggested [17, 18, 19]. Whereas, the energy market in Belgium – as in most countries – is currently organized in a load-driven structure whereby the production side is controlled in order to meet the demand at all times, new market structures, e.g. Smart Grids [20], are suggested. In these Smart Grids, the grid operators can give incentives such as time-of-use prices to consumers to adapt their energy use.
Similar demand-response programs are also explored in the context of 4^{th} generation district heating systems, where local storage and demand-side management are proposed to increase the efficiency of the district thermal system and increase the penetration of renewable production sources [21].

In these active demand response (ADR) programs, the available flexibility at the demand-side is exploited to temporary reduce the peak in the energy demand (peak-clipping), shift demand in time (load-shifting) or temporary increase the load when the incentives are high (valley-filling), as demonstrated in Figure 1.1. Note that the general term 'incentive' is used here as a source to stimulate the change in demand since different methods are still being explored to organize these demand response programs, such as time-of-use-pricing, flexibility markets or direct load control [22, 23, 24, 25]. Although a unified framework is not yet established, these demand response programs have been shown to reduce the

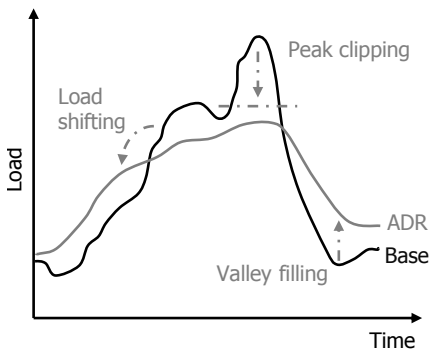

Figure 1.1: Conceptual daily load profile with (blue) and without (red) active demand response.

required investment in grid capacity, large-scale storage systems and peak production units, while increasing the penetration of renewable sources and the overall energy efficiency on an aggregated district or even national level [26, 27, 28, 29].
In a residential context multiple studies [15, 30, 31, 32, 33] demonstrate a significant potential of ADR using thermostatic loads, i.e. heating, cooling and domestic hot water [34] in addition to white-goods, such as dish-washers or refrigerators, and electric vehicles. Thereby the available thermal energy storage capacity in buildings is used to pre-heat or pre-cool buildings when the incentives for ADR are high, e.g. when time-of-use prices are low or (local) renewable production is high. The goal thereby is to enable a reduction of the energy demand during periods with high incentives for demand-reduction, e.g. high energy prices, without jeopardizing the comfort requirements. For ADR using the *structural thermal energy storage capacity* the latter imposes that the indoor temperature fluctuations, needed to activate the storage capacity, may not comprimize thermal comfort [35, 36] and occupant satisfaction.
The use of thermal energy storage to enable these demand response mechanisms is thereby shown to be a cost effective storage technology compared to f.i. battery storage or chemical batteries (Figure 1.2) [37]. Moreover, in the context of thermal energy storage in buildings, this storage capacity is already available today on a large scale in the form of e.g. sanitary hot water tanks and the massive building structure. Investments to integrate this storage capacity in a demand-response market would thus be limited to an upgrade of the control and ICT systems. An important down-side of thermal energy storage, in contrast to f.i. batteries or pumped hydro, is that an efficient reconversion from the stored heat to electricity is in general not possible. Thermal storage can as such only be used when heating or cooling are the required end-uses.

An exploratory study [15], in which a rule-based control strategy was used to shift the peak demand of a heat-pump and increase the self-consumption of renewable electricity from a photo-voltaic (PV) system, showed that by activating the structural thermal mass of a residential building up to 90% of the electricity demand during the peak demand periods can be shifted. Nevertheless, the impact on the self-consumption of the PV system was found limited, since periods with high PV-production coincide with low heat demands, due to the use of passive solar gains in the buildings. Consequently, the potential for load-shifting using the heating system is limited. Moreover, in line with results found in literature [30, 31, 32], an important down-side of the activation of the structural thermal energy storage capacity is the increase in the annual energy use on a building level. This increase was found to depend upon the thermal properties of the dwelling, the type of heat emission system and the efficiency of the control strategy and was explained by the higher thermal losses that correspond to an increase in the indoor temperature when the building is preheated.

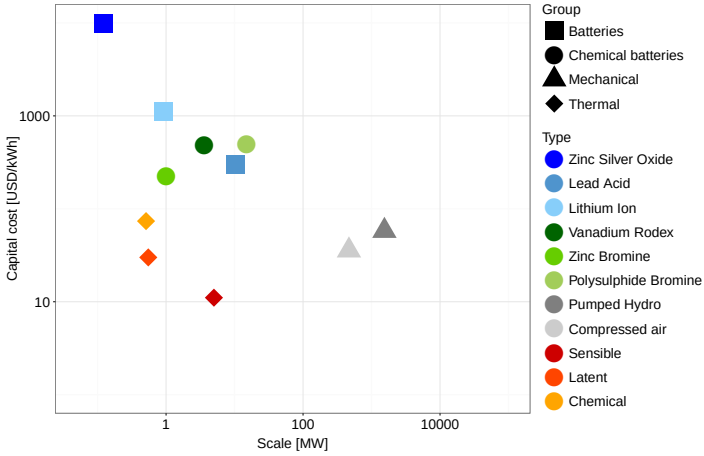

Figure 1.2: Comparison of capital cost of different storage technologies as presented by Sabihuddin et. al [37]

Consequently, the optimal use of structural thermal energy storage in a demand-response context requires an optimization of the thermal characteristics of the building as well as the thermal systems and the control strategies.

For the latter, state-of-the-art control strategies take into account predictions of the future heat demand, comfort requirements and the incentives for demand-response, f.i. time-of-use energy prices provided by smart meters, to optimize the energy use or the energy cost for heating or cooling [38, 39, 40]. Simulation-based and experimental results show that model predictive control (MPC) strategies which take into account both the *structural storage capacity* of the building, i.e. the thermal mass embedded in the building structure, and the *non-structural storage capacity*, i.e. the storage capacity embedded in the thermal systems, may result in energy cost savings of 26 % up to 40 %, while maintaining or even improving thermal comfort [41, 42, 43, 34, 44]. These savings mostly result from the free cooling potential (eg. through night ventilation) [45], a higher contribution of solar and internal gains for passive heating [46] and the price differences between peak to off-peak periods [47]. Although the studies above demonstrate that MPC can maximize these benefits and minimize the storage losses, Privara et al. [48] emphasize that – due to the fact that each building is unique – one of the key challenges for MPC is the development of robust control models which accurately capture the dynamic response of the structural thermal energy storage capacity. Therefore the use of statistical models that have self-learning capabilities is suggested [49, 50, 51].

Moreover, the studies indicate that savings strongly depend on the coupling of the building to the outdoor environment, since the activation of the structural storage increases transmission and ventilation losses. Nevertheless, the literature review revealed that fundamental research on the link between the thermal properties of the building – including its thermal systems – and the availability and efficiency of thermal energy storage capacity for active demand response is missing. Such an analysis may on the one hand provide valuable information for grid operators and aggregators on the level of flexibility that may be expected from the different buildings that are linked to the energy grid. On the other hand it can support building designers in optimizing the energy efficiency of buildings taking into account the requirements of the energy grid.

The main goal of this work is therefore to analyse how the design of the building may affect its suitability for active demand response. Thereby, it should be explicitly emphasized that the scope of the analysis covers both new and existing buildings, since given the low replacement rate of existing buildings (0.2-0.5% per year [52]) the latter group is expected to play a dominant role in the structural storage potential.

1.2 Scope of the work

Since active demand response using structural thermal energy storage is linked to a wide range of research areas – from the impact of variations in the indoor temperature set-point on the efficiency of thermal systems to the assessment of the occupant acceptance of these temperature fluctuations – it is necessary to limit the scope of this work. Based on the gaps identified in the problem statement as well as my personal background in civil engineering and building physics, the focus of this work is on the assessment of the relation between the thermal design of residential building and the suitability for active demand response.

Studies on demand response in literature are mostly focused on office buildings, whereby applications typically assess the potential for reducing peak cooling loads [53, 54, 55, 56, 34]. This work analyses the potential of **residential buildings** in the **heating dominated climate of Belgium**. With an expected increase in the penetration of energy efficient heat pump systems for residential space heating [57], residential buildings will play an important role in the electrification of the energy market. Consequently, demand response using residential heat pumps by activating the structural storage capacity may result in substantial operational savings, CO_2-emission reductions and support the integration of renewable energy sources.

In addition, it was found that the assessment of the potential for structural storage in literature

is mainly covered from a system and control perspective. Studies on optimal control strategies or model predictive control strategies, which take into account predictions of the future heat demand and ADR incentives, are used to demonstrate peak load reductions on the electricity grid level, improve the efficiency of heating systems or optimize the use of passive gains. Nonetheless, a systematic analysis of the impact of the building design parameters on the identified benefits has not been found. To facilitate such a comparison, **simplifications to the thermal systems and control strategies** are introduced.

Rule-based control strategies will be used in contrast to state-of-the-art model predictive control. Although optimal control strategies, such as MPC, show clear benefits in real applications due to the complexity and high amount of control variables in complex thermal systems, for this research the use of rule-based control is found to improve interpretability of the results [58].

Moreover, the impact of ADR on the efficiency of the thermal production and distribution systems, such as a reduced production efficiency due to more frequent on/off-cycling, is not explicitly taken into account. While different studies show that ADR may have a significant impact on the efficiency of these systems, both in positive and negative sense [59, 60, 61, 62, 31], it is assumed here that the overall efficiency of buildings for ADR can be split into the storage efficiency of the structural thermal mass and the efficiency of the heating system.

In contrast to the **simplified heat production system**, the relation between the heat emission system and the activation of the thermal mass is thereby analysed in more detail. Therefore, two types of **hydronic heat emission systems**, i.e. radiators and floor heating systems, are considered as they are commonly used in Belgium and fundamentally differ in the way they activate the structural storage capacity.

Moreover, it is emphasized here that although the presented methodologies can be readily extrapolated to cooling applications, **only heating** is considered in this work , since active cooling applications are not common in the Belgian residential context and can mostly be avoided by a proper passive cooling design.

Finally, the potential for active demand response is in general limited by the range of deviations from normal operation that are acceptable for the user [63, 64, 65, 66]. In the context of structural thermal energy storage, **thermal comfort** plays an important role in the potential of structural storage as it imposes limits to the allowable temperature fluctuations when the building is occupied. In literature, two general approaches are found to take into account the thermal comfort limits into ADR control strategies. A first approach introduces thermal comfort into the cost function that is optimized to calculate the temperature set-points [46, 67]. As such, the cost for deviations from the comfort temperature should be defined and evaluated

against the energy cost for heating. Specifying the cost for comfort violations proves difficult due to the subjective nature of thermal comfort sensation [68]. Therefore, the second approach uses thermal comfort criteria to impose constraints to the optimization problem. The level of allowed temperature fluctuations is then based on thermal comfort standards. Commonly thermal comfort criteria are specified in steady state using the PMV-PPD method introduced by Fanger [69] and employed in the comfort standards such as ISO 7730 standard [70] and EN 15251 [71]. However, Humphreys and Nicol [35] show that due to the flexibility of users in residential buildings, steady state comfort models are no longer valid. Over the last decades the use of adaptive thermal comfort criteria has been suggested in residential buildings to account for the wide range of possibilities to adapt to the thermal environment [72, 73]. Nonetheless, no empirical results are found on the validity of these comfort models in the context of ADR where user requirements may be influenced by incentives from the grid operator. Therefore, in this work the allowed amplitude for temperature fluctuations is added as an additional model parameter to limit the level of temperature variations allowed for activating the structural storage capacity. In addition to the range of temperatures that is available for ADR, also the rate of change is an important factor. According to the ASHRAE standard 55-2004 the indoor temperature should for instance not increase more than 1.1°C in 0.25 h or 2.1 $^{\circ}\mathrm{C}$ in 1 h, although higher values may be allowed if this change is the result of control or adjustments by the user [74]. It may be argued that adjustments for demand response can be considered to fall within the latter category. Therefore, these constraints are not included explicitly in this study.

1.3 Research questions

Whereas, multiple studies have demonstrated that structural thermal energy storage can be a cost effective and efficient technology for demand response, a fundamental study on the relation between the thermal properties of buildings and the potential for active demand response is currently missing. The main research question is therefore formulated as:

> *"How do building design parameters of new and existing residential buildings influence the potential for active demand response using structural thermal energy storage?"*

Three main aspects are embedded in this question. First, a framework needs to be established that allows a quantitative comparison of the ADR potential and flexibility of structural storage. Secondly, we need to understand how the thermal mass is activated and

establish a methodology that allows to identify the active structural storage capacity in new and existing dwellings. Finally, the impact of building design parameters can be evaluated. In order to cover the different aspects, three groups of additional research questions are formulated. The first group of questions aims to develop a methodology to quantify the suitability of a building and its structural storage capacity for active demand response, as such translating flexibility into a quantitative indicator. The main research questions in this part are:

- *How to quantify the availability of the structural storage capacity for active demand response?*
- *How to quantify the amount of heat that is currently stored in the structural storage capacity?*
- *How to quantify the efficiency of the storage process?*

The second group of research questions deals with the analysis and quantification of the activation of the structural storage capacity in dwellings:

- *How is the structural storage capacity activated?*
- *To what extent does the thermal mass of different components contributes to the active storage capacity?*
- *How to quantify the active thermal mass in new and existing buildings?*

Finally, the third group of research questions aims at providing general design guidelines for new buildings and renovation from the perspective of improving the usability of the structural thermal energy storage capacity in a demand response context. The research questions are therefore formulated as:

- *Which buildings are best suited for demand-side management using the structural thermal energy storage capacity?*
- *Which thermal properties have a significant contribution to the demand-side management potential?*
- *What is the link of the usability of structural thermal energy storage with the type and properties of the heating systems?*

1.4 Overview of the dissertation

To answer the research questions, two main tools are presented in this work. On the one hand a simulation-based framework for the quantification of the ADR potential is established. On

the other hand, a grey-box modelling framework is presented to enable the characterisation of the main thermal properties – related to the ADR potential – in existing buildings where these properties are often unknown.
These frameworks are derived using a simulation-based approach to enable a quantitative assessment of the ADR potential of the structural thermal energy storage in new and existing residential buildings. Both frameworks are combined and applied in parameter studies and scenario analyses to quantify the relation between the demand response potential of dwellings and the building design parameters.
Based on this global methodology, the dissertation is organised in 4 main chapters as shown in Figure 1.3.

In **Chapter 2**, the building energy simulation models used to provide a detailed framework for the analysis of structural thermal energy storage are presented. The building models are implemented in Modelica using the IDEAS-library developed at KU Leuven [3]. In addition to a description of the most important models, an assessment of the model accuracy is presented. Thereby a sensitivity analysis on the main numerical aspects is carried out as well as a verification against on-site measurements.

In **Chapter 3**, a generic framework is established that allows for a quantitative comparison of the ADR potential of buildings as function of the building design parameters. As pointed out in Section 1.1, a unified framework – that allows for a comparison of the flexibility of different buildings and even between different storage technologies – was not yet established. However, as explained in the review of the state-of-the-art presented in Chapter 3, recent studies have, during the process of this PhD, developed comparable frameworks based on an optimal control formulation [75, 76]. While such a formulation shows important benefits in practical applications – since it allows to evaluate an aggregated flexibility of different subsystems – a more analytical and rule-based approach is used in this work in order to quantify the fundamental impact of the building design on the ADR potential.
The available storage capacity, the storage efficiency, the power-shift capability and the state-of-charge, are defined as performance indicators to quantify the flexibility of ADR technologies. In the second part of this chapter, a parameter study is carried out to evaluate these performance indicators as a function of the thermal properties of the dwelling.

The parameter study in Chapter 3, shows that the potential of structural storage depends, amongst others, on the type of the heat emission system, the available thermal mass of the dwelling and the heat loss coefficient. While these properties can be readily derived from the building design parameters, one of the goals of this work is to assess the ADR characteristics and related thermal properties of existing buildings. Therefore, a methodology

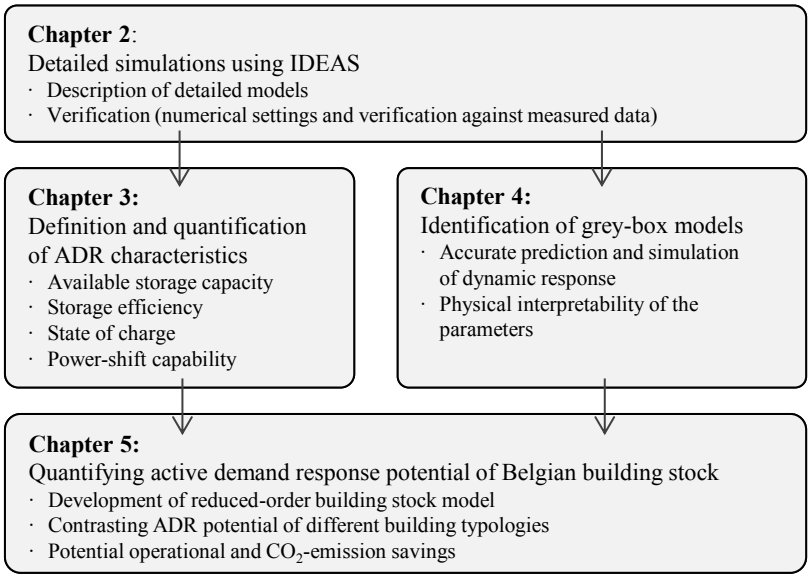

Figure 1.3: Guide to the reader

to find the main dynamic thermal parameters of existing buildings is presented in **Chapter 4**. The methodology is based on system identification and more specific grey-box modelling. Grey-box modelling is a system identification technique whereby the model structure is based on physical knowledge about the system – here the heat balance equations – while the model parameters are estimated using statistical tools on measurement data of the dwelling. While the concept of grey-box modelling is not new and has been applied to buildings in other studies, those applications were mainly focussed on the development of reduced-order models for prediction and control applications. In this work, the main benefit of grey-box models compared to black-box techniques, i.e. the physical interpretability of the model parameters, is evaluated. Thereby, an in-depth analysis of the relation between the design of experiment, the model structure and the model accuracy is carried out, since a literature review demonstrated that due to extensive simplifications this direct physical interpretation is often jeopardized.

In **Chapter 5** the quantification methods for the ADR characteristics developed in Chapter 3 and grey-box modelling framework presented in Chapter 4 are applied to quantify the potential of structural storage in the Belgian residential building stock. Therefore a reduced-order, dynamic, bottom-up building stock model is developed for the single-family dwellings in

the Belgian residential building stock. This model is then used to calculate the available storage capacity and storage efficiency as presented in Chapter 4, contrasting the different typologies in terms of suitability for ADR. Finally, the operational savings, reductions in CO_2-emissions and peak demand reductions that may be expected from a large scale integration of ADR in residential buildings are demonstrated. Therefore, the reduced-order building stock model is implemented in an integrated operational model, which optimizes both demand and production of electricity on a national level taking into account the flexibility of both structural and non-structural thermal energy storage.

Finally, in **Chapter 6** the main conclusions of this work are summarized and suggestions for future research are formulated taking into account both the findings and limitations of this work.

Chapter 2

Simulation of structural thermal energy storage using IDEAS

2.1 Introduction

To assess the impact of building design parameters on the potential of structural thermal energy storage in an active-demand response context, this work relies mainly on a simulation based approach. This chapter presents the building energy simulation models that are used to simulate the dynamic thermal response of buildings. Based on the focus (Section 1.2) and research questions (Section 1.3) of this work, the main model requirements can be formulated as:

- The model should enable the analysis of the impact of the properties of building components on the heat demand, indoor temperature and activation of the thermal mass on a whole-building level.
- The model should capture dynamic effects due to heating, ventilation, climate and occupancy on a high time resolution[1].

Given these requirements a multi-zone nodal modelling approach has been selected for this work. This type of building energy simulation (BES) models is encountered in many commercial and research oriented software packages and is widely used in research and

[1] Typically, 15 min time steps are used for demand response studies as this is the resolution which is also used at the electricity market.

engineering applications [77]. Although more detailed models – using f.i. computational fluid dynamics – are acknowledged to give important insight into the detailed physical phenomena that govern the activation of the thermal mass [78, 79], the zonal approach is selected as the scope of this work is not on the analysis of local effects, such as radiator placement or local convective heat transfer problems, but on an evaluation of the overall potential for structural storage on a building level.

In this work, the BES model from the IDEAS-library (Integrated District Energy Assessment by Simulations) is used. This model is found to be competitive with current state-of-the-art building energy simulation tools in a BESTEST verification [80], while the library has the added value of using the Modelica modelling language[2]. Thereby, the library is built on equation-based, object-oriented models which are relatively easy to interpret and can be readily adapted to the specific requirements of the study. Moreover, the IDEAS-library is specifically designed for energy assessment on a district level. As such, the models developed and used in this work can be readily extended to an evaluation of demand response on a district level.

Layout of the chapter Section 2.2 presents the IDEAS-library focussing on the zone and component models relevant for this work as well as the models used for the heating systems. The accuracy of the building models is evaluated in Section 2.3, showing a sensitivity analysis on the relevant numerical aspects as well as the verification of the model accuracy with on-site measurements.

2.2 Building model implementation in IDEAS

The IDEAS-library[3] is a multi-domain modelling library that enables an integrated dynamic simulation of buildings, thermal systems and electrical systems on a district level using a *bottom-up*, *object-oriented* approach. Bottom-up modelling thereby points to the hierarchical modelling approach whereby aggregated models are composed of physics-based implementations of subcomponents. This bottom-up approach is facilitated by the object-oriented framework realised in Modelica, whereby instances (objects) of submodels with unique functions are assembled using a *connector*-concept to form a high-level model. The paragraphs below summarise the physical equations of the relevant submodels that are available in the IDEAS-library and used in this work, i.e. the zone model (Section 2.2.1),

[2] Modelica is an open-source object oriented and equation based modelling language [81]

[3] The IDEAS-library is publicly available at: `https://github.com/open-ideas/IDEAS`.

opaque components model (Section 2.2.2), transparent components model (Section 2.2.3) and heating system models (Section 2.2.4). Moreover, the implementation of the climate and occupant related boundary conditions are summarised in Section 2.2.5. A more detailed description is found in [82].

2.2.1 Zone model

The zone model implemented in the IDEAS-library consists of both the dynamic heat balance equation for the indoor air and the distribution of long- and short-wave radiation.
The heat balance equation of the indoor air is based on the assumption that the air within the zone is perfectly mixed and can be represented by a single state (T_{air}):

$$C_a \frac{\partial T_{air}}{\partial t} = \sum_{i=1}^{N_s} h_{c,i} A_i \left(T_{s,i} - T_{air}\right) + \dot{Q}_{inf} + \dot{Q}_{vent} + \dot{Q}_{g,c} + \dot{Q}_{sys,c} \qquad (2.1)$$

In this equation T_{air} is the indoor air temperature and C_a the heat capacity of the indoor air calculated as $f_a c_a \rho_a V_a$, where c_a is the specific heat capacity of the air at constant pressure, ρ_a is the density of the indoor air, V_a is the zone air volume and f_a is a correction factor. The latter can be set greater than 1 to account for the additional thermal mass in the zone, f.i. to include furniture. Unless stated otherwise, the default value $(f_a = 5)$ is used as suggested by [83, 84].
The first term of equation 2.1 represents the convective heat transfer between the N_s surrounding components, whereby $T_{s,i}$ is the interior surface temperature of component i with a surface area A_i . $h_{c,i}$ is the convective heat transfer coefficient between the air and surface i as described in Section 2.2.2.

The terms $\dot{Q}_{inf}$ and $\dot{Q}_{vent}$, in Eq. 2.1, represent the heat flow due to respectively natural air infiltration and the ventilation flow induced by the ventilation system. Note that airflow between different zones is, unless explicitly mentioned in the text, not included in the models. Moreover, the mass flow rates are assumed constant and balanced, meaning that the supply and exhaust mass flow rates are equal within each zone. $\dot{Q}_{g,c}$ and $\dot{Q}_{sys,c}$ are the convective fractions of respectively the internal gains – due to occupants and appliances – and the heat emitted by the thermal systems.

Long-wave radiation in the zone is modelled by a *delta-star transformation* and the definition of a fictional *star temperature* (T_r) [85]. This implementation avoids the need for a detailed geometric description of the room and is shown to not significantly affect the overall model

accuracy [86]. Short-wave radiation transmitted through the windows as well as the radiative fractions of the internal gains $(\dot{Q}_{g,r})$ and the heat emitted by the thermal systems $(\dot{Q}_{sys,r})$, is distributed to the different surfaces surrounding the zone using constant weight-factors. For the distribution coefficients of the direct solar gains an area weighted average is used, the other radiative gains are distributed by an area and emissivity weighted average. Note that as such, the distribution of the solar gains within the zone does not depend on the time of day and thus of the position of the sun. Nevertheless, [86] shows that, with a deviation on the maximum cooling load of 0.1-3 %, the overall model is not sensitive to this assumption. Similar deviations were obtained for the average indoor temperature for the different distribution scenarios used in the model verification described in Section 2.3

2.2.2 Opaque components

The model for the opaque components consists of three parts, i.e. the heat balance equations for the interior (i) and exterior surfaces (ii) and the heat conduction between both surfaces (iii).
For both the interior and exterior surfaces the heat balance equation is given by:

$$\dot{q}_T + \dot{q}_c + \dot{q}_{sw} + \dot{q}_{lw} = 0 \tag{2.2}$$

where $\dot{q}_T$ represents the conductive heat flux into the wall, $\dot{q}_c$ is the heat flux by convection, $\dot{q}_{sw}$ the incident direct and diffuse solar radiation and $\dot{q}_{lw}$ the long wave radiant heat exchange to the environment.
At the inner surface, convective heat transfer is modelled using buoyancy driven, temperature dependent, convection correlations defined by Khalifa et al. [87] and Awbi et al. [88], while short- and long-wave radiation are modelled using the distribution coefficients and star network approach described in the previous section. At the outer surface, the convection correlations presented by Defraeye et. al. [89] are implemented and the long-wave heat transfer model is derived from the Stefan-Boltzmann law using the celestial dome temperature T_{sky} [90]. A detailed description of all terms is given in [80, 82].

Thermal conduction within the building components is simplified to a one-dimensional ordinary differential equation using a control volume representation. Thereby the thermal mass of each material layer in a multilayer wall is lumped to n discrete thermal capacities and the heat conduction is modelled as a series of thermal resistances (R_n) and capacities (C_n). R_n and C_n are calculated by dividing the total thermal mass and thermal resistance of the material layer by the number of elements (n), corresponding to a uniform discretisation as

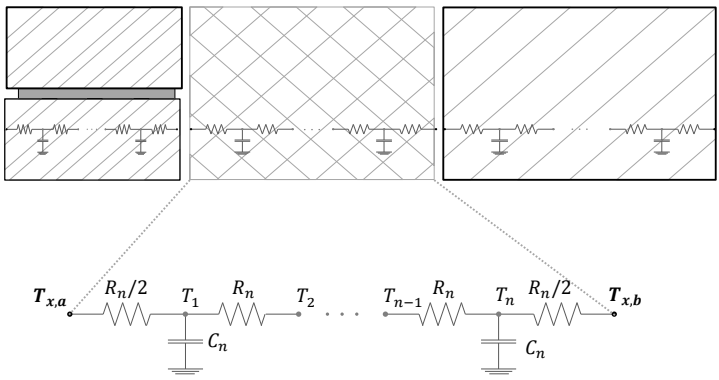

Figure 2.1: RC representation of the one-dimensional control volume method used to simulate thermal conduction for an insulated cavity wall

shown in Figure 2.1. Note that for the boundary elements only half of the thermal resistance is used, conform with the control volume approach. The heat balance equation for the j^{th} thermal capacity, or state, is then given by:

$$C_n \frac{\partial T_j}{\partial t} = \frac{T_{j-1} - T_j}{R_n} + \frac{T_{j+1} - T_j}{R_n} + \dot{Q}_{source,j} \tag{2.3}$$

In this equation $\dot{Q}_{source,j}$ is a source term that may be used for e.g. embedded heating systems. For the remainder of this work, the number of states per material layer is fixed to 8 which is found to be a good compromise between accuracy and calculation time (see Section 2.3).

2.2.3 Transparent components

The thermal model for transparent components is similar to that of the exterior walls but includes the absorption of solar irradiation by the different glass panes, the heat transfer through the gas gaps between the glass panes and the transmission of solar irradiation to the adjacent indoor zone. A detailed description of all terms is given in [80, 82].
The properties for absorption of short wave irradiation by and transmission through the transparent components are taken into account depending on the angle of incidence of solar irradiation and are based on the output of the WINDOW 4.0 software [91] as validated by Aresteh [92] and Furler [93]. The output from WINDOW 4.0 consists of a matrix with angular

dependent transmittances and absorbtances for each glass pane. Similar to other dynamic simulation tools, e.g. TRNSYS, values for different angles are obtained by interpolation.

2.2.4 Heating system model

While component-based dynamic heating system models are available in the IDEAS-library allowing for a detailed simulation of both thermal and hydraulic aspects, a simplified implementation of the heating systems is used for this work. This choice is based on the focus of the work which is on the evaluation of thermal properties of the building on the potential of structural storage in an active demand response context. It should be emphasized, as demonstrated in Chapter 5, that the efficiency of the heat production unit has an important impact on the potential CO_2-emissions and operational savings that can be achieved by ADR. Moreover, multiple studies demonstrate that – using optimal control strategies – the use of thermal energy storage can be optimised in order to increase the system efficiency [59, 60, 61, 62, 31]. Nonetheless, given the scope of this work, we assume that the overall efficiency $(\eta_{ADR,tot})$ for thermal energy storage can be split into the storage efficiency of the building structure $(\eta_{ADR,STES})$ and the efficiency of the heating system $(\eta_{ADR,sys})$. The latter includes the production efficiency as well as distribution and control efficiencies. The overall efficiency of a building for ADR is then given by:

$$\eta_{ADR,tot} = \eta_{ADR,sys}\eta_{ADR,STES} \tag{2.4}$$

The thermal production unit is modelled as a power limited, ideal heat source and is controlled by a thermostat comparing the operative zone temperature (T_{op}) to the temperature set-point (T_{set}) . Unless stated otherwise, the operative temperature is used as control variable as it is directly linked to thermal comfort [69].

Two types of heat emission systems are considered in this work, i.e. radiators and floor heating, as they on the one hand are two commonly used systems in Belgium and on the other hand fundamentally differ in the way they activate the thermal mass of the building (see Chapter 3).
The radiators are modelled as a thermal capacity which exchanges heat by radiation and convection with the zone, as presented by equation 2.5. C_{rad} and H_{rad} are the thermal capacity and heat transfer coefficients of the radiator – obtained by linearising the radiator formula around the design supply temperature. Both properties are based on product data

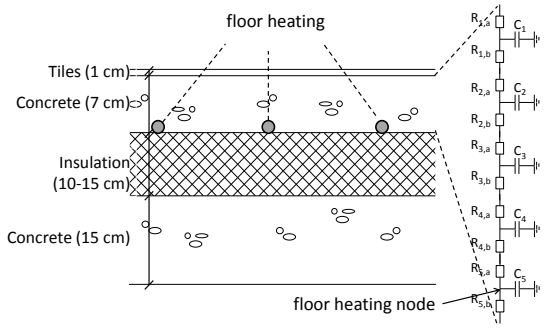

Figure 2.2: Schematic representation of the floor heating model

and scaled to the nominal heating power.

$$C_{rad}\frac{dT_{rad}}{dt} = f_{rad}H_{rad}(T_r - T_{rad}) + (1 - f_{rad})H_{rad}(T_{air} - T_{rad}) + \dot{Q}_{prod} \quad (2.5)$$

The design fraction of heat that is emitted by radiation (f_{rad}) is assumed to be 0.3. T_{rad}, T_r and T_{air} are respectively the radiator temperature and the star and air temperatures of the zone. $\dot{Q}_{prod}$ is output of the ideal heat source. The floor heating system is modelled as a 1D-model with a prescribed heat flow. The heat flow is uniformly imposed at the bottom node of the screed layer in the ground floor using the source term $\dot{Q}_{source,j}$ in Eq. 2.3. Note that, based on the sensitivity analysis presented in Section 2.3, each material layer is subdivided into 8 control volumes. As such, the size of the control volumes varies between 0.1 and 1.5 cm. A schematic representation of the floor heating model is shown in Figure 2.2.
Finally, it is noted that although the indoor temperature profiles obtained by this simplified emission system models showed good agreement with more detailed models in IDEAS, they are evidently not suited to accurately predict the return water temperature which is a prerequisite for a detailed calculation of the system efficiency. Nevertheless, since this work focusses on the efficiency of the building, the simplifications are considered acceptable.

2.2.5 Boundary conditions

The boundary conditions can be divided into two groups, i.e. climate and occupant behaviour. The simulations are carried out for the heating dominated climate of Belgium. Thereby TMY3

data of Uccle are used with a 10-minutes resolution[4] [94].
Occupant related internal gains are implemented using a stochastic user model developed by Baetens and Saelens [95]. In contrast, unless stated otherwise, fixed schedules for the temperature set-point for heating are used to allow a scenario analysis. The specific settings for the schedules will be presented in the different chapters.
Finally, the comfort requirements are specified by minimum and maximum temperatures, limiting the allowed temperature fluctuations for activating the thermal energy storage capacity. As explained in Section 1.2, the allowed comfort range is used as a model parameter in order to estimate the impact of user acceptance on the potential of structural storage for ADR.

2.3 Evaluation of model accuracy

In this section, the accuracy of the models presented above is verified. Since the accuracy of the building model is already shown to be comparable with state-of-the-art building simulation software in a BESTEST-validation [80]. The discussion here is on the one hand limited to an assessment of the impact of the solver settings used to simulate the model in Dymola [96] and the discretisation used for the thermal conduction (Eq. 2.3). On the other hand, the model accuracy is verified in Section 2.3.2 using on-site full-scale measurements of the Twin Houses. These measurements have been collected in the IEA EBC Annex 58 project [97] and provide a high-qualitative data set that allows both a verification of detailed simulation models and the identification of reduced-order building models. The latter will be shown in Chapter 4.

2.3.1 Sensitivity to numerical settings

Before presenting the verification of the model accuracy using measured data, the impact of the solver settings and the discretisation for the conduction equation (Eq. 2.3) is analysed. The analysis is carried out in two steps. First an inter-model comparison for the heat transmission through an insulated cavity wall is given to assess the impact of the number of states in the discretisation of the thermal conduction equations. In the second step, a sensitivity analysis of the solver settings is carried out on a single zone dwelling,

[4] A resolution of 10 minutes for the boundary conditions is used since ADR is typically evaluated at a 15 min resolution.

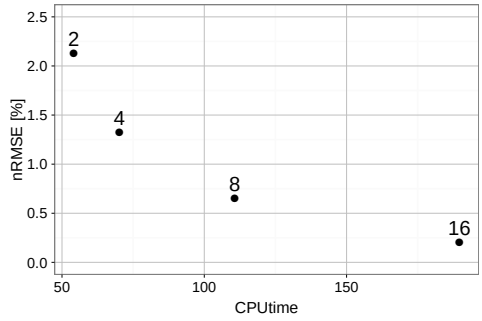

Figure 2.3: Normalised RMSE-value [%] of the difference in heat flux between the simulations using the IDEAS-library model and a detailed simulation in HAMFEM in contrast to the CPU time [s]. The results show the average nRMSE value of the interior and exterior surface as a function of the number of states in each material layer used for the discretisation of the thermal conduction equation.

corresponding to a typical Belgian detached dwelling built before 1945[5], which is chosen as it shows high indoor temperature variations in a day-night heating schedule.

Discretisation of the thermal conduction through a cavity wall The impact of the number of states used to model each material layer in a multi-layer wall is assessed by an inter-model comparison. Thereby a cavity wall is modelled consisting of an outer brick (8 cm), mineral wool insulation (12 cm), an internal brick (14 cm) and an interior plaster finishing layer (1.5 cm). The example of an insulated cavity wall is shown here as it is current practice in Belgian residential buildings and as it shows high temperature gradients over the wall.
As a reference, the model is implemented in HAMFEM [98] which uses a finite element method to simulate heat and mass transfer in building components. Based on a grid-sensitivity study, 200 elements are used to model the wall in HAMFEM, showing a difference in heat flow of less than 1 % compared to a model with 100 elements. The simulations are carried out for a whole year using the outdoor climate of Belgium and a constant indoor air temperature of 20 $^{\circ}\mathrm{C}$ as model inputs. The surface temperatures and heat fluxes on both the indoor and outdoor surface are used as an output and simulated with a time resolution of 1 min.
In IDEAS, the cavity wall is simulated[6] using the surface temperatures obtained by HAMFEM as input signals. The heat flux at the interior and exterior surfaces are selected as model outputs and compared to the HAMFEM results.

[5] The building model is part of the dynamic building stock model developed in Chapter 5. Since for this analysis only the relative impact of solver settings and the discretisation of opaque components is evaluated, we do not include the building description here, but refer to Section 5.1

[6] The simulations are conducted in Dymola [96] using the DASSL-solver with a tolerance of 10^{-12}.

Figure 2.3 shows the normalised RMSE values[7] (nRMSE) of the difference in heat flux between the IDEAS-library and HAMFEM models, averaged for the interior and exterior surface.
A comparison of the model scenarios – using 2 - 16 states for each material layer – shows a significant reduction in the nRMSE values when the number of states increases from 2 to 8. For the latter an nRMSE value for the minutely heat flux of 0.63 % is obtained. At the same time the total annual heat absorbed by the wall is underestimated by 0.18 %. Further increasing the model order does not significantly reduce the nRMSE values which is considered not to outweigh the increase in calculation time. Consequently, for the remainder of the work 8 states are used per material layer. The same number of states is used for every layer to simplify the model implementation, even though less states may be used for thin layers to reduce the simulation time.

Solver settings The impact of the solver settings on the obtained simulation accuracy is quantified for the simulation of a single zone dwelling. This is one of the typical model cases used in this work.
The building is implemented as a single zone model and simulated for a simulation period in spring (April 15^{th} - May 30^{th}) for the Belgian climate. The spring period is chosen as it is characterized by both high dynamic excitation at the exterior surface due to solar gains and at the interior surface due to the heating system. As such, it represents a worst case scenario. The simulations are carried out in Dymola [96] using the radiator heating systems described in Section 2.2.4. Two simulations are carried out for each of the solver settings, corresponding to the two simulations that are used in Chapter 3 to quantify the ADR potential (Figure 3.2). The first simulation, denoted as 'Ref', uses a thermostatic control with a fixed occupant schedule. The second simulation, referred to as 'ADR', includes in addition to the occupant schedule a period of 8 h in which the thermostat set point is increased by $3°\mathrm{C}$. The temperature increase starts on April 15^{th} at 11 AM, the occupied period is set from 8 AM to 10 PM. This latter simulation represents an active demand response event in which the heating system is used to activate the thermal mass of the dwelling. Note however that the settings of the duration and the temperature increase for the ADR event represent an extreme case.

For the sensitivity study, the difference between the two simulations in the total heat produced by the ideal heating system (δQ) is calculated at the end of the 8 h ADR-event (t_1) and at the end of the simulation period (t_2). Both results play an important role in the quantification

[7] the normalised RMSE is defined as: $nRMSE = \sqrt{1/n \sum (\hat{y}(t) - y(t))^2}/(y_{max} - y_{min})$, with $\hat{y}(t)$ and $y(t)$ respectively the simulated and measured signals and n the length of the number of samples

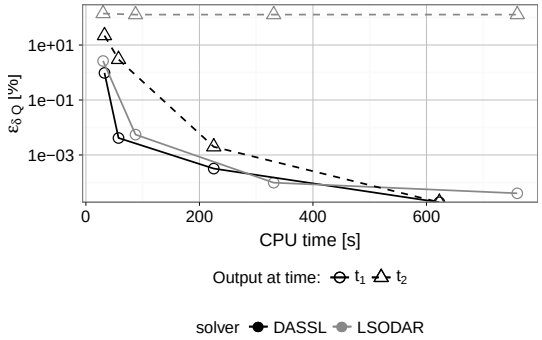

Figure 2.4: Impact of solver settings on the relative simulation error of output δQ [%] and on the CPU time [s]. For both solvers, the markers represent from left to right the tolerances settings, which are set to respectively 10^{-3}, 10^{-6}, 10^{-9} and 10^{-12}.

of the ADR potential of a dwelling as presented in Chapter 3.

$$\delta Q = \int_0^{t_i} \left(\dot{Q}_{sys,ADR}(t) - \dot{Q}_{sys,Ref}(t) \right) dt \tag{2.6}$$

where t_i refers to either the end of the ADR event (t_1) or the end of the simulation period (t_2). $\dot{Q}_{sys}$ is heating power emitted by the ideal heating system.

The sensitivity of the results to the solver settings is analysed by comparing two of the commonly used solvers in Dymola, i.e. DASSL and LSODAR, for a range of solver tolerances varying between 10^{-3} and 10^{-12}. For both solvers a variable step-size is used and the output is in double precision.

Figure 2.4 shows the impact of the solver type and tolerance on the relative error on δQ and on the cpu time. The simulations are run on an Intel(R) Xeon(R) CPU E5-1620v2 processor (3.7 GHz) with 16.0 GB RAM. The error is estimated by comparing the output for each case to the simulated results with the DASSL solver and a solver tolerance of 10^{-12}.

Thereby it is shown that up to t_1, i.e. the end of the ADR period, both solvers show a comparable accuracy and simulation time. Nevertheless, for the output at the end of the dataset a significant difference is found between the LSODAR and DASSL solver. This difference is caused by errors in the event detection for the LSODAR-solver which did not switch off the heating at the end of the ADR period. Consequently, the additional heat delivered by the system at the end of the simulation period (t_2) is an order of magnitude higher.

Based on the results of Figure 2.4, the DASSL solver with a tolerance of 10^{-9} will be used.

For this setting a relative error of 0.001-0.01% was found. Further reducing the tolerances does not compensate for the increased calculation time.

2.3.2 Verification with on-site measurements

Description of the building

In this section the verification of the model with on-site, full-scale measurement data for a multi-zone building is presented. The measurements were conducted – in the framework of the IEA EBC Annex 58 project – in the Twin houses (the O5-building) at the Fraunhofer institute in Holzkirchen (Figure 2.5). The O5-building is one of two identical, single-family houses that have been constructed to allow comparative, full-scale experiments of building components and technical systems with the aim of analysing the energy efficiency under identical weather conditions. A full description of the test facility as well as the experiment design is given in [99].

For the experiment only the ground floor of the building is used, while the attic and cellar are kept at a constant temperature. The ground floor consists of 7 zones (Figure 2.5) and is divided in 2 parts, i.e. the controlled zones and the boundary zones. The controlled zones consist of the 4 south-oriented rooms: the living room (1), the corridor (2), the bathroom (3) and the bedroom (4). They are referred to as controlled zones because in these zones a dynamic heating experiment is carried out which will also be used for the identification of reduced-order building models (Chapter 4). The North-oriented rooms, i.e. the kitchen (5), the doorway (6) and the parent bedroom (7) are referred to as the *boundary zones* since they are heated to a constant set-point equal to that of the attic and the cellar. To separate both parts the doors between the controlled and boundary zones have been sealed. In contrast, the doors between the controlled zones are open to allow for a strong mixing of the indoor air. The building has a ground floor area of 100 m^2 and is constructed and insulated in line with the German energy code (EnEV 2009). The outer walls are exterior insulated brick walls with U-values between 0.20 $\mathrm{W}/(\mathrm{m}^2\mathrm{K})$ and 0.27 $\mathrm{W}/(\mathrm{m}^2\mathrm{K})$. The windows have double-pane thermal insulated glazing with a U-value of 1.2 $\mathrm{W}/(\mathrm{m}^2\mathrm{K})$. The ceiling has a concrete structure with 2 insulation layers respectively at the inner surface adjacent to the controlled zone, and between the concrete structure and the screed top layer. The resulting U-value of the ceiling is 0.17 $\mathrm{W}/(\mathrm{m}^2\mathrm{K})$. The floor has a concrete layer of 6.5 cm adjacent to the controlled zone and a U-value of 0.26 $\mathrm{W}/(\mathrm{m}^2\mathrm{K})$. A balanced ventilation system is used for the controlled zones. The flow rate is kept constant at 60 m^3/h with supply in the living room and the exhaust equally distributed over the bathroom and the bedroom. The supply and

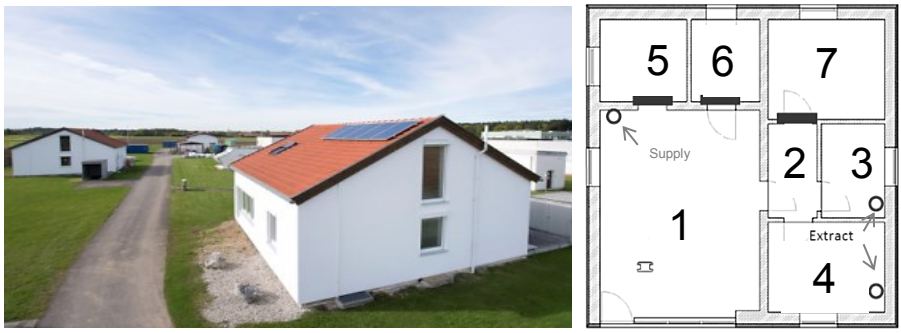

Figure 2.5: Image (left) and floor plan (right) of the Twin Houses

return air temperatures are measured respectively after and before the fan to account for the heat of the fan which is transferred to the air. No ventilation is used in the boundary zones. The air-tightness of the dwelling was measured before the start of the experiment using a blower-door test, resulting in an n_{50}-value of 1.67 ACH.

An overview of the building components and the building geometry is given in Table 2.1. Note that in addition to the surface areas and UA-values the table also shows the total thermal capacity (C_{tot}) and specific effective thermal capacity (C_{eff}), as well as their corresponding area weighted averaged values: U, c_{tot}, c_{eff}. A physical explanation of these capacities is given in Chapter 4.
The data sets and detailed model specifications used to perform the presented validation exercise are accessible from the website of the IEA EBC Annex-58 project [97].

Experiment design and measured data

The experiment consists of three phases in order to enable both detailed building model validation as well as identification of reduced-order models and characterisation of the thermal properties – as was aimed for in the IEA EBC Annex 58 project. The full sequence is shown in Figure 2.6. For the controlled zones the sequence consists of 3 periods with a constant temperature period used as initialisation (init 1, 2 and 3), a free-floating period (free-float) during which the heating is switched off and a period with dynamic heat input (ROLBS).

During this dynamic heating period a ROLBS sequence, or Randomly Ordered Logarithmically

Component	Area m^2	U $\frac{W}{(m^2K)}$	c_{tot} $\frac{MJ}{(m^2K)}$	c_{eff} $\frac{MJ}{(m^2K)}$	UA $\frac{W}{K}$	C_{tot} $\frac{MJ}{K}$	C_{eff} $\frac{MJ}{K}$
Ext. Walls A	18.62	0.27	308	288	5.04	5737	5363
Ext. Walls B	39.34	0.20	305	288	7.85	12012	11329
Int. Walls A	10.89	1.09	264	264	11.88	2874	2874
Int. Walls B	13.89	1.79	163	163	24.87	2264	2264
Ceiling	69.91	0.17	629	6.72	11.62	44000	470
Floor	69.91	0.28	664	130	19.40	46431	9088
Boun. Walls A	8.77	1.09	264	264	9.58	2317	2317
Bound. Walls B	7.48	1.79	163	163	13.40	1219	1219
Bound. Doors	5.47	1.97	24	24	10.77	131	131
Windows	15.08	1.12			16.93		

Theoretic value	Heat transfer coefficient W/K	Effective capacity MJ/K
Ventilation/Indoor air capacity	31.8	0.17
Envelope total	36.6	16.7
Envelope opaque	12.3	16.7
Boundary walls	67.77	13.1
Internal walls		5.1

Table 2.1: Insulation and thermal mass properties of Twin House

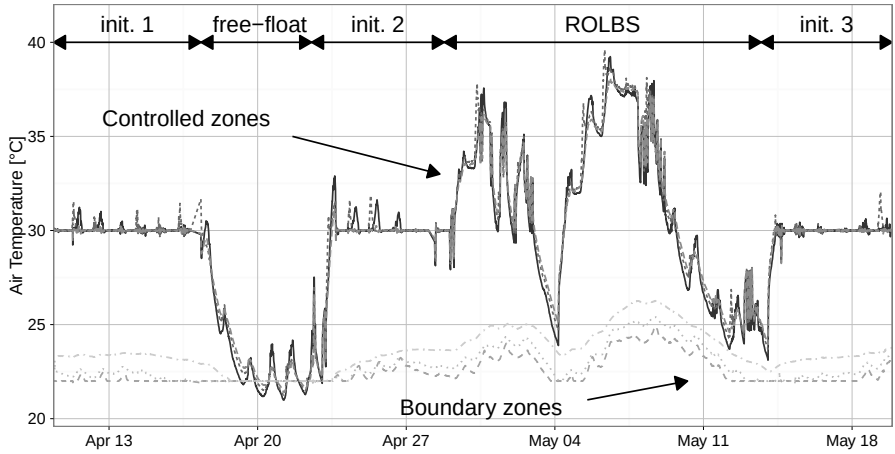

Figure 2.6: Temperature measurements for controlled and boundary zones for the whole test period.

distributed Binary Sequence[8], is applied as control signal for the electric radiators in the controlled zones, while the boundary zones have a constant temperature set point of 22 $^{\circ}\mathrm{C}$.

[8] ROLBS is a pseudo-random sequence that ensures that the heat input is uncorrelated to the other boundary conditions. As such, a persistent excitation is generated to improve the identifiability of grey-box models as shown in Chapter 4.

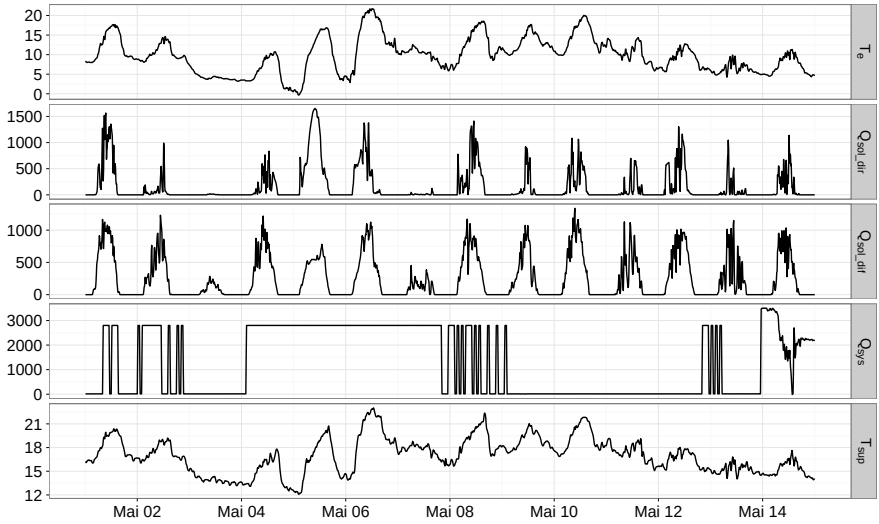

Figure 2.7: Measured input signals. From top to bottom the outdoor air temperature $(T_e\ [^\circ\mathrm{C}])$ *, direct* $(Q_{sol\_dir}\ [\mathrm{W/m^2}])$ *and diffuse* $(Q_{sol\_dif}\ [\mathrm{W/m^2}])$ *horizontal solar irradiation, heating power* $(Q_{sys}\ [\mathrm{W}])$ *and supply air temperature* $(T_{sup}\ [^\circ\mathrm{C}])$ *are shown.*

An extensive set of data is collected of which the indoor (T_i) and outdoor (T_e) air temperatures, solar irradiation $(\dot{Q}_{sol})$, ventilation rate $(\dot{V})$ and supply temperature (T_{sup}) , heating power $(\dot{Q}_{sys})$ and heat flux measurements have been used in this work. Figure 2.7 illustrates a subset of the input measurements during the period with the ROLBS input signal for the heating system. From top to bottom the outdoor air temperature, direct and diffuse solar irradiation, heating power and supply air temperature are shown. The measurements are collected by a central PLC system that also controls all heaters, thereby avoiding possible synchronisation problems. All sensors are read at a 1 second interval and re-sampled with a 60 second interval. A more detailed description of the measurement set up as well as an assessment of the accuracy is found in [99].

Model implementation

The building is implemented using a 7 zone model, i.e. one zone for each room. The thermal properties and building geometry are implemented according to the modelling specifications provided in the common exercise of Subtask 4 of the IEA EBC Annex 58 [97]. Nevertheless, some additional assumptions were needed since some of the physical phenomena, such as

thermal bridges and inter-zone airflow through open doors, are not yet available in the IDEAS-library. In the context of subtask 4 of the IEA EBC Annex 58 project, different assumptions have been tested in a scenario analysis to estimate the sensitivity of the results [100, 101]. For the results shown in this section, thermal bridges are – as a simplification – included directly as a loss term $(\dot{Q}_{TB})$ in the heat balance of the zone (Eq. 2.1). The loss term is given by:

$$\dot{Q}_{TB} = (T_{air} - T_e) \sum \Psi_e L_e + (T_{air} - T_{att}) \sum (\Psi_c L_c) + (T_{air} - T_{cel}) \sum \Psi_f L_f \tag{2.7}$$

where T_{att}, T_{cel} and T_e are respectively the temperatures of the attic, cellar and outdoor air, Ψ_c , Ψ_f and Ψ_e are the linear thermal bridge coefficients in the ceiling, floor and envelope with corresponding lengths L_c, L_f and L_e . Note that the attic and cellar have not been modelled. Instead, the measured temperatures are used as boundary conditions for the floor and ceiling of the zones on the ground-floor.

To account for the high coupling – as a result of the open doors – between zone 2 and respectively zones 1, 3 and 4, an additional term $(\dot{Q}_{\delta,i,j})$ is included in the heat balance equation of the zones (Eq. 2.1):

$$\dot{Q}_{\delta,i,j} = H_{\delta,i,j}(T_{air,i} - T_{air,j}) \tag{2.8}$$

where $T_{air,i}$ and $T_{air,j}$ are the air temperature of room i and j, and $H_{\delta,i,j}$ is the coupling coefficient. Based on a qualitative (visual) analysis of the data, a high coupling coefficient of 50 $\mathrm{W/K}$ is implemented.

The heating system consists of electric resistance radiators, modelled using the ideal radiator heating system presented in Section 2.2.4. Thereby the production efficiency is assumed to be 100% and the radiant fraction (f_{rad}) is set to 0.3, according to the IEA EBC Annex-58 modelling specifications [97].

The control of the heating system for the controlled zones is split into 4 periods in which alternatively the indoor temperature and the heat input are controlled. Between April 9^{th} and 18^{th} and between April 23^{rd} and 27^{th} the heating system is controlled with a thermostat set point equal to the measured air temperature. As such, the measured and simulated heating powers can be compared as an output during these periods (indicated by the grey area in Figure 2.8). Alternatively, during the other periods the measured heating power is used as an input for the model while the indoor air temperatures are used as the model output. Note that for the north zones (zone 5-7) the thermostatic control is used throughout the entire simulation with a set-point temperature of 22 $^{\circ}\mathrm{C}$.

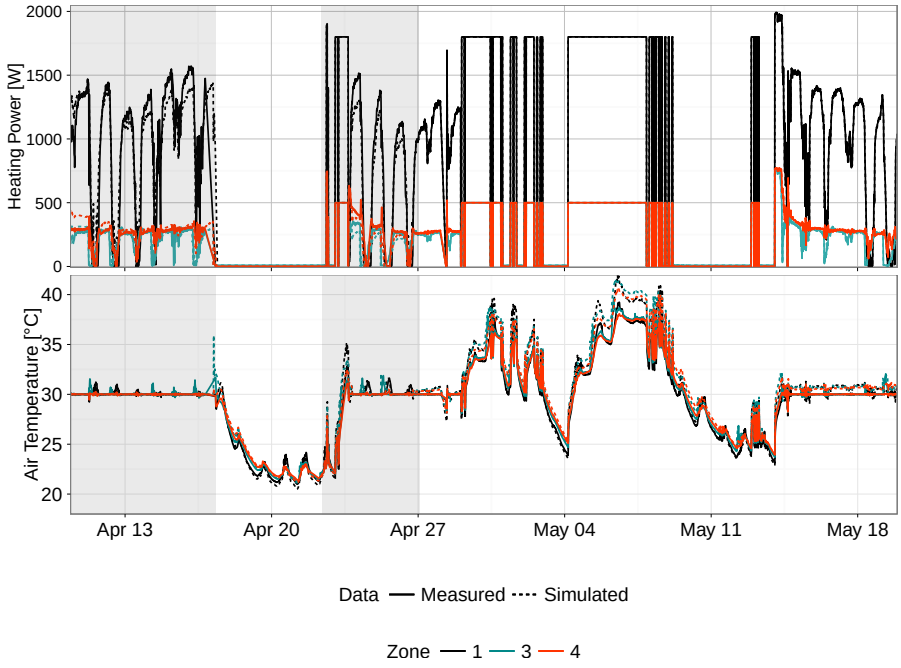

Figure 2.8: Comparison of measured and simulated heating power (top) and air temperature (bottom) for the living room (zone 1), the bathroom (zone 3) and the south bedroom (zone 4). The grey areas indicate the periods where a thermostatic control is used in contrast to a prescribed heating power.

Verification results

The simulated indoor air temperature and heating power for zones 1, 3 and 4 are shown in Figure 2.8. The figure shows a slight underestimation of the heating power, especially for the living room (zone 1), when the thermostat control is used (grey areas in Figure 2.8). Based on the first initialisation period RMSE values of 168 W (11 %), 46 W (15 %) and 55 W (14 %) are found for respectively zone 1, 3 and 4. The highest deviations are thereby found (Figure 2.8) during periods with high solar gains, where high frequent peaks in the residuals are found. Moreover, for zone 3 and 4 the residuals decrease significantly near the end of the initialisation period, from 680 W to 12 W for zone 3 and from 870 W to 18 W for zone 4, indicating that the errors are mainly caused by the initialisation at the start of the simulation. More important differences are found for the indoor temperature during the ROLBS periods (April 29^{th} - May 13^{th}). Since during this period the heat input is controlled to match the measured heating power, an underestimation of the thermal losses or an overestimation of the gains, will result in a systematic deviation of the simulated indoor air temperature from the

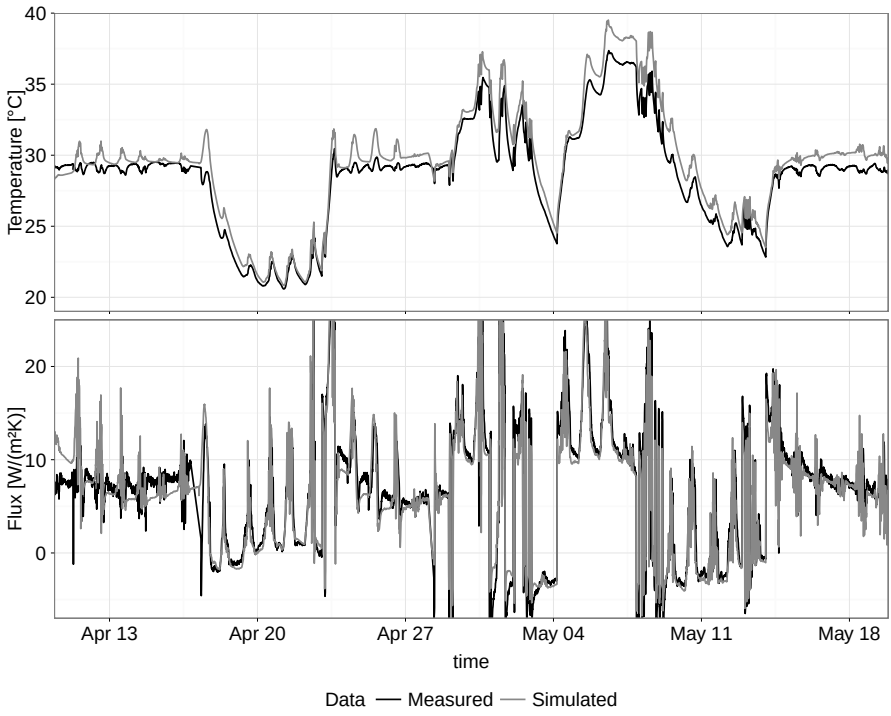

Figure 2.9: Comparison of measured and simulated surface temperatures (top) and heat flux measurement (bottom) at the inner surface of the west wall in the living room.

measured values. Figure 2.8 shows maximum temperature deviations of 3.57 $^{\circ}\mathrm{C}$ (19.6 %), 4.57 $^{\circ}\mathrm{C}$ (29.1 %) and 3.18 $^{\circ}\mathrm{C}$ (23.8 %) for respectively zone 1, 3 and 4. The nRMSE values for the indoor temperature during the ROLBS period and the final constant temperature period (April 29^{th} to May 13^{th}) are 1.0 $^{\circ}\mathrm{C}$ (5.5 %), 0.8 $^{\circ}\mathrm{C}$ (5.1 %) and 0.6 $^{\circ}\mathrm{C}$ (4.5 %) for zone 1, 3 and 4. It should however be noted that the main differences are found during the periods where the measurements showed significant stratification in the rooms (see further in Fig. 4.25). During the cool-down and constant temperature periods, the temperature differences are less pronounced. Moreover, during the last constant temperature period (May 14^{th}-19^{th}) – in which the heating power is used as the input and not the thermostat set point – the air temperature in the simulation is on average 0.5-0.7 $^{\circ}\mathrm{C}$ higher than the measured values.

Finally, Figure 2.9 shows the comparison of the simulated and measured surface temperature and heat flux at the west wall of the living room. The simulated flux is obtained from the model using the term q_T from Eq. 2.2. As for the air temperature (Figure 2.8(bottom))

a significant overestimation of the surface temperature is shown in Figure 2.9(top) during the period with the heating power as input signal, i.e. from April 29^{th} until the end of the experiment. Nevertheless, during this period the simulated heat flux corresponds well to the measured data.
At the same time, an overestimation of the measured surface temperature is also found during the period where the thermostatic control is applied (April 9-18 and 23-27). The flux through the wall is underestimated during this period. Both results point to an underestimation of the transmission losses. This underestimation may result from model errors, but given the level of accuracy found in Section 2.3.1, the results are likely to be caused by discrepancies between the specification of the construction properties provided in the modelling specifications and the as-built values.

2.4 Conclusions

This chapter describes the building energy simulation models that are the basis for the remainder of this work. The models extend from the IDEAS-library in Modelica. Thereby the choice for the IDEAS-library was based on the equation-based and object-oriented framework in Modelica which were found to be strong assets which significantly simplify the implementation of new models and the adaptation of existing components to the specific needs of the study. Moreover, given the district oriented, bottom-up modelling approach that is used in the IDEAS-library, the models and quantification frameworks developed in this dissertation can be readily extended to district energy assessments.

Both the numerical and physical accuracy of the simulations have been analysed. Thereby it was found that the DASSL-solver in Dymola needs more calculation time but is more robust than the LSODAR-solver. Therefore the former will be used in the remainder of the work with a tolerance of 10^{-9}. Moreover, the simulation results were found to depend significantly on the number of states used to discretise the thermal conduction equation. Thereby, a minimum of 8 states per layer was needed to reduce the normalised RMSE-value of the heat flux through a multi-layer wall to less than 1 % for the comparison between a detailed finite element model in HAMFEM and the IDEAS-library model. Consequently at least 8 states per material layer are used for the remainder of the work.

In addition, the model is validated against on-site measurements. A comparison of the indoor air temperature and the heating power showed that on average the model underestimates the thermal losses by 10-15 %. Moreover, a comparison of the heat flux and surface temperature at the inner surface of the outer walls indicated that even in the constant temperature periods,

the losses through the wall are underestimated. As such, part of the deviations between the simulations and the measurements are likely to be caused by discrepancies between the material properties provided in the modelling specifications and the as-built values.
Additional, more detailed measurements are needed to prove these hypotheses. Nonetheless, given the complexity of the experiment, a 10-15 % deviation on the heating power and a temperature deviation of 0.5-0.8 $^{\circ}\mathrm{C}$ during the final constant temperature period are deemed to be acceptable.

Chapter 3

Flexibility for active demand response using structural thermal energy storage

3.1 Introduction

As presented in Section 1.1, multiple studies are found in literature which demonstrate the potential of the structural thermal mass of dwellings for active demand response [102, 44, 47, 43, 46, 56]. A systematic analysis of the relation between the building design parameters and the flexibility of the structural storage capacity for active demand response has not yet been established.

The goal of this chapter is therefore in a first step to develop a generic set of key performance indicators that allows the quantification of the ADR potential of a building. These performance indicators should not only enable a quantitative comparison of the flexibility of different buildings, but also facilitate a comparison with other storage technologies in a Smart Grid context. Therefore this chapter presents a definition and quantification method for these storage metrics that is independent of the energy market structure or demand response mechanism.

In a second step, this chapter aims at quantifying the impact of building design parameters on the suitability of buildings for structural thermal energy storage in an ADR context. Thereby it

should be emphasized that although different studies show that the efficiency of the thermal systems used to activate the structural storage capacity, such as heat pumps or combined heat and power units, is a key parameter in the suitability of a building for ADR, the focus of this work is, as presented in Section 1.2, on the impact of the thermal properties of the building, and its interaction with the thermal emission system, on the ADR potential of the structural storage capacity.

Layout of the chapter Based on the literature study (Section 3.2), the available storage capacity, the efficiency of the storage process, the power shifting capability and the state of charge are identified as key performance indicators for the quantification of the ADR potential of structural thermal energy storage.
In Section 3.3, the definitions of these generic performance indicators and the corresponding quantification methodologies are presented. Thereby, simulation-based quantification methods are developed using a simple rule-based approach. Although, in practice – especially for complex systems – a quantification method using an optimal control approach [75, 76] has important benefits, the rule-based approach is used in this work from a research perspective as it enabled a comprehensive, fundamental comparison of the impact of building design parameters.
In the second part of this chapter, the evaluation of these performance indicators as a function of the building design parameters is presented by means of an extensive parameter study. Given the distinct nature of the defined performance indicators, the analysis and discussion of the results are split into two parts. Section 3.4 presents the parameter study using building energy simulations to evaluate the impact of the building design parameters on the available storage capacity and the storage efficiency. Section 3.5 demonstrates the methodology to quantify the state of charge and the power shifting capability.
Finally, based on the analysis in this chapter, conclusions and suggestions for building and control design are formulated in Section 3.6.

3.2 State of the art in quantification of ADR potential

The potential of structural thermal energy storage for active demand response is commonly evaluated in the context of case studies. These studies can be grouped into two categories: (i) a top-down analysis focusing on the macro-economic benefits of activating flexibility and (ii) a bottom-up evaluation of active demand response focusing on the technological aspects of ADR and storage. The latter starts from an analysis on a technology or component level and

aggregates the results, based on estimates of the impact of individual technologies and the distribution in the total population, to quantify the impact on an aggregated level. In contrast, a top-down approach starts from observations on the aggregated level, typically consisting of historical data, to identify the inter-relations of technological or economical changes in the lower level [103].

In the first group, top-down approaches mostly analyse the macro-economic impact of ADR by taking into account the flexibility of different storage technologies and demand-side management strategies in the energy market. The flexibility for ADR is thereby typically presented as the percentage of the total load profile that can be shifted in a certain time frame, typically 24 h [104]. Alternatively, the flexibility may be implemented by price elasticities[1] [27, 105]. This price-elasticity for demand can then for example be included in a unit commitment problem to optimise the electricity production taking into account the flexible load. Nonetheless, [106] argues that in these studies the physical aspects of the demand-side are often not well represented, eliminating the capability of identifying key areas for improvements for the reduction of energy use. Moreover, [103] emphasizes that the reliance on historical data is also a drawback as top-down models have no inherent capability to model discontinuous advances in technology.

In the second group, bottom-up studies found in literature mostly use case-studies to demonstrate the impact using the flexibility of thermal energy storage on the peak heating and cooling demand, the use of passive gains, the benefits of time of use pricing [102, 44, 47, 43, 46, 56, 58]. Typically optimal control strategies are developed and evaluated for their potential to activate the structural storage capacity of buildings for active demand response. Thereby, the reduction of the energy cost, the shift of peak electricity use or the increased use of local renewable electricity production are used as performance criteria, showing the potential of structural storage for active demand response. In these studies, the flexibility of demand response technologies is often not explicitly defined and the term may refer to various aspects ranging from the response time or the power capacity to the degree of robustness in a given energy market scenario, such as the ability to increase self-consumption or reduce peak demand [107]. However, these performance indicators are found to not reflect the actual flexibility of a building but instead they demonstrate the result of using this flexibility in an optimal control strategy. Consequently, the obtained performance indicators for buildings properties are not only function of the building design but also of the implemented market or control scenario.

[1] In economics, price elasticity of demand is used as a measure to indicate the change in the quantity demanded of a good in response to a price change.

In contrast, Oldewurtel et al. [76] propose a standardised, bottom-up quantification method for the ADR potential based on the definition of the power shifting capability and the power shifting efficiency. The power shifting capability is defined as the maximum upward or downward power shift that is obtained by active demand response. This shift is quantified by performing an optimal control problem with a short, but high, block pulse in the energy price. The corresponding efficiency is defined as the additional energy use compared to the shifted power. A similar formulation is proposed by De Coninck [75], quantifying the flexibility of a building and the associated cost by calculating the activated flexibility as a deviation from the optimal control solution, f.i. minimum energy use or minimum energy cost. While these studies also use optimal control strategies to quantify the buildings flexibility, the optimal control problem is formulated in a generic way – unrelated to a specific market scenario. Consequently, both approaches allow to quantify the generic flexibility of the building for active demand response. The resulting power shifting capability and the power shifting efficiency [76] or the flexible capacity vs. cost relation [75] can be therefore interpreted as a property of the building and its system rather than the result of a scenario-specific optimisation. Nonetheless, it is found that although the use of optimal control provides a strong tool for quantifying the flexibility of complex systems, the interpretation of the results as a function of the contribution of specific building aspects to the flexibility is found to be difficult. For example, it is not always clear whether the increased energy use due to activating the flexibility results from a change in the production efficiency of the heating system, a reduced usability of passive solar gains or increased thermal losses due to higher indoor temperatures.

Whereas these studies demonstrate the potential of ADR, mostly in a specific energy market context, an in-depth analysis of the impact of the building design parameters on the demand-side management potential, taking into account e.g. the insulation quality, the compactness, the infiltration rate is not found in literature. Moreover, unified performance criteria that allow for a systematic comparison of storage and demand response technologies in a general demand response context is not yet established. Such a framework should specify performance indicators that quantify the techno-economic performance of storage technologies, considering both the perspective of the grid developer and the end-user. Thereby the term grid developer is used here as a general term for all stakeholders involved in developing, operating and maintaining energy distribution systems, such as transmission and distribution system operators. Thereby also the government may be considered as a stakeholder which is interested in reducing the CO_2-emissions. These stakeholders are in addition to economic and safety parameters, interested in (i) the total amount of energy that can be stored in the structural storage capacity, (ii) the amount of energy that is currently stored within this capacity and (iii) the additional storage losses that are introduced by

activating the thermal mass. In the case of structural storage for ADR the end-user, i.e. the building owner, is interested in (i) maintaining a comfortable indoor environment and (ii) the potential profit that could result from making the storage capacity of the building available for ADR. Thereby the latter not only refers to monetary savings but also security of supply may be an important factor.
In order to develop such a framework, Ibrahim et al. [108] summarise the techno-economical characteristics of storage systems to establish comparison criteria for selecting the appropriate technology. They state that in addition to operational requirements such as reliability, safety and environmental impact, the main characteristics needed to compare storage technologies are:

- storage capacity: amount of energy that can be stored [kWh]
- energy density: amount of energy that can be stored per unit of mass [kWh/kg] or volume [kWh/m^3]
- autonomy: maximum time the system can continuously release energy [s]
- efficiency: 1 - ratio between self-discharge and stored energy [-]
- available power: maximum power of charge and discharge [W]
- ramp rate: ability to change the power demand or supply [W/s]
- response time: time needed before technology is available [s]
- costs: investment and operational costs of storage [euro]
- durability: maximum number of cycles [-]

Similar performance criteria are used by the International Renewable Energy Agency in a technology assessment report for battery storage [109]. However, it is evident that whereas these properties may be readily available for traditional storage systems, such as battery storage systems or thermal water storage tanks, no literature was that quantifies these properties for structural thermal energy storage in buildings. Nonetheless, it is expected that the first 3 characteristics, i.e. the storage capacity, energy density and autonomy, are closely linked to the available thermal mass of the building. In contrast, the available power, the ramp rate and response time may be linked to the heating system. The storage efficiency is expected to depend both on system characteristics and the building design, since it may be related to the production and distribution efficiency of the system as well as the increased transmission and ventilation losses.

In an ADR context, Oldewurtel et al. [110] extend the use of these performance criteria for storage systems to demand response technologies, contrasting amongst others the *power capacity* [W], *energy capacity* [kWh], ramp rate [W/s] and response time [s] of both storage and DR technologies. Heussen et al. [111] present a similar approach, i.e. the “power node

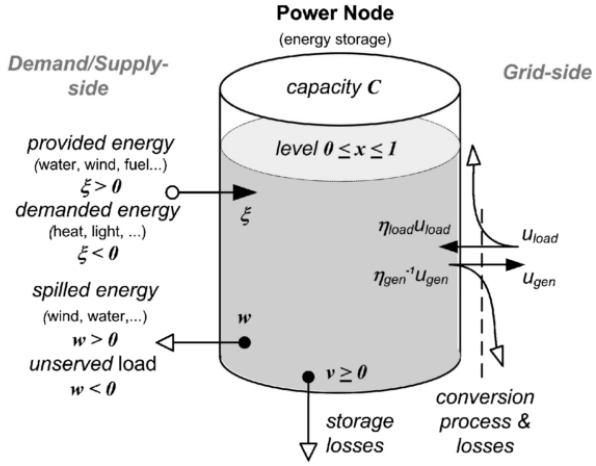

Figure 3.1: Representation of a 'power node' (Heussen et. al [111])

framework", that models demand response technologies as virtual storage units, allowing a comparison with other storage technologies. In the "power node framework" any power source or sink connected to the electric power system enables the conversion of a certain energy vector into electric power and vice versa. From a grid perspective each supply- or sink-process is lumped into a single "power node", making abstraction of the physical properties and internal composition of the process. A representation of a power node is given in Figure 3.1. As indicated in Figure 3.1, the storage capacity of the power node (C), together with the state of charge (x) and the storage losses (v) are used as main characteristics of the storage technology.

Similar to the 'power node' framework the concept of 'Energy Hubs' is introduced in the 'Vision of Future Energy Networks' project. The Energy Hub is defined as a unit where multiple energy carriers can be converted, conditioned and stored [112]. The framework presents a model that links input and output energy vectors of a hub by using coupling matrices that represent the energy conversion and storage structures and their corresponding efficiencies. Both frameworks have shown a strong potential to simulate and assess the operational flexibility in power systems [113, 114, 115, 116]. Their main strength thereby is found in the generic description of demand-side management and storage technologies, allowing for a combined evaluation of a large mix of technologies. Nonetheless, a challenge still lays in a detailed and accurate specification and quantification of the flexibility characteristics needed for the integration of structural thermal energy storage in these generic frameworks.

3.3 Definitions and quantification

In this section the generic key performance indicators for active demand response are defined and quantification methods for the ADR potential of structural thermal energy storage are presented. Based on the literature review presented in Section 3.2, the available storage capacity, the efficiency of the storage process, the power shifting capability and state of charge are defined as main characteristics needed for an energy-related evaluation of a storage technology in an ADR context. Similar parameters were suggested, although the exact definitions may differ from the ones presented here, in the 'power node' and 'energy hub' frameworks [111, 112], as well as in the quantification method for flexibility developed in [110]. Thereby, it is evident that in each of these frameworks 4 aspects are important for the energetic evaluation of the ADR potential of a storage technology, i.e. the maximum energy content, the storage losses, the current energy content and the power at which energy can be exchanged.

Thereby, it will be shown that the available storage capacity for ADR and the storage efficiency – although they vary as a function of the climatic conditions, occupant behaviour and comfort requirements – can be interpreted as performance characteristics of the building in a similar way as f.i. the total heat loss coefficient. As such, they may provide interesting information already in a design phase. In contrast, the power shifting capability and state of charge are characteristics that describe the instantaneous available flexibility for ADR. They are therefore mainly interesting in the operational phase.

3.3.1 Available structural storage capacity for ADR

The first performance indicator quantifies the maximum amount of heat[2] that can be added to the structural storage capacity during the timespan of an ADR-event. An ADR-event is defined as an active, temporary deviation from normal behaviour without violating comfort requirements. In the context of structural thermal energy storage this can be interpreted as a short-term increase of the indoor temperature set-point for heating, compared to normal behaviour (as shown further in Figure 3.2). Note that, this definition can be readily extended to cooling applications as well, but the latter is not explicitly considered here. Moreover, only sensible thermal loads are considered.
In the context of sensible structural storage, which is the focus of this work, the amount of heat that can be stored during an ADR-event is limited by the temperature variations in the

[2] As shown in Section 1.2, only heating is considered in this work as the focus is on the Belgian residential sector. Nonetheless, definitions are readily extended to (sensible) cooling applications.

dwelling and thus depends on the comfort requirements, as well as on the thermal properties of the building and the heating system, the climatic conditions and occupant behaviour. In contrast to typical storage media, such as batteries or water storage tanks, the available structural storage capacity for ADR may thus vary significantly in time.

Definition The available structural storage capacity for active demand response $(C_{ADR}$ $[\text{kWh}])$ is defined as the amount of heat that can be added to the structural mass of a dwelling, without jeopardising thermal comfort, in the time-frame of an ADR-event and given the dynamic boundary conditions.

Quantification methodology To quantify the available storage capacity – as well as the storage efficiency shown in the following paragraph – two scenarios are simulated as demonstrated in Figure 3.2. A first simulation (black line) represents the reference scenario whereby the heating system is controlled to maintain the minimum comfort temperature, resulting in the reference heat demand of the dwelling $(\dot{Q}_{Ref})$. The second simulation (grey line) represents an ADR-event whereby, starting from a building with an indoor temperature equal to the minimum comfort temperature (Fig. 3.2), the temperature set-point for the heating systems is increased by dT_{comf} [°C] for the duration l_{ADR} [s] .
The available storage capacity is then given by the integral of the difference between the heat input during this ADR-event $(\dot{Q}_{ADR}[W])$ and the heat input in normal operation $(\dot{Q}_{Ref}[W])$, represented by the dark grey area in Figure 3.2:

$$C_{ADR}(t, l_{ADR}, U(t), dT_{comf}(t), \theta) = \int_0^{l_{ADR}} (\dot{Q}_{ADR} - \dot{Q}_{Ref})dt \tag{3.1}$$

$$\dot{Q}_{ADR} = f(t, l_{ADR}, U(t), dT_{comf}(t), \theta) \tag{3.2}$$

$$\dot{Q}_{Ref} = g(t, U(t), \theta) \tag{3.3}$$

with l_{ADR} the duration of the ADR-event, $U(t)$ the dynamic boundary conditions such as climate and occupant behaviour, $dT_{comf}(t)$ the comfort range available for ADR which may vary in time, and θ the building and system design parameters.
As discussed in Section 1.2, the comfort range that is available for ADR (dT_{comf}) is treated as a parameter in the analysis. This is done because the aim of this work is to demonstrate the potential of structural storage given the comfort range, i.e. the difference between maximum and minimum operative temperature, rather than attempt to quantify the comfort range, since the latter depends strongly on personal preference and local phenomena that

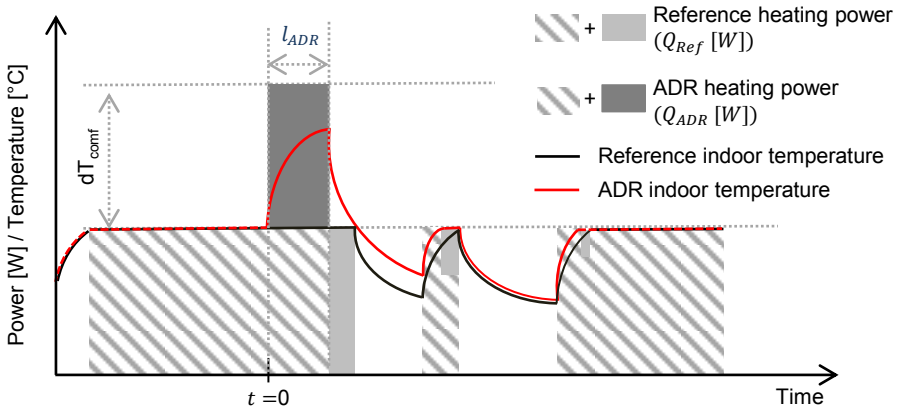

Figure 3.2: Scheme of the simulation experiment used to quantify the available storage capacity and the storage efficiency

are not included in the models.

Note that in this work the duration of ADR-events is varied from 15 min to 12 h, which is expected to be the application range when the thermal mass of the building is activated for ADR.

3.3.2 Efficiency of the storage process

In this section the efficiency of the storage process is defined. As shown in an exploratory study [15], the activation of the storage capacity results in an increased temperature within the building and thus the transmission and ventilation losses increase. As a consequence, only a part of the heat that is stored during an ADR-event, can be used effectively to maintain thermal comfort and reduce the heating power in the period after the ADR-event.

Definition The storage efficiency (η_{ADR} [-]) is defined as the fraction of the heat that is stored during the ADR-event that can be used subsequently to reduce the heating power needed to maintain thermal comfort.

Quantification methodology The efficiency can be calculated using the same set of simulations that are used to quantify the storage capacity. Given the 2 simulations for the

heating power in respectively the ADR scenario $(\dot{Q}_{ADR})$ and the reference scenario $(\dot{Q}_{Ref})$, the efficiency is calculated as:

$$\eta_{ADR}(t, l_{ADR}, U(t), dT_{comf}(t), \theta) = 1 - \frac{\int_0^{\infty} \left(\dot{Q}_{ADR} - \dot{Q}_{Ref}\right) dt}{\int_0^{l_{ADR}} \left(\dot{Q}_{ADR} - \dot{Q}_{Ref}\right) dt} \tag{3.4}$$

The integral in the denominator is equal to the heat stored in the ADR-event or the available storage capacity (C_{ADR}), shown as the dark grey area in Figure 3.2. A part of this heat can be used after the ADR-event to reduce the heating power needed to guarantee thermal comfort as indicated by the light grey area in Figure 3.2. The storage losses induced by activating the thermal mass – used as the numerator in equation 3.4 – thus correspond to the fraction of the heat stored during the ADR-event that is not recovered after a long period. Note that since this study focusses on the performance of the building rather than the heating system, the heat supplied by the emission system to the building and not the energy use of the heating system is used to quantify the efficiency. Nevertheless, the method can be readily extended to include thermal systems.

3.3.3 Power shifting capability

Whereas, C_{ADR} and η_{ADR} can be considered as characteristic properties of the building, the power shifting capability is a measure for the instantaneous flexibility that can be delivered by using the structural storage capacity. The power shifting capability gives the relation between the shift in power that can be obtained and the duration this shift can be maintained.

The amplitude of the power shift (Q_{δ}) [W] is a function of the instantaneous heat demand of the dwelling and the nominal power of the system and can be both positive and negative as the heating power might be increased or decreased compared to the current state. A similar definition was presented in [110]. However, in this thesis, an additional dimension is included in this metric by not only quantifying the range in which the heating power can be varied but also quantifying the time such a deviation can be maintained without jeopardising thermal comfort.

Definition The power shifting capability (PSC [s]) is the duration during which a change in heating power (Q_{δ}) can be maintained, given the dynamic boundary conditions and the current state of charge, before the comfort requirements are jeopardized:

$$PSC = f(\dot{Q}_{\delta}, dT_{comf}, U(t), \theta) \tag{3.5}$$

with dT_{comf} the comfort range as described above, and $U(t)$ the dynamic boundary conditions for the outdoor climate and occupant behaviour and θ the building and system design parameters.

Quantification method Given the current state of the building, a set of dynamic simulations is carried out for a prediction horizon H_t, in practice 48 h. For each simulation, the heating power is kept constant to a fraction (f_{mod}) of the nominal power. The duration for which this heating power can be maintained is quantified by the time until the comfort bounds, either T_{max} or T_{min} are reached. The power shifting capability is then expressed as the duration as a function of the amplitude of the power shift. The latter $(Q_\delta$ [W]$)$ is defined as the difference between the heating power during the ADR-event $(\dot{Q}_{ADR}$ [W]$)$ and the current heating power $(\dot{Q}_{Ref}$ [W]$)$.

$$\dot{Q}_\delta(t, U(t), dT_{comf}, \theta) = \dot{Q}_{ADR} - \dot{Q}_{Ref} \tag{3.6}$$

A distinction is made between the upward and downward shifting capability, representing respectively an increase or a decrease of the heating power compared to the current state.

3.3.4 State of charge

As mentioned above, the power shifting capability of a building depends on the current state of the building. The more energy is already stored within the structural mass of the building, the longer a reduction of the heating power can be maintained. This state is not only given by the current indoor temperature, but also depends on the history of the temperature profile.
The state of charge (SOC) of a storage system is commonly used in battery storage or water storage tanks and relates the current energy content of the storage medium to the minimum and maximum energy content that can be achieved without effecting normal operation. For buildings the latter corresponds to thermal comfort criteria. The maximum energy content $(E_{th,max})$ of the dwelling is obtained by the energy content of the building that is consistently heated to the maximum comfort temperature. Similarly, the minimum energy content $(E_{th,min})$ is obtained when the building is consistently heated to the minimum comfort temperature. Thereby both $E_{th,min}$ and $E_{th,max}$ – and consequently the SOC – depend on the comfort requirements, occupant behaviour and outdoor climate. It is thus important to note that the SOC will therefore vary in time even when the energy content of the building $E_{th}(t)$ is kept constant.

Definition The state of charge (SOC [-]) is defined as the fraction of the energy content of the storage medium at time t compared to the total storage capacity.

Quantification method Following the definition the state of charge is calculated using equation 3.7.

$$SOC = \frac{E_{th}(t) - E_{th,min}(t)}{E_{th,max}(t) - E_{th,min}(t)} = \frac{E_{th}(t) - E_{th,min}(t)}{C_{storage}(t)} \tag{3.7}$$

In this definition $E_{th}(t)$ is the energy content of the storage system, $E_{th,max}(t)$ and $E_{th,min}(t)$ are the time-dependent energy contents of the storage when the system is respectively fully charged or discharged. Note that in practice these values are difficult to quantify. Therefore, in Section 3.5 an alternative quantification method (SOC_T) is evaluated. In this method the indoor temperature is used as an alternative for $E_{th}(t)$ since it is easy to measure in practice and has a close link to the control of the heating system, i.e. when the lower comfort limit is reached the SOC_T is zero and the heating should be switched on.

3.4 Parameter study on the available storage capacity and efficiency

In this section an extensive parameter study is carried out to quantify the impact of the main building design parameters on the available storage capacity and storage efficiency. The power shifting capability and state of charge will be discussed in the Section 3.5, since these properties are more related to the instantaneous flexibility rather than the intrinsic suitability of structural thermal energy storage for ADR.
The parameter study aims at understanding how the usability of structural thermal energy storage is affected by building design parameters. As such, the results may be used as guidelines for grid operators on how they can obtain the most efficient portfolio of buildings that can be used to provide operational flexibility. At the same time the results can be used by building designers to optimize the design of dwellings from an ADR perspective.

Three types of design parameters are analysed in this work: (i) geometric properties of the building, (ii) thermal properties of the components and (iii) type and specifications of the heat emission and ventilation system. Table 3.1 gives an overview of the properties and the range of values that are analysed. Note that the evaluation of building parameters is not limited to

new buildings, since the main potential of structural storage is expected from the thermal mass that is already available in existing buildings.

The following paragraph (§3.4.1) first describes the detailed building model that is used to develop and demonstrate the framework as well as the investigated design and model parameters. Note that, whereas the theoretic example used in this chapter is chosen to cover a wide range of building design parameters, the methodology will be applied to quantify the ADR potential of the structural thermal energy storage capacity in the Belgian residential building stock in Chapter 5.
Paragraphs 3.4.2 and 3.4.3 show the results of the parameter study obtained by respectively a uni- and multivariate analysis. For these analyses simplified theoretical boundary conditions have been used in a first step to facilitate a comprehensive interpretation of the results. A constant outdoor temperature and set point for the operative indoor temperature are applied and neither internal nor solar gains are included. In paragraph 3.4.4 the impact of these simplifications and the generality of the results are discussed on the basis of a step-wise increase of the complexity of the simulation model and the boundary condition.

3.4.1 Model description and parameter definition

The parameter study is carried out on a single-zone building, simulated using the IDEAS-library presented in Chapter 2. Although, the concepts and methodologies presented in this study can also be used for multi-zone buildings, a single-zone model was chosen to simplify the interpretability of the results. Moreover, in order to improve the interpretability of the results, the boundary conditions are in a first step simplified to a constant outdoor temperature and solar and internal gains are not included.
A simplified semi-detached building is implemented as an example comparing both radiator and floor heating systems. The floor is modelled in contact with the ground. The roof is a flat roof adjacent to the outdoor environment. A single window, oriented South, is placed in the wall opposite to the common wall.
The parameters evaluated in the study (Table 3.1) are chosen to cover a wide range of typical construction types found in the Belgian residential stock [117, 118, 119]. They have been selected to allow an evaluation of the impact of the building geometry and thermal properties as well as the type of heat emission systems and control settings used to activate the thermal mass.

The geometric properties are calculated by a parametric building design using only the ground floor area, the ceiling height, the compactness, window to wall ratio and interior wall ratio as

Table 3.1: Overview of the selected parameters and range of values selected for the parameter study

Parameter	range of values
$A_{floor}\ \left[m^2\right]$	75, 100, 125, 150, 200, 250
height $\left[m^2\right]$	2.75, 3, 3.5
compactness $[m]$	0.75, 1, 1.25, 1.5, 1.75, 2, 2.25, 2.5
interior wall ratio $[-]$	0.5, 0.75, 1, 1.25, 1.5, 1.75, 2.0
window to wall ratio $[-]$	0, 0.25, 0.5, 0.75
$d_{insul,roof}\ [cm]$	0, 2, 5, 8, 12, 15, 20, 25
$d_{insul,wall_e}\ [cm]$	0, 2, 5, 8, 12, 15, 20, 25
$d_{brick,wall_e}\ [cm]$	0, 2, 5, 8, 12, 20
$d_{wall_i}\ [cm]$	5, 10, 15, 20, 25, 30
$n_{vent}\ [ACH]$	0, 0.05, 0.1, 0.2, 0.4, 0.6, 0.8
system sizing factor $[-]$	0.8, 0.9, 1, 1.1, 1.25, 1.5, 2
ADR duration $[min]$	15, 30, 45, 60, 120, 180, 240, 480
ADR comfort range [°C]	1, 2, 3, 4

input parameters[3] (Table 3.1). Thereby, the surface areas of the exterior walls are calculated based on the floor area, the height and the compactness of the building. The area of the roof is equal to the floor area, the area of the common wall is based on the floor area and the height. The area of the window and the interior walls are each specified as a fraction of the exterior wall area. The interior wall ratio is the area of interior walls divided by the total exterior wall area, the window to wall ratio is the fraction of the window area to the area of the front facade.

The thermal properties of the dwelling are based on typical construction methods found in the Belgium residential sector [117]. The exterior walls are modelled as cavity walls which is a common construction method in Belgium. Both the insulation thickness $(d_{insul,wall_e})$ as the thickness of the inner brick layer $(d_{brick,wall_e})$ are varied. The former is varied to influence the overall heat loss coefficient. The latter is varied to analyse the impact of the available thermal mass. Thereby an inner brick thickness of 0-2 cm is used to represent light-weight cases, e.g. a building with interior insulation as can be found in renovation projects. Additionally, the available thermal mass is varied by changing the interior wall ratio and the thickness of the massive interior walls (d_{wall_i}). A specific light-weight structure, timber or steel-frame, has not been evaluated since it is not commonly used in the Belgian residential sector. However, a case with an interior wall thickness of 5 cm and an inner brick of 0 cm can be considered as representative for a light-weight building. In contrast, the high values for the interior wall thickness (25-30 cm) are used to assess whether drastically

[3] These geometric input parameters have been selected since they are also available from the building descriptions in the TABULA project [117] which will be used in Chapter 5 to develop a reduced-order building stock model.

increasing the thickness of massive layers, to increase the thermal mass of the building for active storage, has a significant impact on the resulting available storage capacity for ADR.

The ventilation system and the infiltration losses are combined and implemented as a constant air flow. Thereby the ventilation and infiltration rates are fixed and the efficiency of the heat recovery is assumed constant. Both air flows are combined in the analysis using the effective air change rate (n_{vent}) as parameter.

For the evaluation of the impact of the heating system, the scope of this work (Section 1.2) is limited to the analysis of the relation between the heat emission system and the activation of the structural thermal energy storage capacity. Although, active demand response is found to influence the overall efficiency of thermal systems [59, 60, 61, 62, 31], it is assumed that the overall efficiency of buildings for ADR can be split into the storage efficiency of the structural thermal mass and the efficiency of the heating system.
Consequently only the impact of the type of heat emission system and the nominal power of the production and emission systems are included in the parameter study. The production side is modelled, according to Section 2.2.4, as an ideal heat source with a maximum heating power equal to the nominal power calculated according to EN12831 [120]. For the design of the heating system a *system sizing factor* is included which is defined as the ratio of the implemented heating power to the nominal power based on EN12831 [120].
Two types of heat emission systems are modelled: (i) a radiator heating system and (ii) a floor heating system. These emission systems are common in the Belgian residential sector and represent respectively a responsive, mostly convective, emission system and a slow radiant system, resulting in a fundamentally different activation of the thermal mass.

Finally the parameters for the rule-based ADR control strategy are implemented. Although state-of-the-art studies suggest the use of optimal control or model predictive control (MPC) strategies for the practical, real-time quantification of flexibility [76, 75], the simplicity of the presented quantification framework allows for a rule based control strategy. This choice is additionally supported by the fact that the rule based control allows for the analysis of the impact of control choices and identify the framework in which an optimal control strategy would function. More specifically, the duration (l_{ADR}) and the starting time (t_0) of the ADR-event and the allowed comfort range (dT_{comf}) are evaluated in this work. For the latter a constant comfort range is assumed for the theoretic evaluation presented below. Note that, in practice the comfort range, similar to the other boundary conditions, may vary in time as a consequence of occupancy profiles or even occupant preference.

Using these parameter variations, two samples are selected. A first sample is generated in a deterministic way by changing one parameter at the time for a univariate parameter

study. The univariate analysis is used to estimate the impact of the individual building design parameters allowing for an in-depth physical interpretation of the results.
For the multivariate regression analysis, a second sample is generated using a uniform sampling method to generate 2500 data points for both the radiator heating and floor heating cases. The required number of samples was validated by analyzing the convergence of the first and second order moments of the sampled distribution of the building parameters to those of the original distribution from Table 3.1.

3.4.2 Univariate parameter analysis

In this section the results of the univariate parameter study are shown, quantifying the impact of the building design parameters on the available storage capacity and the storage efficiency, defined in Section 3.3. These two ADR characteristics are discussed together since they are closely linked and are calculated using the same simulation procedure, i.e. the simulation of an ADR-event as described in Section 3.3 (Figure 3.2).

Before going into detail on the individual parameters, Figure 3.3 shows an overview of the available storage capacity (top) and the efficiency of the storage process (bottom) as a function of the duration of the ADR-event for the total set of 2500 simulations.
The boxplots in the top graphs of Figure 3.3 demonstrate a wide spread on the available storage capacity obtained for both the radiator (left) and the floor heating system (right). Obtained values vary from near zero up to 800 kWh when the ADR-event lasts for 12 h. The extreme low values occur when the simulated outdoor temperature is equal to the design outdoor temperature of -10 $^{\circ}\mathrm{C}$ that is used for the sizing of the heating system. Consequently, the heating system already operates close to its maximum power and thus no additional flexibility is available for activating the storage capacity.
When the duration of the ADR-event increases, Figure 3.3(top) shows that the rate of increase of the available storage capacity is reduced. During the first minutes the heating system is able to increase its heating power from the level needed to maintain the constant minimum indoor temperature to the nominal power of the system. This increase can be maintained until the upper comfort bound is reached. Afterwards the heating power needs to be reduced to avoid overheating, consequently reducing the rate of increase.
A slight deviation in the available storage capacity for both heat emission systems is observed. Due to its large time constant, the floor heating system is able to maintain the maximum heating power longer than the radiator system. The median capacities available for storage over a 12 h period differ from 90 kWh (2-1050 kWh) to 130 kWh (11-1260 kWh) for respectively the radiator and floor heating systems.

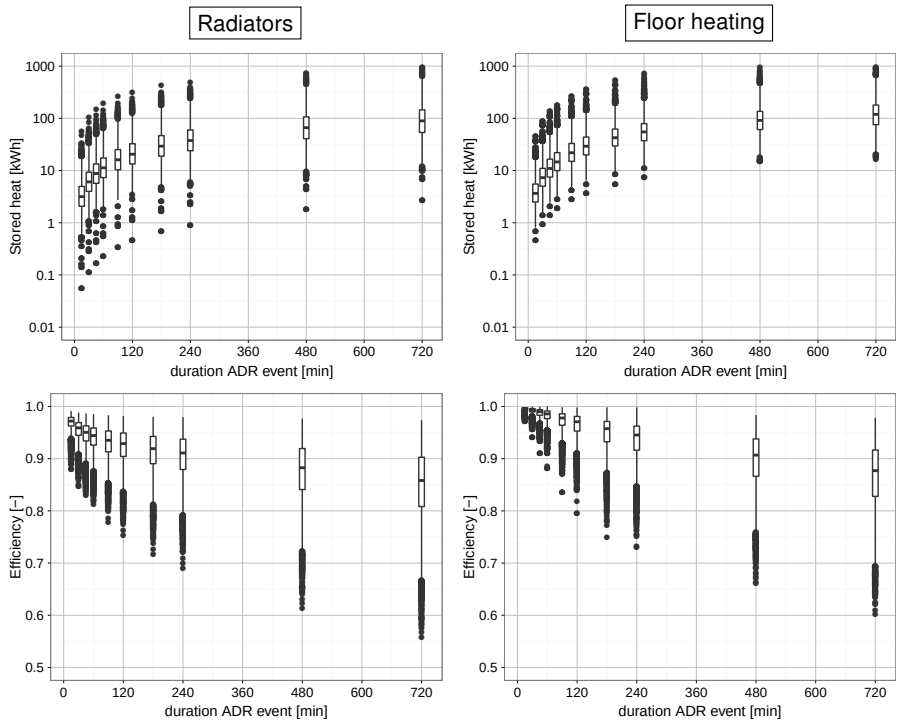

Figure 3.3: Overview of the available storage capacity (top) and storage efficiency (bottom) obtained for the parameter study on 2500 runs for both the radiator (left) and floor (right) heating system. The boxplots indicate the spread on the results due to the variation of building, system and control parameters.

The boxplots in the bottom graphs of Figure 3.3 show two significant trends for the storage efficiency. Firstly, the efficiency decreases with increasing duration of the ADR-event. Secondly, higher storage efficiencies are obtained for the floor heating cases compared to the radiator heating systems. Although a significant spread on the storage efficiency is shown, values above 60 % are obtained for all cases. When ADR-events are limited to a charging time of 3 h, a median value for the efficiency of 93 % (71-97 %) and 96 % (75-97 %) is obtained for buildings with respectively the radiator and floor heating systems. For the radiators, the drop in efficiency as a function of the duration of the ADR-event is sharpest. The floor heating system directly activates the thermal mass of the floor, which results in a higher thermal capacity and relatively small losses to the ground. The heat stored within the floor is released at a low rate, resulting in a less sharp increase of the zone temperature and therefore less thermal losses compared to the radiator heating systems.

Although the average storage efficiency is found to be high, the spread on the results indicates the sensitivity of the storage efficiency to the evaluated design parameters. Moreover, the spread becomes more important for longer ADR-events. In the following paragraphs the impact of the building, system and control design parameters as well as the impact of the boundary conditions are evaluated in a univariate parameter study.

Impact of insulation quality and ventilation rate

The first set of parameters that is considered in this analysis consists of the insulation quality and ventilation rate of the dwellings, defining the thermal losses. Whereas these parameters have a significant impact on the overall energy efficiency of a building, a higher storage efficiency is also expected for increasing insulation levels and lower effective ventilation rates.

To analyse these hypotheses, Figure 3.4 shows the impact of the insulation thickness on the available storage capacity (top) and the resulting storage losses (bottom). In addition to the influence of the duration of the ADR-event discussed above, two important trends are found for the available storage capacity. Firstly, as a result of the higher thermal power of the heating system that is available for ADR, the available storage capacity is higher for the uninsulated buildings. Secondly, the comfort range has a significant impact on the available storage capacity for the radiator heating. Due to the rapid response of the indoor temperature, the maximum comfort level is reached after 30 min. After that time, the heating power is reduced in order to avoid a violation of the comfort limit. The floor heating systems allow to maintain the high heating power for longer periods. Since the heat is directly introduced in the high thermal mass of the floor, the increase of the indoor temperature is less sharp. A clear deviation between the available storage capacity for a comfort range of 1 $^{\circ}\mathrm{C}$ and 4 $^{\circ}\mathrm{C}$ is shown after 3 h, which is in line with the time constant[4] of the floor heating (2.8 h). When a 4 $^{\circ}\mathrm{C}$ temperature variation is allowed, a linear increase of the available capacity is found for both systems since the system is able to operate at its maximum power for the whole period. As a result of the constant boundary conditions a linear increase is obtained with a slope equal to: $\dot{Q}_{Nom} - \dot{Q}_{Ref}$, with $\dot{Q}_{Nom}$ the nominal power of the system and $\dot{Q}_{Ref}$ the reference heating power without ADR. Note that, as both the radiator and floor heating systems have the same nominal power, the differences between both systems disappear. In case of the non-insulated dwelling the available storage capacity obtained for the floor heating

[4] The time constant of the floor heating (τ_{FH}) is calculated as $\tau_{FH} = R_{fh,s}C_{fh,s}$, with $R_{fh,s}$ the thermal resistance of the material layer between the floor heating and the interior surface of the floor and $C_{fh,s}$ the corresponding thermal capacity of this layer

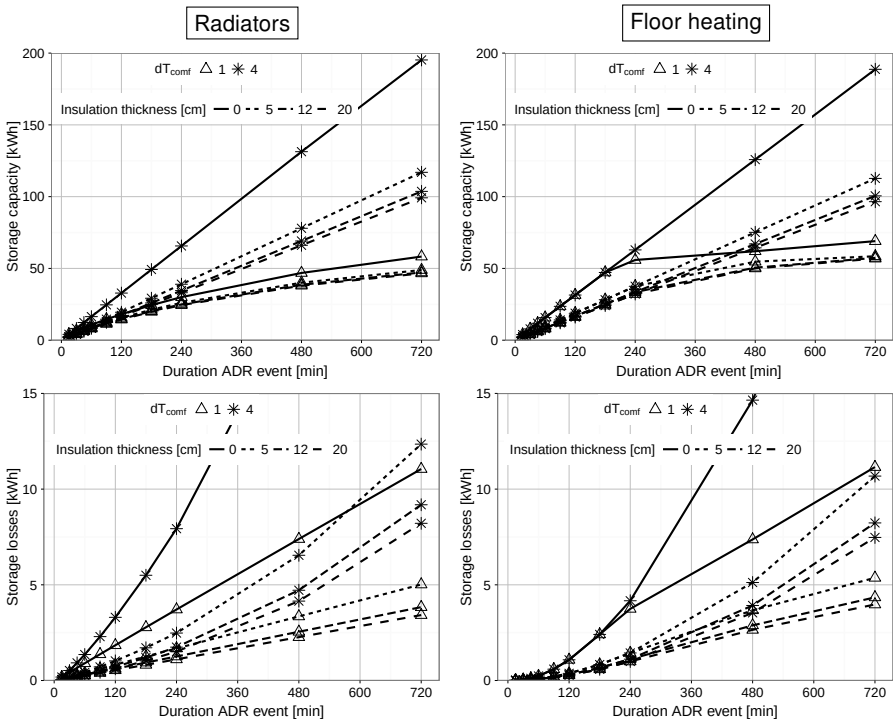

Figure 3.4: Available storage capacity (top) and storage losses (bottom) as a function of the insulation thickness of the exterior walls for both the radiator (left) and floor heating system (right). The results are shown for varying duration of the ADR-event, an outdoor temperature of 0 °C and a comfort range (dT_{comf}) *of 1 °C and 4 °C*

building (180 kWh) is even slightly lower than the one obtained for the radiator building (194 kWh), since $\dot{Q}_{Ref}$ is slightly higher for the floor heated building due to increased losses to the ground.

The bottom graphs of Figure 3.4 show the corresponding storage losses, which correspond to the numerator of Eq. 3.4. Thereby a linear increase of the storage losses is found as a function of the duration of the ADR-event when the comfort range is limited to 1 °C. Taking into account the constant boundary conditions, the heat loss is a linear function of the indoor temperature. As such, after T_{max} is reached, a constant heat loss rate and a linear increase of the storage losses are obtained. For the comfort range of 4 °C, the comfort limit has not been reached, resulting in an exponential increase of storage losses.

As defined in Section 3.3, the storage capacity and corresponding losses can be combined

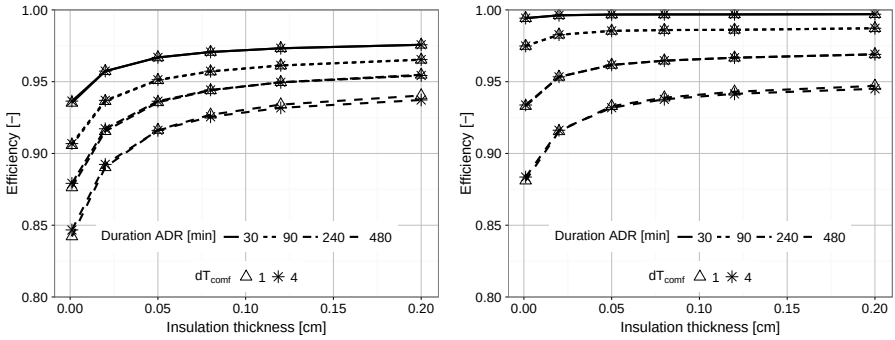

Figure 3.5: Storage efficiency as a function of the insulation thickness of the exterior walls for both the radiator (left) and floor heating system (right). The results are shown for varying duration of the ADR-event, an outdoor temperature of 0 $^{\circ}\mathrm{C}$ *and a comfort range* (dT_{comf}) *of 1* $^{\circ}\mathrm{C}$ *and 4* $^{\circ}\mathrm{C}$

to quantify the efficiency of the storage process. The resulting efficiencies are demonstrated in Figure 3.5 as a function of the thickness of the insulation layer in the exterior walls. In the absence of insulation in the cavity wall $(d_{insul,wall_e} = 0)$, the storage efficiency for the radiator heating system (left) is shown to drop below 85 % for an ADR-event of 480 min, or 8 h, and below 90 % for the floor heating cases (right). Moreover, it is shown that the increase in storage efficiency is sharpest for the first centimetres and for longer storage periods. Moreover, for the floor heating cases, the sensitivity of the storage efficiency to the insulation level of the exterior walls is negligible when the ADR-event is limited to 90 min, since for these short events the heat is mainly stored within the floor itself.

Consequently, in order to guarantee high storage efficiencies, the best performance is found for short ADR-events and high levels of insulation. This is in contrast to the trends shown for the available storage capacity where the highest available capacity is found for uninsulated dwellings and long ADR-events. As such, from a grid perspective an optimum may be expected for average insulation levels whereby a balance is found between a high available capacity and an acceptable storage efficiency. In Chapter 5 this hypothesis will be analysed for the Belgian residential housing stock in a high renewable energy context. Nevertheless, the value of this optimum will strongly depend upon the energy market context.

For the variation of the effective ventilation rate, similar trends are found. Figure 3.6 shows the obtained storage efficiency for both the radiator and floor heating systems, confirming the decreasing efficiencies for increasing ventilation rates. However, due to the smaller share in the overall heat demand, compared to the insulation level, the storage efficiency reductions are found to be smaller, i.e a decrease from 92 % to 88 % and 93 % to 91 % for respectively

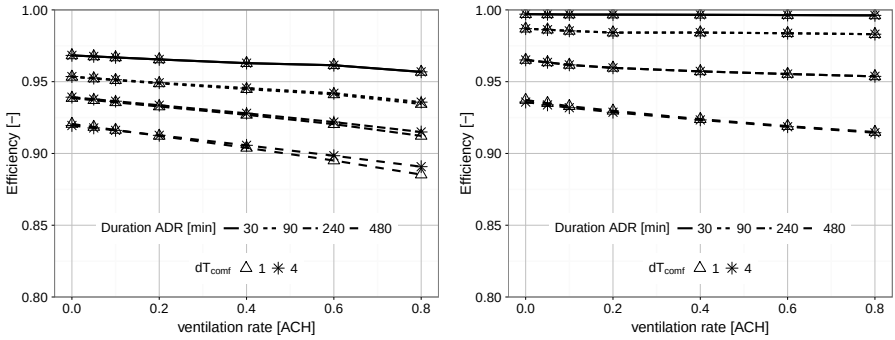

Figure 3.6: Storage efficiency as a function of the ventilation rate for both the radiator (left) and floor heating system (right). The results are shown for varying duration of the ADR-event, an outdoor temperature of 0 °C and a comfort range (dT_{comf}) of 1 °C and 4 °C

the radiator and floor heating cases, assuming an ADR-event of 8 h and a constant outdoor temperature of 0 °C. In line with Figure 3.3, the storage efficiency is found to be significantly higher for the floor heating system especially for shorter ADR-events. This was explained by the fact that most of the heat is stored within the available storage capacity of the heated floor, resulting in only a mild temperature increase and a negligible increase in the transmission and ventilation losses. As a consequence, the impact of an increased ventilation rate on the storage efficiency is less apparent for the floor heating system. Note that for longer ADR-events, the difference in efficiency between floor heating and radiators decreases, due to the fact that the duration of the ADR-event is comparable or even greater than the time constant of the floor heating system. As such, the buffering effect diminishes.

In addition to the overall storage efficiency and available storage capacity, Figure 3.7 shows the contribution of the different components in the available storage capacity for the radiator cases (top) and floor heating cases (bottom) for increasing effective ventilation rates. As such, these figures give an important insight in how the thermal energy storage capacity is activated by the different heat emission systems. For short ADR-events the radiator system is found to mainly activate the indoor air for thermal energy storage, as demonstrated in Figure 3.7. When the duration of the ADR-event is limited to 30 minutes, the thermal mass of the indoor air and furniture[5] represents up to 50 % of the available storage capacity[6], explaining the significant impact of the ventilation rate on the storage losses and corresponding the system efficiency. It takes up to 90 min until the share of the exterior walls in the total storage

[5] As stated in Section 2.2.1 the thermal mass of the air is multiplied by a factor 5 to include furniture.

[6] The heat stored in each component is calculated by integrating the difference between the heat flows at the interior and exterior surfaces. These flows are obtained from the detailed model using the terms q_T in Equation 2.2.

capacity equals that of the indoor air. Moreover, due to the high surface area and thermal mass of the interior walls, they are found to have the highest share in the available storage capacity for ADR-events longer than 1 h.

The share of the indoor air in the available storage capacity is not influenced by the air change rate and decreases significantly when the duration of the ADR-event increases. In contrast, the contribution of the ventilation losses in the overall storage losses (Figure 3.8) increases for both heat emission systems from 0 % to 40 % when the effective ventilation rate increases from 0 to 0.8 ACH.

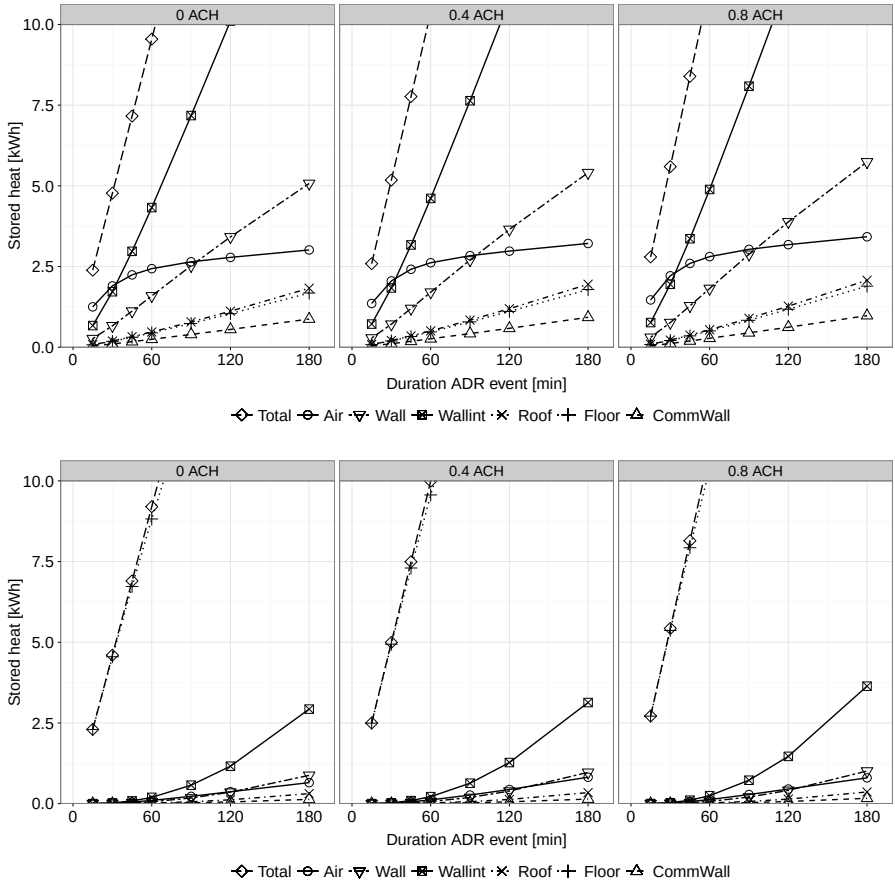

Figure 3.7: Heat stored in different building components as a function of the ventilation rate for both the radiator (top) and floor heating system (bottom). The results are shown for varying duration of the ADR-event, an outdoor temperature of 0 $^{\circ}\mathrm{C}$ and a comfort range (dT_{comf}) of 1 $^{\circ}\mathrm{C}$

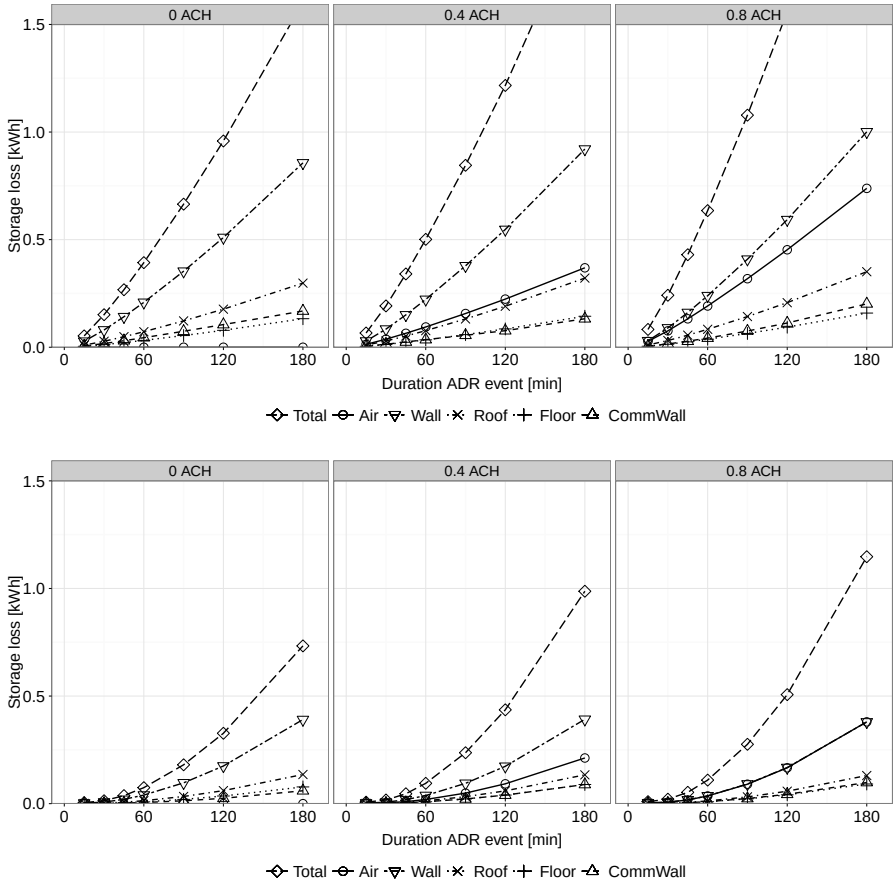

Figure 3.8: Storage losses by different building components as a function of the ventilation rate for both the radiator (top) and floor heating system(bottom). The results are shown for varying duration of the ADR-event, an outdoor temperature of 0 $^{\circ}\mathrm{C}$ and a comfort range (dT_{comf}) of 1 $^{\circ}\mathrm{C}$

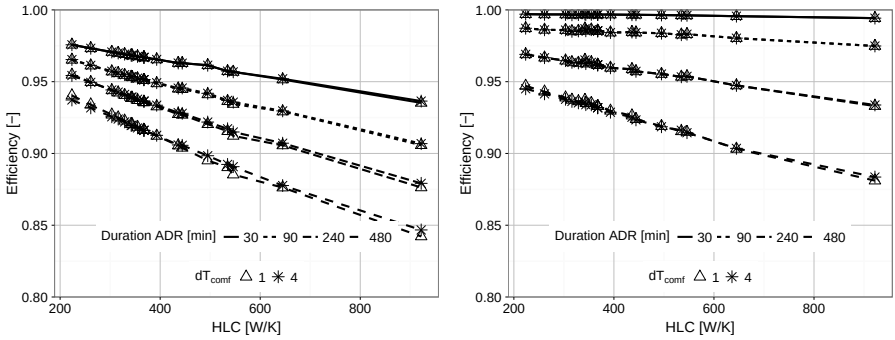

Figure 3.9: Storage efficiency as a function of the total heat loss coefficient for both the radiator (left) and floor heating system (right). The results are shown for varying duration of the ADR-event, an outdoor temperature of 0 °C and a comfort range (dT_{comf}) of 1 °C and 4 °C

Based on the analysis of the ventilation rate and the insulation level, it is concluded that a linear relation exists between the heat loss coefficient of a dwelling and the storage efficiency (Figure 3.9). The heat loss coefficient (HLC [W/K]) is thereby defined as the sum of the total heat transfer coefficient for transmission and ventilation, calculated according to ISO 6946:2007[121]. The buildings equipped with floor heating show both a higher efficiency and storage capacity compared to the radiator system. The reduction in efficiency for increasing heat loss coefficients becomes more important as the duration of the ADR-event is longer. When the heat loss coefficient increases from 200 W/K to 950 W/K the storage efficiency is reduced from 93 % to 84 % for an ADR-event of 8 h and radiator heating. For the floor heating system the efficiency reduces from respectively 95 % to 87 %. When the duration of the ADR-event is limited to 90 min, an efficiency of respectively 90 % and 97% is obtained even for the cases with a high HLC.
As for the overall energy efficiency of buildings, increasing the insulation quality and reducing the infiltration and ventilation losses have a strong positive impact on the storage efficiency. For less insulated buildings it is important to limit the length of the ADR-event.

Impact of thermal mass

To assess the impact of thermal mass properties on the available storage capacity and the storage efficiency, three important aspects are analysed. Firstly, the thickness of the interior walls is varied. Figure 3.7 already demonstrated that the interior walls have a significant contribution to the total structural storage capacity. Thus, varying the interior wall thickness allows to evaluate the impact of increasing thermal mass as well as the concept of the

effective thermal capacity. The latter is defined – as shown further in Chapter 4 – as the fraction of the thermal mass of a component that is activated by the heating system and is limited by the penetration depth of the heat front. As such, the impact of increasing the wall thickness on the available storage capacity is expected to be non-linear with a sharper increase when the thickness is varied from 5 cm to 10 cm as compared to an increase from 10 cm to 30 cm. Moreover, it is expected to depend on the duration of the ADR-event as for longer durations, the penetration depth of the heat front will increase.
Secondly, the thickness of the inner leaf of the cavity wall is varied between 0 cm and 20 cm. A thickness of 0 cm is included as it corresponds to a situation with interior wall insulation where the thermal mass of the envelope is shielded from the inside by an insulation layer. A thickness of 20 cm shows a dynamic response that is close to that of a massive wall with outer insulation, since the thermal mass of the outer leaf becomes less important for the dynamics at the indoor environment.
Finally, the interior wall ratio is increased. Thereby in contrast to increasing the thickness, a linear relation between the available surface area and the structural storage capacity is expected since changing the surface area of a component does not affect its time constant. In this paragraph specific attention is therefore put to the interior wall ratio, defined as the fraction of the interior wall area to the envelope surface area. An evaluation of the impact of the overall geometry of the dwelling is discussed in the next paragraph.

The results of Figure 3.10(top) confirm the expected non-linear relation between the thickness of the interior walls and the available storage capacity. Nevertheless, the impact is negligible for the high comfort range of 4 $^{\circ}\mathrm{C}$, since regardless of the interior wall thickness the maximum comfort limit (T_{max}) is not reached. Moreover, for the floor heating cases even with a comfort range of 1 $^{\circ}\mathrm{C}$ the impact of increasing the interior wall thickness is only visible for event durations longer than 240 min. Again for shorter periods, i.e. less than 2 h and 4 h for respectively the radiator and floor heating systems, the rate of thermal energy storage is thus governed by the difference between the nominal power of the heating system and the heat demand at the minimum comfort range.
The corresponding storage efficiencies are shown in Figure 3.10(bottom), demonstrating the minimal impact on the efficiency when the thickness of the interior walls increases from 5 cm to 30 cm as long as the storage period is limited to 90 min. For a duration of 480 min (8 h), storage efficiencies of 86 % and 92 % are found for respectively an interior wall thickness of 5 cm and 30 cm in case of radiator heating and respectively 90 % and 94% in case of floor heating. Note again that for an 8 h ADR-event the difference in efficiency between the radiator and floor heating case is strongly reduced.

The impact of increasing the thickness of the exterior wall is less pronounced (Figure 3.11).

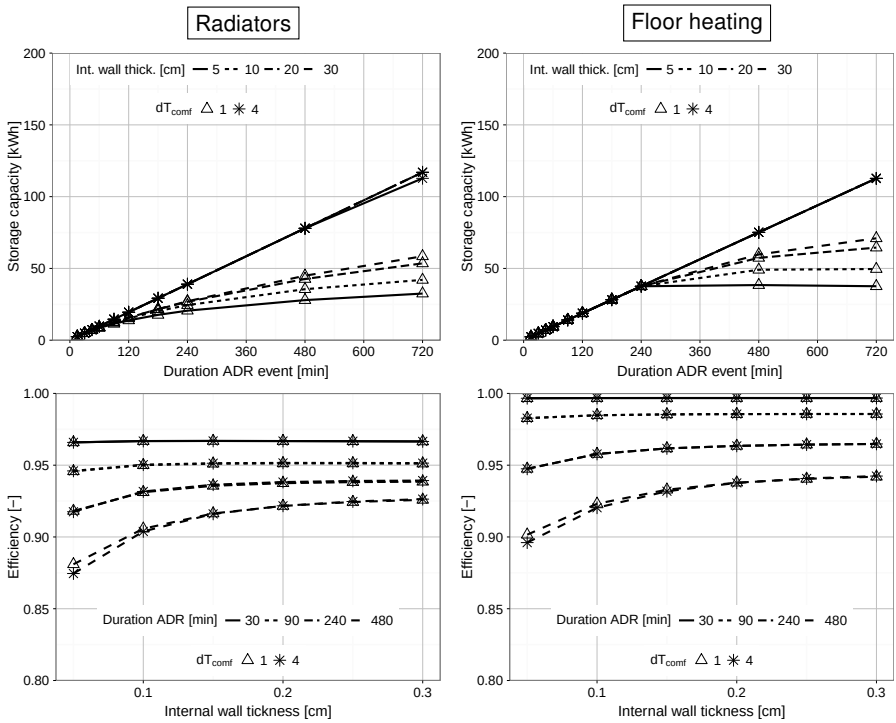

Figure 3.10: Available storage capacity (top) and corresponding efficiency (bottom) as a function of the thickness of the interior walls for both the radiator (left) and floor heating system (right). The results are shown for varying duration of the ADR-event, an outdoor temperature of 0 $^{\circ}\mathrm{C}$ *and a comfort range* (dT_{comf}) *of 1* $^{\circ}\mathrm{C}$ *and 4* $^{\circ}\mathrm{C}$

No significant difference is observed for buildings with inner, cavity or outer insulation, given the thermal capacity of the other structural components is adequate. Reducing the thickness of the inner leaf of the cavity wall to 0 cm, corresponding to an interior insulation scenario, reduced the storage efficiency for an ADR-event of 8 h by 1.5 %, i.e. from 92.5 % to 91 % for the radiator cases and from 94 % to 92.5 % for the floor heating buildings. The reason for this is two-fold. Firstly, due to the lower heat exchanging surface area for thermal energy storage of the exterior walls compared to the interior walls, the contribution of the storage capacity of the exterior walls in the total storage capacity is lower. Secondly, the interior walls are available from both sides. As such, the time constant of a material layer of 10 cm in the exterior wall corresponds to that of 20 cm of interior wall.

Finally, the impact of the interior wall ratio on the storage efficiency and storage capacity is

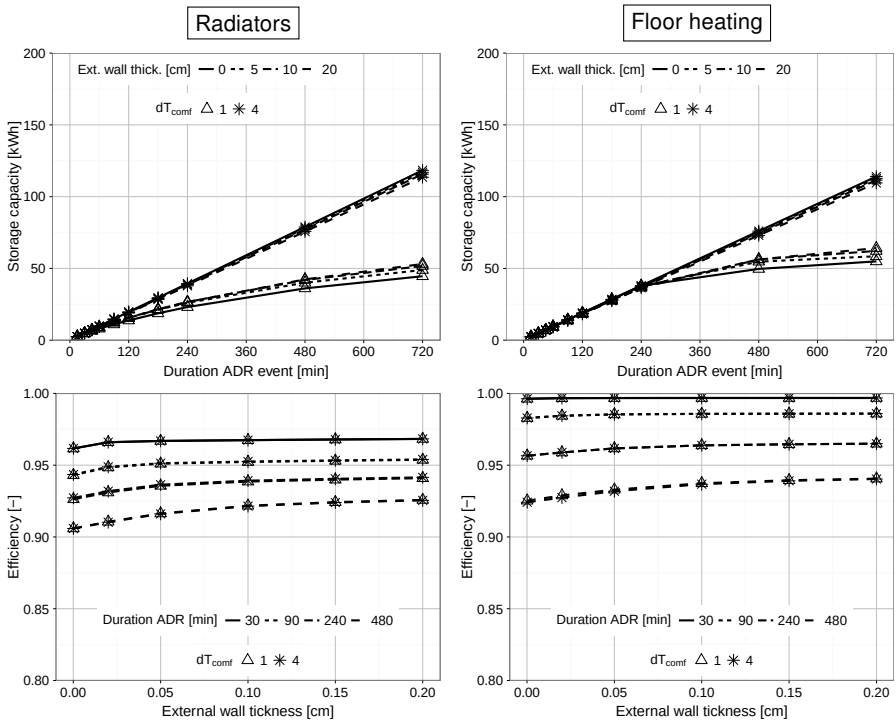

Figure 3.11: Available storage capacity (top) and storage efficiency (bottom) as a function of the thickness of the inner leaf of the exterior walls for both the radiator (left) and floor heating system (right). The results are shown for varying duration of the ADR-event, an outdoor temperature of 0 $^{\circ}\mathrm{C}$ *and a comfort range* (dT_{comf}) *of 1* $^{\circ}\mathrm{C}$ *and 4* $^{\circ}\mathrm{C}$

shown in Figure 3.12. Thereby for a given duration of the ADR-event the expected linear relation between the available storage capacity and the interior wall ratio is again only apparent for the limited comfort range of 1 $^{\circ}\mathrm{C}$ and radiator heating. This linear increase is expected since a uniform surface temperature is assumed in the model and all other parameters are kept constant in the univariate analysis, an increase of the surface area of a component results in a linear increase of the available storage capacity for a given change in indoor temperature. Nevertheless, a clear increase of the storage efficiency with increasing interior wall ratio is observed for all cases. In case of radiator heating, the efficiency varies between 89 % and 93 % for respectively a building with an interior wall ratio of 0.75 and 2 and an ADR period of 8 h. For buildings with floor heating, corresponding efficiencies of 92 % and 95 % are found. Again, the impact of the design parameter is less important for shorter ADR-events, especially for floor heating as the heat is mainly stored inside the floor itself.

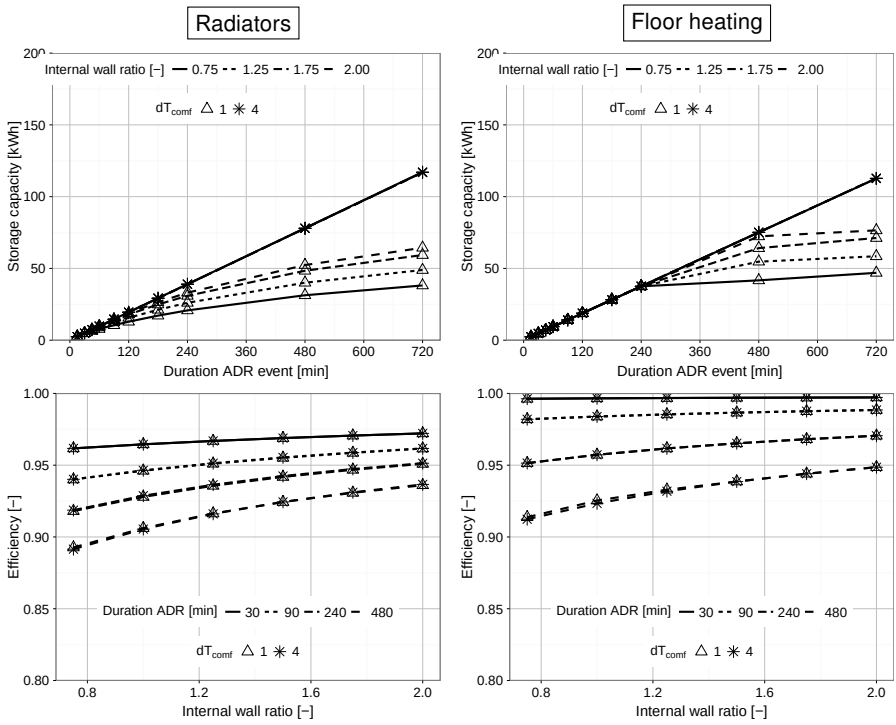

Figure 3.12: Available storage capacity (top) and storage efficiency (bottom) as a function of the interior wall ratio for both the radiator (left) and floor heating system (right). The results are shown for varying duration of the ADR-event, an outdoor temperature of 0 $^{\circ}\mathrm{C}$ and a comfort range (dT_{comf}) of 1 $^{\circ}\mathrm{C}$ and 4 $^{\circ}\mathrm{C}$

Based on this evaluation, it is concluded that the available surface area of the massive components is significantly more important than the thickness of the component. Especially when the comfort range is limited to 1 $^{\circ}\mathrm{C}$, increasing the interior wall ratio from 0.75 to 2 results in a 50-80 % increase of the available storage capacity for ADR-events longer than 2 h for the radiator cases and 4 h for the floor heating cases. Consequently, given the higher available surface area, the impact of increasing the thickness of the massive interior walls is higher than for increasing the thickness of the inner leaf of the exterior walls.

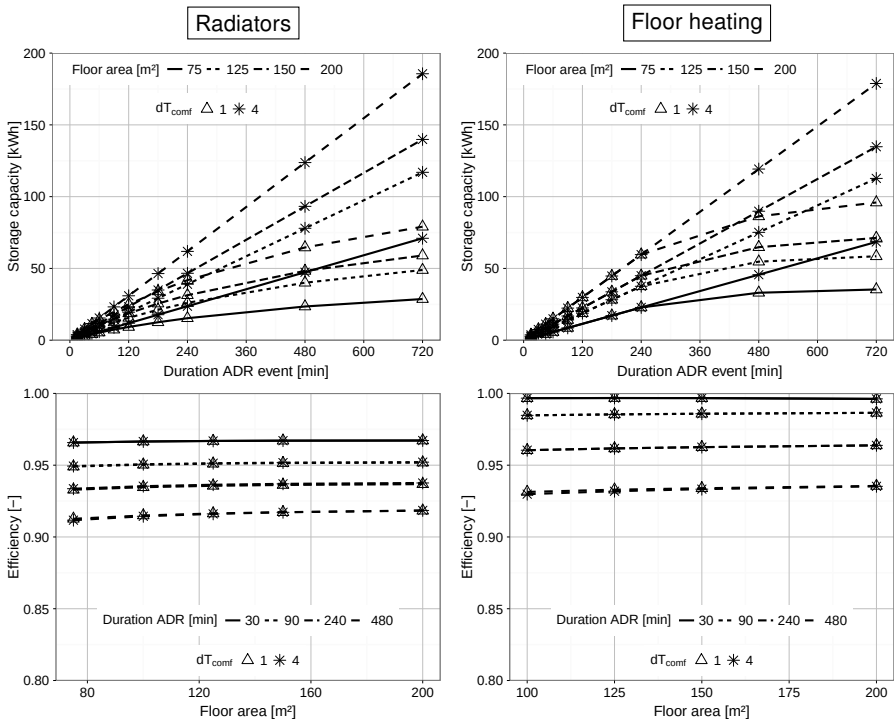

Figure 3.13: Available storage capacity (top) and storage efficiency (bottom) as a function of the ground floor area for both the radiator (left) and floor heating system (right). The results are shown for varying duration of the ADR-event, an outdoor temperature of 0 °C and a comfort range (dT_{comf}) of 1 °C and 4 °C

Impact of geometry

To evaluate the impact of the geometric building parameters, the compactness, floor area, ceiling height and interior wall ratio of the building are varied. Whereas the latter was discussed in the previous paragraph, showing a positive impact of the interior wall ratio on both the available storage capacity and the storage efficiency, the results of the remaining parameters are shown in this paragraph.

Firstly, Figure 3.13 shows an important increase of the available storage capacity when increasing the floor area of the dwelling. The same trend is observed for an increasing ceiling height and can be explained by the parametric design of the geometry of the building. As explained in Section 3.4.1, the floor area and ceiling height of the dwelling are used to calculate the volume of the building and together with the compactness used to calculate the

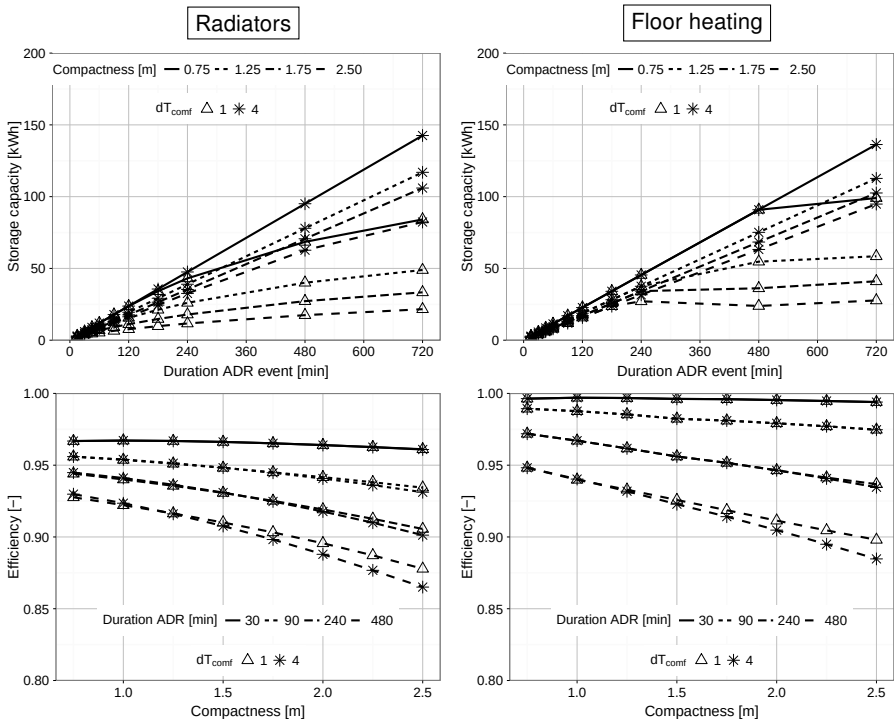

Figure 3.14: Available storage capacity (top) and storage efficiency (bottom) as a function of the compactness of the building for both the radiator (left) and floor heating system (right). The results are shown for varying duration of the ADR-event, an outdoor temperature of 0 $^{\circ}\mathrm{C}$ and a comfort range (dT_{comf}) of 1 $^{\circ}\mathrm{C}$ and 4 $^{\circ}\mathrm{C}$

surface areas of the exterior walls. When respectively the floor area and the ceiling height are increased in the parametric study, keeping the compactness, interior wall ratio and window to wall ratio constant, the volume of the building is scaled uniformly. As a result of this uniform scaling, the efficiency of the storage process does not depend on the floor area and the ceiling height. As such, it can be concluded that although the available capacity is a function of the dwelling size, the efficiency is only dependent on dimensionless parameters. Evidently, the available storage capacity increases linearly when the building is scaled uniformly.

In contrast to changes in the size of the building, the compactness has a significant effect on the storage efficiency (Figure. 3.14). Changing the compactness from 0.75 m to 2.5 m for the buildings with a radiator system, reduces the storage efficiency from 93 % to 86 % for a comfort range of 4 $^{\circ}\mathrm{C}$ and a duration of the ADR-event of 8 h. For the floor heating a similar decrease, from 95% to 89% is found.

Note that not only the storage efficiency but also the available storage capacity reduces with increasing compactness. Both results are explained by the parametric implementation of the geometry. For this implementation, increasing the compactness results in a reduction of the envelope surface area, while keeping the volume constant. Since the interior wall area is based on the envelope area, by means of the interior wall ratio, increasing the compactness drastically reduces the available thermal energy storage capacity. Consequently the indoor air temperature and the resulting thermal losses increase more rapidly during the charging process since a higher compactness results in a higher ratio of indoor air to structural thermal mass.

Impact of boundary conditions

As explained in Section 3.4.1, the climatic boundary conditions and occupant behaviour have been drastically simplified in this parameter study to improve the interpretability of the results. Thereby, the outdoor temperature as well as the temperature set point for the heating systems are assumed to be constant. At the same time solar gains and the impact of occupancy profiles on the internal gains and the set-points for the heating system are ignored. Consequently, the whole dynamic excitation of the building results from the change in the heat input by the heat emissions system during the ADR-event.
In this section, the impact of the outdoor temperature and the comfort range is analysed by including them as independent parameters in the univariate analysis in order to quantify their impact on the available storage capacity and the efficiency of the storage process. Moreover, the sensitivity of these performance indicators to occupant behaviour and solar gains will be analysed. Thereby, the main focus is on investigating how the daily variations introduced by these boundary conditions influence the potential for structural thermal storage, keeping in mind that currently the main peaks in the Belgian electricity demand are located in the morning and evening periods (Figure 3.15). The impact of realistic, dynamic boundary conditions is presented further in Section 3.4.4. The impact of the comfort range has already been handled throughout the section. Thereby it was shown that the comfort range has a significant impact on the available storage capacity for buildings equipped with radiator heating. In contrast for buildings equipped with floor heating, thermal comfort only plays a role for long ADR-events (more than 3 h), since for shorter ADR-events the high thermal mass of the floor was found to limit the temperature increase and corresponding thermal losses.

The impact of the outdoor temperature on the available storage capacity and the

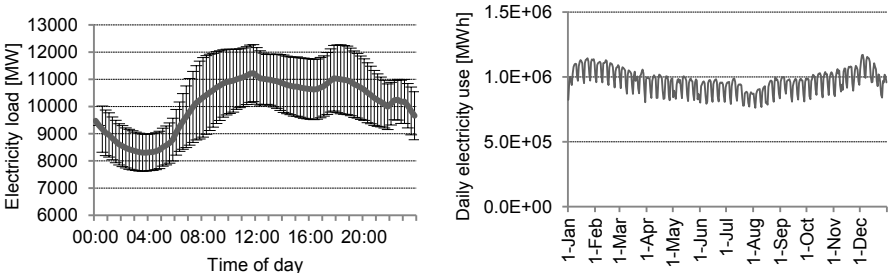

Figure 3.15: Averaged daily electricity load profile (left) and daily demand profile (right) for Belgian electricity use based on national statistics for 2014. The error bars on the left figure show the 90% confidence intervals. [11]

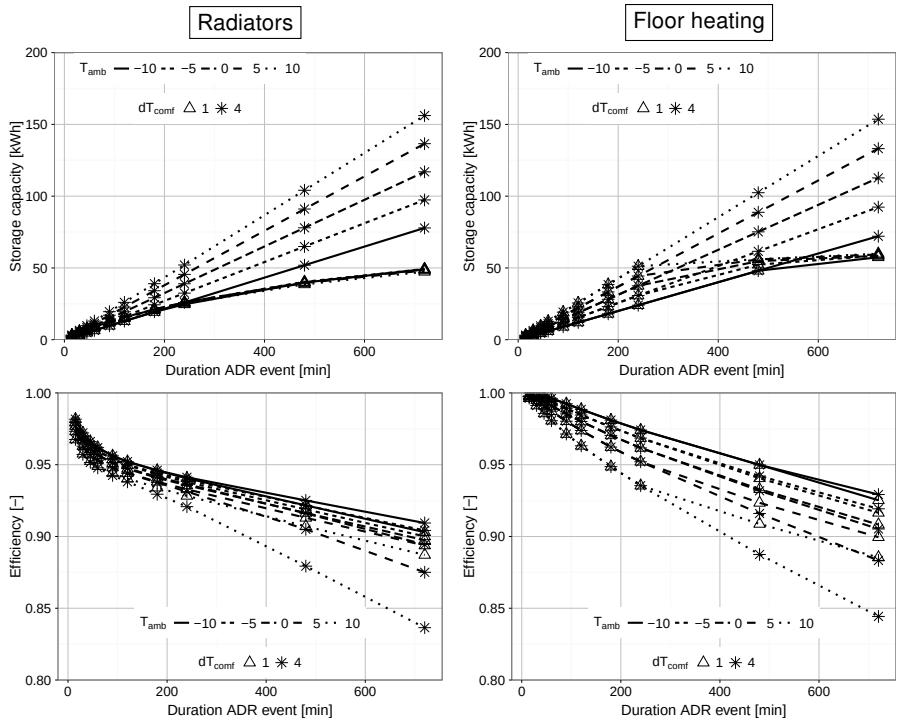

Figure 3.16: Available storage capacity (top) and storage efficiency (bottom) as a function of the stationary outdoor temperature for both the radiator (left) and floor heating system (right). The results are shown for varying duration of the ADR-event, an outdoor temperature of 0 $^{\circ}\mathrm{C}$ and a comfort range (dT_{comf}) of 1 $^{\circ}\mathrm{C}$ and 4 $^{\circ}\mathrm{C}$

corresponding efficiency is shown in Figure 3.16. The figure demonstrates that neither the available storage capacity nor the efficiency are constant, but depend on the climatic boundary conditions. The top panes demonstrate an increasing storage capacity for increasing outdoor temperatures. The increase results from the excess heating power that becomes available for increasing outdoor temperatures and the corresponding decrease in heat demand. Note that for radiator heating, the effect is only apparent for higher comfort ranges, since for a comfort range of 1°C the increase of the heating power and the corresponding available storage capacity is governed by the maximum indoor temperature. For floor heating, the limitation of the available storage capacity is only visible after 4 h.
Note that the results for the efficiency should be handled carefully as they are counter-intuitive. Since the thermal loss of the building decreases with increasing outdoor temperatures, a similar increase in the storage efficiency was expected. The bottom graphs of Figure 3.16 however show that the storage efficiency significantly decreases as the outdoor temperature rises. This is explained by the fact that due to the extra thermal power that becomes available for ADR, the indoor temperature and the corresponding losses increase faster, resulting in decreasing storage efficiencies. Due to this excessive temperature increase, the storage efficiency for the radiator heated buildings with a comfort range of 4$^{\circ}\mathrm{C}$ drops from 91% to 83%, when the ambient temperature increases from -10$^{\circ}\mathrm{C}$ to 10$^{\circ}\mathrm{C}$.

Up to this point, no solar gains have been included in the simulations. To assess the impact of solar gains, a periodic solar input is modelled using the parameter Sun_{amp} as a scaling factor, as described by equation 3.8 as a function of the time of day (t).

$$Q_{dir,per}(t) = max\left(0,\ \sin\left(\frac{2\pi(t-8)}{24} + 0.5\right) Sun_{amp}\right) \tag{3.8}$$

The input signal assumes the sun rises at 06:00, peaks at 14:00 and sets at 22:00, and is used for the direct gains on the plain perpendicular to the sun, no diffuse gains are included. Yet, since both gains are distributed in the room using an area weighted method and only a single window for a single orientation is used for this analysis, this simplification is justified.
Figure 3.17 shows the efficiency and available storage capacity for the radiator heating system as a function of the time of the day the ADR-event starts. The different panes show the impact of the duration of the ADR-event, while the line-type and marker show respectively the comfort range and the window to wall ratio. Note that the latter is specified as the ratio of the window to the front wall, where the window is located.
Firstly, the results show an overall decrease (6-16 %) of the storage efficiency for increasing window to wall ratio, as a consequence of both the decrease of the available thermal mass

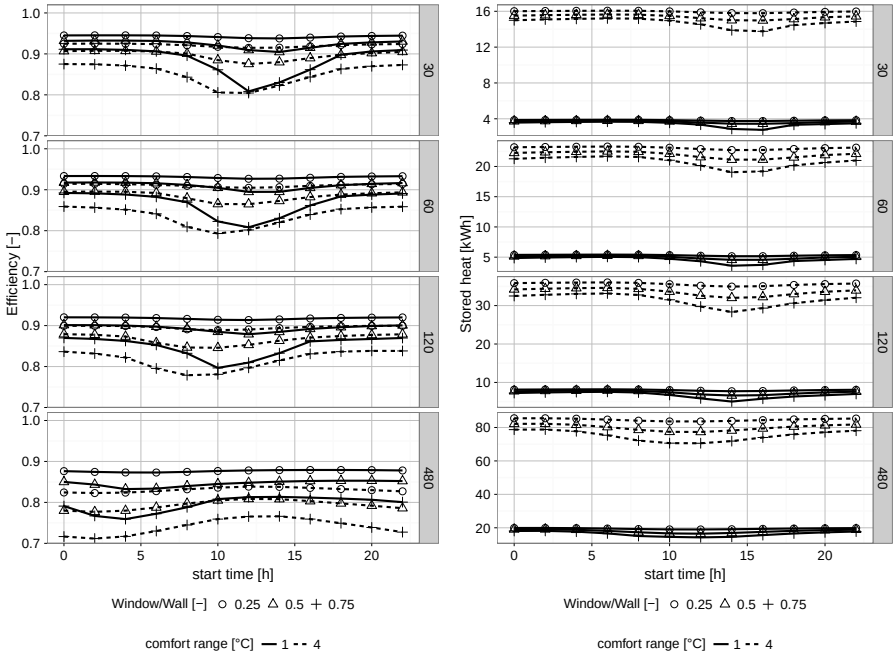

Figure 3.17: Impact of solar gains on the storage efficiency (left) and available storage capacity (right) for increasing window to wall ratio. The results are shown as a function of the starting time of the ADR-event for varying duration of the ADR-event, an outdoor temperature of 5 °C and a comfort range (dT_{comf}) *of 1 °C and 4 °C*

– due to the reduced exterior wall area – and the reduction of the heat demand when introducing solar gains. In addition to the overall reduction a significant temporary reduction of the efficiency is found when the storage capacity is activated just before and during the period of high solar gains. For longer ADR-events, this reduction starts earlier compared to the short ADR-events because preheating the building for a short period at night will not affect what happens during the period with high solar gains.

The right-hand side of Figure 3.17 shows the corresponding storage capacity. Again a reduction of the available storage capacity for ADR is found due to the fact that the solar gains will cover part of the heat load limiting the potential increase of the heating power for ADR. The figure also demonstrates a phase-shift between the reduction of the storage efficiency and the decrease of the available storage capacity. This is a consequence of the fact that by charging the structural storage capacity before the solar peak occurs, results in a lower heat demand in the period after the ADR-event. Consequently, the solar gains that

Zone	Setpoint high	Setpoint low	High setpoint period
Day-zone	$22°C$	$16°C$	07:00–22:00
Night-zone	$18°C$	$16°C$	21:00–09:00

Table 3.2: Thermostat schedule

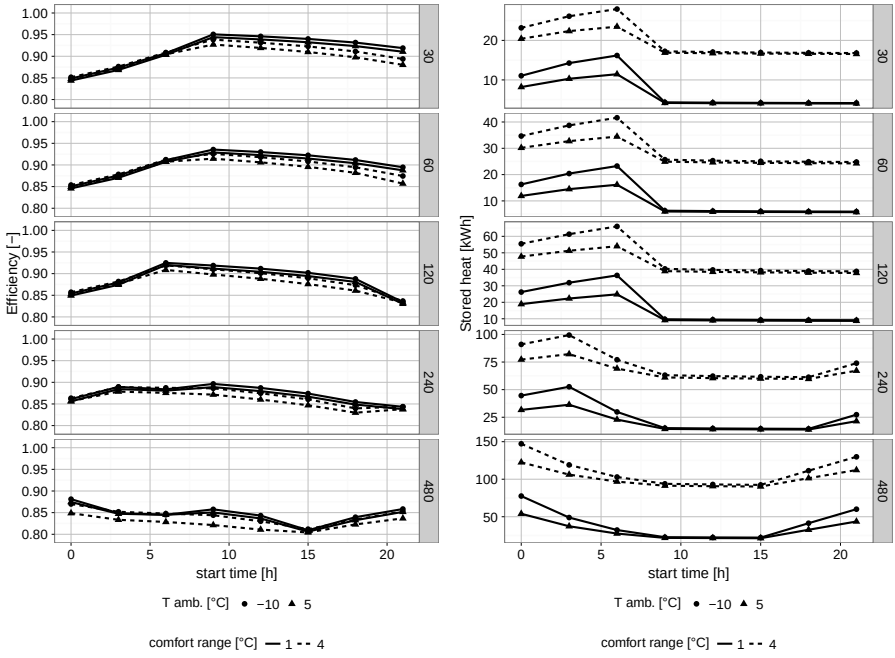

Figure 3.18: Impact of occupant behaviour on the storage efficiency (left) and available storage capacity (right) as a function of the starting time of the ADR-event. The results are shown for varying duration of the ADR-event, outdoor temperature and a comfort range (dT_{comf}) of 1 °C and 4 °C

enter the building may become higher than the heating demand of the building, resulting in higher indoor temperatures in the afternoon and may even lead to overheating problems. In contrast, in the afternoon the building will already be heated by the solar gains, consequently the potential to increase the heating power for ADR and thus the available storage capacity reduces. An efficient control strategy should thus avoid excessive storage prior to periods where high solar gains are predicted, since during these periods the passive gains may be used to charge the storage capacity.

Finally, Figure 3.18 shows the impact of occupant behaviour, and more specific the heating

schedule, on the storage efficiency. The implemented heating schedule imposes a minimum temperature set point of 20°C during the occupied period (between 08:00 and 22:00) and 12 $^{\circ}\mathrm{C}$ during the unoccupied period. The latter is used assuming that heating will not be used at night. The maximum set point for ADR is set to 20 $^{\circ}\mathrm{C} + \delta T_{comf}$ throughout the entire day. As for the solar gains, Figure 3.18 shows a significant variation of the storage efficiency and the available capacity as a function of the time of day on which the ADR-event starts. Due to the night setback, a higher available storage capacity is found for ADR-events which start during the night, f.i. because of high available wind power, since the temperature increase compared to the reference heating scenario is higher at night. Nevertheless, from the left hand plots of Figure 3.18, it is shown that activating the structural thermal energy storage capacity is best done between 6AM and 12AM, immediately before or at the beginning of the occupied period. The fraction of the heat that can be recuperated to reduce the heat demand during the occupied period, decreases as the time between the ADR-event and the start of the occupied period increases. Moreover, it is shown that for longer ADR-events, the efficiency starts to decrease in the late afternoon, as the stored heat cannot be recovered the same day. The highest potential for ADR using the structural storage capacity is thus found in the few hours before the occupied period. This is an interesting result as this demonstrates that the start-up peaks that are typically found at the start of the occupied period [15], can be efficiently shifted and spread over the early morning (eg. 04:00 - 06:00) during which the overall electricity demand is typically low (Figure 3.15). However it should be noted that even for short ADR periods the daily averaged efficiency is always lower in case of the occupancy schedule compared to a constant indoor temperature.

3.4.3 Multivariate parameter analysis

In the second phase of the parameter study, a multivariate regression analysis is carried out for the impact of the building design parameters on the storage efficiency. As observed in the univariate analysis, a significant variation is found on the storage efficiency as a function of the building design parameters and the duration of the ADR-event. However, the impact on the efficiency was not equally large for all parameters. Moreover, it was shown that the impact of the building design, e.g. the heat loss coefficient (Figure 3.9), changes when the duration of the ADR-event increases. Therefore, the multivariate regression model for the prediction of the storage efficiency of a building is calculated in 2 steps, discussed in the following paragraphs. In a first step the dominant parameters are identified for different durations of the ADR-event in order to define a general multivariate regression model for the storage efficiency. In the second step, an additional regression step is used to capture the

time and temperature dependence of the regression coefficients obtained from the first step. As such, a non-linear multivariate model is obtained to predict the storage efficiency based on input data for the general thermal properties of the dwelling, the outdoor temperature and the duration of the ADR-event. Note that, given the fundamental differences that were shown in the univariate analysis, the cases with floor heating and radiators are separated in individual models.

Step 1: multivariate regression for different durations of the ADR-event In the first step, a linear multivariate regression is carried out for the different durations of the ADR-event (0-12 h), using standardised building parameters[7] as inputs. The use of standardised inputs allows for the comparison of the relative importance of the regression coefficients. The building parameters presented in Table 3.3 are used as model inputs. These parameters are a combination of the parameters in Table 3.1 and the resulting aggregated building design properties, such as the HLC. The model is given by equation 3.9,

$$\hat{\eta}_{ADR,j} = \sum \theta_i x_{i,j} + \epsilon_j \tag{3.9}$$

with θ_i the regression coefficients, $x_{i,j}$ the jth observation of the ith building parameters, $\hat{\eta}_{ADR,j}$ is the estimated storage efficiency for observation j and $\epsilon_j \sim N(0, \sigma^2)$.
The regression is carried out using least square estimation in R. A backward selection procedure using the Akaike information criterion (AIC) [122] is used to select the model with the optimal set of building parameters for each duration[8].

As a result of the backward selection process, different models with a different number of significant input parameters are obtained for each duration. These results are compared in order to find a *general model* with the minimum set of building parameters that is required to get a reliable prediction of the efficiency over the time domain. Parameters with only a small contribution to the model for all durations, i.e. the standardised regression coefficients are of a lower order of magnitude, are excluded from the general model even though the AIC showed they should be included. Thereby some input parameters that may not be significant for short-term ADR-events are kept in the general model when they significantly contribute for

[7] standardised building parameter (z) is obtained as $z = (x - \bar{x})/\sigma$, with $\bar{x}$ the mean and σ the standard deviation of building parameter x as obtained from Table 3.1.

[8] A priori, the correlation matrix of the different inputs was analysed to identify correlated building parameters. When high correlations $(\rho > 0.9)$ are found only 1 of the parameters is maintained in order to avoid co-linearity problems. High correlations are for example found between the height of the building, the capacity of the indoor air and the area of the common wall. While these correlations are likely to also occur in a real building stock, the high correlations found here are the consequence of the parametric design method that is used to generate the building models.

Table 3.3: Input parameters for multi-variate regression coefficients. The underlined parameters have been maintained based on the backward selection procedure.

Paramater	Definition	unit
A_{floor}	Ground floor area	m^2
h_{ceil}	Ceiling height	m
int. wall ratio	Ratio of the internal over exterior wall areas	-
compactness	Compactness of the dwelling	m
$A_{wall,i}$	Surface area of interior walls	m^2
$A_{wall,e}$	Surface area of exterior walls	m^2
$A_{wall,c}$	Surface area of common walls	m^2
$d_{brick,wall_e}$	Thickness of inner leaf of exterior walls	m
d_{wall_i}	Thickness of interior wall	m
U_{wall_e}	U-value of exterior wall	$W/(m^2K)$
U_{roof}	U-value of roof	$W/(m^2K)$
n_{vent}	Effective air change rate	h^{-1}
HLC	Total heat loss coefficient (incl. ventilation)	W/K
$HLCperAfloor$	HLC/A_{floor}	$W/(mK)$
C_{TOT}	Total thermal capacity of building components	J
C_{air}	Thermal capacity of indoor air	J
$HLCparCTOT$	HLC/C_{TOT}	$W/(m^2KJ)$
system sizing factor	$Q_{Nom,installed}/Q_{Nom,EN12831}$	-

long-term events, and vice versa. When the structure of the general model is established, an additional regression step is then carried out for each duration using the established *general model* structure. Figure 3.19 shows the impact on the adjusted R^2 (R^2_{adj})[9] of replacing the optimal model structure obtained by the backward selection process by the established general model. The deviations are found to be largest for short durations, especially for the radiator heating cases the R^2_{adj} is on average 0.03 lower for the general model for ADR-events limited to 2 h. Nonetheless, during these short events the storage efficiency is high for all cases and the spread is limited (Figure 3.3). Consequently, the absolute error introduced by the general model is found acceptable.

Figure 3.20 shows the standardised regression coefficients for the obtained general models allowing to compare the relative importance of the building parameters on the storage efficiency. The figure shows for each model parameter the standardised regression coefficients as a function of the duration of the ADR-event (indicated by the grey scale). The shape of the markers indicates a confidence level of the estimate[10].
Firstly, it should be pointed out that for the floor heating case the UA-value of the ground floor is not included in the heat loss coefficient (HLC_e) but as an individual input in the

[9]The adjusted R^2 is a modified version of R^2 that account for the number of model parameters – hence penalizing a high amount of parameters – and is given by: $R^2_{adj} = 1 - (1 - R^2)\frac{n-1}{n-p-1}$ with n the number of samples and p the number of parameters in the model

[10]The confidence level is quantified as $1 - \mid Std.Error(\bar{\theta}) \mid /\bar{\theta}$

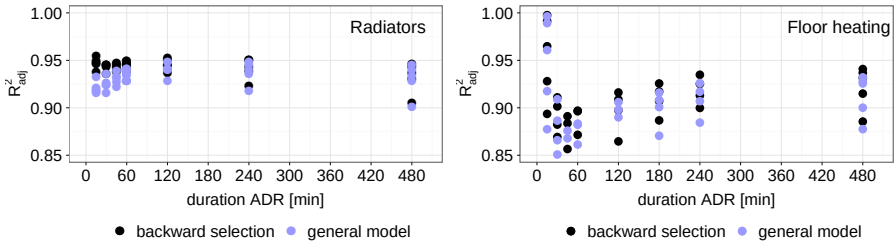

Figure 3.19: Comparison of R^2_{adj} for each duration of the ADR-event the regression models obtained after the backward selection process and for the established general model. The different points for each duration represent different outdoor temperatures.

regression model. For the radiator model, this distinction was not required to improve the model accuracy and thus the UA-value of the floor is included directly in the HLC.

Analysing the standardised regression coefficients shows that for both heating systems the HLC (and HLC_e) and $HLCperCTOT$ parameters are the most important regression coefficients. The latter is defined as the fraction of the heat loss coefficient of the building divided by the total thermal mass of the building fabric. Thereby it is interesting to see that for short ADR-events - less than 60 min. - the HLC is the dominant coefficient, while for longer periods its contribution to the model decreases and the $HLCperCTOT$ becomes dominant. This can be explained by the findings of the univariate analysis (Figures 3.10-3.12) which show that the storage efficiency is influenced by the structural thermal mass (C_{TOT}) for long-term ADR-events (longer than 2 h). For short-term events the impact of increasing the thickness is found to be marginal.

Shown by the positive regression coefficient, the thermal capacity of the indoor air (C_{air}) has a positive impact on the storage efficiency. For dwellings with radiator heating, the contribution is however only important for short ADR-events. A similar positive correlation is found for the floor heating case. However, the uncertainty on the regression coefficients for C_{air} is high and also the link with the ADR duration is less pronounced.
Both the interior wall ratio and the thickness of the interior walls (d_{wall_i}), have a significant positive contribution to the storage efficiency in case of longer ADR periods. The availability of thermal mass at the inside of the exterior walls $(d_{brick,wall_e})$ shows to be insignificant and even a negative correlation is found. The total structural thermal mass (C_{TOT}) has, at least for long ADR-events, a significant positive contribution to the model. Nevertheless, for short-term ADR-events, in case of floor heating, the standard deviation for this coefficient is higher, as demonstrated by the low reliability.

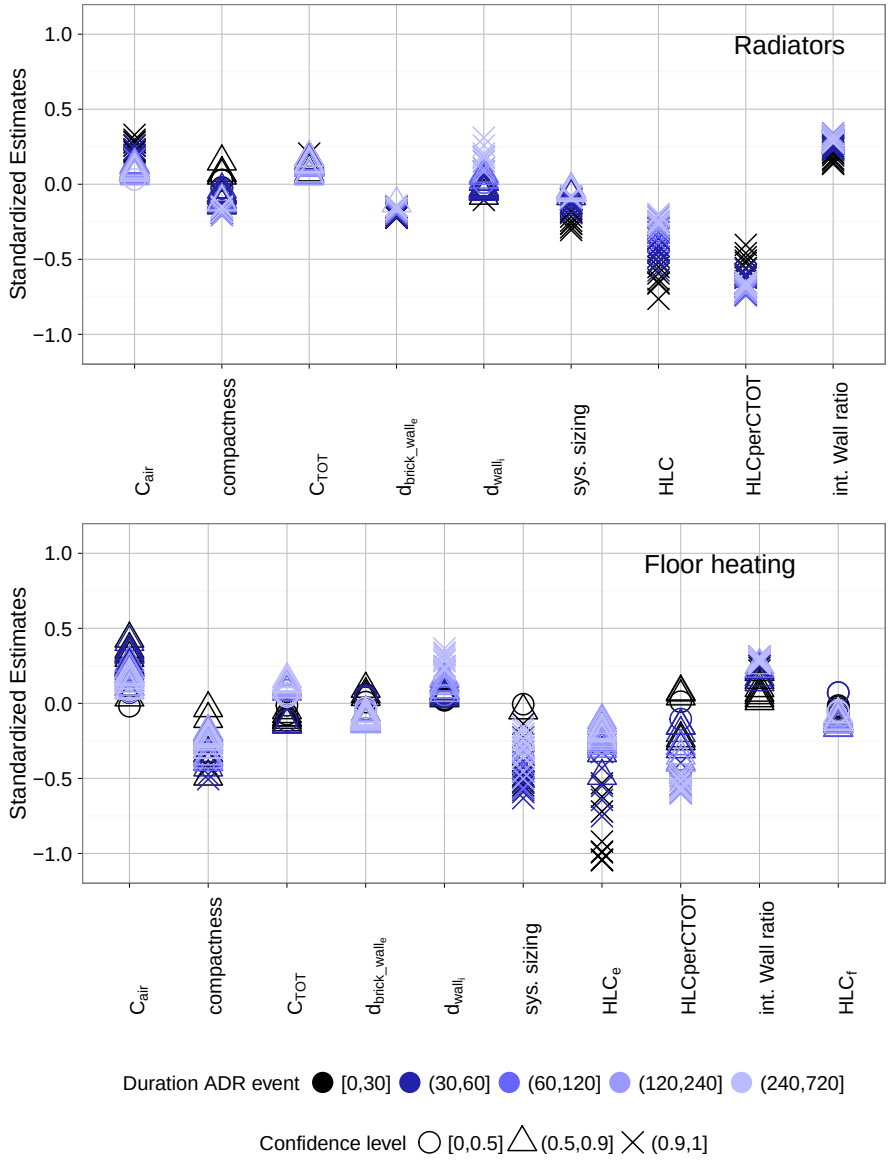

Figure 3.20: Standardized regression coefficients for the general multiple regression model of the storage efficiency for the radiator (top) and floor heating system (bottom) estimated for different durations of the ADR-events. The colour-scale indicates the duration of the ADR-event, the shape of the markers indicates the confidence level of the estimates.

Finally, Figure 3.20 shows that oversizing of the heating system has a significant negative correlation with the efficiency of structural storage for floor heating for ADR periods between 30 and 240 minutes, while for radiator heating the effect is only shown for short periods. Since oversizing results in a higher additional power that is available for charging the thermal capacity of the dwelling, the indoor temperature and the corresponding thermal losses will rise faster. Once the maximum comfort temperature is reached the power of the system is reduced to maintain this temperature, and the effect of oversizing is eliminated. Given the slow thermal response of floor heating systems, it takes longer before this maximum temperature is reached and thus the effect of oversizing lasts longer.

Step 2: identify time and temperature dependent regression coefficients Figure 3.20 shows a clear dependence of the regression coefficients on the duration of the ADR-event. Moreover, the coefficients are found to be influenced by the outdoor temperature. Therefore, in this second step individual models are identified for each regression coefficient θ_i from equation 3.9. As initial model structure, a higher order polynomial for l_{ADR}, T_e and the combined effect of $l_{ADR}T_e$ and $l_{ADR}^2T_e$ is constructed for each coefficient $\theta_i(l_{ADR}, T_e)$ as given by equation 3.10.

$$\begin{aligned}\hat{\theta}_i(t, T_e) = \alpha_0 + \alpha_1 l_{ADR}^{-2} + \alpha_2 l_{ADR}^{-1} + \alpha_3 l_{ADR} + \alpha_4 l_{ADR}^2 \\ +\alpha_5 l_{ADR}^3 + \alpha_6 l_{ADR}^4 + \alpha_7 T_e + \alpha_8 (l_{ADR}T_e) + \alpha_9 (l_{ADR}^2 T_e) + \epsilon\end{aligned} \tag{3.10}$$

with t and T_e respectively the ADR duration in minutes and the outdoor temperature in K. The regression coefficients α_i are again estimated using least squares estimation with a backward selection process using the AIC. The resulting general prediction model for the storage efficiency as a function of the building properties, the duration of the storage event and the outdoor temperature is then given by combining equations 3.9 and 3.10. The regression coefficients (α_j) defining this model are summarised in Table 3.4 for both the floor heating and radiator cases.

Figure 3.21 shows the prediction accuracy of the resulting models by contrasting the calculated storage efficiency using the detailed building energy simulations with the predicted efficiency using the regression model. Thereby higher residuals are found for the floor heating than for the radiator cases. For the latter, the model error is limited to 5 % and increases slightly with decreasing efficiencies, resulting in an R^2-value of 95 %. For the floor heating system deviations up to 15 % are found ($R^2 = 94.8$ %). As such, it is concluded that the established multivariate model is able to accurately predict the storage efficiency, for the simplified boundary conditions, given information is provided about the general thermal

RADIATOR HEATING										
	α_0	α_1	α_2	α_3	α_4	α_5	α_6	α_7	α_8	α_9
intercept	9.62e-01	-4.81e+00	6.96e-01	-1.42e-04	-	-	-	-4.14e-04	-4.23e-06	-
HLC	-2.35e-05	-	9.94e-05	-	-2.47e-11	-	-	1.82e-07	8.48e-10	-
$HLC/CTOT$	-1.69e+04	-	1.33e+05	-3.39e+02	9.34e-01	-9.71e-04	-	-9.02e+02	-	2.30e-03
C_{TOT}	2.01e-12	-	-	1.03e-14	-	-	-	7.21e-14	-	-
C_{air}	1.68e-09	-	-7.29e-09	-	-	-	-	-3.87e-11	-	-
int.Wall ratio	-4.59e-04	-	-	3.62e-04	-2.26e-06	6.81e-09	-7.01e-12	2.84e-04	-7.60e-07	-
sys. Sizing	-1.05e-02	-	-	7.98e-05	-3.50e-07	3.95e-10	-	-	1.40e-06	-1.83e-09
compactness	3.27e-03	-	-	-1.66e-04	5.61e-07	-6.24e-10	-	-	-	-
d_{wall_i}	-1.04e-02	-	-	-	1.86e-06	-2.41e-09	-	-9.25e-04	2.04e-05	-2.06e-08
$d_{brick,wall_e}$	-1.27e-02	-	9.58e-02	-1.45e-04	4.61e-07	-4.95e-10	-	-4.16e-04	1.53e-06	-

FLOOR HEATING										
	α_0	α_1	α_2	α_3	α_4	α_5	α_6	α_7	α_8	α_9
intercept	1.01e+00	-	-1.11e-01	-6.44e-05	-2.91e-07	2.36e-10	-	4.05e-04	-1.50e-05	7.46e-09
HLC_e	-4.04e-06	-	-	-3.69e-08	1.34e-11	-	-	-	-4.89e-10	-
HLC_f	-4.42e-05	-	-	-1.50e-06	1.36e-09	-	-	-	-1.67e-07	1.88e-10
$HLC/CTOT$	3.38e+03	-	-	-1.93e+02	-	5.16e-04	-4.75e-07	-2.30e+02	-9.58e+00	1.27e-02
C_{TOT}	-3.86e-13	-	-	9.12e-15	-	-	-	-	2.36e-16	-
C_{air}	3.14e-10	-	-	8.80e-12	-7.27e-15	-	-	4.52e-11	1.51e-13	-
int.Wall ratio	-1.32e-03	-	-	1.16e-04	-1.53e-07	8.44e-11	-	1.17e-04	3.56e-06	-4.10e-09
sys. Sizing	-9.47e-03	-2.72e+00	3.28e-01	-1.30e-04	2.22e-07	-1.26e-10	-	-3.86e-04	-	1.69e-09
compactness	-2.55e-03	-	3.74e-02	-5.70e-05	3.55e-08	-	-	-9.45e-05	-3.46e-07	-
d_{wall_i}	-1.46e-04	-	-	-	2.20e-06	-4.35e-09	2.67e-12	-9.29e-04	3.49e-05	-3.07e-08
$d_{brick,wall_e}$	2.14e-03	-	-	-9.98e-05	1.97e-07	-1.28e-10	-	-2.21e-04	-2.65e-06	5.27e-09

Table 3.4: Regression coefficients α_j for the regression equation 3.10 for each of the regression coefficients θ_i of Eq. 3.9

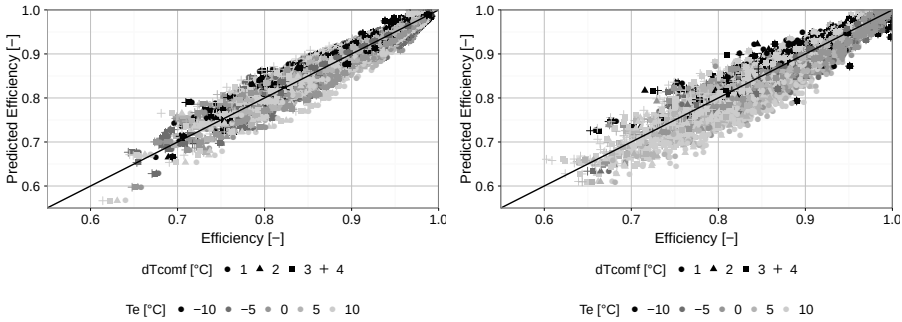

Figure 3.21: Predicted storage efficiency using the general multiple regression models as a function of the outdoor temperature and the considered comfort range for the radiator (left) and floor heating (right) cases.

characteristics of the dwelling, the outdoor temperature and the duration of the ADR-event.

3.4.4 Quantification for realistic boundary conditions

For the multiple regression analysis strong simplifications have been introduced in the simulation model. The climate and minimum indoor temperature are kept constant, while solar gains are not included. As such, a theoretic analysis of the impact of building design parameters on the available storage capacity for ADR and the efficiency of the storage process was possible. Nevertheless, the obtained storage efficiencies and available storage capacities should be interpreted as a theoretic flexibility signature of the dwelling that can support design decisions, rather than instantaneous performance indicators.

In Section 3.4.2 a parametric assessment of the impact of the boundary conditions was already shown for the univariate case. In this section, the potential and limitations of the obtained multivariate regression model are shown in a simulation for a winter period given the climate conditions of Belgium (Uccle). This period has been chosen as it has both cold cloudy days (before Jan 25^{th}) and warmer sunny days (after Jan 28^{th}).

To calculate the available storage capacities (C_{ADR}) and the corresponding efficiencies, the step-up heating experiment (Figure 3.2) has been repeated for each hour of the analysed periods. Figure 3.22 shows the results obtained for ADR-events of 1, 4 and 8 h (60, 240 and 480 min) and a comfort range of 2 $^{\circ}\mathrm{C}$ for both the radiator (left) and floor-heating cases (right). Figures 3.22(a-b) show the resulting indoor temperature at the end of the ADR-events,

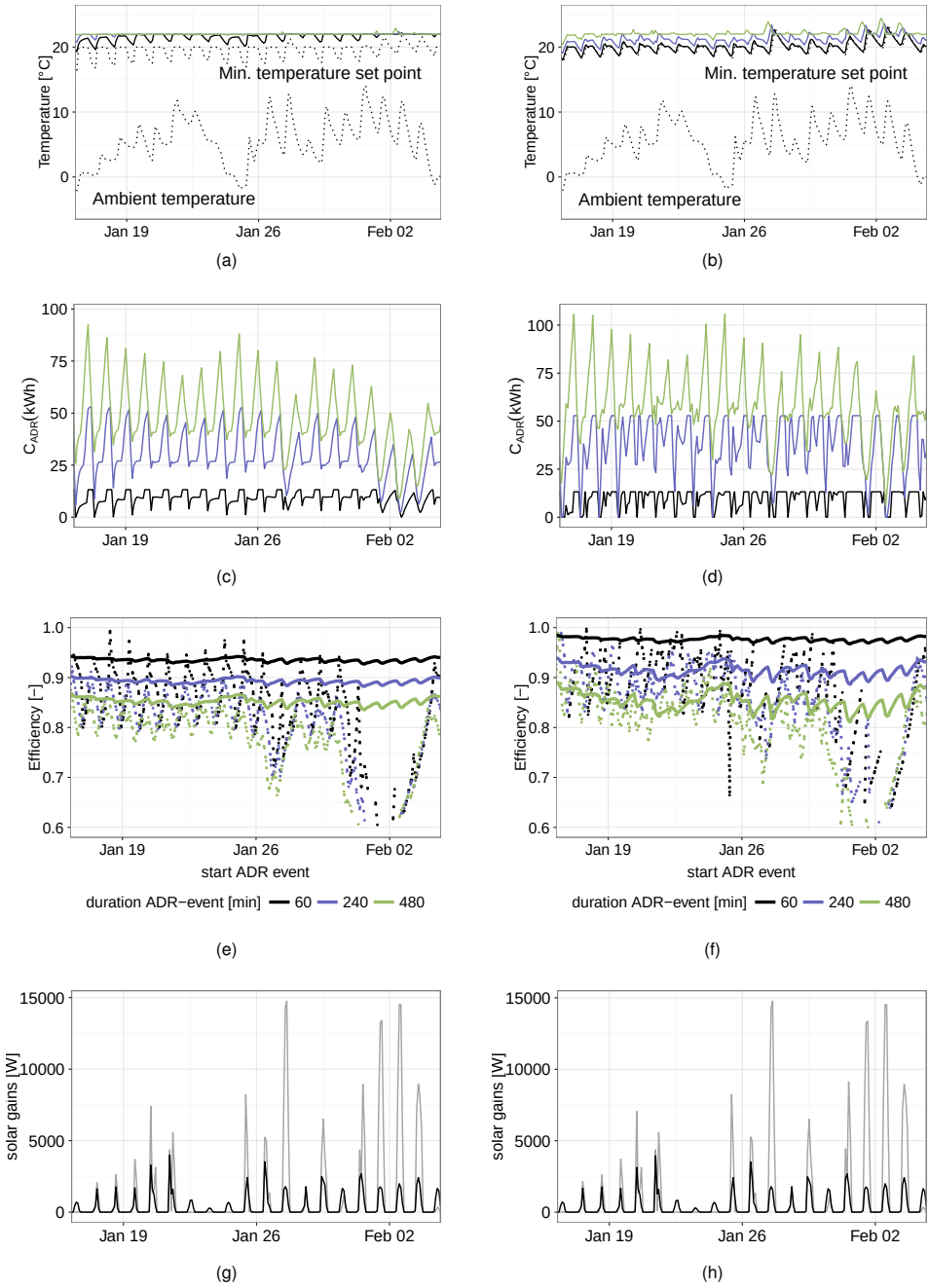

Figure 3.22: Instantaneous storage capacity and efficiency for dynamic boundary conditions for radiators (left) and floor heating (right). (a, b) show the temperature at the end of the ADR event, the ambient and minimum (reference) indoor temperature. (c,d) and (e,f) show respectively the available storage capacity and corresponding efficiency as function of the start time of the ADR event. The colour scale indicates the duration l_{ADR}. The dotted lines in e and f show the efficiency calculated from the detailed simulations, the full lines are the predicted results by Eq. 3.9. (g,h) demonstrate the solar gains.

in addition to the outdoor temperature and the reference temperature profile following the occupancy schedule of Table 4.4. For the radiator heating cases (Fig. 3.22(a)) it is shown that for short ADR-events (60 min and less), the maximum comfort temperature (22 $^{\circ}\mathrm{C}$) is not reached at the end of the ADR-event. Note that the ADR-event always starts from a state equal to the reference scenario (shown by the dotted line). As the duration of the ADR-event increases or the outdoor temperature rises, it is clear that the amount of heat that can be stored within the thermal mass of a building, i.e. the available storage capacity, is limited by the comfort range. For the floor heating cases, as shown on the top-right graph, the maximum temperature is only reached for ADR-events longer than 4 h (240 min) or for days with high solar gains (Fig. 3.22(g-h)). During the latter, the indoor temperature may become higher than the upper bound for ADR (here 22 $^{\circ}\mathrm{C}$). This effect is more pronounced for the floor heating buildings since the thermostat control reacts too late. This is a well-known problem for slow thermal systems such as floor heating, that may be overcome by model predictive control [123]. Since this is not implemented in this work, it is thus important to note that the quantified available storage capacity should be interpreted as upper limits.

The obtained values for the available storage capacity for ADR are shown in Fig. 3.22(c-d), clearly illustrating the day-night fluctuations as a result of the occupancy schedule and – to a limited extent – to the outdoor temperature variations. In addition to the peaks in the available capacity at night, as a result of the larger temperature range when the ADR-events start at a moment where the building has already cooled down in night set-back operation, the figures also show a significant reduction of the available capacity in the early morning. These reductions correspond to a start time of the ADR-event when the building is reheating from the night set-back. During this period, the system already operates at its maximum power and thus no additional increase for ADR is possible.

In addition to the daily variation in the available capacity, the profiles also show a negative correlation with the solar gains. This decrease in capacity with increasing solar radiation directly follows from the increased temperature in the reference profile observed in Fig. 3.22(a-b) and the resulting reduction in the temperature range available for ADR. Corresponding to this reduction in the available storage capacity, a strong reduction in the storage efficiency is demonstrated in Fig. 3.22(e-f).

On Fig. 3.22(e-f), the storage efficiency obtained by the detailed simulation model – which is also used for the other sub-figures – is demonstrated by the dotted lines. For the daily variations, the storage efficiency is shown to be negatively correlated to the available capacity, i.e. low values of the storage efficiency are found at night when the peak in C_{ADR} were found. This result is in line with the findings of Fig. 3.18 and demonstrates that from the perspective of storage efficiency, activating the storage capacity for ADR is best limited to the period just before or at the start of the occupancy period. Moreover, in line with Fig. 3.17,

a strong reduction of the storage efficiency (by 30 % and more) is found for ADR-events during sunny periods. Evidently, from a storage-efficiency perspective, the use of structural storage for ADR (in heating regime) should be avoided on warm and sunny days. To avoid this reduction in efficiency, model predictive control strategies may be used, since using predicted weather data they can f.i. avoid overcharging of the storage capacity by increasing the heat input for ADR in the hours prior to high solar gains.

Finally, the storage efficiencies predicted by the multivariate regression model, taking into account the dynamic outdoor temperature, are shown by the solid lines in Figures 3.22(e-f). Since the regression model is fitted on simulations of a constant indoor temperature, the daily variations in the storage efficiency as a result of the occupancy schedule are evidently not captured by the regression model. Moreover, the regression model does not show the reduction in efficiency due to the high solar gains. Consequently, during the cold cloudy days, the regression model shows an average overestimation of the storage efficiency of 7 %, 5 % and 2 % for respectively the 1, 4 and 8 h ADR-events as a result of the day-night variations and 30 % and more during periods with high solar gains.

In conclusion, it is evident that whereas the identified regression model can be successfully applied to analyse and compare the impact of building, emission system and control design parameters on the suitability of using the structural thermal mass of dwellings for ADR, making it an interesting tool during the building design phase, the absolute and instantaneous values of efficiencies should be handled carefully. The time-dependent solar gains and occupant behaviour have a significant impact on the instantaneous available storage capacity for ADR and the corresponding storage efficiency. As such, for application in grid operation models or control applications on building level, a dynamic evaluation of these performance indicators, using the simulation-based methodology presented in this chapter, is a prerequisite.

3.5 Quantifying the state of charge and power shifting capability

In the previous section, two quantitative performance indicators, i.e. the available storage capacity and the storage efficiency were discussed. These two indicators have been developed and used for the evaluation of the impact of building design parameter on the suitability of structural thermal energy storage for ADR in a more fundamental and theoretic framework. Additionally this section demonstrates the quantification methods, presented in 3.3, for the state of charge and the power shifting capability of a building. These properties

can be interpreted as a momentary snapshot of the flexibility that is available in a building and are therefore useful for control strategies on a local and district level.

3.5.1 State of charge

It is evident that the state of charge is an important property in the control of the storage medium, as it informs the controller about the flexibility that is still available in the system. In the case of thermal energy storage, a state of charge of 0 corresponds to a situation where no heat can be subtracted from the storage medium, while no heat can be added to the storage capacity for a state of charge of 1 without influencing the normal operation of the storage capacity. For structural thermal energy storage the latter corresponds to thermal comfort violations.

In the definition of Section 3.3, the state of charge is defined as the ratio of the instantaneous energy content of a system compared to its total storage capacity and calculated based on the energy content $E(t)$ of the dwelling. Only considering the sensible heat balance, the energy content of the dwelling is given by:

$$E(t) = \sum_{comp} \int_0^d C_i(x) T_i(x,t) dx \tag{3.11}$$

In this equation, $T_i(x,t)$ is the temperature of component i at a depth x within the wall and $C_i(x)$ the thermal capacity of the corresponding material layer. The integral over the total thickness of a component (d) gives the energy content of a single building component. Summation over all components, whereby the indoor air is included as an additional term, gives the total energy content of the dwelling. Note that the internal mass of furniture is not included explicitly in this work, but rather as in a simplified manner by increasing the thermal mass of the indoor air by a factor 5. Nonetheless, it may be included explicitly as an additional term in Eq. 3.11 as well.
Application of this formula requires knowledge of the temperature distribution within each building component and is therefore infeasible in practical applications. Although measurements of the heat flowing in and out each component may be used to quantify the amount of heat stored within the structural storage capacity, an alternative definition is found in literature based on indoor temperature of a dwelling [31]. Thereby the clear link with thermal comfort is used to formulate the state of charge by comparing the indoor temperature

to the comfort bounds, as presented in Equation 3.12.

$$SOC_T = \frac{T_{op}(t) - T_{min}(t)}{T_{max}(t) - T_{min}(t)} \tag{3.12}$$

with $T_{op}(t)$ [$^{\circ}\mathrm{C}$] the time varying operative temperature and T_{max} [$^{\circ}\mathrm{C}$] and T_{min} [$^{\circ}\mathrm{C}$] respectively the maximum and minimum comfort temperature. Note that the latter can also be time varying, depending on occupant behaviour and preference.

Both definitions have been used to demonstrate the evolution of the state of charge when, starting from a steady state condition, a step function is applied to the heating power. Although these definitions are widely used for electrical storage in batteries or thermal energy storage in water tanks, the applicability of both definitions in the context of structural thermal energy storage is found to be limited. Figure 3.23 shows a comparison for SOC$_E$ and SOC$_T$, when a single zone building is heated from an arbitrary steady state condition with an operative temperature of 21 $^{\circ}\mathrm{C}$, T_{max} equal to 24 $^{\circ}\mathrm{C}$ and T_{min} equal to 20 $^{\circ}\mathrm{C}$. Simple constant boundary conditions are considered with a constant outdoor temperature of 0 $^{\circ}\mathrm{C}$ and no solar gains. Both graphs show the simulation of a series of heating experiments where, starting from the equilibrium steady-state conditions, the modulation rate of the heating systems is varied to a value between 0 to 100 %.

Although both graphs are based on the same simulation results, the calculated state of charge significantly differs. Although for both plots the building is initiated with an indoor temperature of 20.5 $^{\circ}\mathrm{C}$, the calculated SOC$_T$ and SOC$_E$ are respectively 12.5 % and 20 %. This difference results from the fact that the temperature increase due to the activation of the structural thermal mass is not uniform for all components, while both SOC$_T$ and SOC$_E$ give a first-order representation of the thermal capacity, i.e. the thermal mass of the building is lumped to a single state.

Secondly, Figure 3.23 shows that the interpretation of the state of charge depends on the definition and may be misleading in the context of control design. For example, when the heating system is shut down (modulation = 0), a control strategy using the state of charge calculated by the indoor temperatures (Equation 3.12), will decide to restart the heating system after 30 minutes when the state of charge becomes 0. Nevertheless, the SOC calculation based on the heat stored in the thermal mass, shows that at this time a significant amount of heat is still stored within the thermal mass. A similar problem exists at the upper comfort boundary, indicating that the SOC calculation based on the indoor temperature would result in an underestimation of the available storage capacity, while a control using the calculation based on the stored heat results in comfort issues.

Moreover, due to the dynamic boundary conditions also the reference values in the denominator are not constant. This results in situations where the state of charge varies

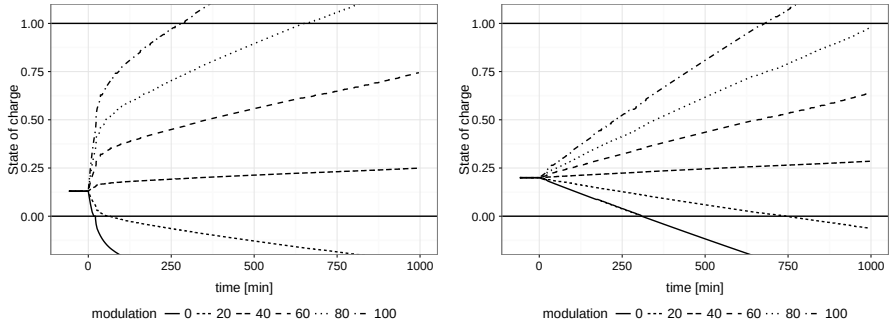

Figure 3.23: Comparison of state of charge (SOC) based on the operative temperature (left) and the stored heat (right).

even though the control strategy does not alter. Therefore it is concluded that whereas the state of charge is widely used for battery storage or water storage tanks, it does not provide the same information and applicability for structural thermal energy storage. The pragmatic definition of the state of charge based on the indoor temperature tends to underestimate the available storage capacity, since a state of charge of 1 is obtained whenever the indoor temperature reaches the maximum comfort temperature. Depending on the heating profile this situation can occur long before the entire thermal mass of the building is activated. In contrast, application of the correct definition of the state of charge (3.7), has no direct link to thermal comfort. Both phenomena can be explained by the fact that the large variations in time constants of the structural components of a building, including the indoor air, is not well captured by a first-order metric. In order to overcome this problem, a time dimension is included in the definition of the *power shifting capability*, presented as a complementary metric to the SOC in the following paragraph.

3.5.2 Power shifting capability

In Section 3.3, the power shifting capability is defined as a complementary metric to the state of charge of the structural storage capacity. In the previous section, the latter is found to be difficult to interpret in terms of control strategies. Moreover the state of charge only describes the current energy content of the structural thermal energy storage capacity. In contrast, the power shifting capability gives information about the extent to which the current operation of the building can be adapted by ADR in the following period.
Figure 3.24 shows the power shifting capability curves for different initial indoor temperatures.

Starting from these steady-state conditions, the thermal response of the building to a change in the heating power is modelled. The duration during which this shift can be maintained is then calculated as the duration until the thermal comfort boundaries, either T_{max} or T_{min} are reached. The power shifting capability is then expressed as the possible power shift as a function of the duration. The power shift ($\dot{Q}_{\delta}\ [W]$) is defined as the difference between the heating power during the ADR-event ($\dot{Q}_{ADR}\ [W]$) and the current heating power ($\dot{Q}_{Ref}\ [W]$).

$$\dot{Q}_{\delta} = \dot{Q}_{ADR} - \dot{Q}_{Ref} \tag{3.13}$$

A distinction is made between the upward and downward shifting capability, representing respectively an increase or a decrease of the heating power compared to the current state. Figure 3.24 shows the power shifting capabilities for buildings initialized at an indoor temperature between 20 $^{\circ}\mathrm{C}$ and 22 $^{\circ}\mathrm{C}$. The plots on the left show the relative power shifting capability. On the right plots the corresponding relative heating power is shown. Both are calculated by respectively dividing $\dot{Q}_{\delta}$ and $\dot{Q}_{ADR}$ by the nominal power of the heating system. Since the heating system operates on approximately 25 % of its power capacity for the outdoor temperature of 0 $^{\circ}\mathrm{C}$, the relative upward power shifting capability is limited to about 75 % for all initial temperatures. Nevertheless, the period for which this shift can be maintained increases significantly for lower starting temperatures and higher comfort ranges. For a comfort range of 2 $^{\circ}\mathrm{C}$ an increase of the heating power to the nominal power can be maintained for 3 h when started from the minimum comfort 20 $^{\circ}\mathrm{C}$, or a SOC of 0. Starting from a steady state condition with an indoor temperature of 21.5 $^{\circ}\mathrm{C}$ the maximum comfort temperature (22 $^{\circ}\mathrm{C}$) is already reached after 30 minutes. For a comfort range of 4 $^{\circ}\mathrm{C}$ and starting from an indoor temperature of 20 $^{\circ}\mathrm{C}$ the maximum heating power in this case can be maintained for almost 18 h.

A similar cooling down period is shown starting from an indoor temperature of 21 $^{\circ}\mathrm{C}$. Evidently, the possible duration of a negative power shift is found to be zero when starting from the minimum comfort temperature of 20 $^{\circ}\mathrm{C}$. Note that for the negative flexibility no difference between the comfort ranges is found, as in both cases the same minimum comfort temperature is used.

Finally, it should be emphasised that the demonstrated power shifting capabilities are calculated here for stationary boundary conditions. As such, the duration goes to infinity for a power shift equal to zero. For dynamic boundary conditions, the required heating power to maintain a constant temperature will not be constant nor equal to the current state. The shape of the power shifting capability functions will therefore depend on these boundary conditions.

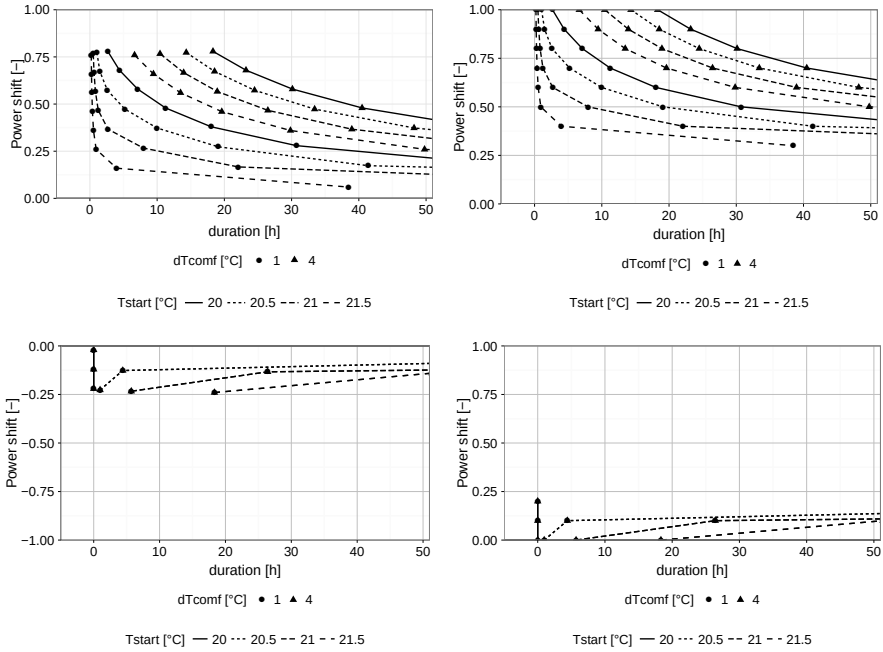

Figure 3.24: Comparison of upward (top) and downward (bottom) relative power shifting capability (left) and corresponding relative heating power of a dwelling for a constant outdoor temperature of 0 °C and varying initial indoor temperatures $(Tstart)$

Figure 3.25 shows the impact of the outdoor temperature on the power shifting capability starting from an indoor temperature of 21 °C. Two interesting trends are shown. Firstly, the relative heating power (right panes) show a clear decrease, for increasing outdoor temperatures, in the time an upward power shift can be maintained. Likewise, a downward power shift can be maintained longer for increasing outdoor temperatures.

Secondly, the relative power shift functions (left hand panes) overlap for all outdoor temperature. The shape of the power shift function is thus defined by the comfort range, the state of charge and the thermal properties of the building, but independent of the outdoor temperature.

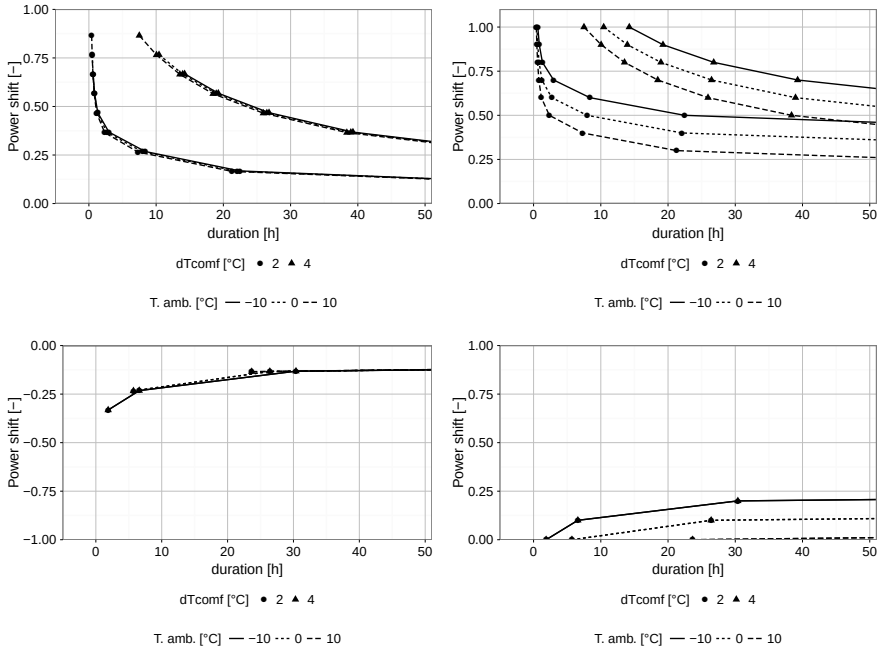

Figure 3.25: Comparison of upward (top) and downward (bottom) relative power shifting capability (left) and corresponding relative heating power of a dwelling for a constant outdoor temperature of 0 $^{\circ}\mathrm{C}$ and varying initial indoor temperatures $(Tstart)$

3.6 Conclusions

Although the potential of active demand response using the structural thermal energy storage capacity of residential buildings shows good potential, a thorough analysis of the impact of the building design on this potential is found to be missing. Therefore in this chapter the available storage capacity, the efficiency of the storage process, the power shifting capability and state of charge are defined and quantified as performance indicators.
The available storage capacity and the corresponding storage efficiency are suggested as storage characteristic that allow a scenario independent evaluation of the suitability of structural thermal energy storage for ADR as a function of the buildings thermal properties, heat emission system and control strategy. Thereby the proposed simplifications in the quantification methods allow a comprehensive interpretation of these characteristics in terms of building thermal performance characteristics.
In contrast, the power shifting capability and state of charge of the building are defined and demonstrated to provide instantaneous knowledge about the available flexibility for ADR. As such, these indicators are concluded to provide useful information for control applications, but do not provide important additional information for the quantification of the impact of building design parameters on the ADR potential.

In order to assess the impact of these building design parameters on the available structural storage capacity for ADR and the storage efficiency an extensive parameter study, using a theoretic quantification framework is carried out. Both the univariate and multivariate parameter study show that high storage efficiencies are obtained for all buildings, assuming the duration of the ADR-event is limited to 1 h. For constant boundary conditions and constant comfort requirements, 95% of the buildings in the multivariate study showed a storage efficiency above 85% for the radiator heated buildings and of more than 93% for floor heated buildings. Lower values are however found for increasing durations of the ADR-event. Thereby buildings equipped with floor heating always show higher storage efficiencies, especially for shorter durations of the ADR-event, since most heat is stored within the heated floor, resulting in a less sharp increase of the indoor temperature and the corresponding transmission and ventilation losses.
Additionally, the parameter study reveals that, as for the overall energy efficiency of buildings, the storage efficiency is strongly correlated to the insulation quality of the dwelling. The overall heat loss coefficient showed to be the most important regression coefficient in the multiple regression model. A minimum level of thermal insulation, as well as an airtight building envelope, are thus a prerequisite for the effective use of structural thermal energy storage for active demand response. Moreover, the availability of the thermal mass, especially

the interior wall ratio, has an important positive effect on the storage efficiency. The impact of the thickness of the interior wall and the inner brick of the exterior cavity wall is found to be less important, demonstrating that the penetration depth of the heat front during the ADR-event is limited. Also, in case of radiator heating, most heat is stored in the air, rather than the building structure if the ADR-event is limited to less than 1 h.
Oversizing of the thermal power of the heating system is found to have a negative impact on the storage efficiency as it results in a faster increase of the indoor temperature and the corresponding thermal losses. Increasing the size of heat production systems, purely for the purpose of ADR, is thus not recommended. This conclusion should however be handled carefully since the production and distribution efficiencies of the heating system are not included in this study.
Finally, the impact of the climatic boundary conditions, occupant behaviour and control parameters were evaluated. Thereby it is shown that due to solar gains and occupancy schedules the storage efficiency varies as a function of the time of day. More precisely, preheating the dwelling just before a period with high solar gains or an unoccupied period results in efficiency reductions of more than 30 %.

In the second part of this section, the calculation method for the state of charge of the building and the power shifting capability are demonstrated. In contrast to the two previous storage metrics these two properties cannot be handled as building characteristics, but provide time-dependent information about the amount of heat that is currently stored within the structural thermal mass and potential for changing the current heating behaviour.
It is shown that although in control strategies often a state of charge based on the indoor air temperature or the thermostat temperature is used, this formulation results in an underestimation of the available storage capacity.
A more correct formulation of the state of charge is based on the actual thermal energy content of the dwelling. Nevertheless, two problems arise with this formulation. Firstly, the energy content is difficult to measure in practice as it is infeasible to measure all the required temperatures. Secondly, the interpretability in terms of thermal comfort and the related control of the heating system is lost.
To overcome this latter problem, the power shifting flexibility was introduced in this chapter. Thereby, compared to similar flexibility metrics found in literature, the added value of the method described in this section lies in the quantification of the relation between the shift in heating power and the time this shift can be maintained.

Chapter 4

Identification of the active thermal capacity of buildings

4.1 Introduction

In the previous chapter, a generic methodology was presented to quantify the potential of structural thermal storage in active demand response programs. Based on prior knowledge of the dominant thermal properties of a dwelling – such as the heat loss coefficient, the volume, the total thermal mass of the components, etc. – and simulations of the dynamic response of the dwelling, the available storage capacity, storage efficiency, state of charge and power shifting capability have been defined and quantified. Nevertheless, accurate data on these thermal properties are often not available or highly uncertain in existing building due to f.i. unknown material properties, partial renovations or bad workmanship. Moreover, the detailed building models used to predict the power shifting capability are found to be computationally intensive, reducing the direct applicability of this method in optimal control applications.
Therefore in this chapter a methodology based on system identification, i.e. grey-box modelling, is introduced to identify reduced-order building models using on-site measurements. The goal of this framework is on the one hand to establish robust, computationally efficient models that can simulate the dynamic response of existing dwellings and on the other hand allowing for the characterisation of the dominant thermal properties.
As explained further, grey-box modelling thereby combines prior knowledge about the physics of the system – here the buildings thermal dynamics – with statistic parameter

estimation methods in order to establish accurate and robust reduced-order models using on-site measurements of existing buildings. Thereby the main benefit of grey-box modelling compared to pure data-driven models or black-box models, lies in the physical interpretability of the model parameters.

Given the context of this thesis, the goal of this chapter is to establish a grey-box modelling framework – including experiment design, parameter estimation and model validation – that allows for the identification of reduced-order models that are suitable for:

- prediction of the heat demand and thermal response on a short prediction horizon (eg. for MPC application)
- long-term simulation of the heat demand and thermal response of dwellings (eg. for implementation in district simulations)
- characterisation of the main thermal properties of dwellings (eg. for the evaluation of the storage efficiency (see Chapter 3))

For the application in MPC, which requires short-term predictions of the heat demand and the indoor temperature variations typically in the range of 15 min to 2 days, the modelling requirements are mainly focussed on capturing the short-term dynamics of the dwelling. In contrast, when reduced-order models are to be applied in long-term simulations, typically over a whole year, e.g. for the simulation of the energy use for heating on an aggregated district or even national level, models should also be able to capture long-term effects such as the heat transfer to the ground.
Characterisation of the thermal properties goes a step further. In order to estimate f.i. the contribution of different building components (e.g. roof, windows and exterior walls) in the effective thermal capacity of the dwelling, the identification process should be able to separate the thermal dynamics of the different components. In this characterisation the identifiability of the model parameters is of significant importance. As will be shown further, whether a parameter can be uniquely estimated – i.e. if a parameter is identifiable – given a certain data set and model structure, is closely related to the model structure and the design of experiment.

In contrast to most studies in literature, that start from measured data of existing buildings, the development of the grey-box modelling framework starts from virtual measurement data generated by detailed building energy simulations. The main benefits of this approach are (i) the access to virtual measurements of all possible temperatures and heat flows within the building, (ii) the absence of measurement noise and (iii) perfect knowledge of the thermal properties of the identified building. As such, the developed framework allows to analyse and improve the experiment design. Thereby specific attention is put on the relation between the

experiment design and modelling approach to the specific application. Nevertheless, as a down-side the use of detailed simulations, as shown further makes it more difficult to obtain uncorrelated white-noise residuals due to the absence of random measurement noise and evidently the detailed models are only an approximation of real behaviour.

Layout of the chapter Firstly, a brief overview of the current state-of-the-art on reduced-order building models and system identification is presented in Sections 4.2 and 4.3. Secondly, the identification framework, including the detailed models used to generate the virtual identification data sets are explained in Section 4.4.
Section 4.5 presents the results of the identification process carried out on the virtual data set. Both a single-zone as well as a multi-zone approach are demonstrated. For each case, different reduced-order models are suggested and a model validation process based on residual analysis of single-step and multi-step predictions, cross-validation by simulation on new data sets and an analysis of the physical interpretation of the model parameters are presented. The goal of this analysis is to assess the relation between the model structure, the available input and output data and the applicability of the model, i.e. for prediction, simulation or characterisation.
Finally, in Section 4.6 the established methodology is applied to develop a reduced-order model using on-site measurements.

4.2 State-of-the-art in system identification for building energy simulation

In general, three approaches are found to derive reduced-order models, referred to as (i) white-box, (ii) grey-box and (iii) black-box modelling. Although, the definitions of these techniques found in literature tend to overlap, the distinction between the methods depends on the balance between the use of prior physical knowledge about the system and the use of data-driven methods.
The first group are physical white-box models, also known as first principle models, which start from the (simplified) fundamental equations established on laws of physics, in this case heat balance equations.
Although in essence all building energy simulations include empirical data for material properties or equations based on empirical correlations, most state-of-the-art building performance simulation packages [77] are considered as white-box models. This is also the case for the building model implemented in the IDEAS-library and used in this thesis.

The use of these white-box building simulation models is widely excepted in engineering and research studies and their reliability is demonstrated in multiple validation studies [124, 125, 126, 99]. In general, the application of these models varies from the preliminary assessment of the indoor comfort and energy performance of buildings in a design stage to the detailed evaluation of new building or system components as well as advanced control strategies. Recently, white-box models have also been applied in the context of demand-side management and model predictive control. For example, Coffey et al [127] developed a software framework with GenOpt to facilitate the use of traditional building energy simulation models for optimization. This framework is however, due to the high computational cost, mainly interesting for research purposes or to deduce heuristic control strategies for complex systems. Zhang et al. [128] compared the use of detailed building energy simulations using TRNSYS with a reduced-order RC model. They showed that the use of detailed models in MPC delivers significantly higher reductions in power demand during on-peak periods (55 % with detailed model, 33 % with simplified model). However, the calculation time for the detailed model is more than 2 orders higher. This high computational cost is generally put forward as the main limitation for their applicability in control applications [129, 51]. Moreover, these models typically require a large amount of detailed building information, that is often not available or highly uncertain in existing buildings. Consequently, a model mismatch may still exist and troublesome model calibration is needed [49].

To overcome the first problem, i.e. the high computational cost, simplified building models have been introduced. Thereby two important approaches are found in literature, which are proven to reduce the computational cost significantly while still capturing the important thermal dynamics of the building and maintaining the physical interpretability. In a first approach, the model complexity is reduced by simplification of the physical representation of the building. These models are generally formulated as state-space models, represented by RC network analogies [130, 131, 84]. Secondly, mathematical model order reduction techniques can be used such as modal decomposition and state aggregation [132, 133, 134]. Nonetheless for both approaches the need for adequate construction data to describe the thermal properties is a prerequisite. Moreover, due to unmodelled system inputs or unknown phenomena a significant bias on the model output may still exist, reducing the practical applicability of the methods for control strategies in existing buildings.

At the other extreme, the use of black-box models is often suggested for control applications. Thereby the input-output relation of the systems is identified using system identification algorithms on measured data. Since no prior knowledge about the system is required, the identification process can be automated reducing the need for modeller interference which is one of the main advantages of black-box modelling. A wide range of black-box modelling

techniques has been applied to identify control models. On the one hand, model-free methods such as fuzzy-logic [135, 136, 137, 138], reinforcement learning [139, 140] and artificial neural networks [141, 142, 143, 144] are shown to have a strong potential for optimal control of complex systems. On the other hand, model-based methods have been applied in various studies. Typical examples are autoregressive models with exogenous inputs (ARX), autoregressive moving average with exogenous input (ARMAX), Box-Jenskins models and subspace identification [145, 146, 147, 148, 129, 149]. Thereby regression based models or transfer function models are used to describe the system dynamics. The main challenge thereby lies in finding the appropriate order of the model that allows for an accurate prediction of the dynamics while maintaining the identifiability of all parameters.
While these black-box methods have shown to accurately predict the input-output relation of the system during normal operation of the building, the robustness of black-box models is low when sudden changes in the building operation occur and extrapolation outside the operation range of the training data needs to be avoided. Moreover, no direct physical interpretation can be given to the model parameters.

A compromise between both stochastic black-box models and deterministic white-box models is introduced by grey-box models [150, 151, 152]. In literature the term grey-box models is used for all reduced-order models that start from a physics-based model structure and use a parameter estimation technique to estimate unknown model parameters from measurements, in this work we follow the more strict definition given in [151]. Thereby a grey-box model is described as a set of stochastic differential equations as explained in Section 4.3. The specification of the set of stochastic differential equations is based on prior knowledge about the building physics and is typically formulated in a state space form. The main advantage of the use of stochastic differential equations lies in the fact that the stochastic framework allows to accommodate random effects. More specific, they allow for a prediction error decomposition, separating the noise into system noise and measurement noise. As such, the unknown model parameters can be estimated using a prediction error method rather than the output error method that is used for fitting the parameters of ordinary differential equations. This avoids the absorption of random effects in the model parameters and enables a whole set of powerful statistical tools [153].
Although grey-box modelling has been used in numerous studies to identify dynamic thermal models for buildings, the application was mostly restricted to the identification of control-oriented models that are able to accurately predicted the heat demand or dynamic thermal response of the building over short prediction horizons [154, 155, 156, 157]. In these studies the focus is mainly on finding reduced-order models which can be used for short-term prediction. Only a limited number of studies are found that exploit the physical interpretability

of the model parameters [154, 158, 159, 160, 161]. Nevertheless, in these studies the interpretation should be handled carefully since the impact of simplifications to the model structure are not always translated correctly to the physical interpretation of the parameters. Moreover, the relation between the model structure, the experiment design and the purpose of the model, i.e. prediction or simulation of the thermal response or characterisation of the physical properties, is not well understood in the context of thermal models for buildings.
Recent developments in the thermal characterisation, using the grey-box modelling framework, of thermal components of buildings as well as whole-building thermal characteristics are found in the IEA EBC Annex 58 project, in which this PhD research was also involved. In the remaining part of this chapter the contribution of this research to the identification of grey-box models for different applications is presented. Thereby specific attention is given to the understanding of the relation between the experiment design, the model structure and the interpretability of the model parameters.

4.3 Grey-box modelling - a theoretic background

Before presenting the developed grey-box modelling framework, a brief theoretic background on grey-box models and the identification process is given in this section. The presented theory is not new and is mainly based on the work of Melgaard [151] and Madsen [162].

4.3.1 Stochastic differential equations

In this work, grey-box models are defined, consistent with [151] as a set of stochastic differential equations given by:

$$dX_t = f(X_t, U_t, \theta_t, t)dt + \sigma(X_t, U_t, \theta_t, t)d\omega_t \tag{4.1}$$

with X_t the states of the system, e.g. the temperatures of the building components. U_t are the measured inputs on time t. These inputs can either be controllable, such as the heating power or the ventilation rate or uncontrollable such as the outdoor climate or occupant gains. θ_t is the set of model parameters.
The main difference between stochastic differential equations and ordinary differential equations, used in white-box models, is the introduction of a system noise model (σ). As such a distinction is made between the deterministic part of the model (f) called the *drift term* and the system noise model (σ) or *diffusion term*. Thereby the former includes the

physical relation between the measured system inputs and outputs, while the latter describes how the system reacts to unmeasured disturbances. These disturbances may result from unmeasured input signals, e.g. opening of windows or wind effects, as well as from physical phenomena that are not included in the drift term, such as long-wave radiation or evaporation. The noise process (ω_t) is a Wiener process, or Brownian motion process, describing Gaussian white noise [151].

Note that although this equation is symbolically written as a differential equation it is interpreted as an integral equation with stochastic integrals [151]. The solution to this stochastic differential equation - which can only be found analytically in simple cases - is thus a stochastic process.

The system is observed through a set of measurements (Y) which are linked to the states of the system and the input signals, by a set of observation equations:

$$Y_k = h(X_k, U_k, k, \theta) + \epsilon_k \tag{4.2}$$

Note that where the system of stochastic differential equations is modelled in continuous time (Eq. 4.1), it is observed in discrete time. ϵ_k is the measurement noise, which is assumed to be Gaussian white noise, thus $\epsilon_k \sim N(0, \sum_k)$.

The grey-box model defined by equations 4.1 and 4.2 is typically formulated in a state-space form:

$$dX_k = (A(\theta)X_t + B(\theta)U_t)dt + \sigma(X_t, U_t, \theta, t)d\omega_t \tag{4.3}$$

$$Y_k = C(\theta)X_k + D(\theta)U_k + \epsilon_k \tag{4.4}$$

with A, B, C and D the system matrices derived from the physical governing equations in terms of the unknown model parameters θ. Thereby, it should be pointed out that the dimensions of A and B may differ from those of C and D, since not all states of the system need to be directly measured. The system equations thus describe the evolution of the stochastic process while the observation equations describe the part that is directly observed.

For the remainder of the chapter, a special case of stochastic differential equations will be used known as a linear, time-invariant grey-box model. Thereby time-invariant points to the fact that the parameters describing the system are assumed constant. The models are said to be linear since the parameters, of both the drift and diffusion terms, do not depend on the states. However, it should be noted that the models are typically non-linear in the parameters as for building simulation often combinations of thermal resistances and capacitors are found.

4.3.2 The estimation process

The estimation of the unknown model parameters in this work is carried out using the Continuous Time Stochastic Modelling toolbox in R (CTSM-R). The software incorporates a maximum likelihood estimation algorithm, which estimates the unknown parameters θ that maximize the likelihood function of a given sequence of measurements $\mathscr{Y}_N = [y_0, y_1, ..., y_N]$:

$$\mathcal{L}(\theta; \mathscr{Y}_N) = \left(\prod_{k=1}^{N} p(y_k \mid \mathscr{Y}_{k-1}, \theta) \right) p(y_0 \mid \theta) \tag{4.5}$$

Note that in this formulation, the joint likelihood function of the parameters given the sequence of measurements, is partitioned into a sequential product of probability densities of one-step-ahead predictions. The parameters are then found as the result of the following optimisation problem:

$$\hat{\theta} = \arg\min\{-ln(\mathcal{L}(\theta; \mathscr{Y}_N))\} \tag{4.6}$$

An exact evaluation of the likelihood function is, apart from simple cases, practically infeasible. However, assuming that the diffusion term is independent of the state variables and driven by a Wiener process, which corresponds to Gaussian noise, the Kalman filter can be used as presented in [163]. The Kalman filter is a recursive filter used to predict the states of the system, given the set of measurements, the model and the known inputs and is shown to be the optimal state estimate under the assumption of Gaussian noise [162]. A full description of the estimation process is presented in [163].

4.4 Description of the identification framework

As explained in the introduction (Section 4.1), the identification framework developed in this chapter starts from detailed building simulations to generate virtual experiments. Compared to the use of experimental data, this approach drastically increases the degrees of freedom in the experiment design, since all modelled temperatures and heat fluxes can be used as virtual input or observation measurements. Moreover, both the boundary conditions and the thermal properties are perfectly known and the impact of measurement noise can be estimated a posteriori.

The main structure of the methodology is shown in Figure 4.1. In a first step, detailed building energy simulations are used to simulate a virtual identification experiment. The main advantage of using simulated data is the high flexibility of possible measurement signals and designs of experiment that can be simulated. In the second step, the actual grey-box model

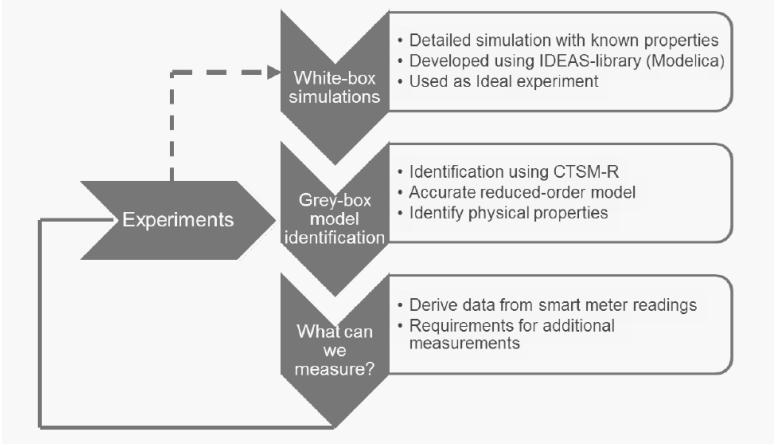

Figure 4.1: Overview of the developed grey-box modelling framework

identification is conducted using the CTSM-R toolbox. Thereby the goal is to evaluate the relation between the design of experiment and the quality of the obtained models in terms of prediction accuracy and physical interpretability of the model parameters. Based on these results guidelines for the design of experiment are deduced, taking into account what signals can be easily measured in practice. In a final step, the identification process is carried out on actual on-site measurement data. The following paragraphs elaborate on the different steps.

4.4.1 Virtual measurements using detailed building simulation

In the first step of the framework, a virtual data set is generated using detailed white-box simulations. The concept and relevant models of the IDEAS-library have already been presented in Chapter 2. Therefore in this section only the model simplifications that are expected to have an impact on the identification process are discussed. Moreover, the set of input and observation variables, that will be used for the identification process, is presented. The main simplifications that are expected to influence the identification process are:

- Assumption of fully mixed, uniform air temperature for complete zone
- Assumption of 1D-heat transfer through building components, assuming uniform surface temperatures and ignoring thermal bridging
- Solar gains and radiant components of internal gains and heating are distributed using area and emissivity weighted distribution factors. Time dependent effects in the

internal distribution of the solar gains – corresponding to e.g. the incident angle of solar radiation – are not accounted for.
- The internal mass of furniture is taken into account by increasing thermal capacity of zone air by a factor 5 [84, 83]
- The infiltration and ventilation rates are constant and not depending on wind conditions
- Internal gains are divided into a radiant and convective component using a constant fraction of 0.5.
- Temperature dependent convection correlations are used for the convective heat transfer at both the interior and exterior surface as specified in Chapter 2

The buildings are simulated using TMY3 weather data for Belgium with a time resolution of 10 minutes [94]. Occupant behaviour is implemented using a stochastic framework described in [3], generating occupancy, thermal gain and electricity demand profiles with a 10 minute time interval. For all cases, simulations are carried out using the variable time step DASSL-solver in Dymola. The solver tolerance is set to 10^{-9} which is found to be a good balance between model accuracy and simulation speed. An equidistant output interval of 5 minutes is used, mimicking typical sample intervals for real measurements.

Two types of virtual experiments are implemented. Firstly, a dedicated identification experiment is simulated for an unoccupied building. Thereby, dedicated input signals are imposed on the heating system in order to have a persistent excitation of the system. In this study, pseudo-random binary sequences (PRBS) are used as input signals to guarantee the input signal is uncorrelated to the climatic boundary conditions. PRBS signals are widely used in the field of system identification and have already successfully been used for grey-box modelling of buildings [164, 151, 161]. Recent studies however argue that these signals may overemphasize the high-frequent response [165, 166], suggesting filtered PRBS signals or multi-sines as an alternative.
Secondly, simulations of dwellings in-use are used as virtual experiments. Thereby the heating system is controlled by a room thermostat, simulating the normal use of the occupied dwelling. The main benefit of this approach, is that the experiments can be carried out in occupied buildings since the heating system is set to maintain thermal comfort. In contrast high indoor temperature variations are obtained using PRBS signals. Nonetheless, important challenges are introduced by the closed-loop control of the heating system and the stochastic occupant behaviour. Moreover, since the persistent excitation obtained by the PRBS-signal is not guaranteed and the temperature variations are typically smaller using a thermostatic control, an important research question is to analyse whether the same model accuracy can be obtained compared to the dedicated heating experiments.

As an output of the virtual experiments, 3 types of output measurements are used in this identification framework. The choice for these signals is based on discussions within the IEA Annex 58 project and corresponds to typical measurements that are also carried out during co-heating tests [167]. Firstly, the indoor air temperature is used. This temperature is directly calculated by the zonal models in IDEAS. Secondly, the surface temperature measurements are included. The surface temperatures are available – from the heatport of the opaque and transparent multi-layer heat conduction models – for each component. A surface area weighted average is used to lump the measurements to the corresponding states when multiple components are modelled as a single state, e.g. the exterior walls. Finally, the heat exchanged between the surface of a component and the zone – by convection and radiation – is extracted from the detailed simulation. The heat flow to each of the states is then obtained by summation of the heat flows of the corresponding components.

4.4.2 Grey-box identification

The identification process consists of three steps. Firstly, a set of reduced-order models of increasing complexity is defined based on the RC-analogy of the building. Secondly, the parameters of the grey-box models are estimated. Thereby the sensitivity to initial values for the unknown parameters is evaluated by repeating the parameter estimation for different initial values. Finally, a validation process is carried out in order to select the optimal model for either short-term prediction, long-term simulation or characterisation of the thermal properties of the dwelling. Note that although they are shown here as three distinct process, in practice the outcome of the validation process may be used to update and extend the model structure in an iterative process, as suggested in [153].

For the first step, generating a set of reduced-order building models, a library of suitable models has been created in this work. This library is the result of grey-box modelling exercises performed on dwellings with a wide range of thermal properties, available observation and input measurements and for the different application purposes. The models are constructed in a forward selection procedure whereby the model complexity is systematically increased in order to find suitable reduced-order models. As explained in [153], systematic improvement of the models is enabled in the grey-box modelling framework by thorough analysis of the characteristics of the diffusion terms and the residuals.
In this forward selection procedure one of the challenges is to preserve the identifiability of the individual model parameters, i.e. all estimated parameters should be uniquely defined in the optimum [168]. Two aspects are important to guarantee the existence of a unique solution. Firstly, the model should be ‘structural identifiable’, meaning that the model is

formulated such that the parameters are uniquely defined. Secondly, the problem of 'practical identifiability' arises when for a given structurally identifiable model, the quality of the data set does not allow to estimate all model parameters. While both problems have not been formally addressed in this work, different internal checks in the model validation process are performed in order to identify such 'over-fitting' problems.
The forward-selection process and the construction of the reduced-order model library, is in a first phase limited to single zone models. In Section 4.5.4 this framework is extended to multi-zone buildings by coupling multiple single-zone models obtained from the individual identification processes. Alternatively, as shown in Section 4.6, zones with a strong thermal coupling may also be aggregated and modelled as a single zone in a pre-processing step.
As will be shown in the results, a limited set of grey-box models is able to cover a wide variety of residential buildings. As such, the construction of the model library allows to automate the identification to some extent. Nonetheless to assure a correct characterisation of the thermal properties, specific adaptation of the models to the specific properties and dynamics of the buildings may be needed and modeller judgement is always required.

When the structure of the model is established, the parameter estimation is carried out using the CTSM-R. Thereby, the solution is shown to be sensitive to the initial values of the parameters and especially of the initial states. This sensitivity is most pronounced for higher order models where the global optimum in the likelihood function is often less clear and the optimizer may converge to local minima. While improvements to the numerical solver in CTSM-R[1] may be considered, it was chosen in this work to check the sensitivity of the parameter estimates to different initial values. Therefore, multiple runs are carried out whereby the different initial values are randomly picked from a normal distribution using the stated minimum and maximum values of the parameters as a 99 % confidence interval.

The final step of the grey-box modelling process is the verification of the accuracy and robustness of the identified grey-box model or the model validation process. As described in [158] the validation process should at least cover the following aspects:

- *Validation on training data.* The 1 step ahead prediction residuals should be 'small' and 'white noise'. A necessary condition for 'white noise' is that there should be neither significant autocorrelation in the residuals nor cross-correlation between the residuals and the input variables.
- *Validation on cross-validation data* The model should be able to predict the output for data that has not been used for the parameter estimation process.
- *Identifiability* All model parameters should be uniquely determined based on the data.

[1] CTSM uses a quasi-Newton method based on the BFGS updating formula and a soft line search algorithm [163]

- *Dynamic stability* In steady state, the model should provide a steady output after transient effects have faded.
- *External validity* The model results should not conflict with previous experience or other known conditions.

To evaluate these criteria three validation steps are carried out. Firstly, the residuals of the 1 step ahead, 1 day ahead and 1 week ahead predictions are analysed to check the validity on training data. Secondly, a simulation of the identified model is carried out for a data period different from the training data, i.e. cross-validation. Finally, the identifiability and external validity of the model are checked in an analysis of the physical interpretability of the identified model parameters. Thereby it is important to note that in practice one would start by specifying minimal model requirements that should be achieved in the validation process in order to accept a model as a function of the application (Section 4.1). In this work however the simulation-based virtual experiments are exploited to identify the potential accuracy that may be expected in ideal circumstances, i.e. noise-less data. Thereby, model refinements in the forward-selection procedure will not be stopped if a certain level of accuracy is reached but continue until problems with the identifiability occur. In practice one may f.i. use likelyhood-ratio tests to decide whether further extending the model is still required [169].

In the residual analysis of step 1, the root mean squared errors (RMSE) as well as the auto-correlation function of the residuals and the cross-correlation of the residuals to the input signals are analysed together with a visual check of the prediction results for any systematic errors.
The RMSE-values quantify the magnitude of the residuals for 1 step ahead, 1 day ahead and 1 week ahead predictions. The 1 step ahead predictions are analysed because they are the output of the prediction error method used for the parameter estimation. The 1 day ahead and 1 week ahead predictions have been included because they cover the range of prediction horizons that may be expected in control applications. As will be shown in the results, a comparison of the RMSE values for the different prediction steps may reveal systematic model errors and over-fitting problems. The latter occurs when not all model parameters can be uniquely estimated given the available data.
The RMSE-values are defined by equation 4.7 with y_k and $\hat{y}_k$ respectively the true and prediction value for the model output at time t and N the length of the data set.

$$RMSE = \sqrt{\frac{1}{N}\sum_{k=1}^{N}(\hat{y}_k - y_k)^2} \tag{4.7}$$

Note that given equation 4.7 the RMSE-value has the same unit as the observation variable

y. To compare the model performance for different data-sets and even different observations, the standardised RMSE-value (sRMSE) is calculated according to equation 4.8 with σ_y the standard deviation of the observation signal over the considered data period.

$$sRMSE = \sqrt{\frac{1}{N\sigma_y^2}\sum_{k=1}^{N}(\hat{y}_k - y_k)^2} \tag{4.8}$$

In addition to the (s)RMSE-values the auto-correlation function of the 1 step ahead predictions is analysed, together with a visual check of the time series plots of the residuals and the inputs of the models. The auto-correlation function (ACF) is defined according to [162] as:

$$ACF(k) = Cor[\epsilon_t, \epsilon_{t+k}] \tag{4.9}$$

i.e. the correlation (Cor) of the residuals at time t (ϵ_t) and the residuals at lag k (ϵ_{t+k}). Based on this definition, white-noise residuals would show an auto-correlation function which is assymptotically equal to 0 except for $k = 0$. Since the grey-box models are defined assuming Gaussian white-noise residuals, it is important to check whether this assumption holds for the identified models. If this is not the case, other statistical tests such as the calculation of the estimated uncertainty of the parameters should be handled carefully. Moreover, as described in [153], the analysis of the auto-correlation function together with correlation of the residuals and the inputs, can be used to pinpoint model deficiencies. As such, a systematic improvement of the model structure in a forward selection procedure is possible. Note that as an alternative to the auto-correlation function, the cumulated periodogram of the 1 step ahead prediction residuals can be analysed, as presented in [154].

In the second validation step, the performance of the model for long-term simulations is evaluated. The use of simulations instead of prediction is made to validate the performance of the model on cross-validation data as well as the dynamic stability of the model. Stability issues are illustrated by a systematic deviation of the simulation output from the measured output. Moreover, the use of simulations also allows to analyse both the high- and low-frequent performance of the model.

Finally, the physical interpretability of the identified parameters is verified. Thereby firstly the covariance matrix of the estimated parameters is verified, checking for statistically insignificant parameters and high correlations between the estimated values, indicating over-fitting problems. Secondly, the identified parameters are compared to the corresponding thermal properties of the building. Note that the main benefit of using simulated virtual experiments is evident here, since the true values for the thermal properties are known.

4.4.3 Application on field measurements

As shown further, the methodology developed in step 1 and 2 of the framework give a good insight in the relation between the experiment, the available measurements, the model structure and the accuracy of the model for prediction, simulation or characterisation. In the third part of the framework, this knowledge is used to apply grey-box modelling on real buildings. Thereby the goal is twofold. On the one hand, it demonstrates the potential of the method in real applications. On the other hand, it is used as feedback on the experiment designs derived from step 2. Where step two demonstrates what should be measured to allow a robust identification, this step will provide feedback on the feasibility of these measurements in real life applications.
The full-scale, on-site measurements used in this work have been collected in the Twin Houses at the Fraunhofer institute in Holzirchen (Germany) in the context of the IEA EBC Annex 58 project, as presented in Chapter 2.

4.5 Identification on simulated data

In this section the system identification process is presented for virtual experiments obtained by detailed simulations using the building simulation models presented in Chapter 2. This section elaborates on the different steps and cases that have been simulated to evaluate the impact of the experiment design and the model structure on the performance of grey-box models. The section consists of three parts. Firstly, the identification process is demonstrated for a single zone dwelling. Thereby both the detailed and grey-box models are modelled using a uniform indoor temperature for the whole dwelling. While this is a strong simplification for real buildings, it allows to clearly analyse the relation between the proposed structure of the grey-box model, the experiment design and the identified thermal properties of the building. Both floor heating and radiator heating systems are compared in this stage, as they significantly differ in the way they excite the thermal mass of the building. As such, different model structures are expected to be optimal for these heat emission systems.
Note that for this first part all input signals are idealised, meaning that the convective and radiative internal gains, solar gains and the heat emitted by the thermal emissions systems – obtained from the simulation results – are directly used as input signals rather than common measurements such as the energy use for heating or the solar irradiation on a horizontal surface. Even though these idealised signals cannot be directly measured in practice, this approach allows to identify an ideal experiment design. In the second part of this section, the translation to realistic measurements is made by analysing the potential of alternative

measurements as well as the impact of noise on the data.
In the third part, the established identification approach is translated to multi-zone buildings. Therefore, a step-wise identification method is presented whereby each zone is identified individually using the temperatures of the adjacent zones as boundary conditions. In Section 4.6, the framework will be demonstrated on actual on-site measurements.

4.5.1 Description of virtual experiments

Simulated buildings and building models The dwellings identified in this section are based on typical Belgian detached houses from respectively the period before 1945 and after 2005, as defined in the TABULA-project [117]. These two buildings have been selected because they represent two extreme cases in terms of insulation level and corresponding dynamic behaviour. While these two buildings are used to demonstrate the methodology in this chapter, all other dwelling typologies of the single family houses presented in the TABULA-project have been analysed as well, resulting in the reduced-order building stock model presented in Chapter 5.
For these typologies only the static thermal properties, required for the degree-day calculations and monthly calculations used in the TABULA-project are specified in the building stock descriptions. In order to evaluate and identify the dynamic thermal properties of the buildings additional assumptions had to be made to translate the stationary building typology descriptions to a dynamic building model:

- The difference between the exterior floor on ground, the floor adjacent to outdoor environment and adjacent to unheated spaces has not been taken into account. The total ground floor is simulated in contact with the ground.
- All roof surfaces are in direct contact to the outer environment. No attic has been implemented in this single zone approach.
- TABULA specifies the total surface area of exterior walls. In order to divide this over the different orientations it is assumed that the front and back wall of the building each cover 27.5 % of the total area. The left and right walls each cover 22.5 % of the total area.
- The internal walls and floor have the same surface area as respectively the exterior walls and the ground floor.
- The building is oriented along the cardinal directions, the facade with the main entrance is oriented North.
- The U-value of the ground floor for the pre-'45 building has been increased to 2.6 $\mathrm{W}/(\mathrm{m}^2\mathrm{K})$, instead of the value (0.85 $\mathrm{W}/(\mathrm{m}^2\mathrm{K})$) defined in the TABULA project,

Table 4.1: Summary of the implemented building properties (pre-'45 (Uninsulated)/ post-'05 dwelling (Insulated))

Zone properties				
Protected volume	766 / 741	m^3		
Infiltration (n50-value)	8 / 1	1/h		
Ventilation rate	0.5 / 0.5	1/h		
Recuperation efficiency	0 / 0.84			
Component properties				
	A $[m^2]$	U $[W/(m^2K)]$	C' $[kJ/(m^2K)]$	g [-]
Exterior walls	255.8 / 201.3	2.2 / 0.4	449.9 / 193.2	
Ground floor	134.3 / 132.0	2.6 / 0.5	449.6 / 96.8	
Roof	158.4 / 152.3	1.7 / 0.3	42.3 /31.9	
Windows	41.2 / 44.1	2.8 / 1.4		0.87 / 0.75
North	10.8 / 11.34	2.8 / 1.4		0.87 / 0.75
East	9.3 / 10.3	2.8 / 1.4		0.87 / 0.75
South	12.2 / 14.11	2.8 / 1.4		0.87 / 0.75
West	8.9 / 8.3	2.8 / 1.4		0.87 / 0.75
Internal wall	255.8 / 201.3	2	150.3/150.3	
Internal floor	134.3 / 132.0	2	168.3/475.8	

since the latter value did not correspond with the suggested floor composition and is argued to be unrealistic.

The main geometrical and thermal properties of the buildings are summarised in Table 4.1. In addition to the zone properties, Table 4.1 shows the surface area (A), heat transfer coefficient (U) , solar transmittance (g) and the effective thermal capacity (C'). The latter, as explained further, is obtained by including the thermal mass of all material layers inside the insulation layer.

The ventilation system is modelled as a constant air-flow corresponding to a balanced ventilation system. Note that this will simplify the identification process since the ventilation losses are not correlated to wind and stack effects. For the post '05 dwelling a heat recovery system is included with a constant efficiency of 84 %. The airflow rate is set to the values stated in the TABULA-project as representative for standard practice.

In line with the previous chapter, two types of heat emission systems are compared, i.e. radiator systems and floor heating systems. Note that, as in the previous chapter, the heat production unit is simplified by an ideal, power limited, heat source. This simplification is allowed since the focus is on the identification of the thermal response of the thermal mass. Therefore the supplied heat will be used as an input to the system rather than the energy use, avoiding the need to include the – mostly non-linear – system efficiency in the identification process.

Input signals In the context of system identification the input signals are typically subdivided in two groups: controllable signals, used in the experiment design to optimally excite the system and uncontrollable signals often called disturbances.

The data sets used for the identification process are obtained using the detailed building simulations described in Section 4.4.1. In order to convert these simulation results into input signals for the identification process, two approaches are compared in this study.
In a first step (Section 4.5.2), idealised input data are used to estimate the maximum accuracy that can be expected for the grey-box model. Thereby, in addition to the ambient air temperature, the effective internal and solar gains obtained from the building simulations are used (Figure 4.2). For the solar gains the effective gains correspond to the calculated fraction of the solar irradiation that is transmitted through the windows. The effective internal gains are directly obtained from the user behaviour model of the IDEAS-library.
Whereas these two inputs are generally available in building simulations, these gains are difficult or even impossible to measure in practice. Therefore in the second step of the study (Section 4.5.3), a step-wise conversion from the effective gains to more realistic measurements is carried out to analyse the impact of the quality of the dataset and the experiment design on the accuracy of the obtained model for simulation and characterisation.

Different scenarios for the alternative input signals are implemented and analysed. As can be seen in Figure 4.2, the internal gains are strongly correlated to the domestic electricity use. For the internal gains, measurements of the domestic electricity use is therefore analysed as an alternative input signal. The latter is selected as it is easy to measure in practice, e.g. obtained by smart meter readings. In addition the obtained model accuracy is compared to a scenario where no information about the internal gains is taken into account.
The use of the effective solar gains is compared against measurements of the global horizontal irradiance, which is relatively easy to measure and often available in local weather stations. Additionally, the total irradiance on the vertical planes along the four cardinal directions are used as input signals. These irradiance data can in practice be directly measured or obtained from the global horizontal irradiance data by preprocessing of the solar data [170, 171].
Finally, it should be noted that the ground temperature is often not measured and therefore the use of the effective ground temperature, measured below the ground floor, is compared against a constant ground temperature of 11 $^{\circ}\mathrm{C}$, i.e. the annual averaged ground temperature obtained by the IDEAS models at a depth of 2 m below the field. The impact of these different input scenarios on the model accuracy is assessed in Section 4.5.3.

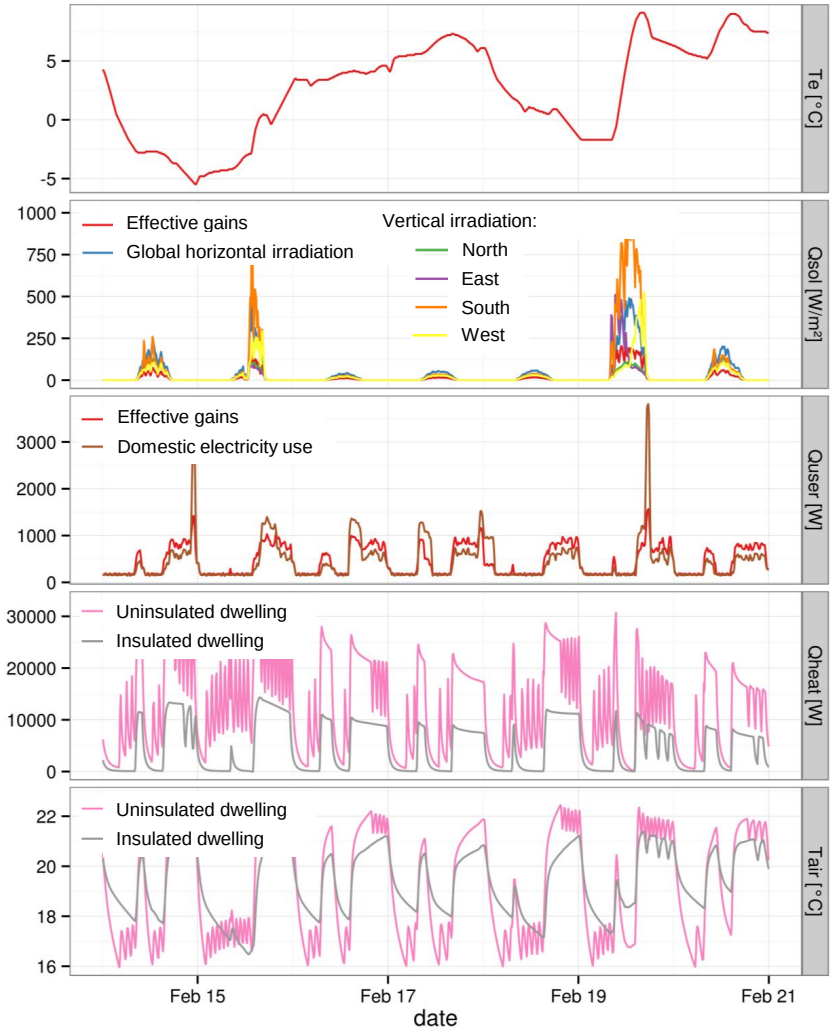

Figure 4.2: Input data and observed indoor air temperature used in the identification on in-use data.

For the controlled input signals, here the heating power, the heat supplied to the emission system is used as a model input. The shape of the input signal itself is the subject of the experiment design. As explained in the introduction again two approaches are considered. Firstly, Section 4.5.2 evaluates a dedicated experiment where a PRBS-signal is used to activate the heating system. Secondly, Section 4.5.3 applies the methodology on an experiment of the building in normal operation, where the heating is controlled by a room thermostat with set point for the operative temperature of 22 $^{\circ}\mathrm{C}$, a dead-band of 1 $^{\circ}\mathrm{C}$ and a setback to 16 $^{\circ}\mathrm{C}$ during the un-occupied periods. For the latter, the resulting indoor air temperature is shown in Figure 4.2. Note however that as an observation in the identification process this indoor air temperature will be used and not the operative temperature, since the indoor air temperature is directly linked to the state that represents the thermal capacity of the indoor air. For both heating experiments the same buildings and climate conditions are simulated.

As explained in the literature review, it is important to properly design the PRBS-signal in order to match it with the dominant time constants of the building. For this study, the PRBS-signal is designed to cover the wide range of frequencies typically encountered in buildings and has a minimum switching frequency of 1 h and a register length of 11 hours, resulting in a total period of 85 days. Higher frequencies are not included since a 15-minute sampling time is used for the identification and since they would be significantly above the dominant time constants of the building. The input signal for the heating system is obtained by multiplying this PRBS signal with 30 % of the nominal power of the heating system, to avoid excessive indoor temperatures when the experiments are carried out in mid-season and summer. Note that when the PRBS signal is used the building is assumed to be unoccupied.

Observation measurements In addition to the system inputs, a good selection and accurate measurement of model outputs is a key to robust system identification. Thereby it should again be emphasised that in the grey-box modelling approach not all states should be included in the observation equation. So called internal states of the systems, in our case the temperatures inside the thermal mass of the components, are updated using the Kalman filter as explained in Section 4.3. Nonetheless, the observability of the system must be guaranteed to allow an identification of all parameters.

Three types of measurements are included with an increasing complexity of the required measurement equipment. Firstly, the indoor air temperature is always included as an observation since it is easy to measure and is an important output for the application in control strategies. Note that the problems of sensor location and stratification are not explicitly evaluated in this Section (see Section 4.6), as we start from simulated data that assume

perfectly mixed zones. To estimate the systematic errors that can result from bad sensor placement or the use of uncalibrated sensors, Section 4.5.3 discusses the impact of (biased) measurement noise on the identification process.
Secondly, surface temperature measurements are included as virtual observation measurements. Thereby the surface temperatures are used as direct observations of the states representing the temperature of the different components. Nevertheless, as will be shown in Section 4.5.2 the surface temperatures of the components are found to not accurately represent the state of the thermal mass of this component since the latter corresponds to the temperature inside the component.
Therefore, as a third alternative, heat flux measurements are included describing the heat flow between the indoor capacity and the building components. Both the total heat flow to the component i ($\dot{Q}_i$ [W]) and the area averaged heat flux ($\dot{q}_i$ [W/m^2]) have been used. For the latter, the area of the component is included as an extra parameter in the grey-box model. For the former, prior knowledge about the surface area of the components is needed. Both are compared here to investigate to what extent this prior knowledge about the building geometry is a prerequisite. Equations 4.10 and 4.11 show the observation equations for respectively the use of heat flow measurements and heat flux measurements to the exterior walls. In these equations T_i and T_w are the indoor temperature and the temperature of the state within the exterior walls, $R_{w,1}$ is the thermal resistance between both states and a_w and f_w are respectively the distribution coefficients for solar gains $(\dot{Q}_s)$ and heating $(\dot{Q}_{heat})$.

$$\dot{Q}_w = \frac{(T_i - T_w)}{R_{w,1}} + a_w \dot{Q}_s + f_w \dot{Q}_{heat} \tag{4.10}$$

$$\dot{q}_w = \left(\frac{(T_i - T_w)}{R_{w,1}} + a_w \dot{Q}_s + f_w \dot{Q}_{heat} \right) / A_w = \dot{Q}_w / A_w \tag{4.11}$$

Note that whereas the use of the heat flow in the observation has the main advantage that only a single model parameter is linked to each of the terms, this is no longer true for the use of the heat flux measurements. As such, difficulties with the identifiability of the model may arise using the latter as observation measurements, as demonstrated in Sections 4.5.2 and 4.6.3.

4.5.2 Identification of single-zone grey-box models for idealised virtual experiments

In this subsection the identification of single zone models using virtual measurements of a dedicated dynamic heating experiment is discussed. Thereby the goal is to find robust and

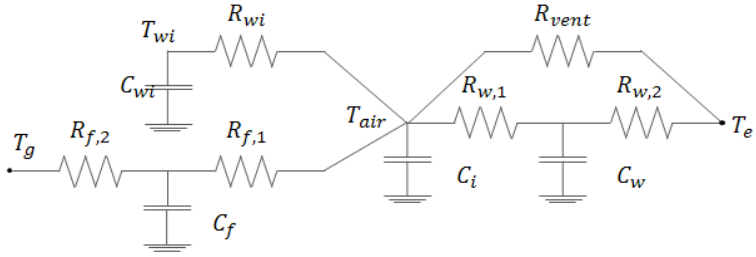

Figure 4.3: RC representation of the 4^{th} order grey-box model. C_i, C_w, C_{wi} and C_f are respectively the indoor air, external wall, internal wall and floor capacity. T_e and T_g are the air and ground temperature used as input for the model. The solar gains and heating input are not shown.

accurate models for the prediction, simulation and characterisation of the dynamic behaviour of residential buildings. An extension to multi-zone dwellings is shown in Section 4.5.4.
Firstly, the model structures evaluated in a forward selection process are presented for both the buildings equipped with radiators and floor heating. Secondly, the input and observation signals used in the identification procedure are presented in the time domain. Note that in this section idealised input signals will be used for solar and internal gains. The impact of these simplifications is assessed in Section 4.5.3.
In the third paragraph, the model validation process is discussed, focusing on the accuracy of the obtained models for short-term predictions as well as simulation. Finally, the physical interpretability of the estimated parameters is discussed. Throughout this analysis the link between the experiment design, the model structure and the quality of the obtained grey-box model is centralised.

Model structures The model structures used to describe the thermal dynamics of the building are derived from resistance-capacitance (RC) networks analogue to electric circuits. Thereby, the distributed thermal mass of the dwelling is lumped to a discrete number of capacitances, depending on the model type. In this work 4 types of models are investigated ranging from 1^{st} to 4^{th} order models. Higher order models have been considered as well but are not presented here as they in most cases resulted in over-fitting problems and thus unreliable results. Figure 4.3 shows the RC representation of the implemented 4^{th} order model. The states of the model are linked to the capacities C_i, C_w, C_{wi} and C_f representing respectively the thermal mass of the indoor air, the envelope, the interior walls and the ground floor. Each of these capacities has been included individually because they are linked to different dynamic boundary conditions and thus excite the thermal mass in a different manner.

Heat transfer through the building components is modelled by two resistances in series with a thermal capacity representing the thermal mass of the component. A parallel resistance (R_{vent}) is included for the ventilation losses. As shown further in the results, this ventilation term will also include the transmission losses through windows, as their thermal mass is negligible to that of the massive exterior and interior walls.
The 4^{th} order model of Figure 4.3 has been established by a forward selection process whereby the model structure is systematically extended starting from a simple first-order model, which only includes C_i. The second order model only includes C_i and C_w, making a distinction between the fast dynamic response of the indoor air and the slower dynamics of the thermal mass of the building structure. The 3^{rd} order model additionally includes a thermal capacity (C_{wi}) for the interior walls to capture the dynamics of the building components are not linked to the outdoor environment. Finally, the 4^{th} order model is obtained by including an additional branch for the heat transfer to the ground.
For all model orders the solar gains, internal gains and heating power are distributed over the capacities, using weight factors that can be specified manually or included in the identification process.

Table 4.2 gives an overview of the different models analysed in this section, the way the thermal gains are introduced into these models, and the observation equations that are used in the identification process. The names of the models are specified by the order of the model, the observation variables, the heating system they are specified for and an optional index when different assumptions for a similar model type are assumed. The stochastic state space equations for each model are found in appendix A.
For the observation variables, the impact of using only indoor air temperature (denoted with Ti) as observation in the identification process is compared to a case where also heat flow measurements (denoted as Q when the flows to all components are considered and Qe when only the flow to the envelope is included) and heat flux measurements (denoted as q) are included. The same models are used for the two building age classes, but different specifications of the observation equations and the allocation of the heating input are used for the floor heating (FH) and radiator systems (Rad). Note however, that for the 1^{st}-, 2^{nd}- and 3^{rd}-order models, the model structures specified for the radiator cases are by means of example also applied to the floor heating cases in order to show the impact of a mismatch in the physics-based model structure.
Models 1_Ti, 2_Ti_Rad_1 and 3_Ti_Rad_1 are respectively the 1^{st}-, 2^{nd}- and 3^{rd}-order models whereby the solar and heating gains are allocated to the indoor air capacity. For model 2_Ti_Rad_2, 3_Ti_Rad_2 and 4_Ti_Rad the distribution coefficients for the solar gains and for the heating power are included in the models estimation process (annotated as 'fitted'

Table 4.2: Summary of the analysed grey-box models, names of the models, the states that are included, the type of observation measurements and the way the gains are allocated to the different capacities.

Model name	States	Observations	Gains
1_Ti	T_i	T_{air}	C_i
2_Ti_Rad_1	T_i, T_w	T_{air}	C_i
2_Ti_FH_1	T_i, T_w	T_{air}	solar: C_i heating: C_w
2_Ti_Rad_2	T_i, T_w	T_{air}	fitted
3_Ti_Rad_1	T_i, T_w, T_{wi}	T_{air}	C_i
3_Ti_FH_1	T_i, T_w, T_{wi}	T_{air}	solar: C_i heating: C_w
3_Ti_Rad_2	T_i, T_w, T_{wi}	T_{air}	fitted
3_Ti_FH_2	T_i, T_w, T_{wi}	T_{air}	solar: C_i heating: C_{wi}
3_TiQe_Rad_1	T_i, T_w, T_{wi}	T_{air}, Q_{fluxe}	C_w
3_TiQ_Rad_2	T_i, T_w, T_{wi}	T_{air}, Q_{flux}	fitted
4_Ti_Rad	T_i, T_w, T_{wi}, T_f	T_{air}	fitted
4_Ti_FH	T_i, T_w, T_{wi}, T_f	T_{air}	solar: fitted heating: C_f
4_TiQ_Rad	T_i, T_w, T_{wi}, T_f	T_{air}, Q_{flux}	fitted
4_TiQ_FH	T_i, T_w, T_{wi}, T_f	T_{air}, Q_{flux}	solar: fitted heating: C_f
4_TiQe_Rad	T_i, T_w, T_{wi}, T_f	T_{air}, Q_{fluxe}	fitted
4_TiQe_FH	T_i, T_w, T_{wi}, T_f	T_{air}, Q_{fluxe}	solar: fitted heating: C_f
4_Tiq_Rad	T_i, T_w, T_{wi}, T_f	T_{air}, q_{flux}	fitted
4_Tiq_FH	T_i, T_w, T_{wi}, T_f	T_{air}, q_{flux}	solar: fitted heating: C_f
4_TiTs_Rad	T_i, T_w, T_{wi}, T_f	T_{air}, T_{surf}	fitted
4_TiTs_FH	T_i, T_w, T_{wi}, T_f	T_{air}, T_{surf}	solar: fitted heating: C_f

in Table 4.2). Compared to the other models, model 3_TiQe_Rad_1 is an exception as here all gains are allocated to the thermal capacity of the exterior walls.

For the buildings equipped with floor heating, additional model structures are proposed, since in contrast to the radiators the heating power of the floor heating is injected directly into the thermal mass of the structure. In the 4^{th}-order models, the heating power is thus directly allocated to the thermal capacity of the floor (C_f), while the distribution coefficients for solar gains are fitted. As such, the '4_xx_FH'-models are obtained. For the 3^{rd}-order models the floor capacity is not included individually into the model therefore two cases are evaluated. In model 3_Ti_FH1 the heating is allocated to the capacity of the exterior walls (C_w) while in model 3_Ti_FH_2 it is allocated to the inner walls (C_{wi}).

Finally, the models 4_TiTs_Rad and 4_TiTs_Rad use the measured surface temperatures as additional observations. Thereby an area weighted average is used to aggregate the surface temperatures of the individual components to respectively the average surface temperature

of the exterior walls, the inner walls and the ground floor.

Identification and validation In this section the results of the model validation process are presented. The validation process is carried out for each of the selected models in order to find the optimal combination of model structure and observation equations that results in accurate models for the prediction, simulation and characterisation of the dynamic response of buildings. This optimal combination is analysed as a function of the building's insulation level, ventilation system and heat emission system. Thereby the goal is to analyse whether the same model structures may be used for different building qualities and heating systems. Moreover the identification process is repeated for different data periods in order to estimate the sensitivity of the results to the data set. In practice this type of test could be done by splitting a measured data set into multiple parts that are alternatively used as training or validation data. However, given the flexibility of using simulated data in this work, three distinct periods in winter and mid-season have been selected. Although other sets with different starting time and duration have been evaluated as well, the results are shown here for a 2-week and 1-month data set in February (Dat 1 and Dat 2) and a 2-week data set in April (Dat 3). Where the latter is shown to demonstrate the impact of the outdoor temperature and more specifically the temperature difference between inside and outside, the former are shown do demonstrate the impact of drastically increasing the duration of the experiment.

As explained in Section 4.4.2, the validation process consists of an analysis of the root mean squared error for short-term predictions, the auto-correlation of the 1 step ahead prediction residuals and the performance of the model for simulation on a cross-validation data set.
Figures 4.4 and 4.5 show the standardised RMSE-values (sRMSE) for both the radiator and floor heating cases and for the uninsulated and insulated dwellings. Thereby, Figure 4.4 demonstrates the impact of different assumptions used to define the model structure, while Figure 4.5 compares the impact of different observation measurements for the 3^{rd}- and 4^{th}-order models.
On the one hand, Figure 4.4 shows a systematic decrease of the sRMSE-values for the 1 step ahead predictions for increasing model orders, i.e. from models 1_Ti to sequentially 2_Ti_Rad_1 and 3_Ti_Rad_1. These decreasing RMSE-values result from the increasing degrees of freedom in the parameter estimation process for increasing model orders when 1 step ahead predictions are carried out on the training data. The decrease is most pronounced when the model is extended from a single state model (1_Ti) to a two state model (2_Ti_Rad_1). For the latter a distinction is possible between the fast response of the indoor air compared to the slower response of the thermal mass of the building structure. The reduction is strongest for the radiator cases, since the radiator heating system directly

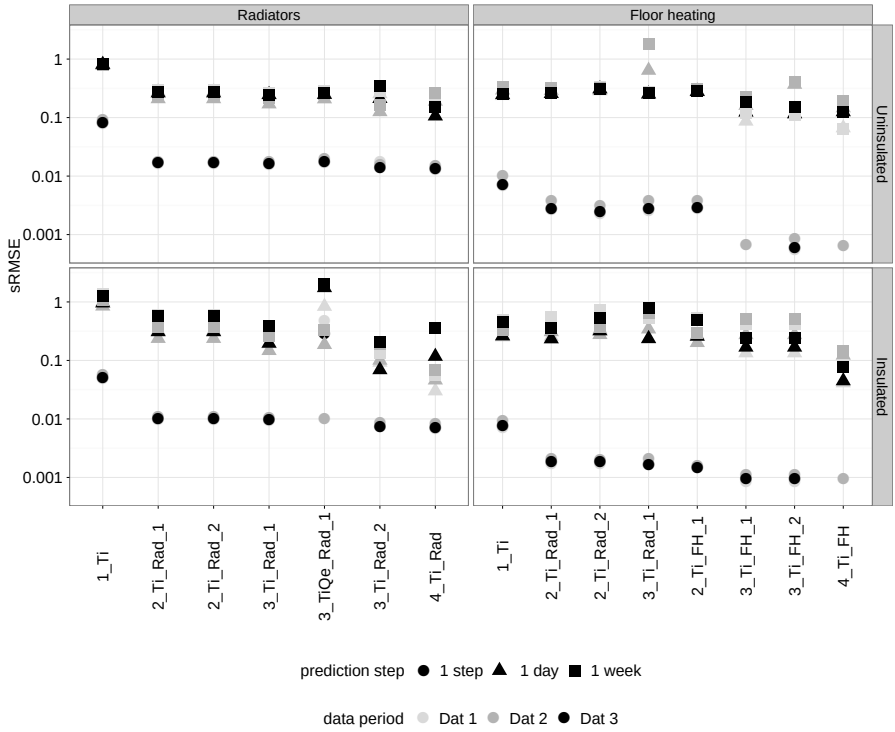

Figure 4.4: Standardised RMSE values (sRMSE) of the 1 step, 1 day and 1 week ahead predictions for both building and heating types as a function of the model structure and the prediction step. The model labels on the x-axis correspond to Table 4.2.

activates both the indoor air and the thermal mass of the structure. Further increasing the model order has a less significant impact on the sRMSE-values for 1 step ahead predictions. For the floor heating cases, an important reduction of the level of the 1 step ahead prediction residuals is also obtained by using the FH-type models whereby the heating power is allocated directly to the thermal mass of the dwelling rather than to the indoor air.

On the other hand, the analysis of the multiple-step ahead predictions shows a significant increase of the sRMSE-values when the prediction step is increased to 1 day and 1 week ahead predictions. Although this increase is expected for all cases due to the propagation of errors over a longer interval, which results in larger temperature deviations, an excessive increase, e.g. by more than 100 %, points out that fundamental errors in the model structure exist or that over-fitting problems occur. This is the case for models 3_TiQe_Rad_1, 3_Ti_Rad_2 and 4_Ti_Rad for the radiator cases and 3_Ti_Rad_1 to 4_Ti_FH_1 for the

floor heating cases. Thereby, as will be explained further, for both heat emission systems the 4^{th} order models using only the indoor air temperature as observation, as well as the 3_Ti_Rad_2 model for the radiator heated building, suffer from over-fitting. This means that inadequate dynamic information is available in the observed signals to estimate all unknown model parameters.

A comparison of the sRMSE values between the radiator and floor heating cases, shows some fundamental differences. Firstly, the sRMSE values of the 1 step ahead predictions are in general lower for the floor heating cases. Due to the thermal mass of the floor which acts as a low-pass filter, the dynamic variation of the indoor air is smoothed. Consequently, lower-order models are able to predict the 1 step ahead temperature response more accurate. Note that the sampling time here is limited to 20 min. In case of floor heating, the 'FH-models', for which the heating is allocated to the thermal capacity of the building components show lower sRMSE values than the models for which the heating power is allocated to C_i, demonstrating the importance of matching the model structure to the physical behaviour of the system. This will become even more important for the physical interpretation of the parameters as discussed further.
Secondly, the significant decrease of the sRMSE values for the long-term predictions that is found for the radiator case (Figure 4.4 (left)) is less pronounced for the floor heating cases. For the radiator heated buildings, the sRMSE-values indicate that the first-order model (1_Ti) is not able to accurately predict the dynamic response of the indoor air to the radiator heating. For the floor heating cases (Figure 4.4 (right)) the decrease in sRMSE value for increasing model orders is less significant since the floor in this case acts as a low-pass filter for the heating system reducing the high-frequent temperature fluctuations. Note that a correct specification of the observation functions and the distribution of the heat input to the system is of significant importance, as higher sRMSE-values are observed when applying the models specified for the radiator heating cases to the floor heated buildings. A similar problem is observed for model 3_TiQe_Rad_1 whereby the heating power of the radiator system is allocated to the exterior wall instead of the indoor air, which again demonstrates the need for a correct physical representation of the system when using

Whereas over-fitting problems are indicated by the sudden increase of the sRMSE values for long-term predictions in Figure 4.4 – as well as by the autocorrelation function of the residuals discussed further – for models 3_Ti_Rad_2 and 4_Ti_Rad for the radiator cases and 3_Ti_FH_2 and 4_Ti_FH for the floor heating cases, Figure 4.5 demonstrates the impact of additional observation equations which are included to increase the identifiability as described above.
In the most detailed case, heat flow measurements to all components are included in the

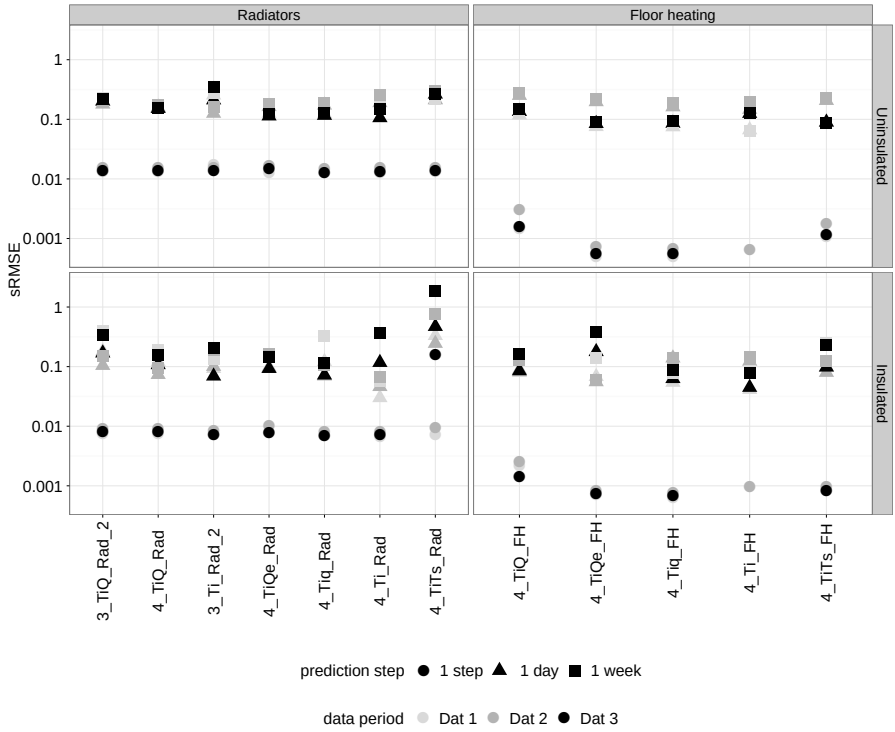

Figure 4.5: Standardised RMSE values (sRMSE), shown on logarithmic scale, of the 1 step, 1 day and 1 week ahead predictions for both building and heating types as a function of the observation variables and data period. The model labels correspond to Table 4.2.

observation equations (models 4_TiQ_Rad and 4_TiQ_FH). For these models Figure 4.5 shows on the one hand increasing sRMSE values for the 1 step ahead predictions. This increase results from the reduction in degrees of freedom as the model needs to follow both the indoor air temperature as the observed heat flows. On the other hand, the difference between 1 step ahead to 1 week ahead predictions is reduced when heat flow measurements to all components are included. This indicates that the model is more stable for long-term simulations.

The same effect is already observed for the radiator cases when only the heat flow measurements to the exterior walls are included in the observation equations (models 4_TiQe_Rad). Nonetheless, this step is less effective in case of floor heating, as explained later in the physical interpretation of the model parameters.

When heat flux measurements are used, no effective improvement of the sRMSE values are apparent since for these heat flux measurement also the surface area of the exterior

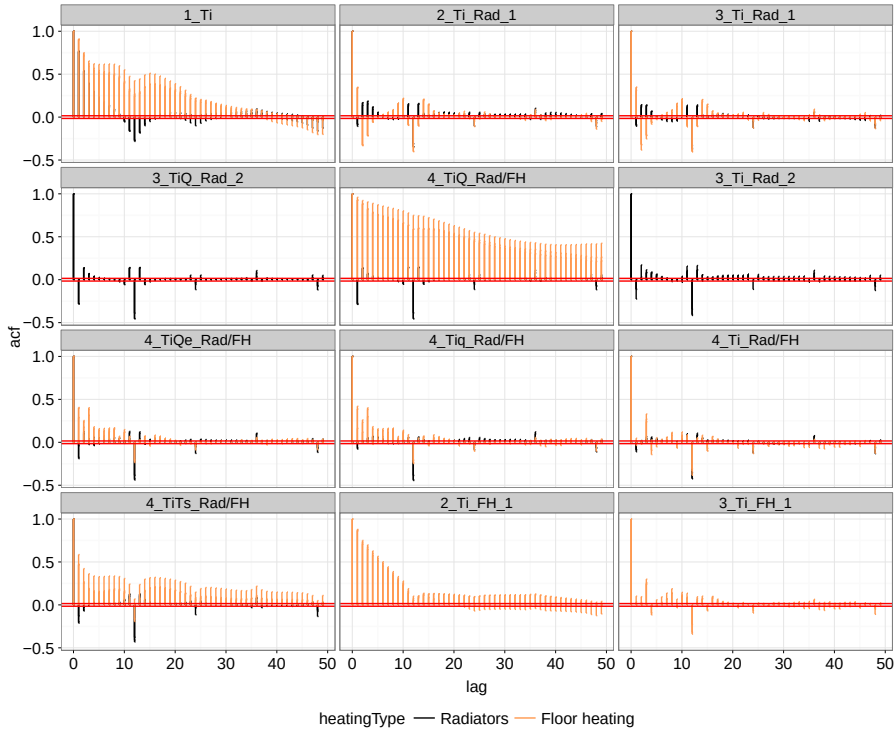

Figure 4.6: Autocorrelation function of the 1 step ahead prediction residuals of the uninsulated building, identified on the 'Dat 2' data period for floor heating and radiator cases.

walls needs to be estimated. This introduces a scaling factor in the observation equation, jeopardizing the identifiability.

Finally, the use of the interior surface temperatures as observation variables (models 4_TiTs_Rad and 4_TiTs_FH) is found to be not effective because the states of the model represent the temperature inside the thermal mass of the components. Consequently, forcing the states to follow the surface temperature does not correspond to the physical representation of the model.

In addition to the size of the residuals, expressed by the (s)RMSE value, Figures 4.6 and 4.7 show the autocorrelation functions (ACF) of the 1 step ahead prediction residuals for respectively the uninsulated and insulated dwelling. In line with the higher RMSE values, a significant level of autocorrelation is found for the 1^{st}-order models, since for almost all lagged time steps the level of the autocorrelation function lays outside the 95 % confidence intervals. This demonstrates that important dynamic information that is available in the data

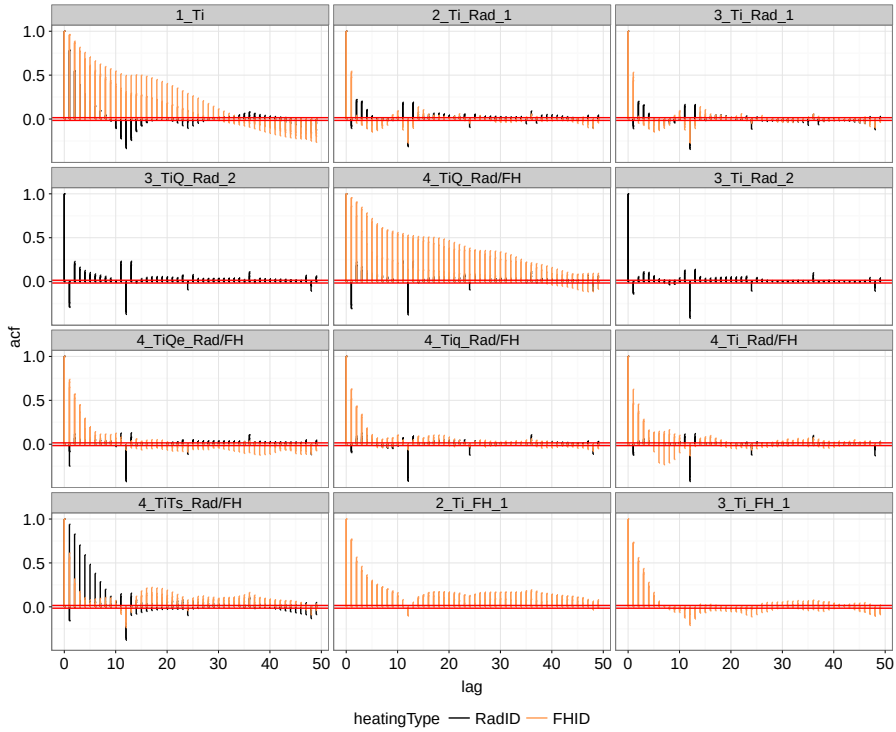

Figure 4.7: Autocorrelation function of the 1 step ahead prediction residuals of the insulated building, identified on the 'Dat 2' data period for floor heating and radiator cases.

is not explained by the model, suggesting that further model extensions are required. Systematically extending the model without including additional measurements results in the expected reduction of the level of autocorrelation in the 1 step ahead prediction residuals. Note that although it is not illustrated here, the cross-correlation function of the residuals and the different inputs has been used together with the estimated scaling factors of the diffusion term to get insight in the cause of the model errors, as described in [153]. Thereby for example a high level of cross-correlation between the residuals and the heating power, together with a high value of the scaling parameter of the noise process for the air capacity revealed that allocating the heating power of the floor heating to the indoor air capacity does not correspond to the actual physical behaviour of the system.

For the floor heating cases, an interesting effect is found whereby the level of autocorrelation of residuals of the models 2_Ti_FH_1 and 3_Ti_FH_1 are higher than those of the corresponding models 2_Ti_Rad_1 and 3_Ti_Rad_1. In the former the heating power

is allocated to the capacity of the exterior walls instead of the indoor air. This was done in order to separate the fast dynamics of the indoor air and the slow dynamics of the thermal mass of the building components, whereby it is expected that allocating the heating power of the floor heating to the massive components rather than the indoor air (i.e. models 2_Ti_FH_1 and 3_Ti_FH_1) would improve the model accuracy. Nevertheless, a comparison of the ACF for models 2_Ti_Rad_1 and 3_Ti_Rad_1 to respectively the ACF for models 2_Ti_FH_1 and 3_Ti_FH_1, reveals that since the floor is in reality not in direct contact to the ambient air temperature the model structure of 2_Ti_FH_1 and 3_Ti_FH_1 does not correspond to the actual thermal dynamics of the building.
The low level of autocorrelation found in models 4_Ti_Rad and 4_Ti_FH indicates that further improvement of the the model structure without including additional information about the system will be difficult since almost all the dynamic information available in the observed indoor air temperature is explained by the 4^{th} order model. The effect of adding heat flow measurements (models 4_Tiq_Rad/FH, 4_TiQe_Rad/FH, 4_TiQ_Rad/FH) is clearly demonstrated by the increased level of auto-correlation in the residuals of the 1 step ahead predictions of the indoor air temperature. Thereby it is evident that when heat flow measurements for all components are included, as is done for models 4_TiQ_Rad and 4_TiQ_FH, a significant amount of dynamics available in the data is not yet explained by the model and further extending the model structure is still possible. Nonetheless, the sRMSE values for these models are found to be small and – as shown further – the simulation performance and characterisation of the thermal properties is found to be reliable. Therefore, it is chosen to stop the forward selection process with the 4^{th}-order models. Moreover, it should be noted that uncorrelated residuals are more difficult to obtain for simulated data due to the absence of random measurement noise on the data. The effect of including measurement noise is illustrated in Section 4.5.3.

In a third step of the model validation process, the performance of the identified models for long-term simulation on cross-validation data is analysed. Thereby the initial values for the internal states are estimated followed by a simulation of the model over a period of 6 months. As such, the accuracy of the model to both short-term and long-term dynamics is evaluated. Moreover, systematic model errors can be easily identified as they will result in a systematic deviation of the model output compared to the observation measurements. These systematic errors result from an over-fitted model, whereby due to a high degree of freedom in the model parameters and inadequate dynamic information in the data, the parameter estimation method converges to a local minimum even though measures were taken to avoid the selection of these solutions. Although in such cases the models show good results for the (s)RMSE values for short-term predictions on the training data, cross-validation is found

to reveal such problems.

Figure 4.8 shows the simulated indoor air temperature for the analysed heat emission systems and building qualities. As already suggested by the sRMSE, a high accuracy is obtained for the 4^{th} order models when heat flux measurements are included (models 4_TiQ_Rad and 4_TiQ_FH). When only the air temperature is used as observation variable (models 4_Ti_Rad and 4_Ti_FH) the simulation performance is found to be unreliable, especially for the insulated building equipped with radiators (Figure 4.8.c) a significant bias is shown, indicating over-fitting problems.
For the lower order models, significant differences exist between the cases. Acceptable performance of the lower order models is found for the uninsulated building equipped with floor heating (Figure 4.8.b). Even for the 1^{st} order models the RMSE value for simulation is limited to 1.1 $^{\circ}\mathrm{C}$ while the average temperature variation is 4.8 $^{\circ}\mathrm{C}$ (sRMSE = 0.23). In contrast, significant differences are found between the model structures for the insulated building (Figure 4.8.d). The residuals for the 1_Ti, 2_Ti_Rad_1 and 3_Ti_FH_1 demonstrate that as a consequence of the simplicity of the model and the mismatch between the model and the actual physics of the system, it is no longer able to describe both the fast response of the indoor air and the long-term dynamics [2] of the thermal mass of the building components. The difference between the two building qualities in performance of the different model orders is explained by the higher difference in time constants of the components in the insulated dwelling on the one hand and to the increasing importance of a correct distribution of the heating and solar gains as the insulation quality improves on the other hand. As such, it is concluded that to accurately simulate the dynamic behaviour of a building, the grey-box model needs to correctly separate heat flow paths that are governed by different boundary conditions and different time-constants. Thereby the required level of detail in the model for simulation applications is more strict than what was found for short-term predictions (Figure 4.5).
Another important observation is that although the level of residuals is typically higher for lower-order models, they are found to be more stable since they show a lower risk for systematic deviations compared to the 4^{th} order models. For the latter, additional observation measurements are needed to guarantee the identifiability of the models and avoid over-fitting problems. This problem of over-fitting is clearly demonstrated for the 4_Ti_Rad model in Figure 4.8.c. Consequently, to guarantee an accurate simulations and avoid systematic deviations, heat flow measurements are a prerequisite for higher-order models. Nonetheless, accurate heat flow measurements may be difficult to obtained on a large scale in practice.

[2] Long-term dynamics here corresponds to time constants of multiple hours up to days.

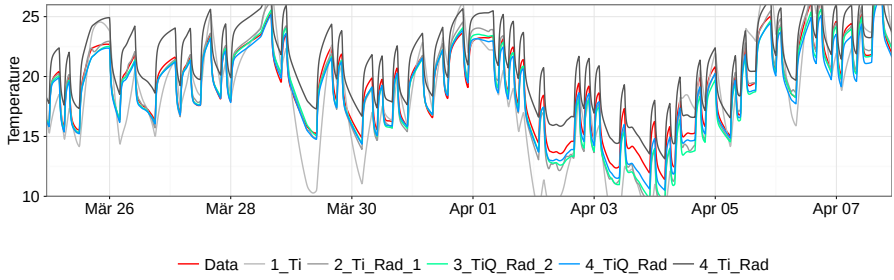

(a) Uninsulated: radiators

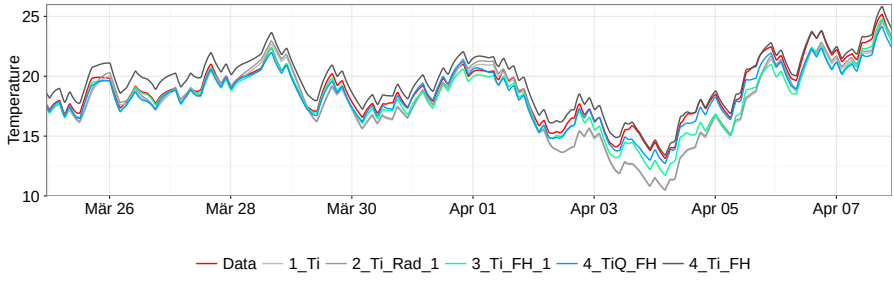

(b) Uninsulated: floor heating

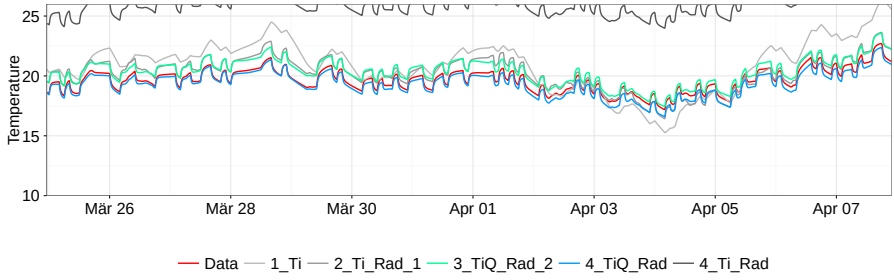

(c) Insulated: radiators

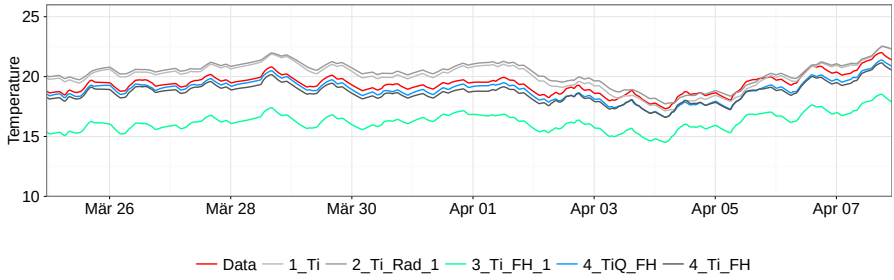

(d) Insulated: floor heating

Figure 4.8: Simulated indoor air temperatures for respectively from top to bottom, the uninsulated dwelling equipped with radiators and floor heating, and the insulated dwelling equipped with radiators and floor heating.

In absence of these detailed measurements, in-depth model validation tests are required to identify potential over-fitting problems. Reducing the model-order may thereby be considered.

Physical interpretation of the parameters As explained in the introduction, the physics-based structure of the grey-box models allows for a direct interpretation of the main thermal properties of the buildings. In this work, the heat loss coefficient (HLC) and the thermal storage capacity of the building are used to asses the physical interpretability of the model parameters. These properties have been chosen as they are closely related to the ADR potential (Chapter 3).

The heat loss coefficient (HLC_e) is defined as the sum of the transmission and ventilation losses per degree of temperature difference between inside and outside and calculated from the identified parameters as:

$$HLC_e = \frac{1}{1/R_{w,1} + 1/R_{w,2}} + \frac{1}{R_{vent}} \tag{4.12}$$

with R_{vent} the resistance for the ventilation losses[3] and $R_{w,1}$ and $R_{w,2}$ respectively the inner and outer thermal resistance of the outer wall, as shown in Figure 4.3. Thereby the roof has been included in HLC_e, as it is subject to the same boundary conditions as the walls. In contrast, the heat loss through the floor (HLC_f), for the 4^{th}-order model, is not included but shown independently as it is not in direct contact with the ambient temperature. HLC_f is calculated from the identified thermal resistances ($R_{f,1}$ and $R_{f,2}$) as:

$$HLC_f = \frac{1}{1/R_{f,1} + 1/R_{f,2}} \tag{4.13}$$

Figure 4.9 shows the impact of the model structure on the estimated heat loss coefficients for both the insulated and uninsulated dwelling when only the indoor air temperature is used as observation variable. The figure demonstrates that for both building qualities, reliable estimates of HLC_e are found for the low-order models (1_Ti and 2_Ti_Rad_1) – shown by the narrow 95 % confidence intervals – with estimated values that lay within the 10 % accuracy range that has been specified for the theoretical value[4]. This is also true for the models 3_Ti_Rad_1 and 3_TiQ_Rad_1 in case of radiator heating. However, the uncertainty

[3] Note that the equivalent thermal resistance for the ventilation losses can be included directly into the definition of HLC_e, as it is implemented as a constant airflow in the detailed simulations. While this assumption is valid for most mechanical ventilation systems, one could for instance try to include the dependence on wind speed and direction to estimate the air flow rate in case of natural ventilated dwellings or high infiltration losses as proposed in [161].

[4] This 10 % accuracy level is chosen arbitrary as an accuracy that is expected to be acceptable for practical applications.

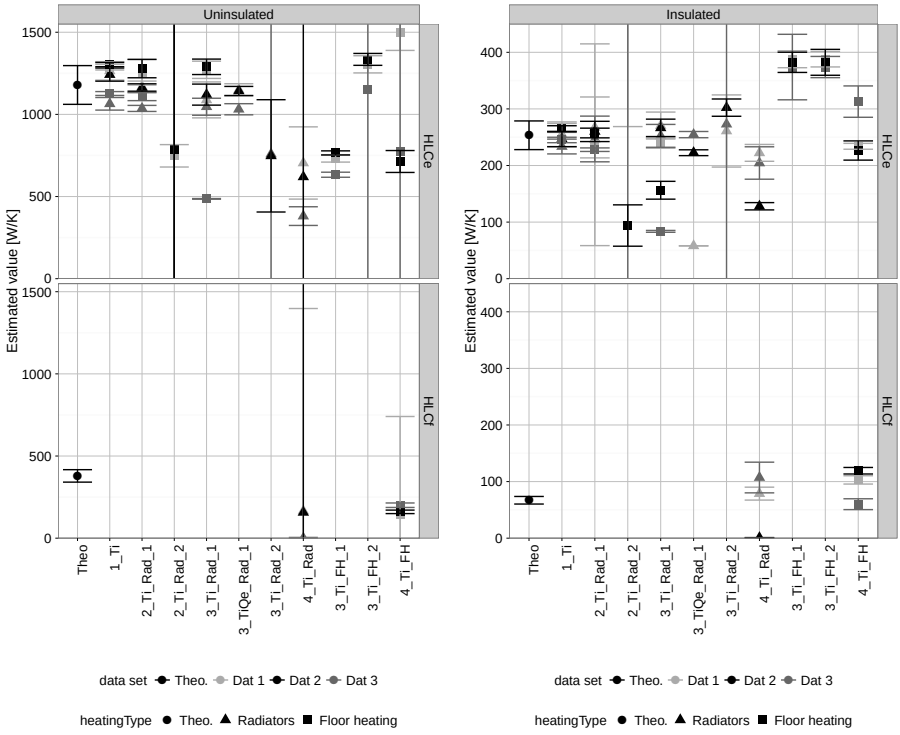

Figure 4.9: Estimated heat loss coefficient as a function of the model structure, with 95% confidence intervals, to the outdoor environment (HLC_e) and to the ground (HLC_f) estimated for the uninsulated and insulated dwellings as a function of the heating system and the data period. For the theoretical values (Theo.) the confidence intervals show the 10% deviation.

on the estimates is found to increase as the insulation quality of the building improves, since the impact of the transmission losses on the dynamic indoor temperature decreases making it harder to estimate an accurate value for HLC_e.

In addition, Figure 4.9 demonstrates that the level of uncertainty drastically increases for higher-order models (3_Ti_Rad_2, 4_Ti_Rad and 4_Ti_FH) when only the air temperature is used as observation. This can be explained by the high degree of freedom in these models, leading to higher levels of correlation between the parameters demonstrating the over-fitting problem.

Finally, it should be pointed out that except for the models 1_Ti and 2_Ti_Rad_1, the spread on the estimated HLC_e for the different data periods is always high for the floor heating cases. This results from the fact that except for model 4_Ti_FH, the floor is not explicitly included in the model. Since the thermal dynamics of the floor are evidently important when

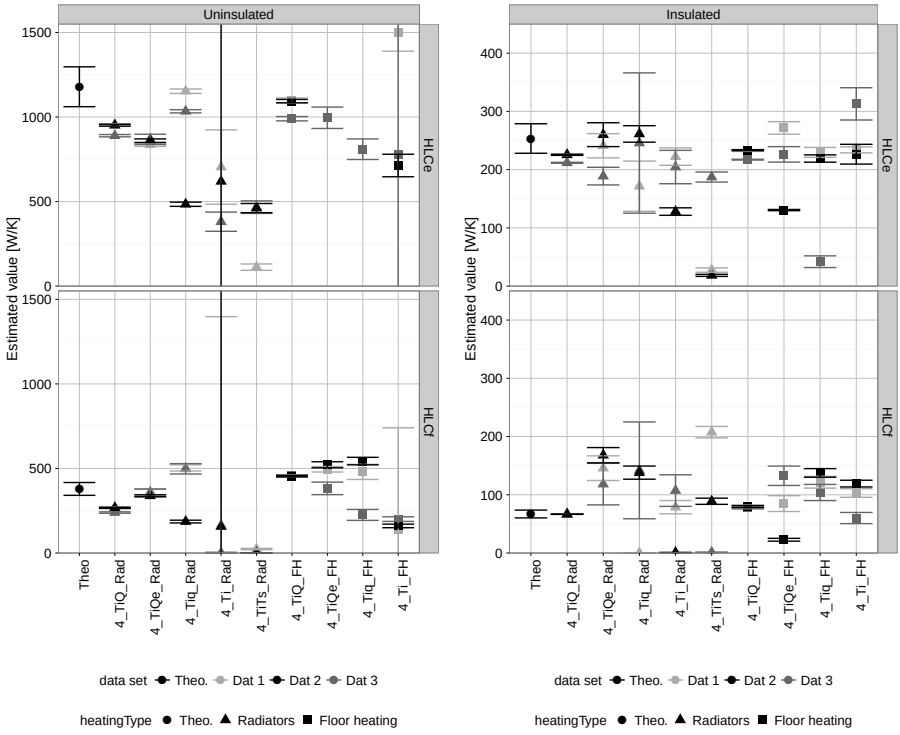

Figure 4.10: Estimated heat loss coefficient as a function of the observation equations, with 95% confidence intervals, to the outdoor environment (HLC_e) and to the ground (HLC_f) estimated for the uninsulated and insulated dwellings as a function of the heating system and the data period. For the theoretical values (Theo) the confidence intervals show the 10% deviation.

floor heating is used, the model structures do not correctly represent the physical behaviour of the dwellings and consequently the model parameters will not have a physical meaning.

To overcome the problem with over-fitting, observed for models 3_TiQ_Rad_1, 4_TiQ_Rad and 4_TiQ_FH, additional observation equations are included. Figure 4.10 shows the impact of adding observation variables to the identification process on the estimated heat loss coefficient. As for the sRMSE-values (Figure 4.5), Figure 4.10 again demonstrates that when only heat flux measurements to the exterior walls are included (models 4_Tiq_Rad and 4_Tiq_FH), the identifiability of the model parameters does not improve significantly since the estimated surface area can be used as a scaling factor. When heat flow measurements to all components are included the level of uncertainty for both the estimated HLC_e and HLC_f is drastically reduced. Nonetheless, given the amount of autocorrelation in the residuals the

confidence intervals should be interpreted carefully. In line with the (s)RMSE-values and the simulation performance, the use of the indoor surface temperatures as observation variables (model 4_TiTs_Rad and 4_TiTs_FH) does not improve the reliability of the estimates.
When the impact of the data period is analysed no significant differences are found between the estimated parameters for the two periods in February ('Dat 1' and 'Dat 2'). The standard deviation of the estimated parameters is however slightly reduced as the length of the data set increases. Nonetheless, it may be concluded that the 2-week period is adequate for an accurate characterisation. For the data period in April ('Dat 3'), the estimated HLC_e for the uninsulated dwellings is found to be lower compared to the other data sets. This effect is likely to be caused by the solar gains on the exterior surface which become important for uninsulated walls and are not included in the reduced-order models. However, this could not be proven since the additional parameters needed to include the solar gains on the exterior surface jeopardised the identifiability of the model.

In order to quantify the ADR potential of dwellings, not only the heat loss coefficient but also the thermal mass that is activated by the heating system should be characterised. Figure 4.11 shows the estimated thermal capacities for the different building components compared to the theoretical value. Thereby it is important to note that these capacities should, as presented in [172, 173], be interpreted as the 'effective' thermal capacity, defined as the fraction of the thermal mass of the structure that is excited by the indoor dynamics induced by the heating system, solar gains and occupant behaviour. Therefore, in line with the findings of [172, 173] only the thermal capacity of the material layers inside the insulation layer is included in order to calculate the theoretical values for the thermal capacities. This assumption is based on the findings that – as shown in Figure 4.12 – only the inner part of a cavity wall, i.e. within the insulation layer, is activated by the short-term dynamics induced by the heating system. If neither insulation nor an air cavity is available, the thermal mass of the entire wall is used to calculate the theoretic value. This is the case for the exterior walls and ground floor of the uninsulated building. The results shown in Figure 4.11 demonstrate, as discussed below, that given a model that is able to capture the dynamics related to the different dominant time constants and taking into account this rule-of-thumb a good correspondence is found between the identified 'effective' thermal capacity and the theoretical values.

Figure 4.11 shows significant differences in the estimated thermal capacity of the building for different model structures and different heating systems. In line with the findings of Figure 4.8, the identification of a single state model for the radiator heating case results in estimated parameters that try to balance the fast dynamics of the indoor air due to the excitation by the heating systems and the slow dynamics of the structural thermal mass. Consequently, as shown on Figure 4.11, total estimated thermal capacity of the 1_Ti model is significantly

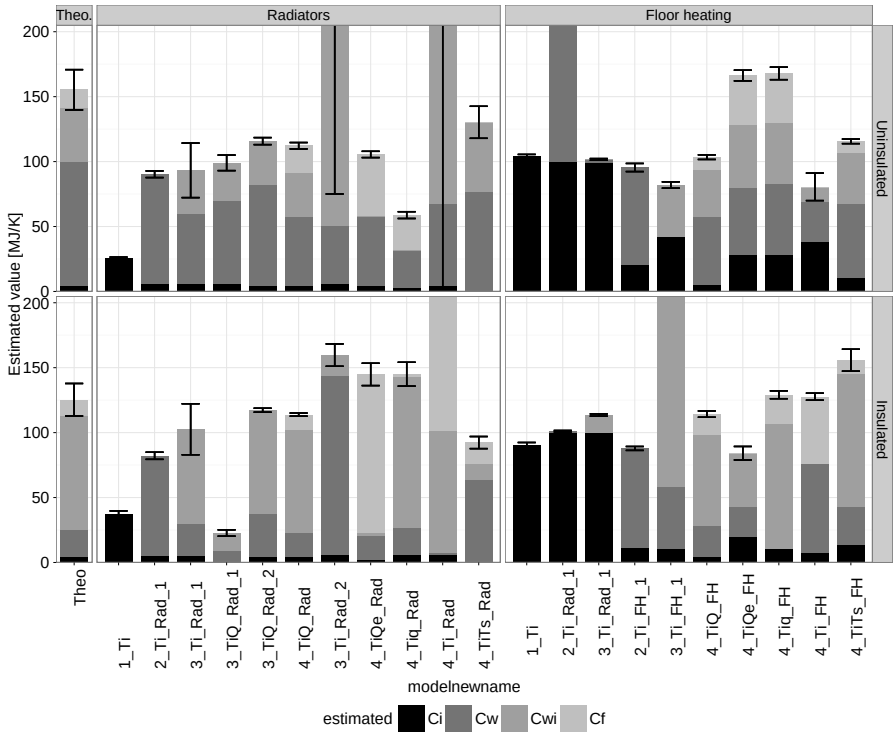

Figure 4.11: Estimated thermal capacities of the exterior walls (C_w), the interior walls (C_{wi}), the ground floor (C_f) and the indoor air (C_i) for the uninsulated and insulated dwellings as a function of the heating system. The theoretical value, shown in the left panes, correspond to the thermal capacity of all material layers inside the insulation layer.

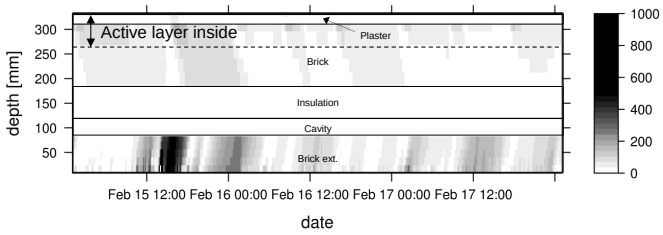

Figure 4.12: Absolute value of the absorbed heat [W] in each point within a cavity wall as a function of time. The outer surface is influence by the outdoor climate, while at the inside the indoor air temperature is controlled by a radiator heating system.

lower than for the other model structures though significantly higher than the estimated thermal mass of the indoor air for the other models and for the theoretic calculation. For the floor heating systems the difference between the total capacity estimated by the 1_Ti model and the higher order models is less pronounced. As discussed in the analysis of the prediction and simulation errors, the floor is acting as a low-pass filter for the heating systems. Consequently, a first-order model is better suited to describe the overall dynamic behaviour of the dwelling compared to the radiator heating case where at least a 2^{nd}-order model is required. In both cases the total thermal mass is lower than the theoretical value of the total thermal mass within the insulation layer and thus also significantly lower than the total thermal capacity of the building fabric.

Extending the model to a 2^{nd}- or 3^{rd}-order model for the radiator heated dwellings results in general in an increase of the estimated total effective storage capacity by on average a factor 3 compared to 1_Ti, resulting in estimated values of the same order of magnitude between the different models and even between the different heating systems. Nevertheless as indicated by the colour-scale the distribution of the total thermal mass over the different components differs significantly between the models. In order to obtain a distribution that corresponds to the theoretic physical values, a 4^{th} order model in combination with heat flow measurements to all components is required. When these heat flow measurements are not available unreliable estimates for the individual thermal capacities are obtained with large variations between the models as a result of the over-fitting problems – even though the total capacity may be in the same order of magnitude.

For the floor heated dwellings, an interesting effect should be emphasised. As discussed in the residual analysis, the low-pass filtering effect of the floor limits the variations in the dynamic response of the different components. Consequently, for models 1_Ti, 2_Ti_Rad_1 and 3_Ti_Rad_1, for which the heating power is allocated to the air capacity, the estimated value for this capacity corresponds closely to the total capacity found by the 4^{th}-order models. This again shows that in case of floor heating, lower order models can be used to accurately simulate the dynamic response of the building. Nonetheless, to interpret the effective capacity of the individual components, heat flow measurements are a prerequisite.

Finally, although the same trends are observed when comparing the estimated thermal capacity for the same models between the insulated and uninsulated dwelling, the estimated capacity for the uninsulated dwelling is generally significantly lower than the theoretical value. For the uninsulated building the entire outer wall is included in the theoretic thermal capacity, which is clearly an overestimation of the effective capacity and demonstrates that not the entire thickness of the 25 cm outer brick wall is activated by the heating system. For the insulated dwellings, the use of the material layers within the insulation layer shows to be a good approximation for the effective thermal storage capacity of the building components.

The latter is therefore considered to be an acceptable rule of thumb when making an initial guess for the active structural thermal capacity of a dwelling.

4.5.3 Sensitivity of identification process to the input data and design of experiment

In the previous section simulated data of a dedicated, dynamic heating experiment were used for the identification of grey-box models. Thereby a PRBS signal was used to guarantee that the input signal is uncorrelated to the climate input. Moreover, the building was simulated without occupants. In this section, the identification process is re-evaluated using virtual measurements for occupied buildings. As such, this section assesses whether the grey-box modelling frame-work may be applied in occupied dwellings. This would drastically improve its practical applicability in both a control and a characterisation context.
Only the radiator heated cases are presented here. Nevertheless the conclusions are also valid for buildings equipped with floor heating. Note that the results of this section were also published in the Energy and Buildings paper: "Quality of grey-box models and identified parameters as a function of the accuracy of input and observation signals [172]."

In contrast to the PRBS-signal of the previous section, normal use of the central thermostat is assumed here, following a fixed heating schedule. The thermostat is modelled with a dead-band of 1 $^{\circ}\mathrm{C}$, a temperature set point of 22 $^{\circ}\mathrm{C}$ during occupied periods and a set point of 16 $^{\circ}\mathrm{C}$ at night and when the building is unoccupied. The internal gains are modelled using a stochastic user-behaviour model as already described in Section 4.5.1. The resulting input signals, as well as the observed indoor air temperatures are shown in Figure 4.2 (see Section 4.5.1).

The following paragraphs firstly describe the results of the identification based on data of the occupied building using the effective gains as input signals, similar to Section 4.5.2. This analysis is carried out to investigate if the same level of accuracy can be achieved as for the dedicated experiment of previous section. Secondly, the impact of replacing the effective gains by more realistic input signals is quantified. Finally, the influence of noise on the virtual measurements is discussed.

Identification on idealised in-use data In this paragraph the performance of grey-box models identified on in-use buildings is verified, analogue to the process discussed in the previous section. The analysed model structures are the same as those of the previous section (see Table 4.2).

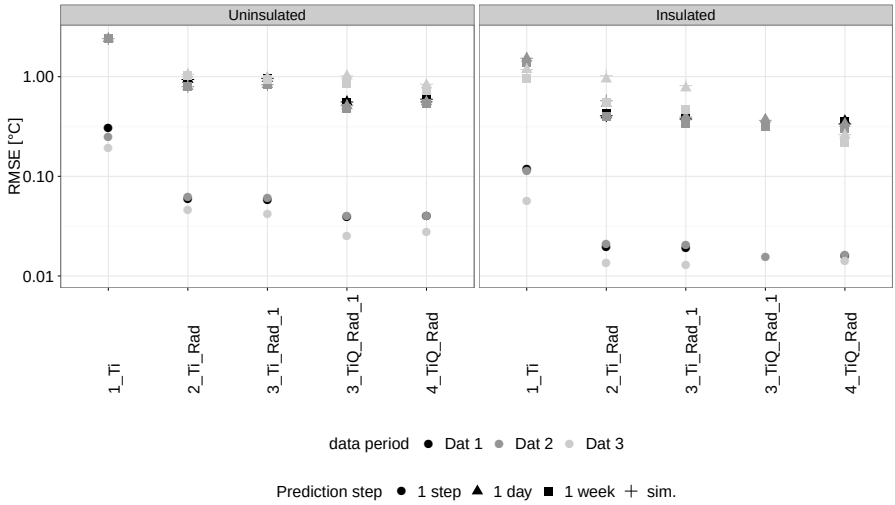

Figure 4.13: RMSE-values of the indoor temperature [$^{\circ}\mathrm{C}$] for 1 step, 2-day and 1 week prediction steps as a function of the data period used to train the model and the model type, for the uninsulated and insulated dwelling.

In the first model validation step, Figure 4.13 shows the RMSE-value as a function of the data period, the model structure, the building type and the prediction step. For both the insulated and uninsulated building it is evident that, as for the PRBS-experiment, a 1^{st}-order model does not allow for accurate predictions of the thermal dynamics of buildings, even for small prediction intervals (10 min) RMSE values up to 0.3 $^{\circ}\mathrm{C}$ are found. In line with the results for the PRBS data, the level of the 1 step ahead prediction residuals decreases significantly when the model is extended to a 2^{nd}-order model. For further extensions of the model structure, the reduction of the RMSE values is less significant.

For both the insulated and uninsulated building the level of residuals increases as the prediction window increases from 1 step predictions to week-ahead predictions and simulations. Compared to the identified models for the PRBS cases (Figure 4.5) where over-fitting problems only occurred for 3^{rd} and 4^{th} order models, here an increase in the long-term prediction errors is already shown for the 2^{nd} order model. In other words, this indicates that it is more difficult to capture the long-term dynamics with in-use data. Due to the thermostatic control, the indoor temperature is only fluctuating within a narrow band following the day-night schedule. Consequently, less dynamic information is available in the data. In order to suppress the increase of the residuals for long-term predictions, additional dynamic information is added to the identification process by including heat flow measurements, as is done for models 3_TiQ_Rad_1 and 4_TiQ_Rad.

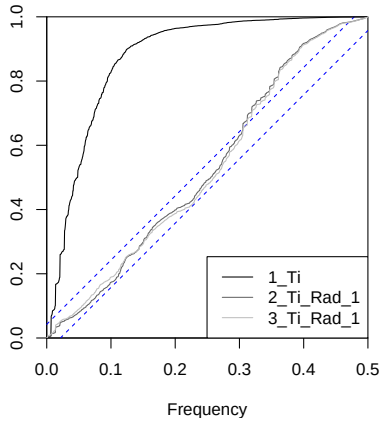

Figure 4.14: Cumulated periodogram for the 1^{st}, 2^{nd} and 3^{rd} order models identified using the air temperature as observation variable.

This need for additional measurements in order to increase the identifiability of the parameters in the higher order models is also demonstrated by the auto-correlation function of the residuals. As shown by the cumulated periodogram in Figure 4.14 the level of auto-correlation in the residuals for the 3^{rd} order model using the air temperature as observation is low. This indicates that the model is able to explain the dynamics contained in the data set. In order to further increase the model order, avoiding over-fitting, additional observation measurements, i.e. heat flow measurements, are required. Note that in the context of demand-side management in Smart Grids and MPC, these observation measurements will not commonly be available and the identifiability of higher order models can therefore not be guaranteed.

Figure 4.13 also demonstrates the influence of the data period on the resulting model quality. This impact is more pronounced than for the PRBS cases. Since the dynamics induced by the heating system are less available for the periods in mid-season and the temperature difference between inside and outside decreases ('Dat 3') over-fitting is more pronounced for these periods. Consequently, to assure the accuracy of the identification process, appropriate climate conditions, i.e. an adequate temperature difference between inside and outside, are a prerequisite. For the analysis of the more realistic input signals data period 1 will be used.

As for the PRBS cases, the parameters of the grey-box models are compared to the theoretical physical properties that were implemented in the detailed simulations. Figure 4.15.a shows the relative estimate of the heat loss coefficient as a function of the ideal input data sets

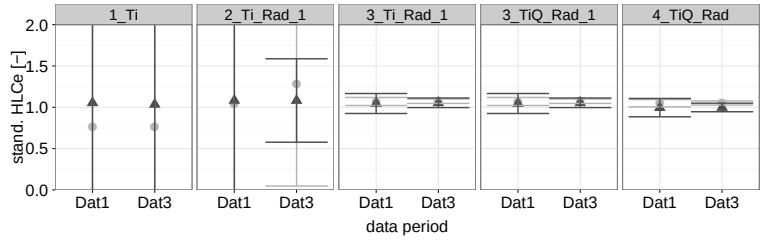

(a) Heat loss coefficient (HLC_e)

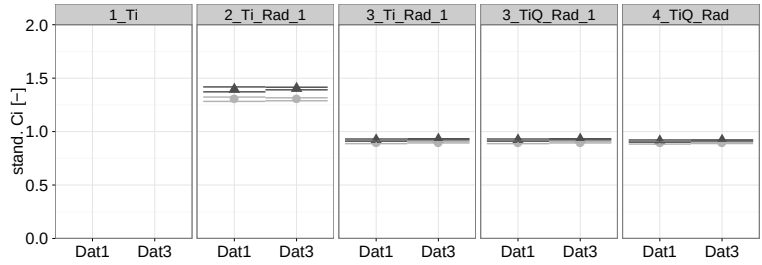

(b) Indoor air capacity (C_i)

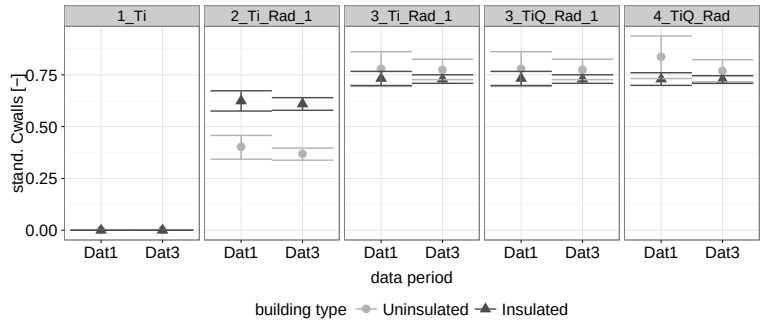

(c) Capacity of envelope, internal walls and floors (C_{walls})

Figure 4.15: Standardised estimates for the heat loss coefficient of the envelope (HLC_e), the indoor air capacity (C_i) and the sum of the capacities of the exterior walls, interior walls and floor (C_{walls}) of the uninsulated and insulated dwelling. Note that theoretical value for the thermal capacity is corrected to include only the capacity within the thermal insulation layer.

and the model order for both the well-insulated and the uninsulated dwellings. The relative estimate is obtained by dividing the estimated value by the theoretical value calculated based on the building properties of Table 4.1.

Figure 4.15.a shows a high uncertainty for the estimated HLC when only the air temperature is used as an observation equation. Whereas these models showed acceptable results for short-term predictions of the thermal behaviour of the building and may therefore be applicable in MPC control, additional measurements and higher order models are required for an accurate characterisation of the physical parameters.

Figure 4.15.b and 4.15.c show the estimated values of respectively the internal air capacity and the thermal capacity of the opaque components of the building envelope. Thereby the theoretical values for the capacity of the walls have been corrected to only include the thermal capacity within the insulation layer. As discussed in the previous section this assumption is based on the fact that mostly the first few centimetres of the walls are excited by the heating system and therefore only the effective thermal capacity can be found in the parameter estimation. Using only the thermal mass of the materials within the insulation layer, good agreement is found between the estimated and theoretical thermal capacities and heat loss coefficients.
Moreover, even though large differences exist between the thermal properties of both buildings, similar model structures could be used to predict their thermal behaviour. Compared to the identification on the PRBS experiments shown in previous section, the identifiability of the parameters is found to be less accurate as demonstrated by higher standard deviations on the estimated values and more over-fitting problems. Nonetheless, the practical benefit of the fact that this method can be used in occupied buildings may outweigh this higher uncertainty. Thereby it should be noted that qualitative heat flow measurements may not be possible in practice.

Identification using realistic input and observation signals In this section the impact of the alternative input data on the properties of the residuals and the estimated parameters is evaluated. As explained in Section 4.5.1, alternative input signals are used as an input for the solar and internal gains. In total, five scenario's have been implemented and are compared against the reference scenario using the ideal inputs as discussed above. The scenario's are summarised in Table 4.3.

Scenario A is the reference scenario using the effective solar and internal gains as input signals. In scenario B, the effective solar gains are replaced by the global horizontal solar irradiance, which is easy to measure in practice. Note that one could think of using the

Table 4.3: Scenario's for the implementation of realistic input signals

Scenario	Solar gains	Internal gains
A	Effective gains	Effective gains
B	Global horizontal irradiation	Effective gains
C	Oriented vertical irradiation	Effective gains
D	Effective gains	Domestic electricity
E	Oriented vertical irradiation	Domestic electricity
F	Effective gains	No input

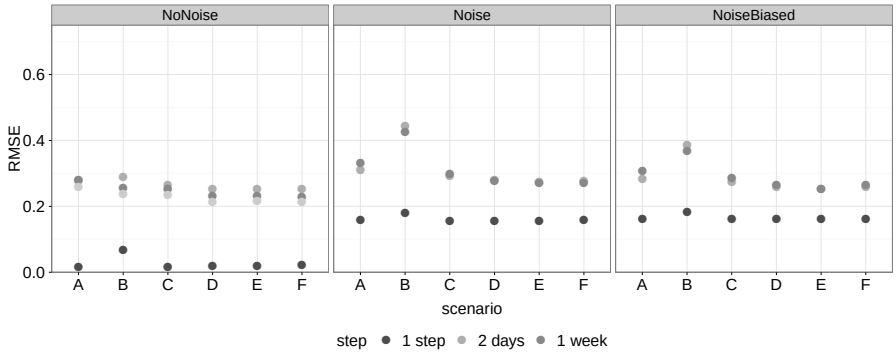

Figure 4.16: RMSE-values for the indoor air temperature for the 4^{th} order model for the insulated dwelling obtained for data period 'Dat 1' as a function of the input scenario and the noise type applied on the measurement data

local electricity production of a photovoltaic system as measure of the solar irradiation as an alternative for the global horizontal irradiation. Scenario C uses the solar irradiance on the vertical planes along the cardinal directions. As such, the orientation of windows can be accounted for. In scenario D, virtual measurements of the domestic electricity use is used as an alternative input for the internal gains. A combination of the alternative inputs for solar and user gains are used in scenario E. Finally, scenario F shows a case where no information of the internal gains is used.
The results show the sensitivity analysis for the insulated dwelling using the 4_TiQ_Rad-model. This 4^{th} order model uses heat flow measurements to all components and is chosen because it showed the best performance for prediction, simulation and characterisation, as demonstrated in the previous paragraphs.

The left hand pane of Figure 4.16 shows the RMSE values as a function of the input scenario, when no measurement noise is added to the simulations. Compared to reference scenario A, the use of the horizontal global solar irradiance results in a significant increase of the RMSE-values. This can be explained by the fact that the g-value of the glazing is not constant but

depends on the incident angle. Also the direct solar gains depend strongly on the orientation of the windows which is not accounted for in scenario B. In contrast, the influence of using the total solar irradiance on the vertical planes along the cardinal directions is negligible. The use of the domestic electricity demand as an input for the internal gains (scenario D) improves the model accuracy compared to scenario F where no user information is available, since the time of use of electricity by the occupants is highly correlated to the moments with high internal gains. Comparing scenario D to the reference scenario shows no significant increase of the RMSE-values. Moreover, scenario E demonstrates that in practice a combination of the solar irradiation along the different orientations and the domestic electricity demand as inputs for respectively the solar and user gains can be used without jeopardizing the model accuracy for short-term predictions and simulations.

Finally, Figure 4.17 shows the comparison of the estimated model parameters to the theoretical values. The estimated values have been standardised by dividing the estimated by the theoretical values. The estimated UA-value and thermal capacity of the walls are found to be estimated accurately and are insensitive for different data scenarios. In contrast, the gA-value obtained for scenario C, calculated as the sum of the estimated absorption coefficients is found to be between 10.3 m^2 and 10.8 m^2 depending on the data period, using the solar radiation on the vertical planes as input. The theoretical value, implemented in the detailed model, is 30.6 m^2 with a g-value of 0.75 and a total window area of 40.8 m^2. Therefore the model tends to drastically underestimate the influence of solar radiation. The estimated ventilation loss and thermal capacity of the indoor air show significant differences for the different models in case of the insulated building. For scenario B the estimated ventilation loss is overestimated by 1.4 %. For scenarios C to F an underestimation of 1.8 - 6.7 % is found. The indoor air capacity is overestimated by 1.3 - 6.8 % using the realistic input signals. A high correlation between both parameters is also shown, indicating over-fitting problems. Nonetheless, the results are considered to be acceptable for typical engineering applications and for the identification of the ADR potential of the building using the methods described in chapter 4.

Influence of noise on the data In this final step of the sensitivity analysis the impact of noise on the measured data is analysed. Thereby both random unbiased and biased noise are investigated. The former corresponds to typical readings of calibrated sensors, whereas the latter emulates un-calibrated sensor or inaccurate sensor placement. For the virtual air temperature measurements a Gaussian random noise is assumed with a mean bias of 0.25 $^{\circ}\mathrm{C}$ and a standard deviation of 0.15 $^{\circ}\mathrm{C}$. For the heat flux measurements the Gaussian random noise term has a mean bias of +10 % of the simulated value and a standard deviation

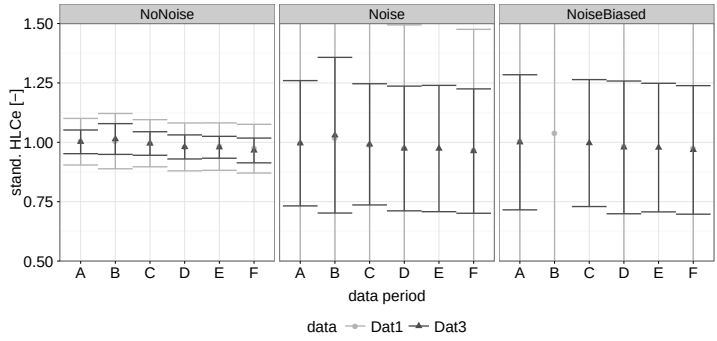

(a) Heat loss coefficient of the envelope

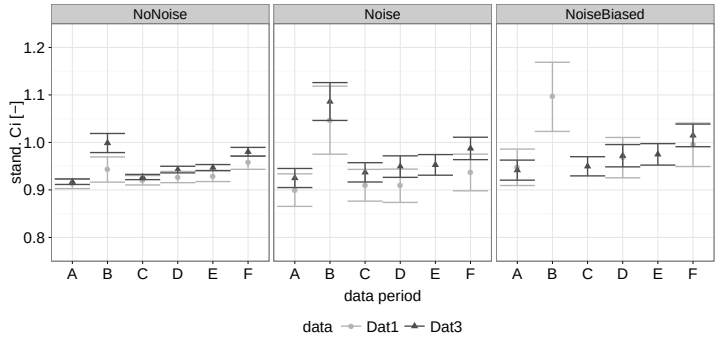

(b) Indoor air capacity

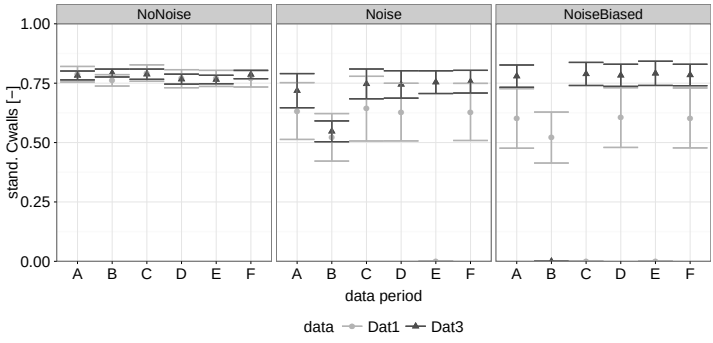

(c) Capacity of envelope, internal walls and floors

Figure 4.17: Standardised estimates for the heat loss coefficient of the envelope (HLC_e), the indoor air capacity (C_i) and the sum of the capacities of the exterior walls, interior walls and floor (C_{walls}) of the uninsulated (grey) and insulated dwelling (black). Contrasting the influence of the noise properties and the input scenario. Note that theoretical value for the thermal capacity is corrected to include only the capacity within the thermal insulation layer.

of 10 %. For the other measurements unbiased random noise has been used, similar to the previous scenario.

The middle and right hand panes of Figure 4.16 demonstrate the impact of the measurement noise on the RMSE values for short-term predictions. On the one hand the figure shows a significant increase of the 1 step prediction errors. This increase is directly related to the fact that the model is logically not able to predict the noise process. On the other hand, the 2 day ahead and 1 week ahead predictions are not significantly influenced by the fact that the models are identified on noise data. Since random noise is used, the dynamic impact of the noise is averaged out when the size of the prediction step increases. Thereby it is interesting to point out that also in case of biased noise, no significant impact on the RMSE-values is found. This shows that the level of residuals between the prediction and simulation results and the measured data is not affected by using biased sensors, since the dynamics in the signal have not changed. Nonetheless, the biased sensors introduce a systematic error between the predicted output and the true value of the variable, leading to biased estimates for the parameters. Note that this is not necessarily a problem for control applications, where typically relative quantities are used, but are of fundamental importance for a correct characterisation of the physical properties.

Figure 4.17 shows the resulting estimated HLC and thermal capacities. Compared to the estimated values on noiseless data, a significant increase of the 95 % confidence intervals is shown when unbiased random noise on the measurement data is added. Although the uncertainty on the estimated parameters increases significantly, no significant influence on the estimated values is found for the insulated building. In contrast, Figure 4.17 shows how the biased noise terms affect the estimated parameter values, especially for the ventilation losses and the thermal capacities. This deviation is in line with the findings of the RMSE values and again demonstrates that whereas the use of biased sensors does not influence the prediction accuracy, it may jeopardize the physical interpretability of the results. Nevertheless, the bias on the estimated values is found to be insignificant compared to the uncertainty on the estimated values induced by the random noise term. Compared to the unbiased noise, the estimated UA-values have increased with 4 % while the estimated ventilation loss is reduced with 4 %. Note that this change is a function of the bias level and the signal-to-noise ratio.

4.5.4 Multi-zone models

In the final part of this section the applicability of the grey-box model framework is extended to multi-zone buildings. Therefore the uninsulated and insulated buildings – presented in the previous parts – have been implemented as 2-zone models by separating the ground and first floor. The former is assumed to be the day-zone while the latter is modelled as the night-zone. Note that the same model structure will be used in Chapter 5 to establish a bottom-up, reduced-order building stock model for the Belgian residential housing stock. Thereby the same grey-box modelling approach as the one presented in this section is applied to each of the different typologies of the housing stock.
Two approaches for the model identification are considered. A single identification step –whereby parameters of the coupled model of both day- and night-zones are estimated together – is compared to a decoupled estimation of the day- and night-zones whereby the indoor temperature of the day-zone is used as an input for the identification of the night-zone and vice versa. The latter, is included since for the coupled approach identifiability problems occurred, as shown in Section 4.5.4.
In line with the previous subsections, first an overview of the model structures is given, followed by a brief description of the data used for the parameter estimation. Next, the model validation process describes the performance of the models for short-term predictions and long-term simulation. The emphasis is thereby put on the evaluation of the model performance to capture the dynamic response of the buildings on a high time-resolution, since these models are to be used in the dynamic reduced-order building stock model presented in Chapter 5.
In the final paragraph of the section, the physical interpretation of the parameters is summarised.

Model structures To obtain the adequate model structure a forward selection procedure has been evaluated. This process has been demonstrated in previous sections and will not be elaborated here. The resulting model structure is shown in Figure 4.18.
The day-zone is modelled using 4 states corresponding to a thermal capacity for the exterior walls (C_w), the ground floor (C_f), the internal walls (C_{wi}) and the indoor air (C_i). The thermal mass of the night-zone is lumped to a capacity for the envelope (roof + walls) (C_w), the internal walls (C_{wi}) and the indoor air (C_i). Both zones are linked by the internal floor which is modelled by 2 thermal capacities (C_{fi1}) and (C_{fi2}).
The coupled model (Figure 4.18) thus consists of 9 capacities. Nevertheless, problems with the identifiability of this model were encountered when the model parameters are estimated

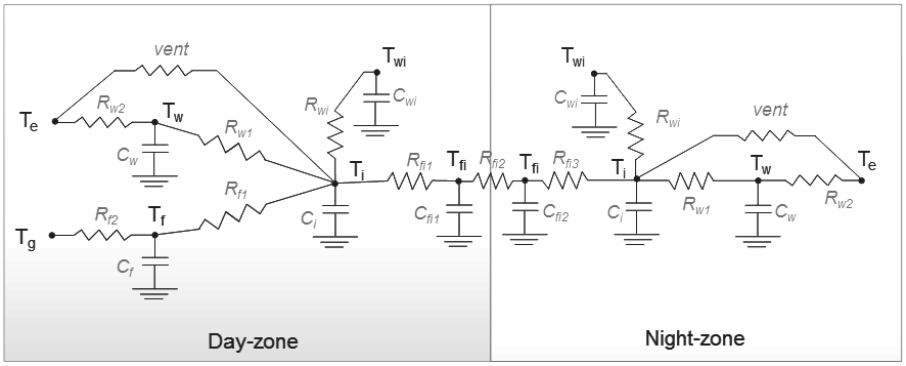

Figure 4.18: Structure of the 2-zone reduced-order models. The day-zone is modelled as a 5-state model with states for the indoor air (T_i), the exterior walls (T_w), the interior walls (T_{wi}), the ground floor (T_f) and the floor between day- and night-zone (T_{fi}). A 4-state model is used for the night zone with states for the indoor air (T_i), the exterior walls (T_w), the interior walls (T_{wi}) and the floor between day- and night-zone (T_{fi}). Note that the gain inputs and the related parameters are not shown.

in a combined parameter estimation process. Therefore, a 7^{th} and 8^{th}-order model are used. The 8^{th}-order model uses only 1 state (C_{fi}) within the floor between day- and night-zone. For the 7^{th}-order model the day-zone is further simplified by excluding the capacity for the ground floor.

As discussed further, an alternative approach for the identification of multi-zone models is suggested whereby the grey-box models for each zone are identified separately using the indoor temperature of the adjacent zone as an input signal. Using this approach both 4^{th}- and 5^{th}-order models are analysed for each zone. For the day-zone the 4^{th}-order model is obtained by excluding C_f from the 5^{th} shown in Figure 4.18. For the night-zone the 5^{th}-order model is an extension of the 4^{th} shown in Figure 4.18, including a separate capacity for the heat transfer through the roof (C_r). Thereby the distinction between C_r and C_w is made to separate the dynamic behaviour of the massive walls and the light-weight roof structure.

In all models, the outdoor temperature (T_e) and ground temperature (T_g) are used as boundary conditions. The solar gains, internal gains and heating are distributed to the different capacities using distribution coefficients, which are also estimated in the identification process. Thereby, in line with the sensitivity study presented in the previous section, the use of the effective solar gains is compared to measurements for the global horizontal irradiation and the global irradiation on the vertical planes along the cardinal axes. These alternatives

are annotated as respectively A, B and C.

Identification and validation data The data set used for identification and validation of the grey-box models is again obtained by detailed building energy simulations using the IDEAS-library. The detailed description of the 2-zone implementation of the detailed models is given in Appendix B. To obtain these model the following assumptions had to be made, in addition to the ones presented in Section 4.5.1, to complete the geometric description of the dwellings:

- the total surface of the ground floor is in contact with the ground. The surface areas of ‘floor in contact with soil’ and ‘floor in contact with unheated space’ have been combined.
- the ground floor is considered to be used as day-zone. The night-zone is considered to be on the first floor and covers the remaining useful floor area.
- the averaged ceiling height is calculated using the total volume and usable floor area.
- The volume of the day-zone is calculated as the product of the ground floor area and the ceiling height. The volume of the night-zone is calculated by subtracting the volume of the day-zone from the total protected volume.
- a pitched roof is assumed with a North-South orientation. As such, the first floor only has exterior walls with an East-West orientation.
- the wall and window areas are distributed between day- and night-zones using a distribution factor of 0.6 for the day-zone and 0.4 for the night-zone.
- the distribution of the windows along the cardinal axes is given in the TABULA data. This distribution has been maintained for both the day- and night-zone.

In line with the previous subsections, two types of virtual experiments have been carried out. In the first experiment the data set is generated by simulating a PRBS experiment. Thereby a pseudo-random binary sequence (PRBS) is implemented on the heating system. Two uncorrelated signals have been used for the day- and night-zone to facilitate the identifiability. In the second experiment in-use behaviour with the deterministic thermostatic control of Table 4.4 is simulated. In both cases measurements of the indoor air temperature and the heat flows to the different components are used as observation variables. Finally, the impact of the data period is analysed. Thereby ’Dat1’ corresponds to 1 week of measurement data in April. ’Dat2’ and ’Dat3’ are 2 week observation data in respectively February and April. The former is chosen to represent a cold winter week with low input for the solar gains, while the latter is a period with high solar gains. Finally, ’Dat4’ and ’Dat5’ are 1 month data sets for respectively February and April.

Zone	Setpoint high	Setpoint low	High setpoint period
Day-zone	$21°C$	$16°C$	07:00–22:00
Night-zone	$18°C$	$16°C$	21:00–09:00

Table 4.4: Thermostat schedule

Model validation Similar to previous sections, two steps have been considered to validate the identified grey-box models. Firstly, an analysis of the residuals has been carried out, taking into account the RMSE values for 1 step predictions and simulation, the auto-correlation function and the correlation of the residuals of to the inputs. Secondly, the performance of the identified grey-box models for long-term simulation is assessed.
Whereas for the models using both the indoor air temperature and heat flow measurements as observations again no white-noise residuals were obtained, the RMSE values showed acceptable results and no significant correlation of the residuals to the inputs was found. Figure 4.19 gives an overview of the RMSE-values for the different models identified for the insulated building on data for the occupied building following the heating schedule (in-use data). It is evident that the model quality is significantly higher when the day- and night-zones are identified separately. For the coupled models the RMSE-values of the indoor air temperature are an order of magnitude higher compared to the separately identified models. For the remainder of the section, only the results for the decoupled identification will therefore be discussed.

In line with previous sections, a comparison is made between models of different order, the type of data used as observation measurements and the data period. For both the day and night-zone 4 and 5 state models have been identified. Although the differences in RMSE value and in the auto-correlation function were marginal, the 4 and 5 state model resulted in the best results for respectively the night- and day-zone. These models correspond to the structure shown in Figure 4.18. In addition to a variation of the order of the model also the impact of the type of input and observation measurements was considered. The variations A, B and C of each model correspond to respectively an identification with idealised inputs, a data set where no information of internal gains was available and solar gains are measured by the global horizontal irradiance and finally a data set that uses the solar irradiance on the vertical planes and the domestic electricity demand as an input for the internal gains. Similar to Section 4.5.3, the results show that data set C results in a similar model quality compared to using idealised inputs, which are often not available in practice.
The impact of the data period on the performance of the identified models shows, as expected, an improvement of the model performance for longer data-sets. In the remainder of this section, the data set of 1 month in February (Dat 4) is used with a sample time of 15 minutes.

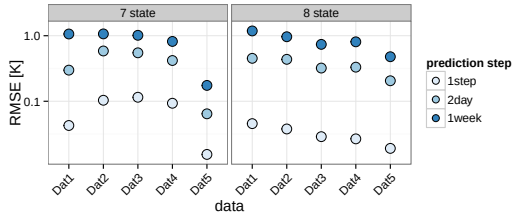

(a) Coupled

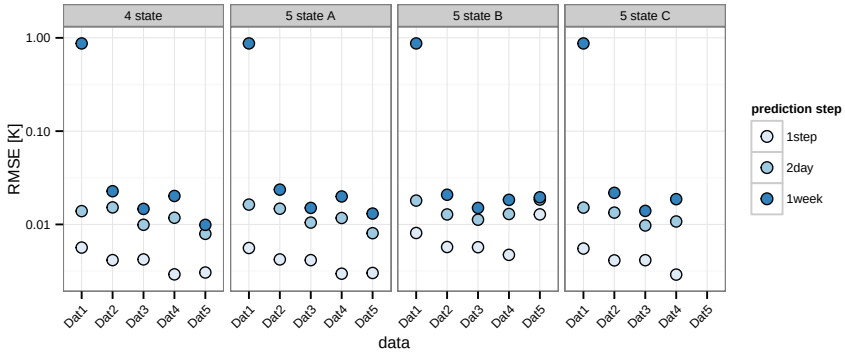

(b) Day-zones

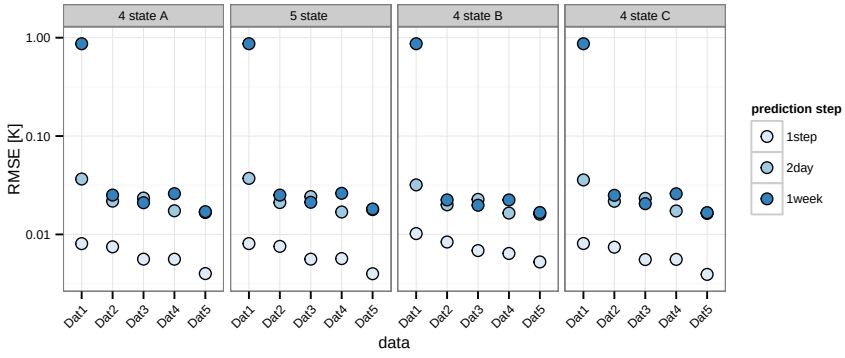

(c) Night-zones

Figure 4.19: RMSE-values for the indoor air temperature obtained for 1 step, 2-day and 1 week predictions (Insulated dwelling with in-use data)

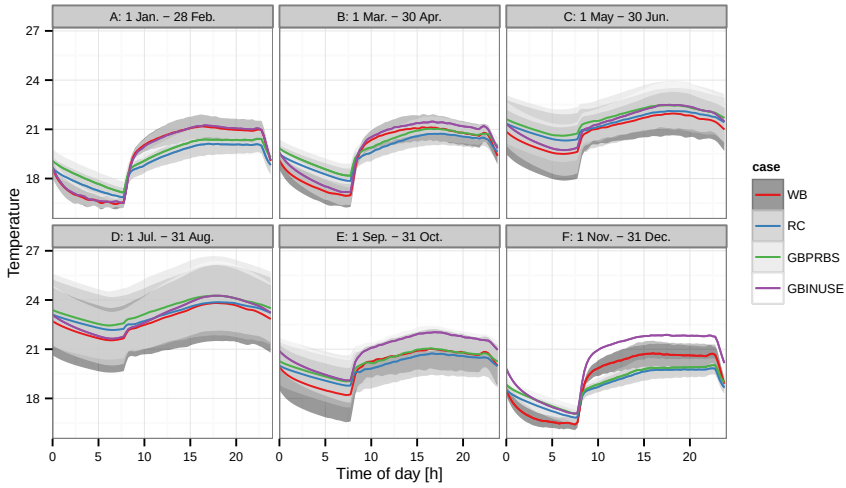

Figure 4.20: Averaged air temperature day zones. (Insulated building)

In the second validation step the performance of the models for simulation is assessed. The focus is thereby on the evaluation of the daily temperature and heat demand profile on a high time-resolution, since both results will play an important role in the evaluation of the ADR potential of the building stock (Chapter 5). For this purpose, the models identified on data of the month February are implemented in the IDEAS-library and simulated for the first half of the year using the same models for the heating system, occupant behaviour and system control. Figure 4.20 shows the averaged daily temperature profile and the 95 % confidence intervals for the insulated building. Thereby, the performance of the grey-box models identified on PRBS (GBPRBS) and in-use data (GBINUSE) is compared against the detailed, white-box simulations (WB) on the one hand and the RC-model implemented using the theoretical values (RC) on the other hand. The different profiles are obtained by averaging over a two-month period, shown in the different panes.

Firstly, Figure 4.20 shows a less sharp response of the air temperature for the grey-box model identified on the PRBS data (GBPRBS) compared to the detailed, white-box, simulations (WB). Consequently the heating system is operated for longer times at high power to provide thermal comfort (Figure 4.21).

Moreover, Figure 4.21 shows the underestimation of the heat demand during the night, as a result of the overestimation of the effective thermal capacity for both the theoretical RC model and the grey-box model fitted on PRBS data (GBPRBS). Secondly, for these model types, the peak heating power during the day is higher and maintained for a longer period to recover

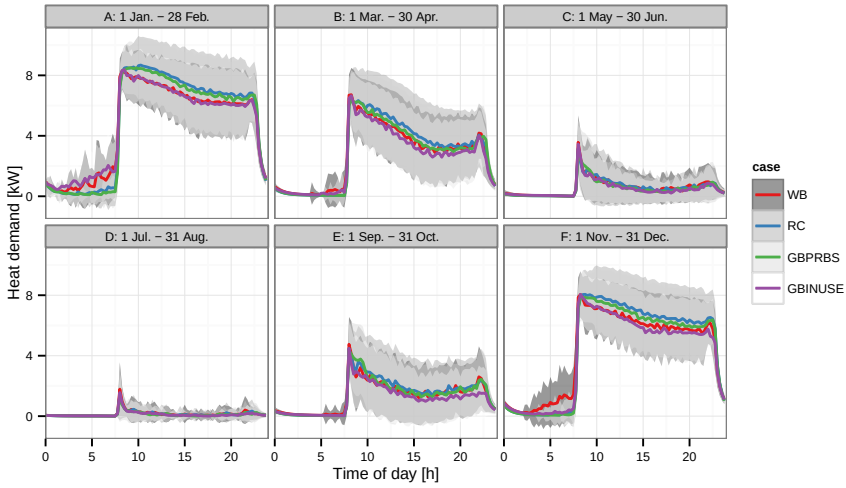

Figure 4.21: Averaged heat demand day zones. (Insulated building)

from night setback. Both results indicate an overestimation of the available thermal mass. In contrast, the grey-box model fitted on the in-use data set is able to capture the sharp temperature swings in the indoor air temperature at the start and end of the occupied periods. As shown further (Figure 4.23), using the in-use data, the latter is explained by the smaller values of the estimated heat transfer coefficient between the indoor air and the building components, indicating that the thermal mass of the components is less available for storage and on a short time-scale most heat is stored in the thermal capacity of the indoor air. Figure 4.20 shows that consequently the temperature profile of the reduced-order model fitted on in-use data (GBINUSE) accurately matches the detailed simulation, especially during winter and mid-season when the potential for demand-side management is highest.
Finally, it is noted that the level of uncertainty on the night zone (Figure 4.22) is much higher than for the day zone. This can be explained on the one hand by an overall lower heat demand of the night-zone compared to the day zone. On the other hand, as shown in Figure 4.23 the identified thermal properties for the internal floor between both zones show a high level of uncertainty. Consequently, the heat transfer between the warmer day-zone and the night-zone, which has a significant impact on the heat demand of the night-zone, is uncertain.

Physical interpretation of the parameters Finally, the identified parameters are compared against the theoretic parameters used for the detailed simulation model and the

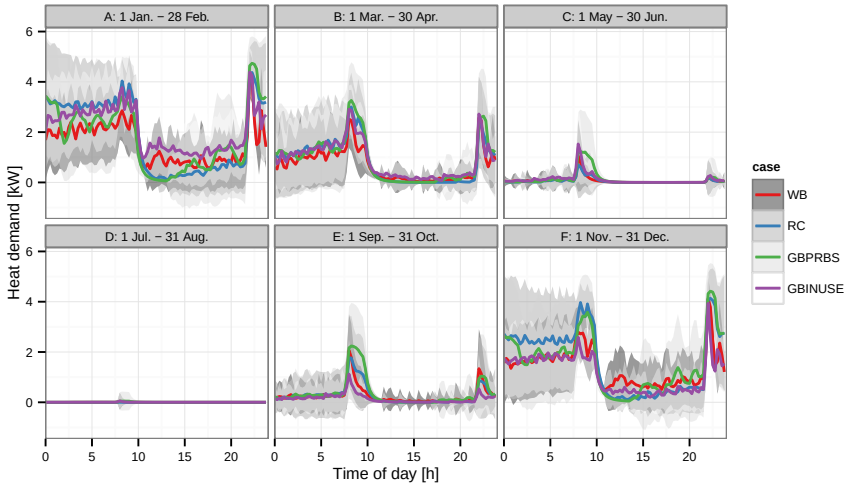

Figure 4.22: Averaged heat demand night zones. (Insulated building)

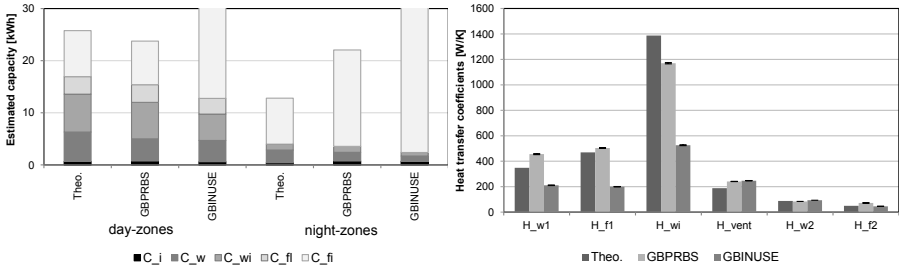

Figure 4.23: Estimated capacities (left) and heat transfer coefficients for the day-zone (right) of the insulated dwelling.

RC-model. Figure 4.23(left) shows the estimated thermal capacities for the models identified on PRBS and in-use data compared to the theoretical values implemented in the RC-model. Firstly, a clear overestimation of the thermal capacity of the floor between day- and night-zone (C_{fi}) is found for the models identified on in-use data. This overestimation is caused by the use of winter data for the identification of the model. For this data, the temperature in both zones varies within a narrow band as specified by the comfort requirements. Consequently, the temperature in the centre of the massive floor is almost constant, leading to over-fitting problems. Thereby, a high correlation is found between the estimated thermal capacities of the interior floor and the heat transfer coefficients between the floor and the adjacent zone

air. As such, the overestimation of the thermal capacity is compensated by low values for the heat transfer coefficients, i.e. 177 W/K and 154 W/K for the heat transfer coefficient at respectively the day- and night-side, compared to a theoretical value of 988 W/K in the theoretic model.
Due to these unreliable estimation of the coupling between day- and night-zone, an overestimation of the heat demand in the night-zone was found in Figure 4.22. In order to overcome this problem, two independent PRBS signals have been applied to the day- and night-zone to guarantee a persistent excitation of both zones in the PRBS case (GBPRBS). Figure 4.23(left) shows, that this approach results in estimates for the effective capacities which closely correspond to the theoretical values for the day-zone. For the night-zone the estimated thermal capacity of the floor between day- and night-zone is still significantly higher than the theoretical values.
In contrast to the internal floor, the estimated effective capacities of the exterior walls, interior walls, indoor air and ground floor, show similar values for the different methods used to establish the parameters.

In addition to the estimated capacities, Figure 4.23(right) shows the different heat transfer coefficients[5] corresponding to the different resistances in the RC-analogy of the day-zone. Note that the theoretical heat transfer coefficients are calculated from the thermal resistance between the middle of the layers within the insulation barrier and the inner air, taking into account standard heat transfer coefficients [121]. For the models identified on the PRBS data, the heat transfer coefficients of the inner walls and the envelope are in the same order of magnitude as the theoretical value. Nonetheless, the estimated values significantly decrease when in-use data is used for the identification. The latter is caused by the temperature dependence of the surface heat transfer coefficients. Given the average temperature difference between the inner surface of the interior walls and the indoor air of 2-4 $^{\circ}\mathrm{C}$, the theoretical value of the convective heat transfer coefficients overestimates the actual heat transfer by a factor 2-3 compared to the value obtained by the temperature dependent convective heat transfer model (Section 2.2.2). As such, less heat is absorbed by the building fabric as the resistance between the indoor air and the fabric increases.

Given these results, it can be concluded that the use of 2 independent PRBS-signals on the one hand results in better estimates of the effective capacity of the floor between day- and night-zone. On the other hand, the higher indoor air temperatures result in an over-estimation of the linearised surface heat transfer coefficients. Consequently the models identified on the in-use data show better results for simulating in-use behaviour.

[5]The heat transfer coefficient H_j is defined is: $H_j = 1/R_j$

4.6 Identification using on-site measured data of a multi-zone dwelling

In this section the grey-box modelling framework is demonstrated using the on-site measurements of the Twin Houses at the Fraunhofer institute in Holzkirchen (Germany) which were presented in Chapter 2 for the verification of the IDEAS building model. Since the building description was already presented in Section 2.3.2, the following paragraphs give a brief summary of the experimental set-up and measured data (§4.6.1) – focussing on the aspects related to the grey-box modelling – and the analysed grey-box model structures (§4.6.2). The two final paragraphs of this section elaborate on the identification results, discussing the model validation process (§4.6.3) and the physical interpretation of the identified parameters (§4.6.4). Thereby, the identification process on measured data is compared against identification using simulated data obtained using the IDEAS library (§ 2.3.2).

4.6.1 Experiment design and measured data

As described in Section 2.3.2, the experiment consists of three phases in order to enable both detailed building model validation as well as identification of reduced-order models and characterisation of the thermal properties – as was aimed for in the IEA EBC Annex 58 project. The full sequence was shown in Figure 2.6. The dynamic heating period (ROLBS) will be used in this study for the identification process, while the final constant temperature and free-floating periods (May 15^{th} - June 1^{st}) are used as cross-validation set. For the identification process the data is averaged with a sample period of 10 min. This sample period is used for both the simulated and measured data.

Figure 2.7 showed the different input signals included in the identification framework. To improve readability, the measured and simulated ambient air temperature (T_e), heating power $(\dot{Q}_{heat})$, and the surface area-weighted temperature of the boundary zones are summarized in Figure 4.24 for the ROLBS-period. Whereas the outdoor temperature and heating power during the ROLBS signal are identical for both the simulated and measured data, significant differences are shown between the simulated and measured temperatures in the boundary zones (T_B) . The latter is calculated as an area-weighted average of the temperatures in the different boundary zones. Figure 2.7 shows that although in both the experiments and the simulations a constant temperature set point of 22 $^{\circ}\mathrm{C}$ is implemented in the boundary zones, a significant amount of overheating occurred during the measurement

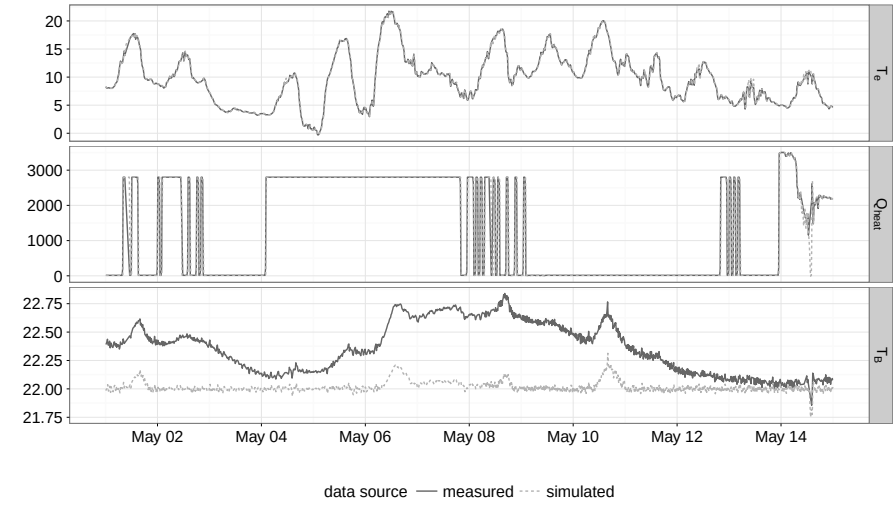

Figure 4.24: Overview of the outdoor temperature (T_e), heating power ($\dot{Q}_{heat}$) and temperature in the boundary zones during ROLBS-period used to train the grey-box models. The measured data are shown in black, the data obtained by the detailed simulations in grey.

Figure 4.25: Measured indoor air temperatures for the different zones and on different heights, together with the aggregated indoor air temperature used as observation measurement.

campaign.

The measured indoor air temperatures are shown in Figure 4.25. It is important to note that whereas the controlled zones will be modelled with a single-zone grey-box model assuming uniform indoor air temperatures, the temperature measurements of the 10 sensors show that

differences up to 5 $^{\circ}\mathrm{C}$ exist between the different rooms. Moreover, significant stratification is found within the rooms, shown (Figure 4.25) by the differences between the temperatures measured near the floor (height = 0.1 m) and on eye-level (height= 1.7), especially when the heaters are activated. In order to find the representative air temperature that can be used as observation for the identification process two steps are followed. Firstly, principal component analysis is carried out on the air temperature measurements within each zone, as proposed by [161]. Secondly, a volume weighted averaging method is used to aggregate the air temperature sensors of the different zones. The resulting, aggregated air temperature for the controlled zones is shown by the full line in Figure 4.25 and corresponds well to the zone temperatures measured at the middle of the room at a height of 1.1 m.

As shown in the previous section, the characterisation of the thermal properties may be improved by including heat flow measurements. Especially in this specific case where both the heat losses to the outdoor environment and to the boundary zones are important, heat flow measurements may reduce potential problems with the identifiability of the individual parameters. Nevertheless, due to practical limitations only heat flux sensors are placed on the interior surfaces of the south-west exterior wall of the living room, the south and east walls of the bed room and the windows of the living and bed room. As such, only the heat flux to the envelope is observed in the measured cases. For the simulated experiment complementary (virtual) heat flux measurements to the boundary zones and the interior walls within the controlled zones are included.

Figure 4.26 shows the heat flux measurements for the exterior walls gathered in the

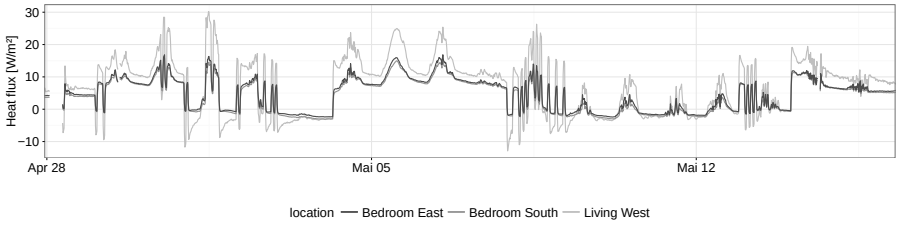

Figure 4.26: Measured heat flux measurements for the south and west wall of the bed room and the west wall of the living.

measurement campaign. As for the temperature measurements, significant differences in the heat fluxes of different rooms are found. This can be explained by the larger temperature swings in the living room where the ventilation supply is located. Moreover, the glazed area is higher for the living room. For the identification process the mean of the three signals is used as observation measurement.

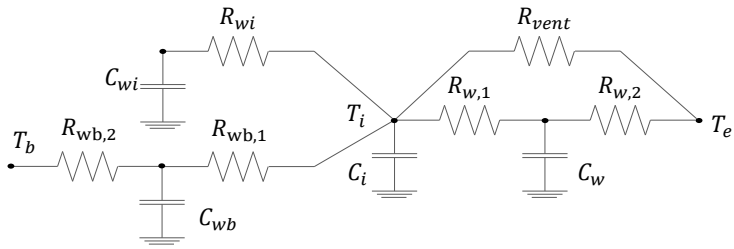

Figure 4.27: RC-network representation of the 4^{th}-order grey-box model established for the Twin House. C_i, C_w, C_{wi} and C_{wb} are the thermal capacities of respectively the indoor air, the exterior walls, the inner walls and the walls and floors between the controlled zone and the boundary zones, connected by thermal resistances $R_{i,j}$. T_e, T_b are measured inputs for respectively the outdoor temperature and the temperature in the boundary zones. T_i and $q_{i,w}$ are the observed indoor temperature and heat flux.

4.6.2 Model structures

As for the identification on the simulated data (Section 4.3), a forward selection procedure is followed to find the optimal model structure. Thereby the same principles are followed, but modifications to the model structures were needed due to the specific requirements of the building, i.e. the influence of the boundary zones in addition to the outdoor environment.
The most detailed model analysed is the 4^{th} order model shown in Figure 4.27 whereby the dynamics of the zone is described by a thermal capacity for the exterior envelope (C_w), the indoor air (C_i), the internal walls (C_{wi}) and the walls and floors adjacent to the boundary zones (C_{wb}). As for the models identified in Section 4.3, the heat transfer through the components is modelled by two resistances in series with the thermal capacity of the wall. No symmetric distribution of these resistances is assumed instead the inner resistance $(R_{i,1})$ and outer resistance $(R_{i,2})$ of component i can take different values. A parallel resistance (R_{vent}) is included for the ventilation losses.
The solar gains and heating power are distributed to each of the capacities by distribution factors that can be defined a priori by the modeller in order to limit the amount of unknown parameters in the identification or included in the parameter estimation problem.
The observed indoor air temperature and heat flux measurements are also indicated in Figure 4.27. Thereby it should be noted that only the heat flux for the exterior walls is available in the measured data. In the analysis this heat flux will also be used as a direct measurement of the heat flow to the envelope by multiplying the measured flux with the surface area of the exterior walls. Nonetheless, given the large spread on the measured heat fluxes for the different locations (Figure 4.26), a higher uncertainty on the estimates may be expected compared to the simulated data where the heat flow is exactly known.

Table 4.5: Summary of the analysed grey-box models, names of the models, the states that are included, the type of observation measurements and the way the gains are allocated to the different capacities.

Model	States	Observations	Gains
2A	T_i, T_w	T_{air}	C_i
3A	T_i, T_w, T_{wi}	T_{air}	C_i
3B	T_i, T_w, T_{wb}	T_{air}	heating: C_i solar: fitted
4A	T_i, T_w, T_{wi}, T_{wb}	T_{air}	heating: C_i solar: fitted
3Bq	T_i, T_w, T_{wb}	$T_{air}, q_{flux,e}$	heating: Ci solar: fitted
4Aq1	T_i, T_w, T_{wi}, T_{wb}	$T_{air}, q_{flux,e}$	heating: C_i solar: fitted
4Aq2	T_i, T_w, T_{wi}, T_{wb}	$T_{air}, q_{flux,e}$	heating: fitted solar: fitted
3BQ1	T_i, T_w, T_{wb}	$T_{air}, Q_{flux,e}$	heating: Ci solar: fitted
3BQ2	T_i, T_w, T_{wb}	T_{air}, Q_{flux}	heating: fitted solar: fitted
4AQ1	T_i, T_w, T_{wi}, T_{wb}	$T_{air}, Q_{flux,e}$	heating: C_i solar: fitted
4AQ2	T_i, T_w, T_{wi}, T_{wb}	T_{air}, Q_{flux}	heating: fitted solar: fitted

As in Section 4.3, the 4^{th} order model of Figure 4.27 has been established in a forward selection procedure whereby – starting from a simplified 2^{nd}-order model – the model structure was systematically extended. The initial 2nd-order model uses only the thermal capacity of the indoor air (C_i) and of the envelope (C_w) to describe the dynamic response of the building. As such, heat transfer to the boundary zones is not taken into account for this simple model.

This model is extended by either including the capacity of the internal walls (C_{wi}), as is done in model '3A' or the capacity of the boundary walls (C_{wb}) as for model '3B.' Finally, these models are further extended to the 4th-order model of Figure 4.27.

For each model order, different assumptions for the distribution of the solar gains and heating power are assumed and different observation measurements are compared. As observation measurements the indoor air temperature (T_{air}) as well as the heat flux $(\dot{q}_{flux,e})$, or heat flow $(\dot{Q}_{flux,e})$ to the exterior walls are used for the measured data, as explained in the experiment design. For the simulated data, also a case with heat flow measurements to all components $(\dot{Q}_{flux})$ is included. An overview of all identified models is given in Table 4.5.

4.6.3 Model validation

The model selection and validation approach followed here is the same as for the identification on simulated results. Three important performance tests are carried out. Firstly, an analysis of the short-term prediction errors is conducted, focusing on the RMSE values of the 1 step ahead, 1 day ahead and 1 week ahead predictions as well as on the auto-correlation and cross-correlation of the residuals for 1 step ahead predictions. Secondly, cross-validation is carried out by simulating the model output for a validation data set. Note that due to the limited length of the data set, the validation data is a combination of the training data set followed by 5 days of the constant temperature period. For the simulated data, also the free floating period at the end of the experiment has been included. An important down-side of this short validation data, is that systematic errors due to over-fitting are less likely to show in the RMSE-values.
The final step in the validation process, i.e. the analysis of the physical interpretability of the identified parameters, is presented in Section 4.6.4.

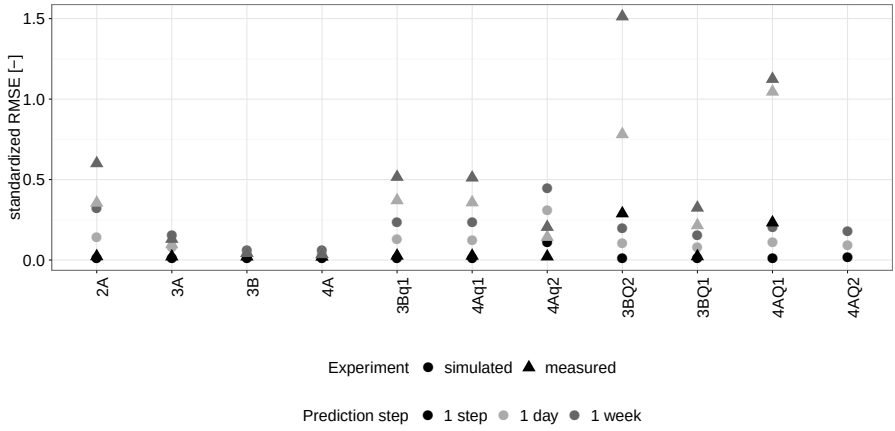

Figure 4.28: Standardised root mean squared errors (sRMSE) for the 1 step, 1 day and 1 week ahead predictions of the indoor air temperature as a function of the models structure and the data set.

In the first step of the validation process, Figure 4.28 shows the standardised root mean squared error (sRMSE) for the 1 step ahead, 1 day ahead and 1 week ahead predictions obtained for the different model structures. As for the results of the previous sections, the lowest sRMSE values for 1 step ahead predictions are obtained when only the indoor air temperature is used as observation variable. Moreover, Figure 4.28 demonstrates that model

2A and 3A, which do not include a separate term for the heat transfer to the boundary zones, result in high RMSE-values. To overcome this problem model 3B uses the thermal capacity of boundary walls (C_{wb}) instead of that of the inner walls (C_{wi}). As such, a distinction between the heat transfer to the outer environment and the boundary zones is possible, clearly resulting in a better prediction of the dynamic response of the building.
Extending model 3B to 4A by including both C_{wi} and C_{wb} has only a minor impact on the prediction accuracy, demonstrated by the insignificant decrease of the sRMSE-values. An important increase of the sRMSE-values for 1 day ahead and 1 week ahead predictions is not shown in the sRMSE-values for model 3B and 4A, suggesting that over-prediction problems do not occur. Given the short duration of the dataset, these results should however be handled carefully, since a comparison of the physical properties (Section 4.6.4) does show unreliable estimates for these models indicating over-fitting problems.
When the observation equations for the measured heat flux (models 3Bq, 4Aq1 and 4Aq2) or the heat flow (models 3BQ1, 3BQ2, 4AQ1 and 4AQ2) are included, a significant increase of the long-term prediction residuals is shown (Figure 4.28). Thereby the introduction of the observation equation for the heat flux (Eq. 4.11) is found to be less efficient than specifying the equations for the heat flow (Eq. 4.10). This is in line with the findings of Section 4.3 and can be explained by the fact that for the heat flux measurements the wall area is introduced as an additional parameter in the identification process, increasing the degrees of freedom. Finally, it should be pointed out that specifying the heat flow measurements for the measured data as the product of the averaged heat flux multiplied by the theoretic wall area results in high RMSE-values for both 1 step ahead and long-term predictions. This confirms the observations of Figure 4.26 that the heat flow is not uniformly distributed over the outer wall surface.

In addition to the RMSE-values, Figure 4.29 shows the autocorrelation functions of the 1 step prediction residuals for the different models. In contrast to the high RMSE-values for the 2A and 3A models, the level of auto-correlation in the residuals is already low for the models identified on measured data and does not significantly reduce for models 3B and 4A. As such, it can be concluded that extending the model complexity to 3B and 4A does not significantly improve the ability of the model to explain the dynamic information available in the observed air temperature. For the models estimated on the measured data the residuals show white-noise behaviour indicating that the model is able to predict all the dynamics that are available in the data. In contrast, a significant level of auto-correlation is still shown for the models identified on simulated data. This observation is in line with what was shown in Section 4.5.3 where random measurement noise on the simulated data was added to mimic real measurements, demonstrating that due to the impact of random measurement noise,

white-noise residuals are easier to obtain than for noiseless simulated data.

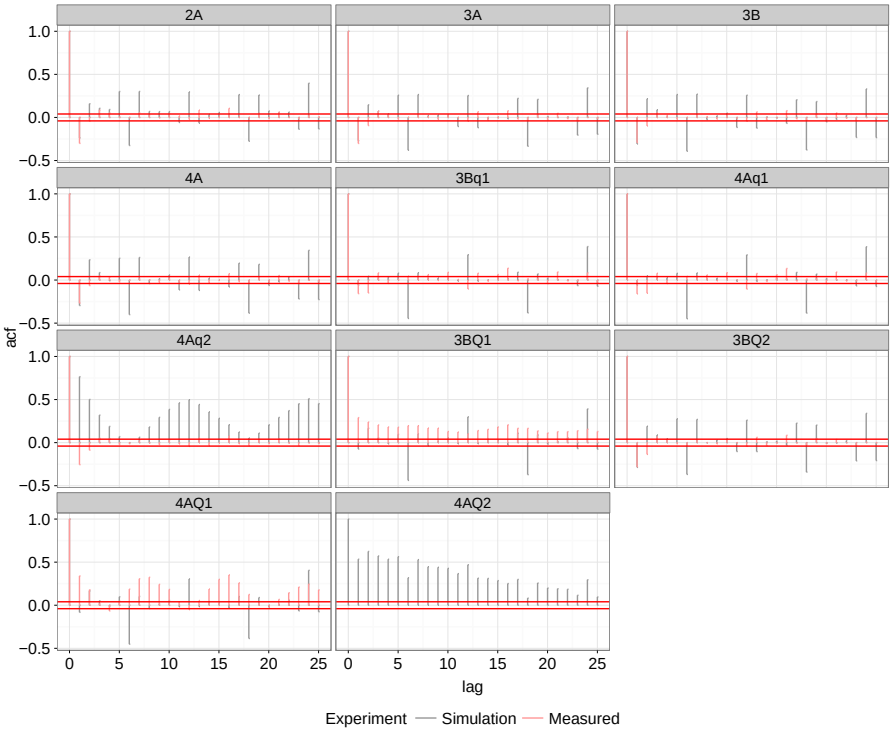

Figure 4.29: Autocorrelation function of the 1 step ahead prediction residuals of the indoor air temperature as a function of the model structure and the data set

Finally, Figures 4.30-4.31 show the performance of the models identified for simulation. Figure 4.30 shows the simulation results for the models identified using only the indoor air temperature as observation. As already indicated by the low sRMSE-values (Figure 4.28) both the 3^{rd} and 4^{th}-order models show a high accuracy for simulation. In contrast, model 2A shows an overestimation of the maximum temperature at the end of the long heating period and an underestimation of the minimum temperature. Both errors can be explained by the model structure which does not take into account the heat transfer to the boundary zones.

When heat flux or heat flow measurements are included, the residuals for the indoor air temperature increase for both the cases identified on simulated and measured data. As was already indicated in the analysis the RMSE-values, the residuals for the 4Aq1 model

Figure 4.30: Simulations results for models identified using only the indoor air temperature for the simulated (top) and measured (bottom) data.

are found to be higher for the case identified on measured data. This can be explained by the high uncertainty on the heat flux measurement on the one hand and the reduction of the degrees of freedom in the model on the other hand. The effect becomes even larger

when the heat flux measurements are used, in combination with the theoretic surface area of the wall to specify the heat flow through the envelope (model 4AQ1). This demonstrates that using the average value for the heat flux does not correspond to reality. More detailed measurements of the heat flux with a higher spatial distribution are required. As shown for the simulated data (Section 4.3 and model 4AQ2), heat flux measurements to components with different boundary conditions can significantly improve the identifiability. Nevertheless, these are difficult to apply in practical on-site tests.
In contrast, for the simulated data where the heat flow measurements correspond exactly to the heat transfer to the exterior walls, a slight improvement of the model accuracy is found going from the use of heat flux data (4Aq1) to data on the heat flow (4AQ1). When heat flow measurements for the heat transfer to all components are included (4AQ2), slightly better simulation performance is found than when only heat flow measurements to the exterior walls are included. Nonetheless, the level of the residuals remains higher than for the models identified using only the indoor air temperature (4A) showing that when only a prediction of the dynamic behaviour of the building is aimed for, given the complexity of the measurements, the added value of heat flux measurements is for this case found to be limited. However, as shown throughout this chapter, one should always test for over-fitting especially if higher-order models are used. Moreover, as will be shown in the next section, heat flow measurements have an important impact on the physical interpretability of the model parameters. This observation is again closely linked to over-fitting problems.

4.6.4 Physical interpretation of the parameters

As a final part of the section, the physical interpretability of the model parameters is analysed. Thereby the focus is on the overall heat loss coefficient to the outdoor environment (HLC_e), the heat loss coefficient to the boundary zones (HLC_b) and the thermal capacities of indoor air (C_i), the exterior walls (C_w), interior walls (C_{wi}) and the walls and floors to the boundary zones (C_{wb}). The heat loss coefficient to the outdoor environment is defined as the combination of the heat transfer coefficient of the exterior walls and the ventilation losses. Consequently, the heat loss coefficient to the boundary zones is defined by the heat transfer coefficient through the walls and floors between the controlled and boundary zones. They are calculated from the identified parameters:

$$HLC_e = \frac{1}{R_{vent}} + \frac{1}{1/R_{w,1} + 1/R_{w,2}} \tag{4.14}$$

Figure 4.31: Simulation results for models identified using indoor air temperature and heat flux measurements as observation.

$$HLC_b = \frac{1}{1/R_{wb,1} + 1/R_{wb,2}} \tag{4.15}$$

	Heat transfer coefficient	Effective capacity
	W/K	MJ/K
Ventilation/Indoor air capacity	31.8	0.17
Envelope total	36.6	16.7
Envelope opaque	12.3	16.7
Boundary walls	67.77	13.1
Internal walls		5.1

Table 4.6: Summary of the calculated thermal properties of Twin House based on prior knowledge

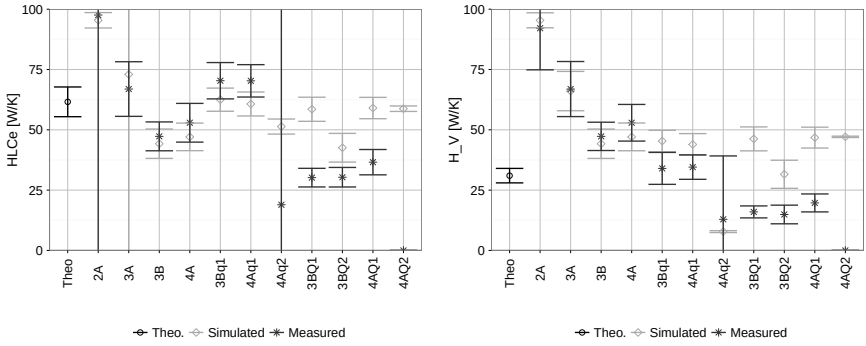

Figure 4.32: Estimated total heat loss coefficient (left) and ventilation loss (right) to the outdoor environment compared to the theoretical value as a function of the model structure and data set.

The thermal capacities representing the different components are obtained directly from the grey-box model. Note that HLC_e can be split in transmission ($H_{T,e}$) and ventilation losses (H_V).

A summary of the relevant thermal properties of the Twin House building is given in Table 4.6. A detailed description of the building is found in [99, 97]. For this study the total transmission losses to both the exterior environment ($H_{T,e}$) and the boundary zones ($H_{T,b}$), the ventilation losses (H_V) and the thermal capacities of the indoor air and the construction components are of interest as these values will be characterised using the grey-box modelling approach.

Figure 4.32 shows the estimated values for HLC_e as a function of the model structure and the data set. Firstly, Figure 4.32 shows that in line with the inaccurate prediction and simulation results the identified values for HLC_e are unreliable for models 2A and 3A. Since the boundary walls are not included in these models, the values for HLC_e are overestimated. For models 3B and 4A, the heat transfer coefficient is underestimated by respectively 25 % and 17 %. As demonstrated by Figure 4.33, these models allocate all transmission losses to boundary zones, resulting in $H_{T,e}$-values which are close to zero and statistically insignificant (Fig. 4.33 left) and an overestimation of HLC_B (Fig. 4.33 right).

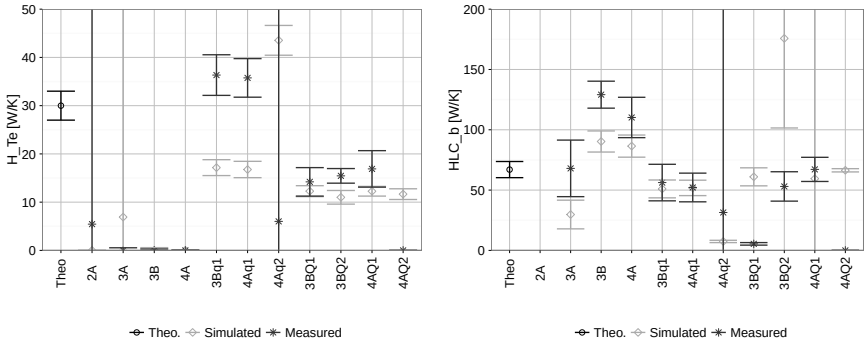

Figure 4.33: Estimated heat transfer coefficient for the transmission losses to the outdoor environment (left) and to the boundary zones (right) compared to the theoretical value as a function of the model structure and data set.

In contrast to the high accuracy for prediction and simulation, obtained for the models 3B and 4A, they prove to be unreliable for characterisation. The latter is caused by identifiability problems, resulting in high correlation between the parameter estimates.

When heat flux measurements are included, the estimated values for $H_{T,e}$, H_V and HLC_B correspond better to the theoretical values. Nonetheless, an overestimation of $H_{T,e}$ is still observed for models $3Bq1$ and $4Aq1$ identified on measured data. Moreover, a high level of uncertainty is shown for model 4Aq2. This high level of uncertainty can be explained due to the fact that a scaling factor is applied to both the supplied heat – in terms of the distribution coefficients – as well as to the observed heat flux – in terms of the wall area (see eq. 4.11). Consequently, the model is no longer structurally identifiable.

This problem has been overcome by using the heat flow rather than the heat flux as an observation equation, specifying the surface area manually. Using this method, the estimated model parameter correspond well to the theoretical value for HLC_e. Except for model 3BQ2 the estimated values all are within 10% of the theoretical value for the models identified on the simulated data.

In contrast, this method demonstrates the problem of unreliable heat flux measurements for the measured data. Using the average of the heat fluxes measured in the living room and the bedroom results in an underestimation of the heat loss through the envelope, explaining the bad performance in simulation and prediction.

Finally, it should be pointed out that the estimated values for $H_{T,e}$ and H_V tend to be respectively lower and higher than the theoretical values. For $H_{T,e}$ the estimates vary between 10 W/K and 14 W/K, corresponding to the theoretical value of the heat transfer coefficient for the transmission losses through the opaque components (12.9

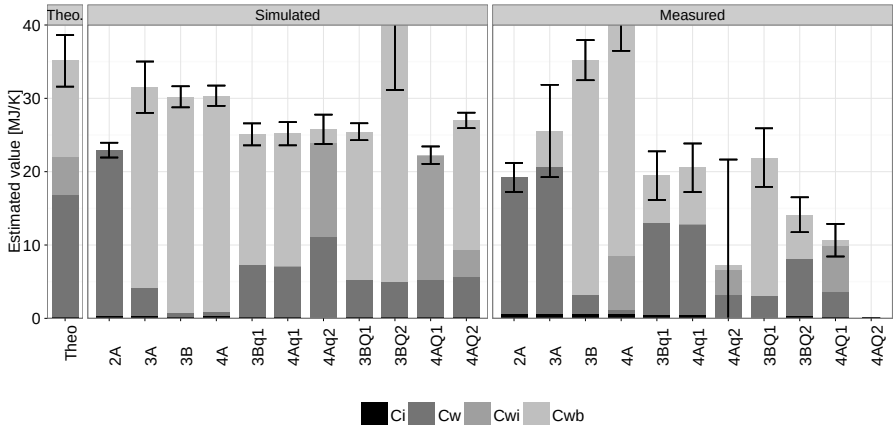

Figure 4.34: Estimated thermal capacities of the indoor air (C_i), the exterior walls (C_w), the interior walls (C_{wi}) and the walls to the boundary zones (C_{wb}) compared to the theoretical value for the models identified on the simulated data (left) and measured data (right)

W/K). Simultaneously, the estimated values for H_V vary between 46 W/K and 48 W/K corresponding to the sum of the theoretic ventilation and infiltration losses (31.8 W/K) and the transmission losses through the windows (15.1 W/K). Since the windows have a negligible thermal mass compared to the opaque components, they are identified as part of the ventilation losses. The same phenomena was found for the identification on the theoretic cases presented in Section 4.3 and should be taken into account when implementing RC-type building models using a theoretic calculation of the parameters.

Finally, Figure 4.34 shows the estimated values for the different capacities. Thereby, a significant difference is found between the models identified on the simulated (left) and measured (right) data. On the one hand a large spread is shown on the estimated values as a function of the grey-box models when measured data is used. On the other hand, the total effective capacity is consistently estimated between 25 and 31 MJ/K for the simulated data, except for model 3BQ2 which for which the model structure is found to not correctly represent the physics of the dwelling. This value is significantly lower than the theoretical value of 35 MJ/K, corresponding to the thermal mass of the material layers within the insulation barrier. In addition, the distribution of the total storage capacity over the different components varies significantly between the different models. In line with the findings of the identification on simulated data presented in Section 4.3, heat flow measurements (model 4AQ2) to the different components are a prerequisite to guarantee the physical interpretation of the individual capacities. Especially the estimated values for C_{wi} and C_{wb} vary significantly

between the different models, due to the minor temperature variations in the boundary zones. The analysis of the estimated values for the model 4AQ2, which proved to give the most reliable estimates for the heat loss coefficients, shows that the exterior walls have a lower contribution to the effective storage capacity than expected by the theoretic calculation. In the theoretical value, the entire brick layer – with a thickness of 30 cm – is assumed to actively contribute to the effective storage capacity of the dwelling. The estimated storage capacity for the exterior walls is a factor 3 smaller, suggesting that only the first 10 cm of the brick contributes to the active storage capacity. However, it should be noted here that the estimated value for C_{wb} is 25 % higher than the theoretical capacity, which shows that despite the heat flow measurements the parameters are still correlated.

In contrast to the consistent estimates of the total effective storage capacity for the models identified on the simulated data, a larger spread is shown for the models identified on the real measurements. Figure 4.34 shows that for models 2A, 3Bq1, 4Aq1 and 3BQ1, the total estimated effective storage capacity varies between 19 and 22 MJ/K. When the observation equations are specified as heat flow measurements the estimated total effective storage capacity of the building is significantly below the theoretical value. This observation is in line with the unreliable estimates of the heat loss coefficients and the inferior performance for prediction and simulation. Consequently, it should be concluded that in absence of adequate heat flux measurements, the characterisation is more reliable if the model order is kept low and only air temperature measurements are used as observations. In that case one should however be prudent when interpreting the physical meaning of the individual parameters, but focus on the overall thermal properties such as the overall heat loss coefficient and total effective storage capacity.

4.7 Conclusions

This chapter evaluated the potential of grey-box modelling to identify reduced-order models that are suitable for accurate (i) prediction of the thermal response and heat demand of dwellings for control applications, (ii) simulation of the dynamic behaviour of buildings for application in district simulations and (iii) characterisation of the main dynamic thermal properties of a dwelling. Thereby, a simulation based framework has been developed and is found useful to asses the link between the model structure, the experiment design and the performance of the identified models for each of the three applications.

Based on an analysis of the identification on simulated data, it is concluded that different model structures and measurement data are required depending on the application of the model. Thereby in general lower-order models suffice to accurately predict the thermal response of a building on time-scales that are typically required for control purposes (15 min up to 1 week). In contrast, higher-order models are required for an accurate simulation of both the short- and long-term dynamics and the characterisation of the thermal properties.
More precise, a 2^{nd}-order model that distinguishes between the fast thermal dynamics of the indoor air and the slow dynamics of the structural thermal mass, is found to be adequate for short-term predictions. When the building is equipped with floor heating, the model may even be reduced to a 1^{st}-order model, due to the fact that the floor itself acts as a low-pass filter smoothing out the temperature variations.
In contrast, if the models are to be used for simulations, 3^{rd} or 4^{th} order models are needed to guarantee accurate simulation of both the short- and long-term dynamics. Thereby, the main reason to increase the model order is found to be the ability to separate thermal capacities that are linked to different boundary conditions, such as the capacity of the outer envelope vs. the capacity of the ground floor. Nevertheless, if only the air temperature is available as observation these higher order models may suffer from identifiability problems or over-fitting, jeopardizing the reliability.
To overcome this problem more detailed experiments, including heat flux or heat flow measurements are required. However, as shown in the identification on on-site measurements, qualitative heat flux measurements are difficult to obtain in practice due to non-uniformities. Moreover, the heat flux measurements should be translated to observations for the heat flow, by including the surface area, in order to avoid problems with over-parametrisation.

The use of heat flow measurements, in combination with higher-order models, is also a prerequisite for a detailed characterisation of the dynamic thermal properties of a dwelling. Thereby the physical interpretability of the parameters is found to be highly sensitive to model assumptions. Consequently, in order to differentiate between the thermal capacities and resistances of different components, the model structure should accurately represent the actual physics of the system. This results in higher-order models and the need for detailed measurements, which in practice may only be feasible in dedicated experiments.
In contrast, if one is only interested in the overall thermal properties, such as the overall heat loss coefficient and total effective capacity, and if no heat flux measurements are available, lower-order models have shown more robust results. Nevertheless, the interpretability of the individual parameters for this models is lost.

Finally, the analysis of the estimated thermal properties demonstrated that when using

dynamic heating signals with excitation frequencies in the same order as normal heating operation or active demand response events, not the entire structural thermal mass but only the inner massive layer is activated. It was found that as a rule of thumb, the identified thermal capacity of the envelope shows good correspondence to the thermal mass of all material layers within the insulation layer. Although, the thickness of this active layer is a function of the time constant of the excitation signal, the estimated values were found to be insensitive to input signal for the heating system even when PRBS-signals were compared against in-use building operation. The obtained estimates for the thermal capacity were therefore defined as the effective thermal capacity.

Chapter 5

Demonstrating the potential of active demand response using structural storage in the Belgian building stock

In the previous chapters, a methodology has been developed – on a building level – to quantify the potential of structural thermal energy storage in residential buildings for active-demand response. In this chapter, the tools developed in the previous chapters are combined and applied to quantify the potential of ADR using structural thermal energy storage in the Belgian residential sector. More specific, a case study is used to estimate how structural storage can support a widespread integration of renewable electricity production and heat pumps in the Belgian residential sector. Thereby the goal is on the one hand to demonstrate the impact of active demand response on the CO_2-emissions and operational savings of the central electricity production for the large-scale introduction of residential heat pumps. On the other hand, given the context of this thesis, the goal is to analyse the suitability of different building typologies for structural thermal energy storage in an ADR context.

To evaluate the ADR potential of the Belgian building stock, an integrated operational model has been developed together with colleagues of the department of Mechanical Engineering of KU Leuven. The model combines detailed operational aspects of both the electricity

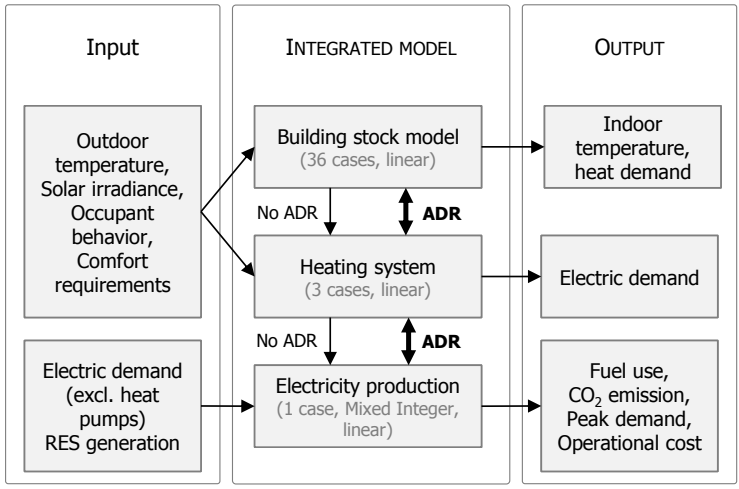

Figure 5.1: The integrated model which simultaneously dispatches electricity generation units and heat pumps in order to deliver the total electricity demand and maintain thermal comfort in the buildings.

generation system as well as single-family residential buildings with heat pumps. Figure 5.1 gives a schematic representation of the model, showing that the integrated model is an optimization problem that simultaneously considers the three subcomponents – i.e. buildings, heating systems and electricity generation.

The model uses dynamic input data on the climate conditions, occupant behaviour and comfort requirements to calculate and predict the heat demand of the dwellings and simulate the indoor air temperature based on the actual heat production by the heat pumps. Thereby the building model is used to calculate the heat demand, while the heat pump model calculates the corresponding electricity demand. This electricity demand is then – in combination with the fixed electricity demand (without heat pumps) and the renewable electricity production – used as input to optimize the electricity production. When ADR is applied, the control of the heating system interacts with the electricity generation system. Hence the bold arrows in Figure 5.1 work in both directions enabling the combined optimization of the electrical demand of heat pumps and production. Thereby, the main contribution of this work to the integrated model lies in the modelling of the residential heat demand and the dynamic behaviour of the structural thermal energy storage capacity.

Layout of the chapter Before explaining and demonstrating the results of the integrated operational model (Section 5.3.1), Section 5.1 goes into detail on the reduced-order building

stock model that is developed and implemented in the operational model. This building stock model is based on the Belgian building stock description presented in the European TABULA-project [117] and has been used to set up a dynamic reduced-order building stock model using the grey-box framework presented in Chapter 4. The main research question thereby is to evaluate whether reduced-order models can provide the required accuracy needed to evaluate the ADR potential on an aggregate level. Thereby the focus is explicitly on the ability of the reduced-order models to capture the dynamics of the heat demand profile and indoor temperature variations at the high time resolution (15 min - 60 min) used to evaluate ADR.

Using this building stock model the available storage capacity for ADR and storage efficiency – introduced in Chapter 3 – are evaluated for the different building typologies (Section 5.2). The goal is thereby to understand how the thermal properties of the different building types, age classes and renovation levels in the Belgian building stock affect the theoretical potential for ADR.

In the second part of the chapter, the integrated operational model is presented (Section 5.3.1) and applied (Section 5.3) in order to demonstrate the CO_2-emission reduction and operational savings that can be obtained by active use of the structural thermal energy storage capacity of the Belgian building stock.

5.1 Building stock model

In this section, a reduced-order, dynamic, bottom-up building stock model is developed to quantify the demand-side management potential of the structural storage capacity of the Belgian building stock. A bottom-up framework is used as it enables a physics-based simulation and evaluation of different building typologies and aggregates the results – based on the distribution of the individual building typologies [103, 174].

The goal of this model is to enable an accurate simulation of the instantaneous heat demand and indoor temperatures of buildings with a low computational cost. In the context of ADR, an accurate simulation of the instantaneous heat demand as well as the indoor temperature is a prerequisite (Chapter 3) since optimal control strategies optimize the heat demand – e.g. to reduce the peak demand and increase the match with renewable electricity production – by adapting the temperature set-point for heating. As such, these control strategies have a direct impact on the thermal comfort of the occupants. Inadequate prediction of the indoor temperature and the dynamic response of the building may thus not only influence the efficiency of smart buildings and districts, it may also jeopardize thermal comfort.

Additionally, since the performance of the electricity production is strongly affected by the

shape of the load duration curve and the peaks of the instantaneous electricity demand, the reduced-order building stock model should capture the dynamics in the heat demand at a high time resolution. For this study hourly data will be used.

Although, a number of studies have been published on the inventory and modelling of the Belgian housing stock [117, 118, 175, 52], the modelling approaches typically do not support dynamic simulations needed for this work, but consist of monthly averaged heat balance and degree-day calculations. Moreover, the available data is mostly focused on geometry, insulation thickness, ventilation type and glazing properties and does not provide the detailed information needed for the dynamic modelling of buildings e.g. material properties, properties of internal walls and floors, etc.
Therefore in this section, the framework and building descriptions obtained from the TABULA-project are elaborated using engineering assumptions and knowledge about traditional construction methods to develop suitable dynamic reduced-order models (Section 5.1.1).
To develop this dynamic reduced-order building stock model, the grey-box framework developed in Chapter 4 is applied. The main research question is thereby formulated as:

> *To what extent are reduced-order models suitable for simulation of the dynamic behaviour and instantaneous heat demand of buildings with the high temporal resolution needed for the quantification of the demand-side management potential?*

The method used to establish the reduced-order models is evaluated by comparing two approaches to calculate the model parameters: (1) parameter identification using the grey-box modelling framework presented in Chapter 4, and (2) a theoretical calculation of the building parameters based on the building stock data completed by assumptions and the rules-of-thumb that were deduced from the results of Chapter 4. The performance of the obtained reduced-order models is evaluated by a quantitative and qualitative comparison of the instantaneous heat demand and indoor temperature profiles against detailed building energy simulations. The latter are, in the absence of qualitative time-series data on the heat demand for the different building typologies, used as a reference case.

In Section 5.1.1 the data and assumptions regarding the Belgian building stock are discussed. As a basis the TABULA-project is used [117]. Sections 5.1.2 and 5.1.3 describe the detailed and reduced-order models respectively. Section 5.1.4 shows the verification of the building models as well as the aggregation of the results to the national level.

5.1.1 Building stock description

The development of the dynamic building stock model is based on the typology data presented in the TABULA-project [176]. The TABULA-project is a European project that focuses on the evolution of energy-related properties of buildings as well as the possibilities for improvement. The 13 partners and 2 associated partners involved in the European TABULA project have committed themselves to develop a housing typology for their respective countries. Thereby, a harmonized framework has been established, which is considered as an added value since it allows for an extension of the methodology presented in this chapter to other European countries.

In addition to the TABULA-project, multiple studies have presented and used a description of the Belgian residential stock [117, 118, 175, 52]. Nevertheless, a literature review revealed that most studies rely on the same data-bases – such as [52, 177, 178] – to deduce the building stock descriptions. Thereby most studies define building typologies to categorize the buildings into different types and age classes. Nevertheless, a significant difference is found in the way these typologies are defined and how typical buildings for each typology are composed. For example, Allacker (2010) selected existing buildings which are considered to represent a specific type and age-class [118]. In contrast, Hens [179] composed fictional buildings for each age-class and building type based on statistical data of the thermal characteristics.
The latter approach is also implemented in the TABULA-project and is used in this thesis. Thereby the use of statistical data on the buildings thermal properties is considered to give a more representative estimate of the average available storage capacity and storage efficiencies of the different buildings in the building stock. A comparison of the simulated heat demand for the TABULA building stock description and the recently developed building stock model by ULg – which uses the buildings presented in [118] to define the geometry – showed however a difference of 65 % between the heat demand of the total residential stock. The difference was mainly caused by the difference in geometry, whereby the TABULA buildings were on average 175 % larger than the ones in the ULg-building stock. Nevertheless, it was found that the relative differences between the building types and age classes show the same trends for both building stock descriptions in [180]. Consequently it should be noted that although a quantitative methodology will be used in this chapter, the conclusion should be interpreted qualitatively. Thereby the main goal of the work is to demonstrate the relative differences between the building typologies.

In the TABULA project, the Belgian residential building stock is represented by 30 typical dwellings grouped in 5 age classes and 6 types of which only the 3 types of single family

Figure 5.2: Main matrix of the Belgian housing typology following the harmonized TABULA approach. The figure shows the three single family building types (detached, semi-detached and terraced) for the 5 age classes [117].

houses are considered in this work (Figure 5.2). The term 'typical dwelling' indicates that these dwellings are fictional houses that are composed of typical elements and technical installations. In this work only the single family houses are addressed, representing 75 % of the total building stock [52]. Multi-family houses are not considered since their dynamic behaviour as well as the required modelling approach significantly differ from single-family dwellings. Note that two of these single family dwellings, i.e. the detached dwellings from before 1945 (D1) and after 2005 (D5) have already been presented and used as examples in Chapter 4.

The geometry and U-values of the envelope components are specified for each dwelling together with a typical infiltration and ventilation rate. Although the exact material properties used to calculate the U-values of the envelope components are not specified, a typical composition of the components is provided for the envelope components. Based on these

proposed compositions, the material properties used in the detailed model have been obtained by reverse engineering to match the U-values given in the TABULA specification. Note that the geometry and material properties of the interior walls and floors have not been specified. As such, it is evident that whereas the data specified in the TABULA project suffices for the static calculation methods used in the project, additional assumptions are required to implement a dynamic building energy simulation model. The main assumptions are summarized in Appendix B. Since the TABULA project uses a single zone heat balance calculation, most assumptions are related to convert the geometry description to a two-zone model.

In addition to the specification of the original building characteristics, 2 renovation scenarios are implemented in this work. Note that these renovation scenarios differ from those presented in the TABULA project. In the TABULA renovation case 1, the thermal performance of the building components is upgraded to the level prescribed in the Flemish energy regulation for new buildings in 2010. In the second renovation case, presented in TABULA, an advanced energy upgrade level is proposed, i.e. the Low-Energy level with U-values of 0.25 $\mathrm{W}/(\mathrm{m}^2\mathrm{K})$, 0.15 $\mathrm{W}/(\mathrm{m}^2\mathrm{K})$ and 1.6 $\mathrm{W}/(\mathrm{m}^2\mathrm{K})$ for respectively the exterior walls, roof and windows. Nevertheless, it is argued that a renovation to the low-energy scenario is not likely to become standard practice in the Belgian building stock. Therefore, the EPB2010-level used in TABULA is defined in this work as the *thorough renovation scenario*, referred to as Ref. 2, and an intermediate scenario (Ref. 1) is defined. For this intermediate level of energy refurbishment, the windows have been upgraded (U-value = 2 $\mathrm{W}/(\mathrm{m}^2\mathrm{K})$), the air tightness is improved ($v_{50} = 6$ h^{-1}) and the roof has been insulated to a U-value of 0.3 $\mathrm{W}/(\mathrm{m}^2\mathrm{K})$. In Ref. 2 the outer walls and floor are also insulated in addition to Ref. 1, to a U-value of 0.3 $\mathrm{W}/(\mathrm{m}^2\mathrm{K})$, which is slightly below the 0.4 $\mathrm{W}/(\mathrm{m}^2\mathrm{K})$ used in the TABULA specification. Note that the thermal mass of the dwellings is, apart from the added insulation material, not affected by these renovations.

The aggregation of the heat demand of each building typology to the demand of the entire stock is not explicitly carried out in the TABULA project for the typical housing approach. As stated in the introduction the typical housing approach merely presents a set of typical dwellings for each building type and age class. In order to get an estimate of the heat demand of the whole stock the heat demand of each dwelling is multiplied by the number of dwellings of each building typology. The number of dwellings is obtained from the SuFiQuaD project [52], which is also mentioned as a data source in the TABULA project and is in line with – though more detailed than – the Belgian land register. However, there exist some discrepancies between the numbers shown in SuFiQuaD and our implementation for the TABULA building stock. The 4^{th} period in the SuFiQuaD data ends in 2007 instead of 2005

Table 5.1: Number of buildings used for aggregation of TABULA building stock

Age class	D: Detached	SD: Semi-detached	T: Terraced
A: Pre 1945	269 771	375 000	766 884
B: 1946-1970	309 263	275 838	242 952
C: 1971-1990	446 481	158 123	87 706
C: 1991-2005	266 050	81 677	54 519
D: Post 2005	74 135	29 046	19 388

as for the TABULA project. Moreover, there is no data for period 5 (2005-2012). Therefore the number of buildings for period 4 (1991-2005) and period 5 (2005-2012) are obtained by respectively linear interpolation and extrapolation of the SuFiQuaD data for the period of 2005-2007. The results are summarized in Table 5.1.

5.1.2 Detailed building stock energy simulations

In this section the building energy simulations used to generate dynamic heat demand profiles for the single family houses of the Belgian building stock are presented. Since disaggregated dynamic measurement data on the energy use for heating are not available for Belgium, the simulations presented in this section will be used as validation set for the reduced-order models presented in Section 5.1.3.

The detailed simulations are carried out using the IDEAS-library described in Chapter 2. According to the simulations in previous chapters, only the heat demand of the building – and not the energy use – is considered to develop and verify the reduced-order building stock model (Section 5.1.3) and quantify the theoretic potential of the structural thermal mass for ADR (Section 5.2). Therefore an ideal heating system is implemented for the development of the building stock model. In the integrated operational model (Section 5.3.1), the heating system is included by a separate sub-model, representing air-to-water and ground-to-water heat pumps (see Section 5.3.1).

The nominal power of the production unit is designed for each building according to EN12831 [120].

As in previous chapters both radiators and floor heating systems have been compared in the scenario analysis. However, the floor heating is only applied in dwellings constructed after 1990 or after thorough renovations (Ref. 2) have been carried out. This is done since for the older, un-renovated dwellings the high heat loss coefficient does not allow to apply low temperature heat emission systems, such as floor heating [181].

Ventilation and infiltration are simplified to a constant airflow model. Hygienic ventilation is

Table 5.2: Deterministic schedule for indoor temperature setpoints

Zone	Setpoint high	Setpoint low	High setpoint period
Day-zone	21 °C	16 °C	07:00–22:00
Night-zone	18 °C	16 °C	21:00–09:00

only implemented after 2005 with a constant ventilation rate of 0.4 ACH, in accordance with the TABULA report.
To verify the building models, the use of the thermostat is implemented by a deterministic pattern based on [182] shown in Table 5.2. Note that, as explained further, stochastic user behaviour is implemented according to [95] in the integrated operational model (Section 5.3.1).

In order to check if the simulation results show the correct order of magnitude, the results of the detailed simulation using the 'white-box model' (WB) are – in absence of adequate measurement data – compared against the annual heat demand calculated for each typology in the TABULA-project. The latter was obtained by the monthly-averaged calculation method implemented in the EPB software [117]. For the total annual heat demand, an average difference of 13 % is found between the detailed simulation model and the results specified in the TABULA-report [180]. Given the differences that were found by Protopapadaki et. al. (2014) for the comparison between the TABULA- and ULg-descriptions of the Belgian building stock, the accuracy of these detailed simulations is considered to be acceptable. More important, relative differences for the heat demand of the different typologies show the same trends for both building stock descriptions confirming the usability of the model for inter-building comparison. Nevertheless, the absolute value of the heat demand, and consequently of the available storage capacity of the residential stock, should be handled carefully in the absence of more reliable statistical data on the Belgian building stock.

5.1.3 Reduced-order building models

In order to reduce the computation time, the grey-box modelling framework presented in Chapter 4 is applied in this section to develop reduced-order models in the form of lumped-capacity models for each typology.
The reduced-order model structure is shown in Figure 5.3 and has been established on a forward selection process as presented in Chapter 4 (Section 4.5.4). For all typologies the thermal dynamics can be described by 4 thermal capacities for the day-zone, 3 thermal capacities for the night-zone and 2 thermal capacities for the floor between day- and night-

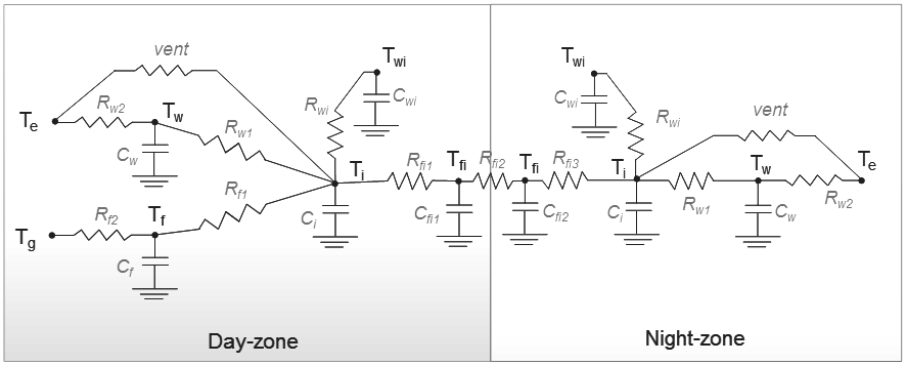

Figure 5.3: Structure of the 2-zone reduced-order models, with in each zone states for the indoor air (T_i), the exterior walls (T_w), the interior walls (T_{wi}) and the floor between day- and night-zone (T_{fi}). T_f represents the ground floor in the day-zone. Note that the inputs for the thermal gains and the related parameters are not shown.

zone. The resulting model structure (Figure 5.3) is thus the same as the model obtained in Section 4.5.4.

Two approaches are used to calculate the model parameters. Firstly, the parameters are estimated using the *grey-box modelling* approach presented in Chapter 4. Thereby the detailed simulations are used to generate the identification data set. Secondly, *theoretical RC-models* are implemented whereby the model parameters are obtained directly from the building stock description. This approach is included here to analyse whether it is possible to skip the system identification process by taking into account the findings of the physical interpretations of the parameters analysed in Chapter 4. Both approaches are presented in the following paragraphs.

Grey-box modelling The first approach to establish the reduced-order building stock models is based on the grey-box modelling framework discussed in Chapter 4. In Section 4.5.4, the identification process has already been presented for the multi-zone detached dwellings from before 1945 (D1) and after 2005 (D5). The same process has been followed to identify reduced-order models for the other typologies.
The data for the identification process has been generated using the detailed simulation model described in Section 5.1.2. Two types of virtual experiments have been carried out. In the first experiment, the dataset is generated by simulating a PRBS experiment. Thereby a pseudo-random binary sequence (PRBS) is implemented on the heating system. Two uncorrelated signals have been used for the day- and night-zone. In the second experiment,

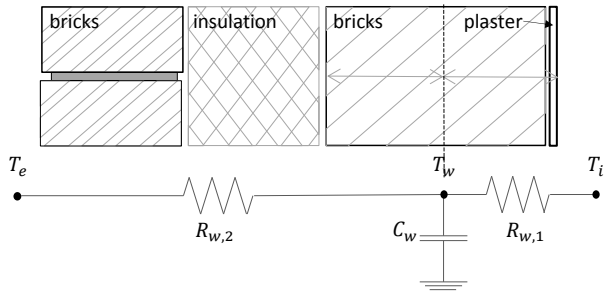

Figure 5.4: Representation of the first order model used for the outer walls. The state of the walls is, based on Chapter 4, assumed in the middle of the material layers inside the insulation barrier.

in-use behaviour with the deterministic thermostatic control of Table 5.2 is simulated. In both cases measurements of the indoor air temperature and the heat flows to the different components are used as observation variables.

The identified models are validated by analysing the residuals for 1-step ahead, 1-day ahead and 1-week ahead predictions as well as the performance for long term simulation on a cross-validation set as presented. Thereby, it is found that although minor over-fitting problems were found for the uninsulated dwellings, the same model structure (Figure 5.3) can be used for all typologies. The resulting model parameters for each of the building typologies are summarized in Appendix B. The validation results are briefly discussed in Section 5.1.4.

Theoretical RC model For the theoretical RC model, the lumped parameters are calculated directly from the building stock specification, taking into account the assumptions presented in Section 5.1.1 and the rules of thumbs that have been deduced from the identified grey-box models (Chapter 4). More precise, the identification of the active thermal mass in buildings showed that the active thermal mass of the envelope can be estimated by the thermal mass of the material layers within the insulation barrier. This rule of thumb is applied to quantify the thermal capacities of the envelope and the ground floor.
The thermal resistance for the envelope (R_w) is calculated using the wall compositions defined for the detailed model. In line with the calculation of the thermal capacity of the wall, the internal resistance $(R_{w,1})$ is defined as the thermal resistance between the indoor environment and the middle of the material layers within the insulation barrier. $R_{w,2}$ is then defined as the thermal resistance between the middle of the layers within the insulation barrier and the outdoor environment, as shown in Figure 5.4.
For the internal walls and floor the entire thermal mass has been taken into account, since

the components are entirely within the insulation barrier. The thermal resistance between the indoor air and the thermal capacity of the interior walls R_{wi} is taken equal to 50 % of the total resistance of the wall. As such, the thermal mass is assumed to be in the centre of the wall and is accessible from both sides.
In addition, the UA-values of the windows have been combined with the ventilation and infiltration losses. This is done since the thermal mass of the windows is negligible compared to the massive building structure and is in line with the results found in Chapter 4.
In all cases, standard surface resistances at the interior surfaces are used according to [121].
The convective and radiative heat flow from the low temperature radiators are combined with the internal gains as 1 input signal for the model. Since the radiators have a radiative heat fraction of 0.3, 70 % of the heat input is distributed to the indoor air. The remaining 30 % is distributed to the capacities of the different components using area weighted distribution factors, hence assuming that all emissivity factors are equal. Solar gains are, in line with the approach of the WB model, entirely allocated to the states of the opaque components using area weighted distribution coefficients.

5.1.4 Comparison of modelling approaches

The following paragraphs present respectively a comparison of the annual heat demand as well as a verification of the aggregated load-duration curves. Note that the accuracy of the reduced-order models for simulation of the dynamic behaviour of the dwellings has already been verified on a building level in Section 4.5.4. The aim of this section is therefore to analyse the aggregation to the national stock level.

Annual heat demand Figure 5.5 gives an overview of the annual energy demand for the different model and building types. Comparison of the theoretical RC-model (RC) with the detailed simulations (WB) shows an overestimation of the energy demand for the RC-models of on average 20 %. The overestimation is more pronounced for the night-zones and is mainly caused by an overestimation of the heat transfer coefficient between the indoor air and the thermal capacities of the components. As shown in Section 4.5.4 the constant, theoretical heat transfer coefficients implemented in the RC models were up to a factor 2 higher than those obtained by detailed simulations. Consequently, the total thermal resistance is underestimated compared to the detailed simulations. For the well insulated dwellings this effect is less pronounced (4-6 %) than for the uninsulated walls (12-31 %), since the relative impact of the interior heat transfer coefficient in the total thermal resistance of the wall becomes smaller.

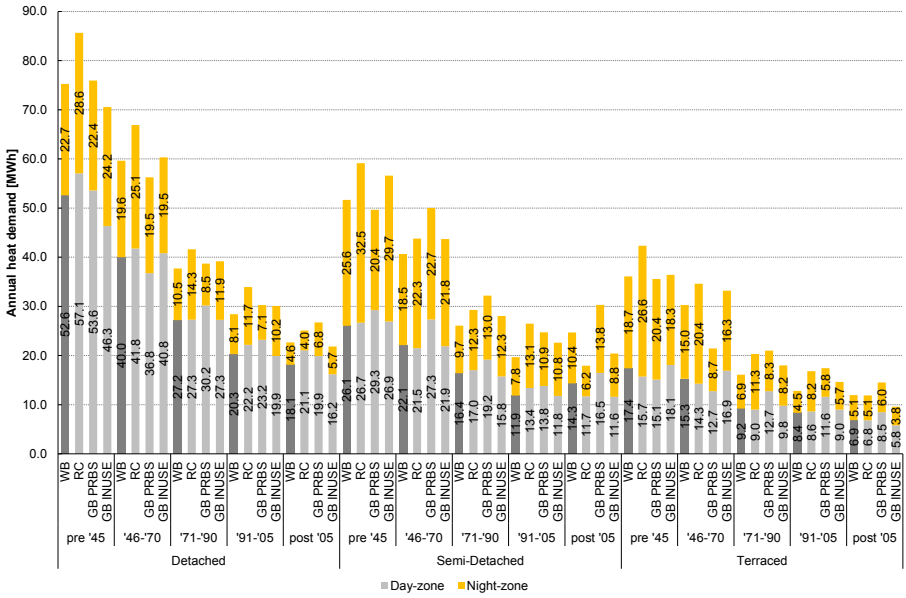

Figure 5.5: Calculated annual energy demand [MWh] as a function of the age class and building type for the radiator heated buildings. 'WB' and 'RC' correspond to the detailed simulation model and the theoretical RC-model respectively. The grey-box models estimated on the PRBS data and the in-use data are referred to as 'GB PRBS' and 'GB INUSE' respectively.

For the reduced-order models obtained by system identification (GB INUSE and GB PRBS in Figure 5.5), the difference with the detailed simulation is less pronounced. For the buildings before '05 (periods A to D), the average difference is reduced to 7 % and 10 % for respectively the models identified on in-use and PRBS data. The estimated models for the buildings after '05 (period E) show higher deviations. Analysis of the physical parameters showed that for these buildings, the absorption of solar gains is overestimated. This overestimation is mainly caused by the fact that the models are trained on winter data, during which the excitation by solar gains are low, resulting in a high level of uncertainty. Nonetheless, as shown in Chapter 4, the use of in-use mid-season data or summer data resulted in a higher uncertainty on the heat loss coefficient due to the decreasing difference between the indoor and outdoor temperatures. Here, the underestimation of solar gains is considered to be of lesser importance since the focus of the simulations will be on the heating period.

Comparing the results for the different building types, an overestimation of the heat demand is generally shown for the identified models. The overestimation is more pronounced for the semi-detached and terraced buildings (11-23 %) compared to the detached dwellings

(10-13 %) and is mainly due to an overestimation of the heat demand in the night-zone. As a result of the high level of uncertainty on the estimated thermal properties of the internal floor between the day- and night-zone, the identification is found to significantly overestimate the thermal resistance and thermal capacity of the internal floor. Consequently, the heat transfer between day- and night-zone for the grey-box models is strongly underestimated, resulting in lower indoor temperatures and a higher heat demand for the night-zones. These unreliable estimates result from the almost constant temperature within the centre of the floor due to the fixed thermostat schedule during the identification process. As a consequence the model is not able to accurately simulate the heat demand during summer when the mean temperature in the building rises. A dedicated identification experiment, activating the thermal mass of the internal floor is therefore necessary.
Regardless of the large deviations in summer, the reduced-order models show acceptable correspondence to the detailed simulations during the winter period, especially for the day-zone. As such the models are considered acceptable for the evaluation of the ADR potential, since as indicated in Chapter 3 and further in Section 5.2.2 the available storage capacity for ADR decreases significantly in summer, due to the limited thermal losses and higher passive gains. Moreover, in the integrated model (Section 5.3.1) the heating system is assumed only to be active during the heating season.

Impact at aggregate level As explained in Section 5.1.1, the aggregation of the heat demand of each building type to the demand of the entire stock is not explicitly carried out in the TABULA project for the typical housing approach. As stated in the introduction the typical housing approach merely presents a set of typical dwellings for each building type and age class. In order to get an estimate of the heat demand of the whole stock the heat demand of each dwelling is multiplied by the number of dwellings of each building case (Table 5.1).
Figure 5.6 shows the resulting load duration curve for the aggregated Belgian residential stock. Although small differences are shown, an acceptable prediction of the load-duration curve is obtained using the reduced-order models. Where the theoretical reduced-order models show a more accurate prediction of the peak demand, the grey-box models identified on the in-use data show good correspondence for medium and lower loads.
Taking into account the uncertainty on the building stock description that was found by Protopapadaki et. al. [180], the use of both the theoretical and the identified reduced-order model for building stock simulations is considered as acceptable.

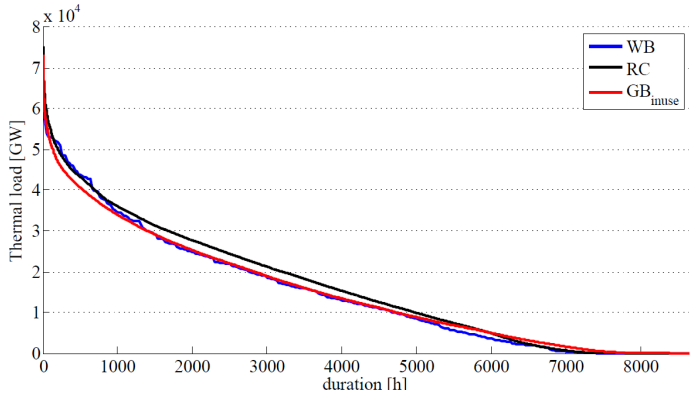

Figure 5.6: Load duration curve for the aggregated heat demand

5.1.5 Conclusions for the reduced-order building stock model

Reduced-order building models have been evaluated for their application in a dynamic bottom-up model for the Belgian building stock. In a first phase, detailed building models were implemented, based on the building stock description of the TABULA project, in the IDEAS-library in Modelica. Thereby the lack of qualitative statistical data on the building stock, required a significant amount of assumptions ranging from material properties, wall compositions to the allocation of the useful area to day- and night-zones. Verification of the detailed models against the heat demand calculation provided by TABULA showed a difference of less than 10 % of the annual heat demand of the dwellings. Validation of the heat demand profile against measured data could not be carried out, since no dynamic data are available on national level.

In the second part of this section, the accuracy of the reduced-order models is compared against the detailed simulations. Thereby both the grey-box modelling approach presented in Chapter 4 and a direct implementation of the physical parameters based on the building stock data have been compared. The analysis showed that for all cases the simulation of the heat demand profile during the heating season was acceptable. However the relative differences in the annual heat demand with the detailed simulations are in general smaller for the identified grey-box models compared to the theoretical RC-models and increase as the absolute heat demand decreases. The main differences are found in the night-zone, where the unreliable estimate of parameters of the floor between day- and night-zone results in an over-prediction of the heat demand. This is especially the case during the summer period. During winter season, when the heat demand is high, good agreement is found between the

reduced-order models identified on in-use data and the detailed simulations.

5.2 Quantifying ADR characteristics of the Belgian residential stock

In this section the theoretical potential for ADR using the structural storage capacity is quantified for the different typologies of the Belgian residential building stock. Thereby the goal is to get insight in the ADR characteristics for the Belgian stock, which will help to understand the results of the integrated model presented in Section 5.3.
The quantification uses the simulation-based methodology that has been developed in Chapter 3. More specific, the available storage capacity and the storage efficiency are discussed here as they can be interpreted as intrinsic building properties. The state-of-charge and available power flexibility are not presented here, since it was concluded that the latter only show an instantaneous snapshot of the available flexibility.

The ADR characteristics are calculated using the grey-box models that have been identified in Section 5.1.3. The results are compared for both simplified static boundary conditions (Section 5.2.1) as well as dynamic boundary conditions (Section 5.2.2). Thereby the former correspond to the static approach followed in Section 3.4 and allows for a theoretical comparison of the potential of different building typologies and renovation levels. The latter are used to additionally evaluate the impact of the time of use of the storage capacity in relation to the occupancy schedule and the outdoor climate. Note that in both cases only the heat delivered by the emission systems is used as an input. As in Chapter 3, the production efficiency is hence not considered. The impact of the efficiency of the heating system is discussed further in Section 5.3 using the integrated operational model.

5.2.1 Available storage capacity and storage efficiency for static boundary conditions

Figure 5.7 shows the available storage capacity (top) and storage efficiency (bottom) as a function of the building typology and renovation level for the buildings equipped with radiator heating. Similar trends are found for the floor heating cases, but the results are only shown for the radiator cases. Although both the available capacity for ADR and the storage efficiency were found to depend on the outdoor temperature and the comfort range (Chapter

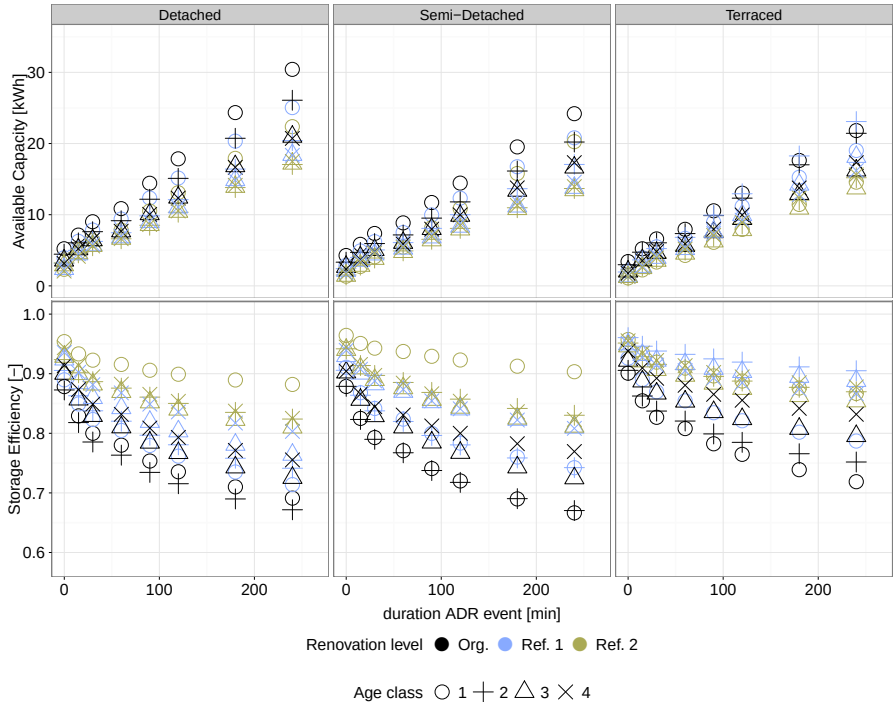

Figure 5.7: Available storage capacity for ADR (top) and storage efficiency (bottom) for the different building types, age classes and renovation levels for the radiator heated buildings, a constant outdoor temperature of 5 °C and comfort range of 2 °C

3), here only the results for a comfort range of 2 °C and an outdoor temperature of 5 °C are shown. Thereby the comfort range is similar to the one used in the operation model (Section 5.3.1), while the outdoor temperature of 5 °C is a representative outdoor temperature during the heating season. Note that the indoor temperature set-points are – except during the ADR-event – kept constant at 20 °C and 18 °C for respectively the day- and night-zone.

Figures 5.7 (top) shows a significant increase of the available storage capacity as the age of the dwelling increases and renovation level decreases. Due to the higher nominal heating power, the available capacity of the oldest buildings in their original state is about twice the size of the thoroughly renovated buildings. For the same reason, the available capacity is on average 20 % higher for detached dwellings than for semi-detached and terraced houses. When the storage capacity is activated for a period of 4 h, the available capacity varies between 12 kWh for the thoroughly renovated terraced dwellings and 30 kWh for the original detached house built before 1945. As a comparison, this is equivalent to a water storage tank

of respectively 520 l and 1300 l assuming a temperature difference of 20 $^{\circ}\mathrm{C}$ in the storage tank. For the buildings equipped with floor heating similar trends are found. Nevertheless, in line with the results of Section 3.4.2, the available capacity is in general higher for the floor heated buildings, ranging from 16 kWh for the thoroughly renovated terraced dwellings and 66 kWh for the original detached house built before 1945, equivalent to water storage tanks of respectively 690 and 2840 l.
Consistent with the findings of Chapter 3, the available storage capacity increases with the heat loss coefficient and the size of the dwellings. Consequently, Figure 5.7 (top) also demonstrates that when the buildings are renovated to a similar insulation level, the relative differences between the age classes is reduced. An exception to this is found for the buildings built before 1945 (Age class 1). For these dwellings the outer walls consists of a 25 cm brick wall, whereas a cavity wall is used for the newer buildings. The thermal mass inside the insulation layer is thus significantly higher for the oldest period, even though the entire thickness does not contribute equally to the available capacity as shown in Chapter 4.

The corresponding storage efficiencies are shown in Figure 5.7 (bottom). As in Chapter 3, the storage efficiency also depends significantly on the heat loss coefficient, as shown by the increasing efficiencies for increasing renovation levels and decreasing age of the building.
For the uninsulated detached dwellings, the storage efficiencies vary between 66 % and 75 % for an ADR-event of 4 h (81-93 % for floor heating). Thereby it should be noted that as an exception the detached buildings of Age Class 1 show a slightly higher efficiency (2 %) compared to the dwellings of Age Class 2, which is linked to the high thermal mass of the massive outer walls for Age class 1 compared to the uninsulated cavity wall for Age class 2.
A mild renovation (Ref. 1) does not drastically improve the efficiency for the detached dwellings. Since for these dwellings most heat is stored in the day-zone, improving the insulation quality of the roof (Ref. 1) does not drastically affect the storage efficiency. For the terraced and semi-detached dwelling the contribution of the night-zone in the total capacity for ADR is higher, hence the larger impact of refurbishment scenario 1.
When also the outer walls and floor are insulated (Ref. 2), storage efficiencies above 80 % (90 % for floor heating) are found for all cases if the duration of the ADR-event is limited to 4 hours. Moreover, the relative differences between the age classes are reduced after insulation, with the exception of the oldest dwellings as the ratio of the thermal mass to the heat loss coefficient is significantly higher for these dwellings.
Finally, comparing the building types, the higher ratio of the thermal mass to the heat loss coefficient for the terraced buildings results in storage efficiencies that are 5-10% higher than for the other building types equipped with radiator heating. Moreover the effect of the mild renovations (Ref. 1) is more pronounced for the terraced buildings. The same level of

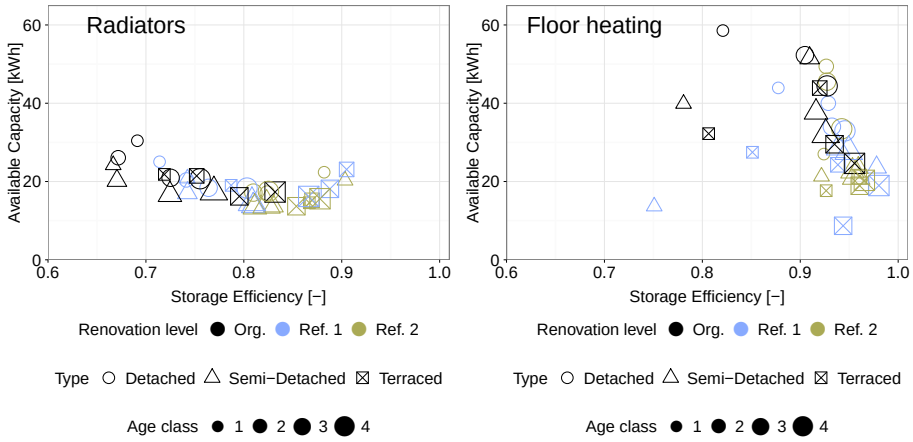

Figure 5.8: Scatter plot of the available storage capacity as a function of the storage efficiency for the radiator (left) and floor heated building typologies. The shape and size of the markers show respectively the building type and age class, while the colour indicates the renovation level.

increase in the storage efficiency is not shown for the terraced houses when the insulation quality is improved further to renovation level 2. Nevertheless, it should be noted here that for the thoroughly renovated dwellings the remaining differences in the results fall within the level of uncertainty of the reduced-order models and should be handled carefully.

As a summary, Figure 5.8 shows the relation between the available capacity for ADR and the storage efficiency for the different buildings in the Belgian building stock for a storage period of 2 h. Based on these theoretical characteristics, the highest operational savings due to ADR, when implemented in the integrated operational model of Section 5.3, are expected for the floor heating buildings since they do not only show higher storage efficiencies, but also significantly higher available capacities. For the floor heated buildings, except for specific cases, all efficiencies are above 90 %, compared to variations between 65 % and 91 % for buildings equipped with radiators.
For the latter, the highest potential for ADR is expected for the mildly renovated terraced buildings built after 1990, since they show both high efficiencies (87 % - 91 %) and higher available capacities compared to the thoroughly renovated buildings. For the floor heating cases the operational savings due to ADR are expected to be less sensitive to the storage efficiency since high values are obtained for most buildings. Consequently, buildings with a higher capacity, i.e. the older and mildly renovated dwellings, are expected to have a higher impact on the operational savings and CO_2-emission reductions.

5.2.2 Impact of dynamic boundary conditions on storage efficiency and available capacity for ADR

While the results of the previous section – obtained for simplified, static boundary conditions – allowed to assess and contrast the theoretic potential of dwellings as a function of their thermal properties, the storage efficiency and available capacity were also shown (Section 3.4) to depend strongly on the starting time of the ADR-event. Thereby, the storage efficiency was found to decrease up to 10 % when the ADR-event increases the set-point temperature at night when it would have been reduced in the reference case following the occupancy schedule. A similar reduction was found when the thermal capacity was activated in an ADR-event prior to – or during – a period with high solar gains.
In this section, the time-dependency of the ADR properties is assessed for the different building typologies of the Belgian residential stock. Therefore, the available storage capacity and storage efficiency are quantified as a function of the start time of the ADR-event. The simulations are conducted for the Belgian climate and the occupancy schedule shown in Table 5.2, a duration of the ADR-event of 2 h and a comfort range of 2 $^{\circ}\mathrm{C}$. The duration of 2 h has been chosen based on the findings of Section 3.4.4. There the dependency of the efficiency on the start time of the ADR-event was found to be averaged out for longer ADR-events, since the ADR-event is more likely to cover both occupied and unoccupied periods.

Figure 5.9 shows the available storage capacity as a function of the start time of the ADR-event. While similar trends are found for the other building typologies, the figure contrasts the radiator heated detached (left) and terraced buildings (right) built before 1945 (Age class 1) and between 1990-2005 (Age class 4). They are shown here since they represent two significantly different cases in terms of insulation quality and heat loss to capacity ratio. Moreover, the figure shows the available capacity of the original buildings before renovation (top) and after thorough renovation (bottom). Thereby the available capacity shows significant variations on two time scales. A long-term variation is found for the available capacity, showing decreasing values in mid-season when the outdoor temperature rises and solar gains become important. In addition an important daily variation is shown. An averaged daily profile is illustrated further in Figure 5.10.
The long-term variations result from the increasing outdoor temperatures and high solar gains in mid-season. As such, the free-floating indoor temperature will rise above the minimum comfort temperature, reducing the temperature difference that is available to activate the structural thermal energy storage capacity. Note that the impact is more pronounced for the detached dwelling due to the higher glazed area and therefore the higher solar gains.

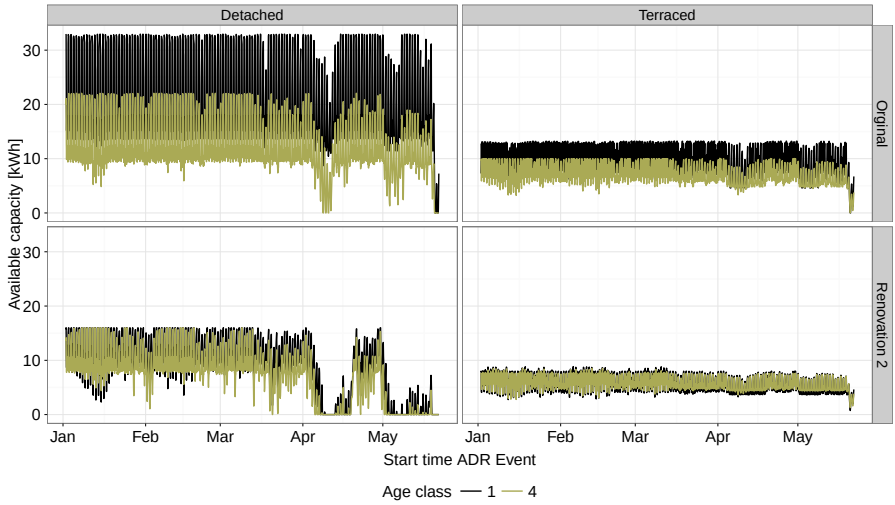

Figure 5.9: Available storage capacity as a function of the start time of the ADR-event for an ADR-event of 2 h with a comfort range of 2 °C, contrasting the detached (left) and terraced (right) dwellings for both the original (top) and thoroughly renovated (bottom) cases. The different colours represent the buildings built before 1945 (Age class 1) and between 1991-2005 (Age class 4).

In the renovated scenario, the high solar gains for the detached dwelling and the fact that shading is not included in the model, results in indoor temperatures above 22 °C for the period between April 2^{nd} and April 12^{th} and after May 4^{th}. Consequently, the heating system can no longer be used to activate the thermal mass and the resulting available capacity for ADR is 0 kWh. Note that active cooling systems can be considered for ADR at this point, however this has not been investigated in this Belgian context. Moreover, one may argue that the use of shading devices may avoid the overheating and prolong the active use of the structural thermal energy storage capacity. In both cases, it is the authors opinion that passive strategies should always be given priority to deliver thermal comfort. This statement is supported by the results of the storage efficiency shown further in Figure 5.11.

In addition to the long-term variations, daily fluctuations induced by the occupancy schedule are illustrated in Figure 5.10. Since, the maximum temperature in the ADR-event ($T_{max,ADR}$) is calculated based on the temperature set-point for the occupied period, a larger range of temperature variations is available during the set-back periods.
To analyse this effect in more detail – keeping in mind the national electricity demand profile for Belgium (Figure 3.15) – Figure 5.10 shows an average daily profile of the available storage capacity for the same cases shown in Figure 5.9. Thereby a clear difference is found between

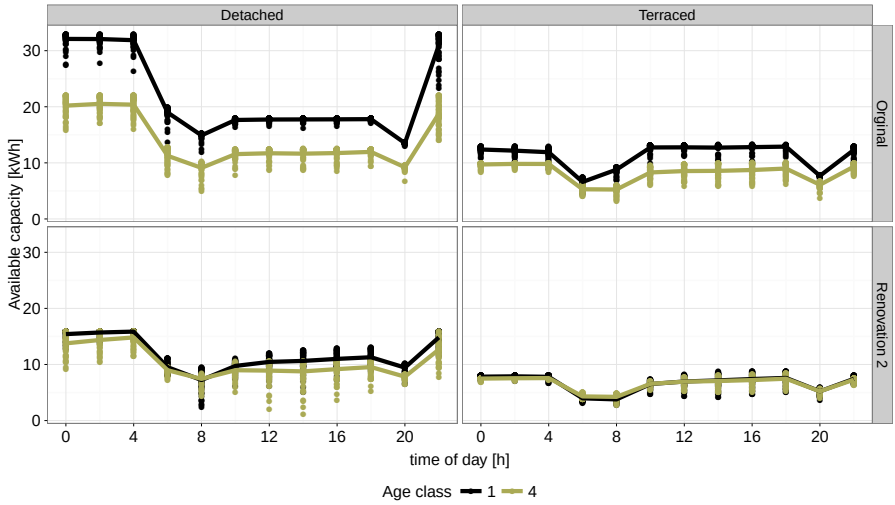

Figure 5.10: Daily profile of the available storage capacity, contrasting the detached (left) and terraced (right) dwellings for both the original (top) and thoroughly renovated (bottom) cases. The different colours represent the buildings built before 1945 (Age class 1) and between 1991-2005 (Age class 4), for an ADR-event of 2 h with a comfort range of 2°C. The points show the values for each day, while the curve represents the daily profile averaged over the whole period.

the profile of the terraced and the detached dwelling. Whereas for the detached dwelling the available capacity is almost 2 times higher between 10 PM and 4 AM, the available capacity for the terraced building is almost equal during day-time as at night. This can be explained by the significant difference between the share of the day- and night-zone in the total heating power. For the detached dwelling the heating power for the day-zone is on average twice as high as for the night-zone. Consequently, the additional capacity that is available in the day-zone during the temperature set-back at night, is higher than the additional capacity that is available in the night-zone between 9 AM and 9 PM. For the terraced buildings, both zones have an equal share in the heating power.
The reduction in the capacity between 6AM and 8AM and at 8 PM, coincide with the start-up of respectively the day- and night-zone. During this period the heating in the reference case already operates at its maximum capacity to recover from the temperature setback and is therefore not available for ADR.

Complementary to the available storage capacities for ADR, Figure 5.11 shows the evolution of the storage efficiency. Thereby, a systematic decrease of the efficiency is found as a function of time, in addition to the daily variations and the significant reduction of the storage efficiency for periods with high solar gains. While the latter are directly linked to the variations

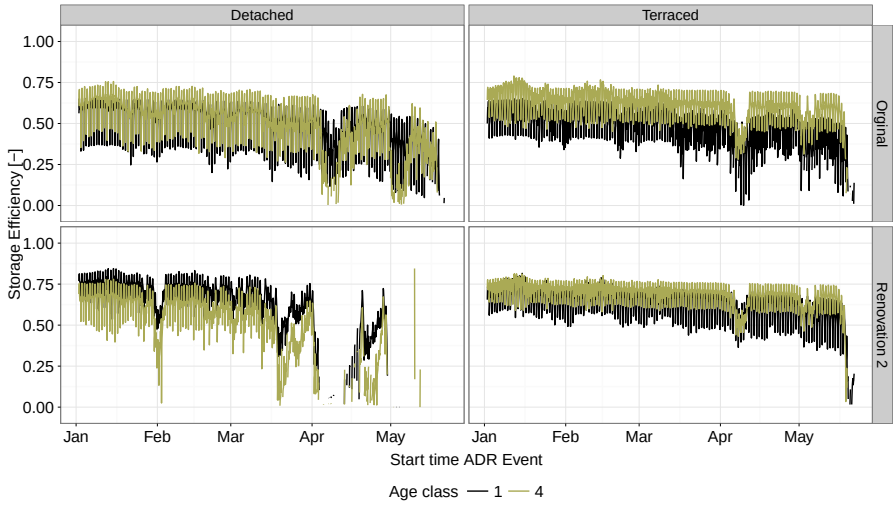

Figure 5.11: Storage efficiency as a function of the start time of the ADR-event for an ADR-event of 2 h with a comfort range of 2 °C, contrasting the detached (left) and terraced (right) dwellings for both the original (top) and thoroughly renovated (bottom) cases. The different colours represent the buildings built before 1945 (Age class 1) and between 1991-2005 (Age class 4).

found in the available storage capacity (Figure 5.9), the systematic reduction is explained by the decreasing heat demand of the dwellings as the outdoor temperature rises. To analyse this effect the relative available storage capacity ($C_{ADR,rel}$) is calculated as:

$$C_{ADR,rel} = \frac{C_{ADR}}{\int_0^{24h} Q_{Ref} dt} \tag{5.1}$$

with Q_{Ref} the heat demand without ADR. Thereby, a systematic increase of the relative storage capacity is shown (Figure 5.12) as a function of time – due to the increasing outdoor temperature – which corresponds to the systematic reduction of the efficiency found in Figure 5.11. During the winter period, the heat stored during the ADR-event with a duration of 2 h corresponds on average to 3 % - 10 % of the daily heat demand for the original dwellings and between 5 % and 20 % for the thoroughly renovated buildings. Moreover, the relative available capacity increases rapidly in periods with high solar gains, especially for the detached dwelling given the higher window to floor area ratio. Consequently the storage efficiency during these periods drops to 0 % as the relative available capacity is close to 100 %. The potential for ADR using the structural storage capacity using only heating systems is thus clearly limited to the heating season.

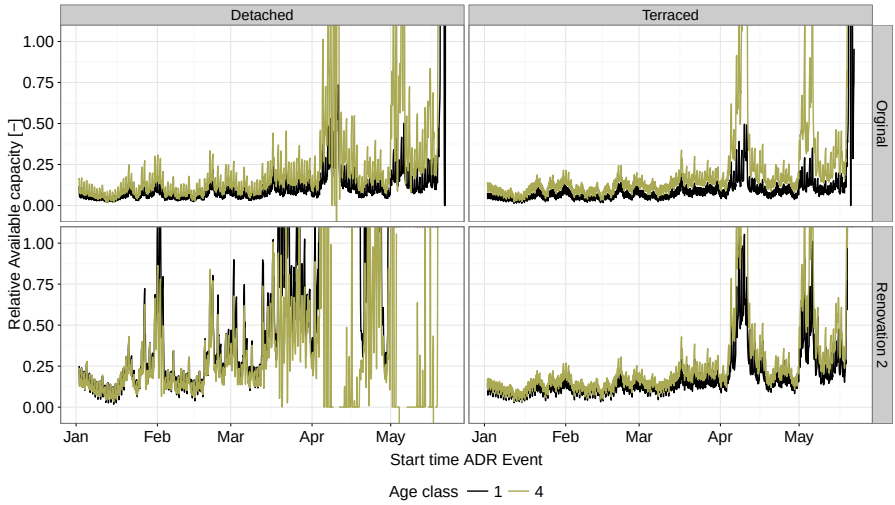

Figure 5.12: Relative available capacity as a function of the start time of the ADR-event for an ADR-event of 2 h with a comfort range of 2 °C, contrasting the detached (left) and terraced (right) dwellings for both the original (top) and thoroughly renovated (bottom) cases. The different colours represent the buildings built before 1945 (Age class 1) and between 1991-2005 (Age class 4).

5.2.3 Conclusions of the quantification of ADR characteristics for the Belgian building stock

In this section the available storage capacity for ADR and the corresponding storage efficiency were quantified for the different typologies of the Belgian residential building stock. Therefore the simulation-based quantification method developed in Chapter 3 has been applied using the reduced-order building stock model developed in Section 5.1.

Firstly, the ADR characteristics were calculated for simplified, static boundary conditions to allow a comprehensive comparison of the impact of building design properties on the potential for ADR. The results showed that the highest available capacities for ADR are obtained for the oldest uninsulated dwellings, since these buildings have the highest heat loss coefficient and hence the highest installed heating power. Nevertheless, the high heat loss coefficient also resulted in a significant reduction of the storage efficiencies. On average storage efficiencies of 66 % to 83 % were found for the original building typologies, for and ADR-event of 4 h with a comfort range of 2 °C. After thorough renovation, the efficiency increased significantly for the older buildings (80-91 %). At the same time, the reduction of the nominal power and the fact that the upper comfort boundaries are reached earlier in an ADR-event for the renovated dwellings resulted in a reduction of the available storage

capacity for ADR (10-25 %). For both the efficiency and the available storage capacity it was found that as the buildings were renovated to the same insulation level, the relative differences between the different age classes became negligible.
Secondly, a quantification of the ADR characteristics using dynamic boundary conditions – also taking into account the occupancy schedule for the day- and night-zone – revealed that in practice the storage capacity is reduced with 10-25 % depending on the starting time of the ADR-event. Thereby the highest potential – showing both a high efficiency and available capacity – was found in the early morning or late afternoon to preheat the zones right before the occupied period starts. Moreover, active use of the structural thermal energy storage capacity should be avoided in mid-season when the outdoor temperature rises and solar gains become important, since excessive efficiency losses were obtained when the fraction of the stored heat to the daily demand is higher than 30 %.

5.3 Demonstration of ADR potential in high renewable scenario using an integrated model

The previous section showed the analysis of the flexibility characteristics, i.e. available storage capacity for ADR and storage efficiency, for the different building types, age classes and renovation levels. Thereby the analysis is carried out on a building level. In this section, the quantification of the potential of using the structural storage capacity for ADR is carried out on a national level. As such, this final section aims at demonstrating the operational savings and CO_2-reductions that can be expected from ADR using residential heat pumps in a high RES system.
To evaluate these operational savings, the integrated operational model (Figure 5.1), developed by Patteeuw et al. (2014), has been extended in collaboration with the authors by integrating the reduced-order dynamic building stock model presented in Section 5.1.
The results presented below are based on the work carried out for the journal paper submitted to Applied Energy, titled: "CO_2-abatement cost of residential heat pumps with Active Demand Response: demand- and supply-side effects" [33]. The goal in that paper was mainly to quantify the CO_2-abatement cost[1], taking into account both the operational aspects of the production side and the physical properties of the demand side. In the discussion of the results presented in this section, the focus will be on the impact of ADR using the structural thermal energy storage on: the need for peak production capacity (§ 5.3.3), the operational

[1] The CO_2-abatement cost is defined as the sum of the difference in annual operational costs of the system and the annuity, of the additional investment, divided by the annual CO_2-emission savings

aspects (§ 5.3.4) and the CO_2-emission reductions (§ 5.3.5). Thereby, compared to the results presented in [33] more emphasis is put on the comparison of the impact of the building type and renovation level on the potential of ADR.

The following paragraphs first briefly summarize the concepts of the integrated operational models (§5.3.1). In §5.3.2 different cases are presented that have been simulated in order to assess the impact of ADR. Finally, §5.3.3, §5.3.4 and §5.3.5 present the results for respectively the peak production capacity, the operational aspects and the CO_2-emission savings.

5.3.1 Description of the integrated operational model

The general framework of the integrated operational model is formulated as an optimization problem that optimizes the operational cost for electricity production on the national level taking into account both the operational aspects of the electricity production system and the physical behaviour of the demand-side. As such, the main added value of this integrated operational model lies in the combined optimization of both demand and supply side. The model structure has already been illustrated in Figure 5.1 and consists of three main parts: (i) the building stock model, (ii) the heating system models and (iii) the electricity production system. The building stock model has already been elaborated, as it is my main personal contribution to the integrated model. The other two parts are briefly summarized below. A more detailed description can be found in [33].

Electricity generation The electricity generation system is modelled by a merit order, which considers efficiencies, minimal and maximal power output of power plants and neglects all other technical constraints. As shown by Patteeuw et al. [183], this approach can approximate the cost savings determined via a state-of-the-art unit commitment and economic dispatch model.
For the electricity generation side, data related to the fixed electricity demand and electricity generation from RES is taken from the Belgian transmission system operator Elia [11] for the year 2013. A high RES scenario is implemented with 30 % and 10 % of the electricity use covered by wind and photo-voltaic (PV) systems respectively. The residual demand – defined as the electricity demand of the heat pumps that is not covered by RES – is assumed to be fully covered by combined cycle gas turbines (CCGT) and open cycle gas turbines (OCGT). For RES based electricity generation, it is assumed that the marginal cost is zero. Curtailment costs are zero since these are assumed to be internal transfers within the model.

Table 5.3: Range of heat pump SPF for the different building cases.

Renovation Level	Mild	Thorough	Thorough	Thorough
Heat pump source	Air	Air	Air	Ground
Heat emission	Radiator	Radiator	Floor	Floor
Min SPF	1.8	2.3	2.5	3.3
Max SPF	2.1	2.6	3.0	4.0

Note that this is an optimistic scenario for ADR, since excessive use of the storage capacity to buffer renewable production, is not penalized.

Heating systems For the application of heat pumps, three main cases are considered: (i) an air coupled heat pump (ACHP) with radiators, (ii) an ACHP combined with floor heating and (iii) a ground coupled heat pump (GCHP) with floor heating[2]. In each case, the heat pump also supplies the domestic hot water demand (DHW). For the lightly renovated building, depending on the age category, the nominal supply water temperature for zone heating can be higher than 60 $^{\circ}\mathrm{C}$. This is too high to be supplied by a standard heat pump, in which case a double-compression, high-temperature air coupled heat pump is considered [184]. The heat pump's efficiency is typically expressed by the coefficient of performance (COP). In this study, the COP is determined according to Bettgenhäuser et al. [185], which results in an SPF[3] as shown in Table 5.3, assuming that the COP is constant during each week and not effected by ADR.
In addition to space heating, the central heating system also produces domestic hot water. For the latter a water storage tank of 200 l is included. The water temperature inside this tank can also be modified for demand response as described in [33].

5.3.2 Definition of the cases

Before the results of the study are presented, this paragraphs briefly summarizes the different case studies that are used for a step-wise evaluation of the impact of heat pumps and ADR on the national electricity production.
As it is the aim of this study to identify whether specific building types are better suited for installing heat pumps with ADR, multiple building typologies (36 cases) and heating system

[2]The radiators in the thoroughly renovated buildings are assumed to have a nominal supply water temperature of 45 $^{\circ}\mathrm{C}$. For the lightly renovated buildings, the water temperature is adjusted to allow a recuperation of the existing emission systems, since replacing the heat emission system in a light renovation scenario was found to be not cost-effective in [184]. GCHPs are in general not combined with this kind of radiators.

[3]The seasonal performance factor (SPF) is defined as the ratio of the heat delivered throughout the year to the yearly electricity use of the heat pump.

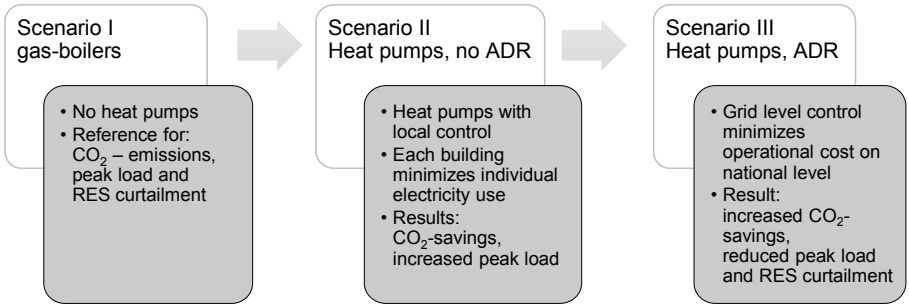

Figure 5.13: Flow chart of the scenarios evaluated for each building and heat pump case.

types (3 cases) are considered. Thereby, in contrast to Section 5.2.1, the original buildings without renovation built before 2005 are not considered since the supply water temperature for these buildings would be too high to be efficiently supplied by a heat pump. Moreover, as was shown in Section 5.2.1, the un-insulated dwellings show significantly lower storage efficiencies.

For every combination of building and heating system, the CO_2-emission reduction, operational cost savings and peak electricity demand are determined. In order to have a significant impact on the electricity generation side, it is assumed that for each case (combination of a building case and heating system case) the electricity demand is scaled up to 250 000 buildings[4]. According to the study for the European heat pump association [185], this is the number of heat pumps that is expected to be installed in Belgium by 2030.

Three simulation scenarios are simulated for all building and heating system combinations (Figure 5.13). First, the CO_2-emissions, the electricity use without heat pumps and the RES curtailment losses are calculated for the reference scenario, assuming all buildings are heated with gas-boilers. This reference electricity demand covers residential plug-loads, lighting, etc. but also non-residential electricity use. The RES curtailment losses correspond to loss of renewable production that occurs when renewable production units need to be shut down to avoid voltage peaks in the grid. One of the important challenges for ADR is therefore to reduce these losses.

In the second scenario, heat pumps are introduced and the impact on the total electricity use, the curtailment losses, peak electricity demand and CO_2 emissions is quantified. In this case

[4] The number of buildings is taken to be identical for all combinations of building types and heating system types, in order to make the relative comparison between these types independent of the number of buildings. Each case is calculated separately meaning that the 250 000 buildings are always of one single building type with one single heating system type. Thereby for the other buildings types no heat pump is implemented and hence no ADR potential exists.

without ADR, the consumers minimize their own electricity use regardless of the implications for the electricity generation side. The electricity generation system then minimizes the cost for supplying the resulting electricity demand profile.
Finally in the third step, the impact of ADR is quantified. Thereby, the use of the structural thermal energy storage capacity and the domestic hot water storage are optimized to obtain the minimal total cost for electricity production.

In order to represent occupant behaviour regarding temperature set points and domestic hot water demand, 52 user stochastic behaviour profiles were generated using the method of Baetens and Saelens [95]. In order to reduce calculation time, this user behaviour is aggregated by averaging the predetermined, effective lower temperature bounds according to [186]. The upper bound for the indoor temperature set-point is 22 $^{\circ}\mathrm{C}$ and 20 $^{\circ}\mathrm{C}$ for respectively the day and night-zone [72]. For the weather data, measurements in Uccle (Belgium) for 2013 are used. This climate data differ from the TMY3 data used in previous sections and are used since they match with the data for the RES generation and fixed electricity demand as mentioned before. In this data set, the average outdoor temperature is 10.2 $^{\circ}\mathrm{C}$, the minimal temperature -9.3 $^{\circ}\mathrm{C}$ and the number of heating degree days is 2474 with respect to a reference indoor temperature and outdoor bound of 16 $^{\circ}\mathrm{C}$.

In the following paragraphs respectively the impact of the heat pumps and the use of ADR on the required peak production capacity, operational aspects and CO_2 emissions are discussed. As shown in [33], all three aspects have an important impact on the CO_2-abatement cost. The results are reported for one year, obtained by solving the optimization problem for each week of the year using a receding horizon approach[5] and assuming perfect prediction of disturbances. Hence, the presented results serve as an upper bound of the practically attainable operational and CO_2-emission savings.

5.3.3 Peak capacity

A transition from gas-boilers to heat pumps will evidently result in an increase of the electricity use that has to be covered – given the production system assumed in this work – by either the renewable energy sources or an increased production of the OCGT and CCGT plants. When the electricity demand of the heat pumps coincides with the electricity demand that already exists in the network, this may significantly increase the total peak demand in the network and thus additional peak production units need to be installed. At an investment cost of 750

[5] A receding horizon is employed, in which the states of the system at the end of a week are passed on to the next week.

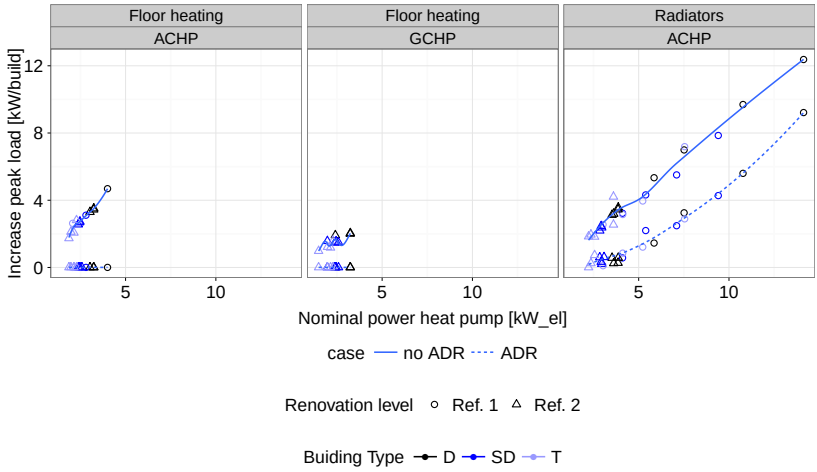

Figure 5.14: Contribution of each building to the increase of the peak demand by introducing heat pumps with (full line) and without (dashed line) ADR as a function of the electric nominal power of the heat pump. The colour-scale indicates the type of building (D: detached, SD: semi-detached, T: terraced). The markers indicated the state of the building (Ref. 1: mild renovation, Ref. 2 thorough renovation)

EUR/kW [187], this additional capacity can be an important term in the CO_2-abatement cost, which is typically not included in heat pump CO_2-abatement cost in the literature. Therefore in this section, the potential of ADR to reduce the peak demand is evaluated as a first performance indicator.

The required peak production capacity is for each building scenario determined through an a-priori optimization of the critical week, i.e. the week with the highest residual electricity demand[6]. When ADR is applied, the demand of the heat pumps during this week is optimized by using the flexibility of both the structural and non-structural storage capacity to minimize the required capacity of the power plants. Note that this installed capacity is then applied as an upper bound for the production capacity throughout the considered year.

Figure 5.14 shows the contribution of each building to the increase of the peak electricity demand [kW/build] by introducing heat pumps with (full line) and without (dashed line) ADR as a function of the electric nominal power of the heat pump. The colour-scale indicates the type of building (D: detached, SD: semi-detached, T: terraced). The markers indicated the state of the building (Ref. 1: mild renovation, Ref. 2 thorough renovation). When no

[6]The residual electricity demand is defined as the electricity demand from which the generation from renewable energy sources is subtracted. Hence, this is the demand which the traditional power plants need to deliver.

ADR is applied, Figure 5.14 shows that the additional peak demand per building is strongly correlated with the nominal power of the heat pump. The lowest increase is thus obtained for the thoroughly renovated terraced buildings. Regarding buildings with the same heat demand, a ground-coupled heat pump performs best because this system has the highest COP and therefore the lowest peak electricity demand.

ADR is found to significantly reduce the need for additional peak power plants, as indicated by the dashed trend line (Figure 5.14). For the floor heating cases and the thoroughly renovated dwellings, the use of the structural and non-structural thermal energy storage allows to shift almost all demand away from the period with the highest electricity use. The buildings with floor heating generally perform better than the same building with radiators. This is in line with the findings of Section 5.2.1, demonstrating that the available storage capacity is lower for the radiator heated buildings. Hence, the heat stored within the thermal mass is found to be inadequate to cover the peak demand period, especially for the less insulated dwellings (Ref. 1 on Figure 5.14).

Consequently, active demand response using the structural thermal mass is found to be an effective measure to avoid the need for additional production units when applied in thoroughly renovated buildings. When heat pumps are to become common practice in less insulated buildings (Ref. 1), ADR cannot avoid the need for additional production capacity. However it is able to reduce the required capacity on average by 30 %, by shifting the heat pump operation away from periods where a peak demand is already present.

5.3.4 Operational aspects

In addition to the reduction of the peak capacity, an important potential of ADR is the increase of the penetration of RES to cover the heat pump electricity use and at the same time reducing the use of traditional power plants. Nonetheless, the analysis of Chapter 3 demonstrated that activating the structural thermal energy storage capacity for ADR comes at the cost of an increase of the heat demand. The main research questions, tackled in this section, are therefore to analyse to what extent ADR leads to an increase of the electricity use on a building level and whether this increased local electricity use due to ADR is balanced by an increased penetration of RES.

To evaluate these research questions the reduction in curtailment losses is compared to the reference scenario when heat pumps with and without ADR are introduced. This reduction in curtailment losses is on the one hand compared to the increase in electricity use on a building level and on the other hand to the change in the production of the OCGT and CCGT

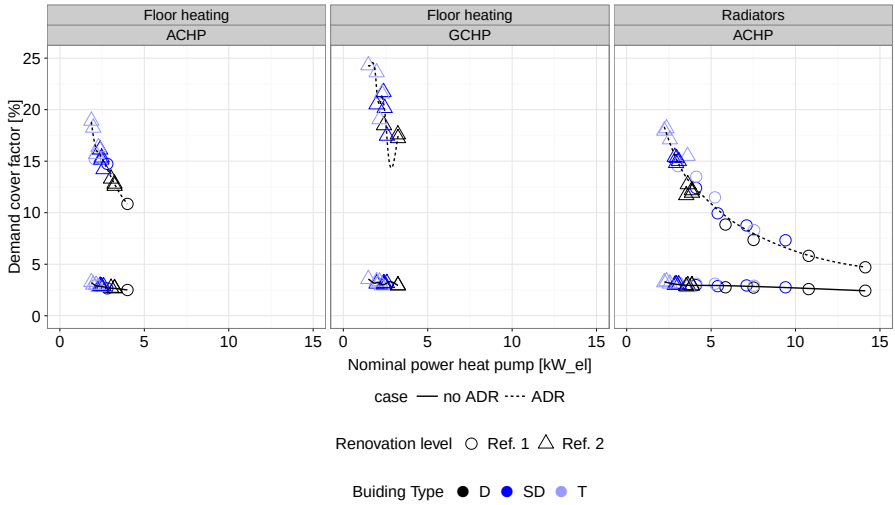

Figure 5.15: Fraction of the annual electricity demand of the heat pumps that is covered by renewable production, with (dashed line) and without (full line) ADR and as a function of the nominal electrical power of the heat pumps.

power plants. The analysis can also be interpreted in terms of a storage-efficiency, whereby the reduction of RES curtailment can be interpreted as the gains from ADR and the increase in the local electricity use as the losses.

As shown in Figure 5.15, the heat pump demand is mainly covered by a higher generation from the gas-fired power plants, since only 2.4-3.5 % of the heat pump demand is covered by RES when no ADR is applied. This reduces the curtailment losses compared to the scenario without heat pumps with 5-30 % (Figure 5.16). The highest reduction of curtailment losses is found for the mild renovation cases since these buildings have the highest electricity use. Note that the latter implies that for the thoroughly renovated buildings the availability of RES, to be used when ADR is applied, is higher.

When ADR is implemented, the share of the heat pump electricity use that is covered by renewable production increases to 6 % for the mild renovation detached dwellings built before 1970 and up to 24 % for the thoroughly renovated terraced dwellings, resulting in a corresponding reduction of the curtailment losses by 35 % to 60 % compared to the scenario without heat pumps (Figure 5.16).
On average, this results in an increase of the use of RES by 0.15 TWh on average, while a reduction of the electricity produced by the power plants by 0.10 TWh is obtained. Consequently increasing the total energy use by 0.05 TWh.

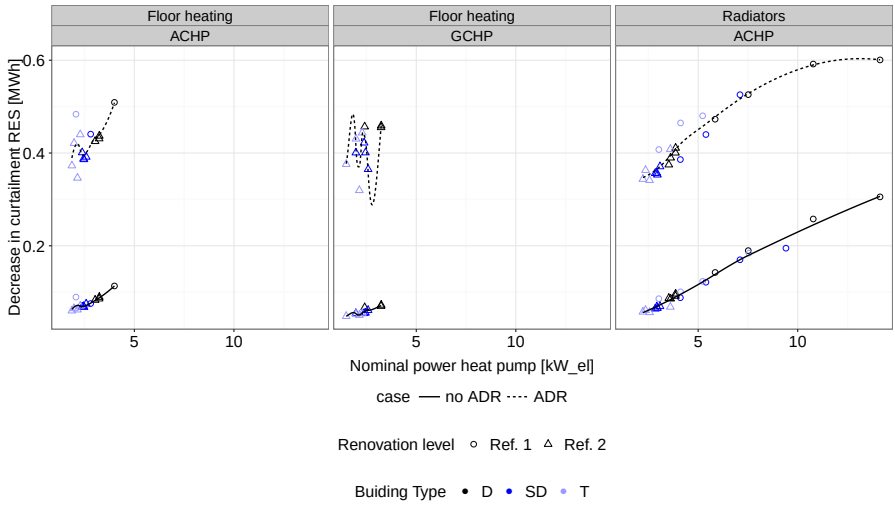

Figure 5.16: Reduction of the RES curtailment losses when introduction heat pumps, with (dashed line) and without (full line) ADR relative to the curtailment losses for the reference case without heat pumps. The markers indicate the renovation level, while the colour of the markers shows the building type.

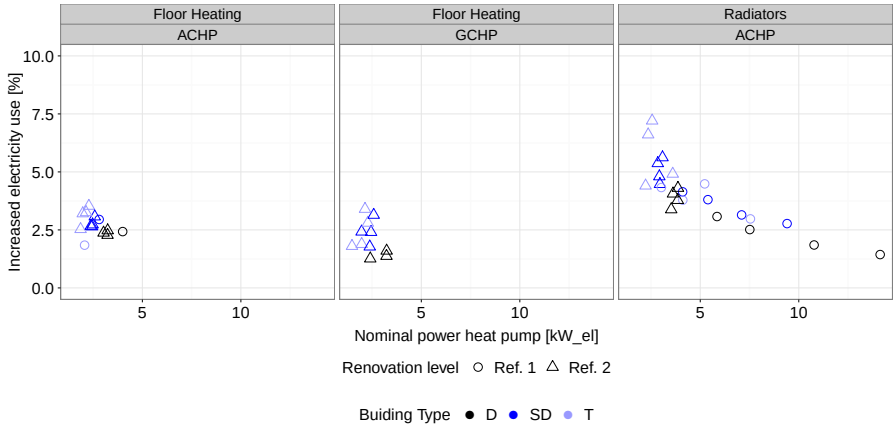

Figure 5.17: Rise in electricity use for space heating when ADR is applied as a function of the nominal electrical power of the heat pump. The markers indicate the renovation level, while the colour of the markers shows the building type.

The latter is caused by the higher average temperatures and hence higher thermal losses and higher energy use as a result of the load shifting. Fig. 5.17 shows this increase in energy use associated with load shifting in terms of the annual heat demand. For all heating systems a clear trend is observed, i.e. relatively more electricity is used for decreasing nominal powers of the system. This effect is counter-intuitive and contradicts the findings of Section 5.2.1 where higher storage-efficiencies where found for better insulated buildings. However, as was already pointed out for the reduction of the curtailment losses, the driving forces for activating the storage capacity differ since relatively more renewable energy is available for the well insulated building. Consequently, since the price for renewable production is assumed to be 0 EUR/kWh, the storage capacity of the well-insulated dwellings will be used more. The latter is also demonstrated by the stronger increase of the indoor temperature.
Comparing the results of the air-coupled heat pump with radiators and floor heating shows that for the same building typologies, the floor heating system shows an increase of the electricity use which is 2 times as high as for the radiator buildings as a result of the higher storage efficiency.

One may argue that the extra energy use is just wasted in higher thermal losses. To see whether this is the case, the decrease in RES curtailment per building is plotted against the increase in electricity use per building in Fig. 5.18. For example, applying ADR causes a building to consume 300 kWh_e of electricity more but reduces 600 kWh_e of RES curtailment, then on a net basis the gas-fired power plants produce 300 kWh_e less. This can be interpreted in terms of a storage-efficiency. In the case of this example the storage efficiency would thus become 50 %, since the increased activation of the heat pumps that charge the thermal energy storage capacity when RES production is high results in a 50 % reduction of the electricity demand when RES is able to cover the load.
Figure 5.18 shows that the decrease in curtailment is always higher than the increase in electricity use due to ADR. Hence on a net basis, less electricity from gas-fired power plants is used. For the air-coupled heat pumps (ACHP) with floor heating, this difference is the highest, resulting in an average storage efficiency of 70 %. For the radiator heating and ground coupled heat pump cases the storage efficiencies are significantly lower, i.e 35 % for the ground coupled heat pump and 25% - 50% for the radiator heating cases. The reason for these low values are however different for the two systems. For the ground-coupled heat pump, the low efficiency results from the increased use of the inefficient auxiliary heater to increase the temperature in the domestic hot water tank. For the radiator heating cases the decreasing efficiencies can be directly related to the differences in thermal properties of the building similar to the analysis carried out in Section 5.2.1. The highest reduction in RES curtailment with an efficiency of about 50 % is thereby obtained for the mildly renovated

terraced dwellings. These buildings were also identified to have the highest storage potential in Figure 5.8, since they combine a high storage efficiency with an adequate thermal load. Nonetheless, the storage efficiencies are for all cases significantly lower than the theoretical values obtained in Section 5.2.1. Thereby it should be emphasized that due to the assumed price for RES of 0 EUR/kWh, excessive and inefficient use of the storage capacity to absorb RES is not penalised. Consequently the increased total energy use may be considered as an upper value.

5.3.5 CO_2-emissions

Due to the reduction of the use of fossil fuel and the increased penetration of renewable energy sources, the introduction of heat pumps significantly affects the CO_2-emissions, especially when ADR is considered.

Figure 5.19 shows the relative change in CO_2-emissions associated with replacing the condensing gas boilers with heat pumps. The relative CO_2-emission savings are highly dependant on the SPF of the heat pump, for which four groups can be distinguished based on Table 5.3. The first group consists of the mildly renovated buildings which are all equipped with a high temperature ACHP and radiator heating (SPF 1.8 to 2.1) and shows CO_2-emissions are reduced by 15 % to 25 % compared to the CO_2-emissions for the scenario without ADR (no ADR), depending on the building type as indicated by the circular markers in the middle pane of Figure 5.19. For the second group, consisting of the thoroughly renovated buildings (indicated by the triangular markers) with an ACHP and radiators (SPF 2.3 to 2.6), the CO_2-emission reduction compared to the no ADR scenario varies between 25 % to 35 %. The third and fourth groups represent the buildings with floor heating combined with an ACHP (SPF 2.5 to 3) or a GCHP (SPF 3.3 to 4) respectively. For these groups the reductions in CO_2-emissions compared to the no ADR scenario are respectively 30 % to 40 % and 40 % to 55 %.

Including ADR leads to an average additional reduction in emission of approximately 15 %. However the relative reduction in CO_2-emissions by ADR depends significantly on nominal power of the heating system and hence on the insulation level of the building. Thereby an additional reduction of the relative CO_2-emissions by up to 25% is found for the thoroughly renovated terraced buildings, indicated by the light-blue triangular markers. In contrast, for the mildly renovated detached dwelling equipped with radiators no significant reduction of the CO_2-emissions is found. The latter is in line with the findings of Figure 5.15, where it was shown that for the mildly renovated dwellings equipped with radiator heating ADR has no significant impact on the heat demand that is covered by renewable production.

Table 5.4: Equivalent electricity generation-system efficiency, $\bar{\eta}_{EGS}$, which can also be interpreted as the inverse of the primary-energy factor (PEF). The reference values are obtained from [188]

Case	Reference values	no ADR	ADR
$\bar{\eta}_{EGS}$	40 %	56 %	71 %
PEF	2.5	1.8	1.4

Note that these are all relative reductions in CO_2-emissions. As buildings get better insulated and the annual heat demand lowers, the absolute CO_2-emissions for the heat pump cases will converge. To illustrate this, Figure 5.20 highlights the CO_2-savings that are obtained by ADR. The figure shows the CO_2-emission savings for the different heating systems as a function of the nominal power of the heating system – which is strongly correlated to the heat loss coefficient. Thereby, two important trends are shown, depending on the heat emission system.

For the buildings equipped with floor heating the additional CO_2-savings for the ADR scenario compared to the no ADR scenario increase with increasing nominal heating power. This confirms the findings of Section 5.1.4 where for increasing heating power a higher available storage capacity was found. In contrast, for the buildings heated by radiators, a parabolic trend is shown. As suggested in Section 5.2.1, this indicates that for a high nominal power – which corresponds to the mildly renovated buildings built before 1990 – the low storage efficiency jeopardizes additional CO_2-savings. This effect is amplified here since the driving force for ADR, i.e. the remaining curtailed RES production after installing the heat pumps without ADR, is already lower for the uninsulated dwellings (Figure 5.16).

The reduction in CO_2-savings is not shown for the floor heated building, since on the one hand the old buildings are not equipped with floor heating and on the other hand the storage efficiency is in general higher for floor heated dwellings. For both emission systems the highest absolute CO_2-savings due to ADR are found for the mildly renovated detached dwellings, although the optimum is not well defined.

5.4 Conclusions

In this chapter the potential for active demand response using the structural thermal energy storage capacity is demonstrated for the Belgian building stock. Therefore a bottom-up dynamic reduced-order building stock model has been developed using the grey-box modelling framework developed in Chapter 4. The accuracy of the reduced-order building

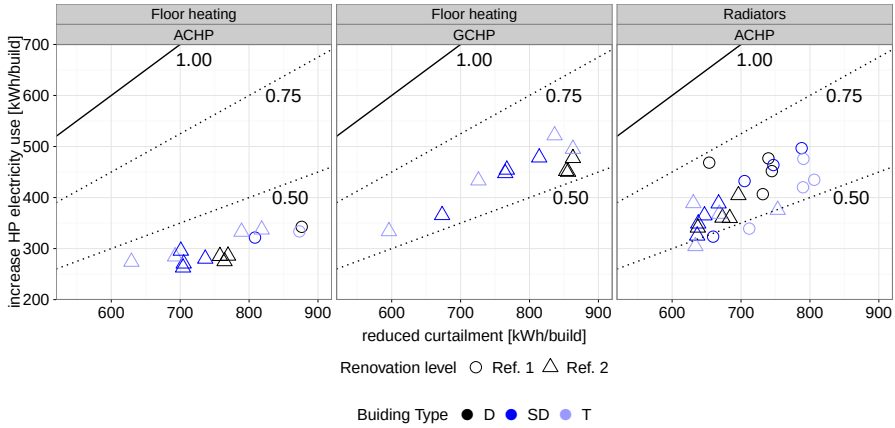

Figure 5.18: Extra electricity use per building when applying ADR with respect to the decrease in curtailing RES per building. The marker and colours indicate respectively the building type and renovation class. The thick contour line depicts the situation in which, on a net basis, no net reduction is achieved. The dashed lines show the contours whereby the increase in energy use is 0.75 and 0.5 times the reduction in curtailment.

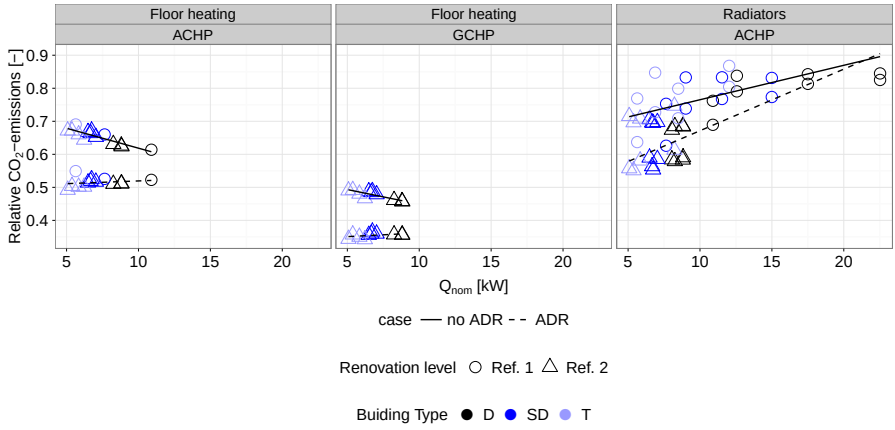

Figure 5.19: Relative CO_2-emission compared to the reference scenario without heat pumps, for the heat pump scenarios with ADR (dashed trendline) and without ADR (full trendline). The results are function of the nominal thermal power of of the heat pump. The markers indicate the renovation level, while the colour of the markers shows the building type.

models is verified against detailed building energy simulations for the different typologies. Two reduced-order modelling approaches have been compared, i.e. (i) a direct calculation of the model parameters based on the construction data and (ii) an estimation of the model parameters using the grey-box modelling framework developed in Chapter 4. Comparison of the reduced-order models showed that for all cases the simulation of the annual heat demand is acceptable, with an average difference of 7 % between the detailed simulations and the identified models. For the short term dynamic effects, the theoretical RC-models overestimated the contribution of the thermal mass of the building, underestimating the temperature fluctuations and overestimating the heat demand. In contrast, simulations using the grey-box models identified on the in-use data, show good agreement of the temperature and heat demand profiles of the day-zone to those obtained with the detailed models for the winter and mid-season period. The major differences between the models were found in the estimated properties of the internal floor between the two zones, the heat transfer coefficients between the air and building components and the distribution factors for solar gains.

In a second part of the chapter, the developed building stock model is used to quantify the ADR characteristics according to the theoretical quantification framework developed in Chapter 3. Thereby significant differences between the building types, age classes and renovations levels were found. In general the available capacity for ADR is found to increase with the age of the building and reduces with increasing renovation level – and thus with

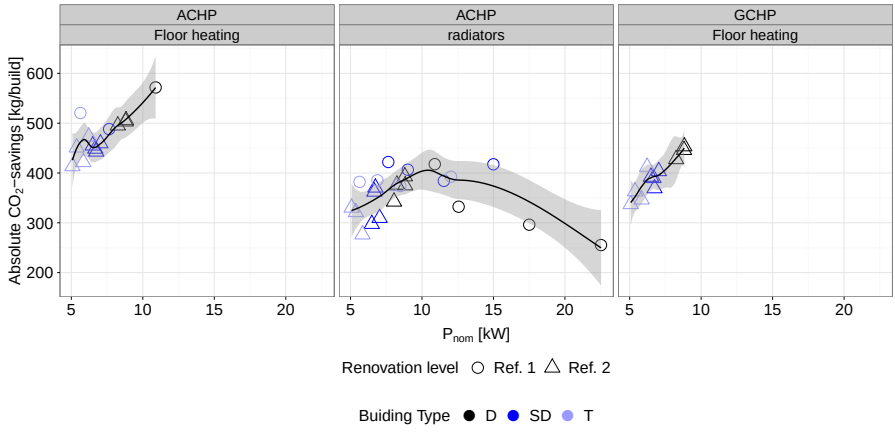

Figure 5.20: Absolute additional CO_2-savings due to ADR as a function of the nominal power of the heat pump for the floor heating and the radiator cases and for the air coupled heat pump (ACHP) and ground coupled heat pump (GCHP). The marker types and colours show respectively the different building types (D: detached, SD: semi-detached, T: terraced) and renovation levels.

increasing heat loss coefficient of the dwelling. The available storage capacity for an ADR-event of 4 h and a comfort range of 2 $^{\circ}\mathrm{C}$ was found to vary between 12 kWh and 30 kWh (16 - 66 kWh for floor heating) for respectively the terraced house built between 1990 and 2005 and detached dwelling built before 1945.
In contrast the storage efficiency for the radiator heated buildings, is found to improve significantly when buildings undergo energy related renovations. For the original buildings storage efficiencies vary between 66 % and 85 % for an ADR-event of 4 h and using constant boundary conditions. For the renovated building all efficiencies were found above 80 % and the relative differences between the different age classes were significantly reduced. For buildings equipped with floor heating the impact of the renovation level is less pronounced as for most cases efficiencies above 90 % where already obtained.
Based on these findings, it was concluded that for the radiator heated buildings the mildly renovated buildings built after 1990 showed the highest potential for ADR since they combine both a high available storage capacity and high storage efficiency. For the floor heating cases, due to the high overall efficiency, the highest CO_2-emission reductions and operation savings are obtained for the buildings with the highest available capacity.
Nevertheless, it was demonstrated that including dynamic boundary conditions and occupant behaviour showed to have a significant impact on both the available capacity and the storage efficiency. Although the relative ranking between building typologies, that was found using the static boundary conditions, is also observed for the dynamic conditions, the storage efficiency was found to decrease up to 20 % due to typical day-night variations in the occupancy profile. Moreover, as the ratio of the stored heat to the daily heat demand increases, due to solar gains and rising outdoor temperatures, the storage efficiency drops and even becomes zero. This clearly demonstrates that active demand response using the structural storage capacity by means of heating systems, can only be used efficiently in winter and emphasises that the dynamic evaluation method – developed in this work – is a prerequisite in order to quantify the dynamic variation of the ADR performance characteristics.

Finally, in the third part of this section, the building stock model is implemented in an integrated operational model for the Belgian electricity system. This allows a thorough assessment of the peak-capacity investment, fuel and renewable energy usage, CO_2-emissions.
The results show that as a consequence of the electrification of the energy demand for heating, a significant increase in the required peak production capacity is found when introducing heat pumps without ADR. Thereby the required peak production capacity increases linearly with the installed power of the heat pump. For the floor heating cases and the thoroughly renovated radiator heated buildings, the need for investments in the peak production capacity can be almost entirely avoided when ADR is taken into account. For the mildly renovated

buildings with radiator heating the available storage capacity is found to be inadequate to shift the entire peak load to off-peak periods. Nevertheless even for these cases the required production capacity is reduced by 30 % compared to the scenario without ADR.

In addition to the reduction in peak demand, ADR is able to increase the fraction of the electricity use of the heat pumps that is covered by RES from 2.4-3.5 % to 6-24 %. As a down-side of this increased RES penetration, the total electricity use of the heat pumps increases by 1.5-7.5 %. Based on both results the efficiency of the storage was estimated at 70 % for the floor heating buildings in case an air coupled heat pump is used. For the radiator heated buildings the efficiency strongly depended on the building typology and renovation level. Thereby, efficiencies up to 55 % are obtained for the terraced buildings, while efficiencies below 30 % were found for the mild renovation case.

As a result of the increased penetration of renewable energy sources, a reduction in CO_2 emission is obtained. This reduction is dominated by the seasonal performance factor of the heat pump and the application of ADR. This ADR allows a higher uptake of RES-based electricity generation that would have otherwise been curtailed, reducing the CO_2 emission on average by 15 %.

Chapter 6

Conclusions and future research

Based on a literature review – which demonstrated that although the use of structural storage is often suggested as a high-potential and low-cost technology for active demand response (ADR), the impact of the thermal properties on the suitability of a building for ADR is not well understood – the main research question was formulated as:

> *"How do building design parameters of both existing and new buildings influence the potential for active demand response using the structural thermal energy storage?"*

This general question was further divided into three parts that have been tackled in the different chapters of this work. The first part aims to establish a quantification framework that allows for a quantitative analysis of the ADR potential. The second part deals with the analysis of how the structural storage capacity is activated. Thereby one of the goals was to establish a methodology that allows for the characterisation of the thermal properties related to the ADR potential of the structural storage capacity in both new and existing buildings. Using both developed tools the third part then aimed to quantify the impact of building design parameters on the ADR potential, as such answering the main research question, in this work. The scope of the work has been limited to the analysis of the structural thermal energy storage capacity of residential buildings for ADR using heating systems.

To answer **the first group of sub-questions**, one of the main achievements of this work was the development of a generic, simulation-based framework for the quantification of the ADR potential of structural thermal energy storage capacity. The goal of the framework was thereby

to enable a quantitative analysis of the potential of structural thermal energy storage in an ADR context as a function of the building design parameters. A literature review, as well as the results of this study, showed that the flexibility of a building for ADR cannot be expressed by a single variable, but is a combination of different characteristics. In this framework 4 key performance indicators have been defined to allow a quantitative comparison of the ADR potential between buildings with different design parameters and by extension between buildings and other storage technologies. Based on the analysis and interpretation of the results, these performance indicators could be grouped into two categories. On the one hand, the *available storage capacity for ADR* and the *storage efficiency* were introduced as building related ADR characteristics that allow to evaluate the intrinsic ADR potential of a dwelling. On the other hand, the *state-of-charge* and *power shifting capability* were defined as metrics for the instantaneous flexibility of a dwelling. As such, the latter are mainly useful to provide instantaneous information to control systems. In contrast, the available storage capacity for ADR and the storage efficiency can be used to assess the overall potential of a dwelling for the application in an ADR context. Nonetheless, it was emphasized that all four performance indicators depend – in addition to the building design parameters – upon the dynamic boundary conditions for the outdoor climate and occupant behaviour, as well as upon control settings such as the allowed temperature variations and the duration of the ADR-event.

In order to quantify the instantaneous values of the performance indicators, dynamic, simulation-based evaluation quantification methods were presented for each of the indicators. However, in order to facilitate a comprehensive analysis of the impact of building design parameters on the ADR potential, a simplified rule-based approach using stationary boundary conditions has been introduced. Although it is acknowledged that in practical applications and for more complex systems quantification methods using an optimal control framework have a strong potential, the simplified rule-based framework was found to enable an in-depth physical interpretation of the relation between the building properties, heat emissions systems and control settings. As such, the theoretic framework was concluded to be a comprehensive tool to assess the impact of the building design parameters on the ADR potential and is therefore used in the third part of the study to answer the main research question in this work.

In order to answer **the second group of research questions** – concerning the analysis of how different building components contribute to the active storage capacity – two steps were taken. First, detailed building energy simulations were used for a detailed analysis of the dynamic behaviour of the structural thermal energy storage capacity on a building level, focussing on the contribution of the different building components. Therefore, the building energy simulation model implemented in the IDEAS-library was used. A

verification of this zonal model against on-site, full-scale measurement data of the Twin House dwellings obtained in the context of the IEA Annex 58 project showed acceptable accuracy. Consequently, the detailed model was concluded to be a useful tool from a research perspective. Nonetheless, a high amount of prior knowledge about the physical properties was needed to set up the model and due to the high amount of model parameters a calibration of the model is found to be cumbersome. Consequently, the practical applicability of these detailed simulations for a large-scale analysis of the ADR potential in existing buildings or the use in control strategies is deemed to be limited.

Therefore in a second step, a grey-box modelling framework was presented, to enable this dynamic simulation of the active use of the structural storage capacity in both new and existing buildings. The grey-box modelling framework was developed to allow on the one hand a robust and computational efficient prediction and simulation of the dynamic thermal response of buildings and on the other hand to characterize the main dynamic thermal properties that define the ADR potential of dwellings. To develop this grey-box modelling framework, this work starts from the simulations of virtual experiments using the detailed BES models. In contrast to other studies found in literature, which start from measured data, the flexibility of these virtual experiments was exploited in this work, allowing a detailed analysis of the relation between the model structure, the design of experiment and the required application. Based on this analysis guidelines for the experimental design as well as the development of adequate model structures were deduced based on the specific purpose of the model. Thereby, this work showed that the physical interpretability of the individual model parameters, e.g. the capacities of the interior or the exterior walls, should be handled carefully, since typically higher-order models are needed to correctly separate the dynamics related to the different components. In general, 1 state for each of the components linked to different boundary conditions, was found to give a reliable interpretation of the thermal parameters of the individual components. However, the practical identifiability of the model parameters in these higher-order models requires a qualitative set of observation variables, including heat flow measurements. These detailed measurements are typically not required when grey-box modelling is used to identify control-oriented models, since lower-order models – that are less sensitive to over-fitting – in most cases suffice to capture the short-term dynamic response needed for control applications.

Moreover, it was emphasized that, even for the higher-order models, the identified parameters should always be interpreted in relation to the model, especially for the characterisation of the thermal capacities of the building components. For the latter, it was demonstrated that using grey-box modelling it is only possible to characterize the effective thermal capacity, defined as the thermal mass of the components that is activated by the indoor dynamics. Thereby, the sum of the thermal mass of the material layers within the insulation barrier was identified

as a good first estimate of the effective capacity. Additionally, the physical interpretation of the results showed that the transmission losses to the windows are always included in the estimated ventilation losses, since due to the negligible thermal mass of the windows, both loss terms cannot be separated in the identification process.

Finally both developed tools, i.e. the quantification method for the ADR potential and the grey-box modelling framework, are combined to answer **the third group of sub-questions** and quantify the ADR potential of the structural thermal energy storage capacity as a function of the building design properties. In a first step, a theoretical assessment of the available structural storage capacity and storage efficiency is carried out using the theoretical, rule-based, quantification framework with simplified boundary conditions. This parameter study has been conducted using detailed simulations of a single zone dwelling, taking into account the geometric and thermal design parameters of a dwelling, as well as the type and sizing of the heat emission system and the settings for the ADR control strategy.
The results of this theoretical assessment demonstrated that both the available storage capacity and the storage efficiency strongly depend on the duration of the ADR-event and the allowed temperature increase by thermal comfort, in addition to the building design properties and characteristics of the heating system.
For the *available storage capacity* a linear increase as a function of the duration of the ADR-event was found for short-term ADR-events (15-90 min) and high comfort ranges. This linear relation was found since during these short ADR-events the heating system was able to operate at its nominal power when the indoor temperature at the end of the ADR-event did not reach the maximum comfort boundary. For longer storage events the heating power during the ADR-event had to be reduced as the indoor temperature reaches the maximum comfort boundary to avoid overheating and guarantee thermal comfort. As a result, the rate of increase of the available storage capacity decreases as a function of the duration of the ADR-event. Thereby it was pointed out that despite the large variation in the obtained values for the available storage capacity, buildings equipped with floor heating and a high available thermal mass show higher available storage capacities compared to radiator heated buildings, since they allow the heating system to operate at the maximum power for significantly longer periods. Moreover, the available storage capacity for ADR was found to increase with the nominal thermal power of the building, since a higher power capacity is available to activate the thermal mass.
Complementary to the available storage capacity, the *storage efficiency* was found to significantly decrease for increasing duration of the ADR-event. As for the available storage capacity a high variation in the storage efficiencies was obtained as a function

of the building design parameters. In addition to the theoretic efficiencies obtained for the simplified boundary conditions, a dynamic evaluation of the storage efficiency showed a strong dependence on the dynamic boundary conditions.
Again the floor heating cases were found to out-perform the radiator heated buildings, since for the former most heat is stored in the thermal mass of the floor limiting the increase in ventilation and transmission losses due to the activation of the thermal mass. Nonetheless, high overall values for the storage efficiency were obtained for the theoretic framework using simplified boundary conditions. Taking into account the wide range of parameter values used in the parameter study, a median value for the efficiency of 93 % (range 71-97 %) and 96 % (range 75-97%) is obtained for buildings equipped with respectively a radiator or floor heating system, when ADR-events are limited to a charging time of 3 h. However, the instantaneous value of the efficiency is found to be highly sensitive to dynamic variations induced by the solar gains and occupant behaviour. Thereby reductions of 30 % and more were found when the storage capacity is activated prior to a period with high solar gains of close to the end of the occupancy period. Activating the structural storage capacity is thus most efficient prior to periods with a high heat demand, since the stored heat can as such be directly recovered.
In addition to impact of the type of heat emission system, the heat loss coefficient, the ratio of the heat loss coefficient and the total thermal mass, the internal wall ratio, the thermal capacity of the indoor air and the total thermal capacity of the building components were identified in a multivariate regression analysis as dominant thermal properties which influence the storage efficiency. Thereby a significant negative correlation was found for the ratio of the heat loss coefficient to the total thermal capacity of the components, demonstrating that an adequate insulation quality and efficient ventilation system are a prerequisite to guarantee a high storage efficiency. The thermal mass of the indoor air, the internal wall ratio and the total thermal capacity of the components are positively correlated with the efficiency. Nonetheless, the values of the regression coefficients in the regression models were found to significantly depend on the duration of the ADR-event. Analysis for the results showed thereby that for short ADR events (less than 60 min) the capacity of the indoor air has the highest contribution to the available structural storage capacity for the radiator heating. For long ADR-events the internal walls were found to have the highest contribution to the available storage capacity.

In a second step, the potential of ADR using the structural storage capacity of the Belgian residential building stock is assessed. Therefore a reduced-order building stock model has been established using the developed grey-box modelling framework. Thereby it was shown that a 9 state, 2 zone grey-box model was able to capture both the long- and short-term dynamics needed for the evaluation of the ADR potential of the structural storage capacity on an aggregated level.

Firstly, using the developed reduced-order building stock model, the ADR-potential of the different typologies in the Belgian stock has been evaluated, quantifying the available storage capacity for ADR and the corresponding storage efficiency for the presented *theoretical quantification framework*. In line with the results of the theoretical parameter study, the analysis demonstrated a significant decrease of the available storage capacity and improvement of the storage efficiency as the age of the building decreases and renovation level of the dwelling improves. As such, for the different building typologies an available storage capacity for ADR between 12-30 kWh was obtained for the radiator heated buildings and 16-66 kWh for the floor heating cases, assuming an ADR-event of 4 h and a comfort range of 2 $^{\circ}\mathrm{C}$. The corresponding efficiencies obtained for the simplified boundary conditions, assuming a constant outdoor temperature of 5 $^{\circ}\mathrm{C}$, were found to vary between 66 % and 85 % for the original dwellings equipped with radiator heating, while after renovation all efficiencies were found above 80 %. For the floor heating cases, the impact of renovation was less pronounced since for most cases efficiencies above 90 % were already obtained for the simplified boundary conditions.
Nevertheless, the available storage capacity and storage efficiency drastically decreased with the decreasing heat demand for increasing outdoor temperatures and high solar gains. As such, in mid-season and summer the potential for ADR by activating the structural storage capacity using heating systems is marginal, due to the low values of the available storage capacity and storage efficiency. Based on these high variations in the available storage capacity and the storage efficiency, as a result of the dynamic boundary conditions, it was concluded that whereas the multivariate regression model and the simplifications of the boundary conditions allowed for a comprehensive evaluation of impact of building design parameters on the ADR potential, dynamic simulations are a prerequisite to capture the fluctuation of the performance indicators as a function of the boundary conditions.

Secondly, the building stock model was implemented in an *integrated operational model* for the electricity market evaluating the impact of ADR on the operational costs and CO_2-emission for a wide-spread integration of heat pumps and renewable electricity production. Thereby the main benefits from ADR using both the structural and non-structural thermal energy storage capacity of dwellings were shown to be the reduction of required peak production capacity and the increased penetration of renewable energy sources, due to a reduction of the curtailment losses.
For the building equipped with floor heating and the thoroughly renovated dwellings the available storage capacity for ADR was adequate to avoid the need for additional peak production units completely. For the less insulated dwellings equipped with radiators a complete elimination of the demand peak was not possible although a reduction of 30 %

compared to the scenario without ADR was still obtained.
Additionally, the use of the structural thermal energy storage capacity in the thoroughly renovated dwellings resulted in an increase of 25 % of the fraction of the heat demand that was covered by RES. As a downside however, an average increase of the annual electricity use by the heat pumps of approximately 5 % was obtained. However, it was pointed out that these increased losses should be interpreted as upper limits since the production cost of RES was assumed to be 0 EUR/kWh. Consequently, excessive use of RES to activate the storage capacity was not penalized. Nonetheless, it is concluded that activating the structural storage capacity comes at an important cost, i.e. an increase of the energy use for heating, and is therefore only useful when it can be compensated by a reduction of the primary energy use, or the cost for energy conversion, on the aggregated – district or even national – level. Accounting for both the increased penetration of renewable electricity production and the increase in electricity demand, an overall reduction of CO_2-emissions of 0.25-0.55 ton/year or 6-25 % could be obtained per building by applying ADR. The highest relative reduction of CO_2-emissions was thereby obtained for the thoroughly renovated terraced dwellings. This is in line with the findings of the ADR characteristics where, due to the low ratio of the heat loss coefficient over the total thermal mass, these dwellings showed the highest storage efficiency. Nevertheless, in absolute terms the impact of ADR on the CO_2-emissions showed an optimum for the radiator heated dwellings, although it was not well pronounced, for the mildly renovated buildings built after 1990 since these buildings combine an acceptable storage efficiency with a high available storage capacity. For the floor heated dwellings this optimum was not found, but a quasi-linear increase of the CO_2-emissions as a function of the heating power was found. The latter was explained by the higher overall storage efficiency for floor heated buildings and the lower heating power, since floor heating was only applied in the recent or thoroughly renovated dwellings.

Based on these findings it is concluded that the structural thermal energy storage capacity can be an important storage technology in an ADR framework, since high available storage capacities are generally found in the Belgian building stock. Nonetheless, activating the structural storage capacity comes at a cost of increasing the local energy use for heating. Although, in general high storage efficiencies could be obtained – even for mildly renovated dwellings – the use of structural storage for ADR should therefore always be analysed in the perspective of reducing primary energy use, the cost of energy production or the CO_2-emissions, on an aggregated level. To facilitates this assessment, the simulation-based quantification framework presented in this work, is therefore concluded to be a step forward in optimising the use of structural thermal energy storage in an ADR context.

Future research Based on the findings of this work and taking into account the simplifications and assumptions that were introduced to define the scope of the dissertation, this paragraph summarizes several paths for future research:

- In order to focus on the impact of the building properties on the ADR potential, the thermal systems have been simplified significantly. A logic next step would therefore be to analyse the impact of activating the structural storage capacity on the system efficiency. Thereby taking into account the impact of f.i. changing supply and return water temperatures on the production efficiency.
- Moreover, for multi-zone buildings – where the heat demand may differ significantly between zones – new control challenges arise since the thermal energy storage capacity may not be activated to the same extent in the different zones.
- It is also acknowledged that a zonal modelling approach is not able to capture all local effects that are occurring when activating the thermal mass. While these effects were considered to be of lesser importance for this work, as the focus was on an evaluation of the potential of structural thermal energy storage on a building or aggregate level, a further refinement of the simulation of these local effects is suggested as an important step to allow the optimization of building components for structural thermal energy storage.
- The quantification methods developed in Chapter 3 have been applied to quantify the potential for ADR in a heating dominated residential context. Nevertheless, given the generic formulation of the methods, they can be readily extended to cooling applications or other building types, such as offices or schools. Since these buildings are subject to different boundary conditions – i.e. internal gains, occupancy, comfort etc. – an interesting research question could be to analyse if these buildings can be used as a complementary storage capacity to structural storage in residential buildings.
- Moreover the analysis can be extended to more complex systems including different storage technologies, e.g. a building with both structural thermal mass, a water storage tank for domestic hot water and a bore-hole heat exchanger for long-term storage. For these complex systems, an evaluation using rule-based control may no longer be feasible and optimal control methods (as presented in [58, 189]) may be required to evaluate the instantaneous values of the ADR-characteristics.
- The impact of ADR using structural storage has been demonstrated in Chapter 5 in the context of the electricity production on a national level. Nonetheless, ADR is in

literature also suggested to avoid stability issues on the distribution grid [10]. Thereby the analysis on a district level may introduce specific challenges since the law-of-large numbers that has been assumed on the national level, may no longer be applicable. As such, a detailed evaluation of f.i. stochastic occupant behaviour and discrete control actions (such as on/off cycling of a heat pump) should be analysed in-depth.

- In the context of on-going research on the 4^{th}-generation district heating (and cooling) systems, local thermal energy storage has been introduced as one of the key technologies to increase the energy efficiency and RES penetration in district thermal systems [21]. Given the generic evaluation presented in this work, the presented methodologies – and even the conclusions regarding the impact of the thermal properties of different buildings on the ADR potential – may be applied to these systems as well.

- Finally, since it was shown that the ADR characteristics of a dwelling are significantly effected by the level of allowed temperature evaluation needed to activate the thermal mass, fundamental knowledge about the user acceptance of these temperature variations is required. Thereby the validity of traditional formulations of comfort requirements was questioned in the context of ADR since on the one hand the methodologies to identify them were based on steady-state of slow-varying conditions and on the other hand they do not take into account the potential impact of (financial) incentives from grid-operators. Large-scale research and demonstration projects, such as the LINEAR-project [190], may be used to get insight in this matter although socio-logic studies may also give important fundamental knowledge about the psychological aspects of thermal comfort.

In addition to these more general topics, specific remaining challenges and opportunities were identified in each of the chapters. Thereby a first step for further research evidently lies in the detailed evaluation of all assumptions and simplifications that have been introduced in this work.

Appendix A

Specification of grey-box models

In this appendix the model and observation equations for the grey-box models used in Chapter 4 are listed. The names of the models correspond to the convention used in Table 4.2. The equations are formulated as stochastic differential equations and are presented as implemented in CTSM-R. The conventions listed in Table A.1 are used.

Table A.1: Names and conventions for variables used in grey-box model implementation in CTSM-R

Name	Variable of parameter	Unit
Ti	State for indoor air	[K]
Tw	State for exterior walls	[K]
Twi	State for interior walls	[K]
Tf	State for floor	[K]
Te	Ambient air temperature	[K]
Tground	Ground temperature	[K]
Q_s_dir	Direct solar gains	[W]
Q_s_dif	Difuse solar gains	[W]
Q_g_c	Convective internal gains	[W]
Q_g_r	Radiative internal gains	[W]
Q_heat	Heat emitted by heating system	[W]
Tx	observed temperature of state x	[K]
Qfluxe(NoFloor)	heat flow to outer walls (excluding the floor)	[W]
Qfluxi	heat flow to inner walls	[W]
QfluxFloor	heat flow to the floor	[W]
qfluxe(NoFloor)	heat flux to outer walls (excluding the floor)	[W/K]
qfluxi	heat flux to inner walls	[W/K]
qfluxFloor	heat flux to the floor	[W/K]
abs*x*	absorption coefficient for solar gains for state *x*	[-]
f*x*	absorption coefficient for heating for state *x*	[-]

1_Ti

```
Linear state space model with 1 state, 1 output and 6 inputs
System equations:
        dTi ~ (1/Re/Ci * (Te - Ti) + (Q_s_dir + Q_s_dif + Q_g,c +
            Q_g,r + Q_heat)/Ci) * dt + exp(p11) * dw1
Observation equations:
        yTair ~ Ti
Inputs:  Te, Q_s_dir, Q_s_dif, Q_g,c, Q_g,r, Q_heat
```

2_Ti_Rad_1

```
Linear state space model with 2 states, 1 output and 6 inputs
System equations:
        dTi ~ (inf/Ci * (Te - Ti) + hcAw/(Ci) * (Tw - Ti) + (Q_s_dir +
            Q_s_dif + Q_g,c + Q_g,r + Q_heat)/Ci) *
            dt + exp(p11) * dw1
        dTw ~ (1/(Cw * Re) * (Te - Tw) + hcAw/(Cw) * (Ti - Tw)) * dt +
            exp(p22) * dw2
Observation equations:
        yTair ~ Ti
Inputs:  Te, Q_s_dir, Q_s_dif, Q_g,c, Q_g,r, Q_heat
```

2_Ti_Rad_2

```
Linear state space model with 2 states, 1 output and 6 inputs
System equations:
        dTi ~ (inf/Ci * (Te - Ti) + hcAw/(Ci) * (Tw - Ti) + f1 * (Q_s_dir +
            Q_s_dif + Q_g,c + Q_g,r + Q_heat)/Ci) *
            dt + exp(p11) * dw1
        dTw ~ (1/(Cw * Re) * (Te - Tw) + hcAw/(Cw) * (Ti - Tw) + f2 *
            (Q_s_dir + Q_s_dif + Q_g,c + Q_g,r +
                Q_heat)/Cw) * dt + exp(p22) * dw2
Observation equations:
        yTair ~ Ti
Inputs:  Te, Q_s_dir, Q_s_dif, Q_g,c, Q_g,r, Q_heat
```

3_Ti_Rad_1

```
Linear state space model with 3 states, 1 output and 8 inputs
System equations:
        dTi ~ (inf/Ci * (Te - Ti) + hcAw/(Ci) * (Tw - Ti) + hwi/Ci *
            (Twi - Ti) + (Q_s_dir + Q_s_dif + Q_g,c +
            Q_g,r + Q_heat)/Ci) * dt + exp(p11) * dw1
        dTw ~ (1/(Cw * Re) * (Te - Tw) + hcAw/(Cw) * (Ti - Tw)) * dt +
            exp(p22) * dw2
        dTwi ~ (hwi/Cwi * (Ti - Twi)) * dt + exp(p33) * dw3
```

```
Observation equations:
        yTair ~ Ti
Inputs:  Te, Q_s_dir, Q_s_dif, Q_g,c, Q_g,r, Q_heat
```

3_TiQ_Rad_1

```
Linear state space model with 3 states, 2 outputs and 6 inputs
System equations:
        dTi ~ (inf/Ci * (Te - Ti) + hcAw/(Ci) * (Tw - Ti) + hwi/Ci *
            (Twi - Ti) + (Q_s_dir + Q_s_dif + Q_g,c +
            Q_g,r + Q_heat)/Ci) * dt + exp(p11) * dw1
        dTw ~ (1/(Cw * Re) * (Te - Tw) + hcAw/(Cw) * (Ti - Tw)) * dt +
            exp(p22) * dw2
        dTwi ~ (hwi/Cwi * (Ti - Twi)) * dt + exp(p33) * dw3
Observation equations:
        yTair ~ Ti
        Qfluxe ~ (Ti - Tw) * hcAw
Inputs:  Te, Q_s_dir, Q_s_dif, Q_g,c, Q_g,r, Q_heat
```

3_TiQ_Rad_2

```
Linear state space model with 3 states, 3 outputs and 8 inputs
System equations:
        dTi ~ (inf/Ci * (Te - Ti) + hcAw/(Ci) * (Tw - Ti) + hwi/Ci *
            (Twi - Ti) + abs3 * (Q_s_dir + Q_s_dif)/Ci + f3 *
            (Q_heat + Q_g,c + Q_g,r)/Ci) * dt +
            exp(p11) * dw1
        dTw ~ (1/(Cw * Re) * (Te - Tw) + hcAw/(Cw) * (Ti - Tw) + abs1 *
            (Q_s_dir + Q_s_dif)/Cw + f1 * (Q_heat + Q_g,c +
            Q_g,r)/Cw) * dt + exp(p22) * dw2
        dTwi ~ (hwi/Cwi * (Ti - Twi) + abs2 * (Q_s_dir + Q_s_dif)/Cwi +
            f2 * (Q_heat + Q_g,c + Q_g,r)/Cwi) *
            dt + exp(p33) * dw3
Observation equations:
        yTair ~ Ti
        Qfluxe ~ (Ti - Tw) * hcAw + abs1 * (Q_s_dir + Q_s_dif) +
            f1 * (Q_heat + Q_g,c + Q_g,r)
        Qfluxi ~ (Ti - Twi) * hwi + abs2 * (Q_s_dir + Q_s_dif) +
            f2 * (Q_heat + Q_g,c + Q_g,r)
Inputs:  Te, Q_s_dir, Q_s_dif, Q_g,c, Q_g,r, Q_heat
```

4_TiQ_Rad

```
Linear state space model with 4 states, 4 outputs and 9 inputs
System equations:
        dTi ~ (inf/Ci * (Te - Ti) + hcAw/(Ci) * (Tw - Ti) + hwi/Ci *
            (Twi - Ti) + hfAf/Ci * (Tf - Ti) + abs3 * (Q_s_dir +
```

```
            Q_s_dif)/Ci + f3 * (Q_heat + Q_g,c + Q_g,r)/Ci) *
            dt + exp(p11) * dw1
        dTw ~ (1/(Cw * Re) * (Te - Tw) + hcAw/(Cw) * (Ti - Tw) + abs1 *
            (Q_s_dir + Q_s_dif)/Cw + f1 * (Q_heat + Q_g,c +
            Q_g,r)/Cw) * dt + exp(p22) * dw2
        dTwi ~ (hwi/Cwi * (Ti - Twi) + abs2 * (Q_s_dir + Q_s_dif)/Cwi +
            f2 * (Q_heat + Q_g,c + Q_g,r)/Cwi) *
            dt + exp(p33) * dw3
        dTf ~ (hfAf/Cf * (Ti - Tf) + 1/(Rf * Cf) * (Tground - Tf) + abs4 *
            (Q_s_dir + Q_s_dif)/Cf + f4 * (Q_heat + Q_g,c +
            Q_g,r)/Cf) * dt + exp(p44) * dw4
Observation equations:
        yTair ~ Ti
        QfluxeNoFloor ~ (Ti - Tw) * hcAw + abs1 * (Q_s_dir + Q_s_dif) +
            f1 * (Q_heat + Q_g,c + Q_g,r)
        Qfluxi ~ (Ti - Twi) * hwi + abs2 * (Q_s_dir + Q_s_dif) +
            f2 * (Q_heat + Q_g,c + Q_g,r)
        QfluxFloor ~ hfAf * (Ti - Tf) + abs4 * (Q_s_dir + Q_s_dif) +
            f4 * (Q_heat + Q_g,c + Q_g,r)
Inputs:  Te, Q_s_dir, Q_s_dif, Q_g,c, Q_g,r, Q_heat, Tground
```

3_Ti_Rad_2

```
Linear state space model with 3 states, 1 output and 8 inputs
System equations:
        dTi ~ (inf/Ci * (Te - Ti) + hcAw/(Ci) * (Tw - Ti) + hwi/Ci *
            (Twi - Ti) + abs3 * (Q_s_dir + Q_s_dif)/Ci + f3 *
            (Q_heat + Q_g,c + Q_g,r)/Ci) * dt +
            exp(p11) * dw1
        dTw ~ (1/(Cw * Re) * (Te - Tw) + hcAw/(Cw) * (Ti - Tw) + abs1 *
            (Q_s_dir + Q_s_dif)/Cw + f1 * (Q_heat + Q_g,c +
            Q_g,r)/Cw) * dt + exp(p22) * dw2
        dTwi ~ (hwi/Cwi * (Ti - Twi) + abs2 * (Q_s_dir + Q_s_dif)/Cwi +
            f2 * (Q_heat + Q_g,c + Q_g,r)/Cwi) *
            dt + exp(p33) * dw3
Observation equations:
        yTair ~ Ti
Inputs:  Te, Q_s_dir, Q_s_dif, Q_g,c, Q_g,r, Q_heat
```

4_TiQe_Rad

```
Linear state space model with 4 states, 2 outputs and 9 inputs
System equations:
        dTi ~ (inf/Ci * (Te - Ti) + hcAw/(Ci) * (Tw - Ti) + hwi/Ci *
            (Twi - Ti) + hfAf/Ci * (Tf - Ti) + abs3 * (Q_s_dir +
            Q_s_dif)/Ci + f3 * (Q_heat + Q_g,c + Q_g,r)/Ci) *
            dt + exp(p11) * dw1
        dTw ~ (1/(Cw * Re) * (Te - Tw) + hcAw/(Cw) * (Ti - Tw) + abs1 *
            (Q_s_dir + Q_s_dif)/Cw + f1 * (Q_heat + Q_g,c +
            Q_g,r)/Cw) * dt + exp(p22) * dw2
        dTwi ~ (hwi/Cwi * (Ti - Twi) + abs2 * (Q_s_dir + Q_s_dif)/Cwi +
```

```
            f2 * (Q_heat + Q_g,c + Q_g,r)/Cwi) *
            dt + exp(p33) * dw3
        dTf ~ (hfAf/Cf * (Ti - Tf) + 1/(Rf * Cf) * (Tground - Tf) + abs4 *
            (Q_s_dir + Q_s_dif)/Cf + f4 * (Q_heat + Q_g,c +
            Q_g,r)/Cf) * dt + exp(p44) * dw4
Observation equations:
        yTair ~ Ti
        QfluxeNoFloor ~ (Ti - Tw) * hcAw + abs1 * (Q_s_dir + Q_s_dif) +
            f1 * (Q_heat + Q_g,c + Q_g,r)
Inputs:  Te, Q_s_dir, Q_s_dif, Q_g,c, Q_g,r, Q_heat, Tground
```

4_Tiq_Rad

```
Linear state space model with 4 states, 2 outputs and 9 inputs
System equations:
        dTi ~ (inf/Ci * (Te - Ti) + hcAw/(Ci) * (Tw - Ti) + hwi/Ci *
            (Twi - Ti) + hfAf/Ci * (Tf - Ti) + abs3 * (Q_s_dir +
            Q_s_dif)/Ci + f3 * (Q_heat + Q_g,c + Q_g,r)/Ci) *
            dt + exp(p11) * dw1
        dTw ~ (1/(Cw * Re) * (Te - Tw) + hcAw/(Cw) * (Ti - Tw) + abs1 *
            (Q_s_dir + Q_s_dif)/Cw + f1 * (Q_heat + Q_g,c +
            Q_g,r)/Cw) * dt + exp(p22) * dw2
        dTwi ~ (hwi/Cwi * (Ti - Twi) + abs2 * (Q_s_dir + Q_s_dif)/Cwi +
            f2 * (Q_heat + Q_g,c + Q_g,r)/Cwi) *
            dt + exp(p33) * dw3
        dTf ~ (hfAf/Cf * (Ti - Tf) + 1/(Rf * Cf) * (Tground - Tf) + abs4 *
            (Q_s_dir + Q_s_dif)/Cf + f4 * (Q_heat + Q_g,c +
            Q_g,r)/Cf) * dt + exp(p44) * dw4
Observation equations:
        yTair ~ Ti
        qfluxeNoFloor ~ ((Ti - Tw) * hcAw + abs1 * (Q_s_dir + Q_s_dif) +
            f1 * (Q_heat + Q_g,c + Q_g,r))/Aext
Inputs:  Te, Q_s_dir, Q_s_dif, Q_g,c, Q_g,r, Q_heat, Tground
```

4_Ti_Rad

```
Linear state space model with 4 states, 1 output and 9 inputs
System equations:
        dTi ~ (inf/Ci * (Te - Ti) + hcAw/(Ci) * (Tw - Ti) + hwi/Ci *
            (Twi - Ti) + hfAf/Ci * (Tf - Ti) + abs3 * (Q_s_dir +
            Q_s_dif)/Ci + f3 * (Q_heat + Q_g,c + Q_g,r)/Ci) *
            dt + exp(p11) * dw1
        dTw ~ (1/(Cw * Re) * (Te - Tw) + hcAw/(Cw) * (Ti - Tw) + abs1 *
            (Q_s_dir + Q_s_dif)/Cw + f1 * (Q_heat + Q_g,c +
            Q_g,r)/Cw) * dt + exp(p22) * dw2
        dTwi ~ (hwi/Cwi * (Ti - Twi) + abs2 * (Q_s_dir + Q_s_dif)/Cwi +
            f2 * (Q_heat + Q_g,c + Q_g,r)/Cwi) *
            dt + exp(p33) * dw3
        dTf ~ (hfAf/Cf * (Ti - Tf) + 1/(Rf * Cf) * (Tground - Tf) + abs4 *
            (Q_s_dir + Q_s_dif)/Cf + f4 * (Q_heat + Q_g,c +
```

```
            Q_g,r)/Cf) * dt + exp(p44) * dw4
Observation equations:
        yTair ~ T
Inputs:  Te, Q_s_dir, Q_s_dif, Q_g,c, Q_g,r, Q_heat, Tground
```

4_TiTs_Rad

```
Linear state space model with 4 states, 4 outputs and 9 inputs
System equations:
        dTi ~ (inf/Ci * (Te - Ti) + hcAw/(Ci) * (Tw - Ti) + hwi/Ci *
            (Twi - Ti) + hfAf/Ci * (Tf - Ti) + abs3 * (Q_s_dir +
            Q_s_dif)/Ci + f3 * (Q_heat + Q_g,c + Q_g,r)/Ci) *
            dt + exp(p11) * dw1
        dTw ~ (1/(Cw * Re) * (Te - Tw) + hcAw/(Cw) * (Ti - Tw) + abs1 *
            (Q_s_dir + Q_s_dif)/Cw + f1 * (Q_heat + Q_g,c +
            Q_g,r)/Cw) * dt + exp(p22) * dw2
        dTwi ~ (hwi/Cwi * (Ti - Twi) + abs2 * (Q_s_dir + Q_s_dif)/Cwi +
            f2 * (Q_heat + Q_g,c + Q_g,r)/Cwi) *
            dt + exp(p33) * dw3
        dTf ~ (hfAf/Cf * (Ti - Tf) + 1/(Rf * Cf) * (Tground - Tf) + abs4 *
            (Q_s_dir + Q_s_dif)/Cf + f4 * (Q_heat + Q_g,c +
            Q_g,r)/Cf) * dt + exp(p44) * dw4
Observation equations:
        yTair ~ Ti
        yTw ~ Tw
        yTwi ~ Tw
        yTf ~ Tf
Inputs:  Te, Q_s_dir, Q_s_dif, Q_g,c, Q_g,r, Q_heat, Tground
```

2_Ti_FH_1

```
Linear state space model with 2 states, 1 output and 6 inputs
System equations:
        dTi ~ (inf/Ci * (Te - Ti) + hcAw/(Ci) * (Tw - Ti) + (Q_s_dir +
            Q_s_dif + Q_g,c + Q_g,r)/Ci) * dt + exp(p11) *
            dw1
        dTw ~ (1/(Cw * Re) * (Te - Tw) + hcAw/(Cw) * (Ti - Tw) + (Q_heat)/Cw) *
            dt + exp(p22) * dw2
Observation equations:
        yTair ~ Ti
Inputs:  Te, Q_s_dir, Q_s_dif, Q_g,c, Q_g,r, Q_heat
```

3_Ti_Rad_1

```
Linear state space model with 3 states, 1 output and 8 inputs
System equations:
        dTi ~ (inf/Ci * (Te - Ti) + hcAw/(Ci) * (Tw - Ti) + hwi/Ci *
            (Twi - Ti) + (Q_s_dir + Q_s_dif + Q_g,c +
```

```
            Q_g,r + Q_heat)/Ci) * dt + exp(p11) * dw1
        dTw ~ (1/(Cw * Re) * (Te - Tw) + hcAw/(Cw) * (Ti - Tw)) * dt +
            exp(p22) * dw2
        dTwi ~ (hwi/Cwi * (Ti - Twi)) * dt + exp(p33) * dw3
Observation equations:
        yTair ~ Ti
Inputs:  Te, Q_s_dir, Q_s_dif, Q_g,c, Q_g,r, Q_heat
```

3_Ti_FH_1

```
Linear state space model with 3 states, 1 output and 8 inputs
System equations:
        dTi ~ (inf/Ci * (Te - Ti) + hcAw/(Ci) * (Tw - Ti) + hwi/Ci *
            (Twi - Ti) + (Q_s_dir + Q_s_dif + Q_g,c +
            Q_g,r)/Ci) * dt + exp(p11) * dw1
        dTw ~ (1/(Cw * Re) * (Te - Tw) + hcAw/(Cw) * (Ti - Tw) + Q_heat/Cw) *
            dt + exp(p22) * dw2
        dTwi ~ (hwi/Cwi * (Ti - Twi)) * dt + exp(p33) * dw3
Observation equations:
       yTair ~ Ti
Inputs:  Te, Q_s_dir, Q_s_dif, Q_g,c, Q_g,r, Q_heat
```

3_Ti_FH_2

```
Linear state space model with 3 states, 1 output and 6 inputs
System equations:
        dTi ~ (inf/Ci * (Te - Ti) + hcAw/(Ci) * (Tw - Ti) + hwi/Ci *
            (Twi - Ti) + (Q_s_dir + Q_s_dif + Q_g,c +
            Q_g,r)/Ci) * dt + exp(p11) * dw1
        dTw ~ (1/(Cw * Re) * (Te - Tw) + hcAw/(Cw) * (Ti - Tw)) * dt +
            exp(p22) * dw2
        dTwi ~ (hwi/Cwi * (Ti - Twi) + Q_heat/Cwi) * dt + exp(p33) *
            dw3
Observation equations:
        yTair ~ Ti
Inputs:  Te, Q_s_dir, Q_s_dif, Q_g,c, Q_g,r, Q_heat
```

4_TiQ_FH

```
Linear state space model with 4 states, 4 outputs and 9 inputs
System equations:
        dTi ~ (inf/Ci * (Te - Ti) + hcAw/(Ci) * (Tw - Ti) + hwi/Ci *
            (Twi - Ti) + hfAf/Ci * (Tf - Ti) + abs3 * (Q_s_dir +
            Q_s_dif)/Ci + (Q_g,c + Q_g,r)/Ci) * dt +
            exp(p11) * dw1
        dTw ~ (1/(Cw * Re) * (Te - Tw) + hcAw/(Cw) * (Ti - Tw) + abs1 *
            (Q_s_dir + Q_s_dif)/Cw) * dt + exp(p22) * dw2
        dTwi ~ (hwi/Cwi * (Ti - Twi) + abs2 * (Q_s_dir + Q_s_dif)/Cwi) *
```

```
            dt + exp(p33) * dw3
        dTf ~ (hfAf/Cf * (Ti - Tf) + 1/(Rf * Cf) * (Tground - Tf) + abs4 *
            (Q_s_dir + Q_s_dif)/Cf + (Q_heat)/Cf) * dt +
            exp(p44) * dw4
Observation equations:
        yTair ~ Ti
        QfluxeNoFloor ~ (Ti - Tw) * hcAw + abs1 * (Q_s_dir + Q_s_dif)
        Qfluxi ~ (Ti - Twi) * hwi + abs2 * (Q_s_dir + Q_s_dif)
        QfluxFloor ~ hfAf * (Ti - Tf) + abs4 * (Q_s_dir + Q_s_dif)
Inputs:  Te, Q_s_dir, Q_s_dif, Q_g,c, Q_g,r, Q_heat, Tground
```

4_TiQe_FH

```
Linear state space model with 4 states, 2 outputs and 9 inputs
System equations:
        dTi ~ (inf/Ci * (Te - Ti) + hcAw/(Ci) * (Tw - Ti) + hwi/Ci *
            (Twi - Ti) + hfAf/Ci * (Tf - Ti) + abs3 * (Q_s_dir +
            Q_s_dif)/Ci + (Q_g,c + Q_g,r)/Ci) * dt +
            exp(p11) * dw1
        dTw ~ (1/(Cw * Re) * (Te - Tw) + hcAw/(Cw) * (Ti - Tw) + abs1 *
            (Q_s_dir + Q_s_dif)/Cw) * dt + exp(p22) * dw2
        dTwi ~ (hwi/Cwi * (Ti - Twi) + abs2 * (Q_s_dir + Q_s_dif)/Cwi) *
            dt + exp(p33) * dw3
        dTf ~ (hfAf/Cf * (Ti - Tf) + 1/(Rf * Cf) * (Tground - Tf) + abs4 *
            (Q_s_dir + Q_s_dif)/Cf + (Q_heat)/Cf) * dt +
            exp(p44) * dw4
Observation equations:
        yTair ~ Ti
        QfluxeNoFloor ~ (Ti - Tw) * hcAw + abs1 * (Q_s_dir + Q_s_dif)
Inputs:  Te, Q_s_dir, Q_s_dif, Q_g,c, Q_g,r, Q_heat, Tground
```

4_Tiq_FH

```
Linear state space model with 4 states, 2 outputs and 9 inputs
System equations:
        dTi ~ (inf/Ci * (Te - Ti) + hcAw/(Ci) * (Tw - Ti) + hwi/Ci *
            (Twi - Ti) + hfAf/Ci * (Tf - Ti) + abs3 * (Q_s_dir +
            Q_s_dif)/Ci + (Q_g,c + Q_g,r)/Ci) * dt +
            exp(p11) * dw1
        dTw ~ (1/(Cw * Re) * (Te - Tw) + hcAw/(Cw) * (Ti - Tw) + abs1 *
            (Q_s_dir + Q_s_dif)/Cw) * dt + exp(p22) * dw2
        dTwi ~ (hwi/Cwi * (Ti - Twi) + abs2 * (Q_s_dir + Q_s_dif)/Cwi) *
            dt + exp(p33) * dw3
        dTf ~ (hfAf/Cf * (Ti - Tf) + 1/(Rf * Cf) * (Tground - Tf) + abs4 *
            (Q_s_dir + Q_s_dif)/Cf + (Q_heat)/Cf) * dt +
            exp(p44) * dw4
Observation equations:
        yTair ~ Ti
        qfluxeNoFloor ~ ((Ti - Tw) * hcAw + abs1 * (Q_s_dir + Q_s_dif))/Aext
Inputs:  Te, Q_s_dir, Q_s_dif, Q_g,c, Q_g,r, Q_heat, Tground
```

4_Ti_FH

```
Linear state space model with 4 states, 1 output and 9 inputs
System equations:
        dTi ~ (inf/Ci * (Te - Ti) + hcAw/(Ci) * (Tw - Ti) + hwi/Ci *
            (Twi - Ti) + hfAf/Ci * (Tf - Ti) + abs3 * (Q_s_dir +
            Q_s_dif)/Ci + (Q_g,c + Q_g,r)/Ci) * dt +
            exp(p11) * dw1
        dTw ~ (1/(Cw * Re) * (Te - Tw) + hcAw/(Cw) * (Ti - Tw) + abs1 *
            (Q_s_dir + Q_s_dif)/Cw) * dt + exp(p22) * dw2
        dTwi ~ (hwi/Cwi * (Ti - Twi) + abs2 * (Q_s_dir + Q_s_dif)/Cwi) *
            dt + exp(p33) * dw3
        dTf ~ (hfAf/Cf * (Ti - Tf) + 1/(Rf * Cf) * (Tground - Tf) + abs4 *
            (Q_s_dir + Q_s_dif)/Cf + (Q_heat)/Cf) * dt +
            exp(p44) * dw4
Observation equations:
        yTair ~ Ti
Inputs:  Te, Q_s_dir, Q_s_dif, Q_g,c, Q_g,r, Q_heat, Tground
```

4_TiTs_FH

```
Linear state space model with 4 states, 4 outputs and 9 inputs
System equations:
        dTi ~ (inf/Ci * (Te - Ti) + hcAw/(Ci) * (Tw - Ti) + hwi/Ci *
            (Twi - Ti) + hfAf/Ci * (Tf - Ti) + abs3 * (Q_s_dir +
            Q_s_dif)/Ci + (Q_g,c + Q_g,r)/Ci) * dt +
            exp(p11) * dw1
        dTw ~ (1/(Cw * Re) * (Te - Tw) + hcAw/(Cw) * (Ti - Tw) + abs1 *
            (Q_s_dir + Q_s_dif)/Cw) * dt + exp(p22) * dw2
        dTwi ~ (hwi/Cwi * (Ti - Twi) + abs2 * (Q_s_dir + Q_s_dif)/Cwi) *
            dt + exp(p33) * dw3
        dTf ~ (hfAf/Cf * (Ti - Tf) + 1/(Rf * Cf) * (Tground - Tf) + abs4 *
            (Q_s_dir + Q_s_dif)/Cf + (Q_heat)/Cf) * dt +
            exp(p44) * dw4
Observation equations:
        yTair ~ Ti
        yTw ~ Tw
        yTwi ~ Tw
        yTf ~ Tf
Inputs:  Te, Q_s_dir, Q_s_dif, Q_g,c, Q_g,r, Q_heat, Tground
```

Appendix B

Implementation and parameters for reduced-order building stock model

This appendix consists of two main parts. In Section B.1 the parametric implementation of the building models is presented, demonstrating how the building stock data of the TABULA project are used to implement a dynamic 2-zone model. Section B.2 presents the parameters of the 2-zone grey-box models used in Chapter 5 for the whole building stock as they have been obtained by grey-box modelling and a direct use of the theoretical values.

B.1 Parametric implementation of TABULA dwellings

In the TABULA-project [117] a building stock description for the Belgian residential sector has been established as presented in Section 5.1.1. Additional assumptions had to be made in order to translate these properties – formulated for stationary, single-zone calculation framework – to the model parameters needed to implement a 2-zone dynamic building energy simulation model. In this section, the parametric methodology used for this dynamic implement ion of the building models is presented. Most of these assumptions are related to the transformation from a single-zone to a two-zone model.

The parametric implementation of the building geometry starts from data on the ground floor area $(A_{fl,D})$, total floor area $(A_{fl,use})$, protected volume (V), total envelope area (A_{env}), roof area (A_{roof}), window areas for each orientation (A_{win}) and the area of the doors (A_{door}). The detached dwellings are modelled as 2 floor buildings $(n_{fl} = 2)$. The semi-detached and terraced dwellings are implemented with 3 floors $(n_{fl} = 3)$. Thereby the whole ground floor is assumed to be in contact with the ground and is simulated as a day-zone. The other zones are used as night-zone, following a different occupancy schedule. Thereby the surface area of the floor between day- and night-zone is assumed to have the same surface area as the ground floor $(A_{fl,D})$. The total floor area for the night-zone $(A_{fl,N})$ is calculated as:

$$A_{fl,N} = A_{fl,use} - A_{fl,D} \tag{B.1}$$

The surface area of the internal floor of the night-zone is given by:

$$A_{fl,N-N} = A_{fl,N} - A_{fl,D} \tag{B.2}$$

The height of the zones is calculated using the volume (V) and the total floor area of the dwelling $(A_{fl,use})$:

$$h_{fl} = V/A_{fl,use} \tag{B.3}$$

The volume of the day-zone (V_D) and night-zone (V_N) can as such be calculated as:

$$V_D = A_{fl,D} h_{fl} \tag{B.4}$$

$$V_N = V - V_D = A_{fl,N} h_f l \tag{B.5}$$

The calculation of the exterior wall areas along the different orientations slightly differs for the three building types. For the detached dwellings, 55 % of the walls are assumed to be oriented to the north and south facade, while 45 % are allocated to the east and west. As such assuming the front wall, with the main entrance, is oriented north.
For the semi-detached dwellings, the east wall is assumed to be the common wall. For the outer walls, the envelope area (A_{env}) is distributed to the different orientations assuming a rectangular floor plan with the depth of the dwelling equal to 2 times the width.
For the terraced dwellings only the front and back facade are adjacent to the outdoor environment. The surface area of each of these walls is thus half of the total envelope area A_{env}. The width (w) and depth (d) of the dwelling are then given by:

$$w = \frac{A_{env}}{2 h_{fl} n_{fl}} \tag{B.6}$$

$$d = A_{fl,d}/w \tag{B.7}$$

The surface area of the interior walls is taken equal to the surface area of the exterior walls. Except for the terraced dwellings where the internal wall area is the sum of the exterior wall area and half of the common wall area. The fraction of these wall areas that is allocated to the day-zone (f_{day}) is calculated as:

$$f_{day} = A_{fl,D}/A_{fl,use} \tag{B.8}$$

B.2 Reduced-order building stock description

The structure for the two-zone reduced order building stock model has been obtained by a forward-selection process using the grey-box modelling framework developed in chapter 4. The RC-equivalent of the model structure has been illustrated in Figure 4.18. The model equations for the day-zone, night-zone and the intermediate floor are given below. In these equations the conventions of Table A.1 are followed.

B.2.1 Grey-box model equations

Day-zone model:

```
Linear state space model with 5 states, 5 outputs and 9 inputs
System equations:
        dTi ~ (inf/Ci * (Te - Ti) + 1/(Re*Ci) * (Tw - Ti) + hwi/Ci *
            (Twi - Ti) + UfiA/Ci * (Tfi - Ti) + hfl/Ci * (Tfl - Ti) +
            abs3N * (Q_s,N)/Ci + abs3E * (Q_s,E)/Ci + abs3S * (Q_s,S)/Ci +
            abs3W * (Q_s,W)/Ci + f3 * (Q_g+Q_heat)/Ci) * dt + exp(p11) * dw1
        dTw ~ (1/(Cw * Re) * (Te - Tw) + hcAw/(Cw) * (Ti - Tw) + abs1N *
            (Q_s,N)/Cw + abs1E * (Q_s,E)/Cw + abs1S * (Q_s,S)/Cw +
            abs1W * (Q_s,W)/Cw + f1 * (Q_g,r+Q_heat)/Cw) * dt + exp(p22) * dw2
        dTwi ~ (hwi/Cwi * (Ti - Twi) + abs2N * (Q_s,N)/Cwi + abs2E *
            (Q_s,E)/Cwi + abs2S * (Q_s,S)/Cwi + abs2W * (Q_s,W)/Cwi +
            f2 * (Q_g+Q_heat)/Cwi) *
            dt + exp(p33) * dw3
        dTfl ~ (Ufl/Cfl * (Tground - Tfl) + hfl/Cfl * (Ti - Tfl) + abs4N *
            (Q_s,N)/Cfl + abs4E * (Q_s,E)/Cfl + abs4S * (Q_s,S)/Cfl +
            abs4W * (Q_s,W)/Cfl + f4 * (Q_g+Q_heat)/Cfl) * dt + exp(p44) * dw4
        dTfi ~ (UfiA/Cfi * (Ti - Tfi) + UfiB/Cfi * (TB - Tfi) + abs5N *
            (Q_s,N)/Cfi + abs5E * (Q_s,E)/Cfi + abs5S * (Q_s,S)/Cfi +
            abs5W * (Q_s,W)/Cfi + f5 * (Q_g+Q_heat)/Cfi) * dt + exp(p55) * dw5
Observation equations:
        yTair ~ Ti
        QfluxeNoFloor ~ (Ti - Tw) * hcAw + abs1N * (Q_s,N) + abs1E *
```

```
            (Q_s,E) + abs1S * (Q_s,S) + abs1W * (Q_s,W) + f1 *
            (Q_g+Q_heat)
        Qfluxi ~ (Ti - Twi) * hwi + abs2N * (Q_s,N) + abs2E * (Q_s,E) +
            abs2S * (Q_s,S) + abs2W * (Q_s,W) + f2 * (Q_g+Q_heat)
        QfluxA ~ (Ti - Tfi) * UfiA + abs5N * (Q_s,N) + abs5E * (Q_s,E) +
            abs5S * (Q_s,S) + abs5W * (Q_s,W) + f5 * (Q_g+Q_heat)
        QfluxFloor ~ (Ti - Tfl) * hfl + abs4N * (Q_s,N) + abs4E * (Q_s,E) +
            abs4S * (Q_s,S) + abs4W * (Q_s,W) + f4 * (Q_g+Q_heat)
Inputs:  Te, Q_s,N, Q_s,E, Q_s,S, Q_s,W, Q_g, Q_heat, TB, Tground
```

Night-zone model

```
Linear state space model with 4 states, 4 outputs and 8 inputs
System equations:
        dTi ~ (inf/Ci * (Te - Ti) + hcAw/(Ci) * (Tw - Ti) + hwi/Ci *
            (Twi - Ti) + UfiA/Ci * (Tfi - Ti) + abs3N * (Q_s,N)/Ci +
            abs3E * (Q_s,E)/Ci + abs3S * (Q_s,S)/Ci + abs3W *
            (Q_s,W)/Ci + f3 * (Q_g + Q_heat)/Ci) *
            dt + exp(p11) * dw1
        dTw ~ (1/(Cw * Re) * (Te - Tw) + hcAw/(Cw) * (Ti - Tw) + abs1N *
            (Q_s,N)/Cw + abs1E * (Q_s,E)/Cw + abs1S * (Q_s,S)/Cw +
            abs1W * (Q_s,W)/Cw + f1 * (+
            HeatingQTotal)/Cw) * dt + exp(p22) * dw2
        dTwi ~ (hwi/Cwi * (Ti - Twi) + abs2N * (Q_s,N)/Cwi + abs2E *
            (Q_s,E)/Cwi + abs2S * (Q_s,S)/Cwi + abs2W * (Q_s,W)/Cwi +
            f2 * (Q_g + Q_heat)/Cwi) *
            dt + exp(p33) * dw3
        dTfi ~ (UfiA/Cfi * (Ti - Tfi) + UfiB/Cfi * (TB - Tfi) + abs4N *
            (Q_s,N)/Cfi + abs4E * (Q_s,E)/Cfi + abs4S * (Q_s,S)/Cfi +
            abs4W * (Q_s,W)/Cfi + f4 * (+
            HeatingQTotal)/Cfi) * dt + exp(p44) * dw4
Observation equations:
        yTair ~ Ti
        Qfluxe ~ (Ti - Tw) * hcAw + abs1N * (Q_s,N) + abs1E * (Q_s,E) +
            abs1S * (Q_s,S) + abs1W * (Q_s,W) + f1 * (-
            UserGainsRad Q_g + Q_heat)
        Qfluxi ~ (Ti - Twi) * hwi + abs2N * (Q_s,N) + abs2E * (Q_s,E) +
            abs2S * (Q_s,S) + abs2W * (Q_s,W) + f2 * (-
            UserGainsRad Q_g + Q_heat)
        QfluxA ~ (Ti - Tfi) * UfiA + abs4N * (Q_s,N) + abs4E * (Q_s,E) +
            abs4S * (Q_s,S) + abs4W * (Q_s,W) + f4 * (-
            UserGainsRad Q_g + Q_heat)
Inputs:  Te, Q_s,N, Q_s,E, Q_s,S, Q_s,W, Q_g, Q_heat, TB
```

Internal floor between day- and night-zone

```
Linear state space model with 2 states, 2 outputs and 13 inputs
System equations:
        dTfiD ~ (UfDN/CfiD * (TiD - TfiD) + Ufi/CfiD * (TfiN - TfiD) +
            abs5D * (Q_s,D)/CfiD + f5D * (Q_g,D + Q_heat,D)/CfiD) * dt
            + exp(p99) * dw9
```

```
        dTfiN ~ (UfND/CfiN * (TiN - TfiN) + Ufi/CfiN * (TfiD - TfiN) +
            abs5N * (Q,s_N)/CfiN + f5N *
            (Q_g,N + Q_heat,N)/CfiN) * dt + exp(p55) * dw5
Observation equations:
        QfluxiDayNight ~ (TiD - TfiD) * UfDN + abs5D * (Q_s,D) + f5D * (Q_g,D + Q_heat,D)
        QfluxiNightDay ~ (TiN - TfiN) * UfND + abs5N * (Q_s,N) + f5N * (Q_g,N + Q_heat,N)
Inputs:  Te, TiD, TiN, Q_s,D, Q_g,D, Q_heat,D, Q_s,N, Q_g,N, Q_heat,N
```

B.2.2 Model Parameters

Table B.1: Grey-box model parameters for original detached buildings (Estimated values (Est.) and standard error of estimation (Std.))

Parameters	D1		D2		D3		D4		D5	
	Est.	Std.	Est.	Std.	Est.	Std.	Est.	Std.	Est.	Std.
abs1ED	8.73E-01	8.30E-02	9.56E-01	5.53E-02	1.05E+00	4.79E-02	1.23E+00	3.63E-02	6.40E-01	4.91E-02
abs1ND	3.78E+00	1.86E-01	2.50E+00	1.36E-01	1.38E+00	1.17E-01	1.45E+00	9.87E-02	2.60E-01	1.06E-01
abs1SD	1.71E+00	3.88E-02	1.58E+00	2.84E-02	1.31E+00	2.20E-02	1.40E+00	1.80E-02	7.66E-01	2.18E-02
abs1WD	9.97E-01	3.67E-02	1.04E+00	2.91E-02	1.02E+00	2.38E-02	1.13E+00	2.16E-02	3.77E-01	2.16E-02
abs2ED	2.21E+00	1.66E-01	1.92E+00	8.63E-02	1.95E+00	7.55E-02	2.44E+00	5.87E-02	1.25E+00	6.13E-02
abs2ND	3.14E+00	4.81E-01	3.24E+00	2.21E-01	3.30E+00	1.93E-01	3.50E+00	1.54E-01	1.91E+00	1.31E-01
abs2SD	2.46E+00	6.82E-02	2.52E+00	4.67E-02	2.36E+00	3.58E-02	2.66E+00	2.87E-02	1.77E+00	2.80E-02
abs2WD	2.71E+00	5.63E-02	2.41E+00	4.59E-02	2.32E+00	3.94E-02	2.51E+00	3.19E-02	1.04E+00	2.74E-02
abs3ED	1.16E+00	4.49E-01	9.95E-01	2.52E-01	6.46E-01	1.91E-01	5.97E-01	1.78E-01	3.74E-01	1.23E-01
abs3ND	1.53E-01	9.23E-01	1.01E+00	4.49E-01	5.65E-01	3.44E-01	9.14E-01	3.06E-01	2.67E+00	2.24E-01
abs3SD	5.80E-01	1.02E-01	7.24E-01	8.63E-02	7.58E-01	6.11E-02	7.90E-01	5.38E-02	3.77E-01	4.91E-02
abs3WD	5.19E-08	1.17E-07	1.30E-01	1.13E-01	4.37E-01	8.14E-02	7.09E-01	7.53E-02	3.87E-01	4.76E-02
abs4ED	8.19E-01	4.24E-02	8.94E-01	3.57E-02	1.15E+00	3.45E-02	1.19E+00	2.23E-02	5.65E-01	2.47E-02
abs4ND	1.38E-14	3.66E-14	1.05E-09	2.11E-08	1.02E+00	8.53E-02	1.13E+00	5.97E-02	6.84E-01	5.02E-02
abs4SD	7.64E-01	2.04E-02	9.10E-01	1.93E-02	1.26E+00	1.63E-02	1.22E+00	1.08E-02	7.53E-01	1.12E-02
abs4WS	7.92E-01	1.94E-02	9.14E-01	1.96E-02	1.14E+00	1.72E-02	1.09E+00	1.24E-02	4.28E-01	1.06E-02
abs5ED	8.40E-02	4.31E-02	4.54E-01	2.17E-02	4.25E-01	1.70E-02	6.25E-01	1.74E-02	5.82E-01	4.35E-02
abs5ND	2.07E-01	9.91E-02	4.18E-11	1.65E-09	1.66E-07	1.74E-06	8.75E-08	5.38E-07	4.67E-01	9.19E-02
abs5SD	4.38E-01	2.26E-02	5.26E-01	1.09E-02	4.78E-01	8.17E-03	6.45E-01	8.67E-03	7.51E-01	1.98E-02
abs5WD	1.54E-01	2.43E-02	4.15E-01	1.13E-02	3.96E-01	8.30E-03	5.19E-01	8.92E-03	2.81E-01	1.81E-02
f1D	7.21E-02	5.49E-04	6.50E-02	3.27E-04	6.29E-02	3.69E-04	6.37E-02	3.80E-04	7.29E-02	3.43E-04
f2D	1.41E-01	8.25E-04	1.30E-01	5.72E-04	1.32E-01	5.61E-04	1.35E-01	5.53E-04	1.47E-01	4.42E-04
f3D	7.20E-01	1.62E-03	7.30E-01	1.67E-03	7.20E-01	1.38E-03	7.20E-01	1.54E-03	6.81E-01	9.46E-04
f4D	4.62E-02	2.36E-04	5.05E-02	2.24E-04	6.65E-02	2.51E-04	5.89E-02	2.21E-04	6.11E-02	1.61E-04
f5D	2.32E-02	2.19E-04	3.74E-02	1.32E-04	3.46E-02	1.16E-04	4.20E-02	1.33E-04	5.60E-02	2.85E-04
CflD	2.35E+08	3.36E+07	4.87E+07	3.63E+06	1.36E+07	1.67E+05	1.35E+07	1.45E+05	1.09E+07	1.92E+05
CiD	2.32E+06	2.61E+04	2.25E+06	1.70E+04	2.47E+06	1.32E+04	2.39E+06	1.42E+04	2.22E+06	7.69E+03
CwD	7.57E+07	1.62E+06	3.73E+07	5.88E+05	2.72E+07	4.67E+05	1.97E+07	2.56E+05	1.47E+07	4.05E+05
CwiD	2.27E+07	2.19E+05	2.42E+07	2.24E+05	2.39E+07	2.51E+05	2.65E+07	2.32E+05	1.82E+07	1.96E+05
hwD	5.31E+02	1.95E+00	4.03E+02	1.32E+00	3.09E+02	1.29E+00	3.06E+02	1.19E+00	2.38E+02	1.70E+00
hflD	2.29E+02	1.55E+00	2.07E+02	8.45E-01	2.33E+02	9.19E-01	2.09E+02	7.37E-01	1.92E+02	8.73E-01
hwiD	8.63E+02	2.70E+00	6.08E+02	2.24E+00	5.10E+02	2.41E+00	5.36E+02	2.02E+00	5.28E+02	2.31E+00
infD	2.65E+02	1.20E+00	2.74E+02	8.60E-01	2.23E+02	4.28E-01	2.00E+02	3.70E-01	1.79E+02	2.01E-01
UflD	1.09E-02	4.71E-03	2.24E+02	1.48E+01	9.10E+01	1.73E+00	6.91E+01	1.21E+00	6.81E+01	1.36E+00
Uwd	1.30E+03	9.35E+04	5.59E+02	5.68E+04	2.59E+02	2.31E+04	1.29E+02	1.56E+04	8.71E+01	4.79E+03
abs1EN	3.60E-07	9.11E-06	5.17E-12	7.27E-10	1.27E-08	1.50E-07	8.52E-07	5.82E-05	3.20E-01	2.60E-02
abs1NN	9.01E-01	1.87E-01	1.50E-12	2.36E-10	1.98E-29	1.05E-26	1.52E-01	1.52E-01	8.74E-01	5.50E-02
abs1SN	8.99E-01	5.41E-02	1.06E-10	1.28E-08	8.21E-01	4.48E-02	8.38E-01	4.48E-02	7.52E-01	1.19E-02
abs1WN	1.28E+00	4.83E-02	1.62E+00	3.63E-02	1.54E+00	3.74E-02	1.56E+00	3.63E-02	4.26E-01	9.49E-03
abs2EN	7.39E-01	4.34E-02	5.95E-01	2.92E-02	5.35E-01	2.35E-02	5.51E-01	2.20E-02	2.17E-01	8.51E-03
abs2NN	5.18E-01	1.10E-01	7.03E-01	7.23E-02	4.17E-01	5.27E-02	4.00E-01	4.79E-02	8.93E-08	1.24E-05
abs2SN	5.70E-01	3.23E-02	7.44E-01	1.50E-02	5.36E-01	1.10E-02	5.49E-01	9.96E-03	1.99E-01	3.76E-03
abs2WN	1.24E-01	1.88E-02	6.30E-02	1.30E-02	1.90E-01	9.33E-03	2.58E-01	7.97E-03	1.31E-01	3.25E-03
abs3EN	1.18E-06	3.75E-05	3.22E-11	4.43E-09	1.65E-09	1.34E-08	1.48E-01	1.21E-01	8.98E-10	2.22E-07
abs3NN	2.20E-08	5.15E-07	5.16E-10	6.08E-08	7.76E-13	1.81E-11	5.00E-07	2.93E-05	1.78E-08	3.01E-06
abs3SN	6.51E-02	8.58E-02	5.76E-08	3.80E-06	8.89E-02	5.86E-02	1.42E-01	6.27E-02	7.52E-02	2.05E-02
abs3WN	2.99E-01	1.25E-01	1.07E-07	7.07E-06	1.25E-01	6.13E-02	1.74E-01	5.32E-02	4.22E-02	2.48E-02
abs5EN	9.71E-01	8.49E-02	1.32E+00	6.93E-02	1.16E+00	5.43E-02	1.41E+00	6.24E-02	6.72E-01	2.82E-02
abs5NN	1.10E-06	2.60E-05	1.65E+00	1.47E-01	1.51E+00	1.10E-01	1.79E+00	1.21E-01	4.04E-01	5.59E-02
abs5SN	9.87E-01	6.12E-02	1.81E+00	2.77E-02	1.21E+00	2.68E-02	1.41E+00	2.88E-02	6.39E-01	1.25E-02
abs5WN	1.37E-02	6.99E-02	1.07E-10	1.23E-08	3.05E-01	2.18E-02	4.81E-01	2.39E-02	3.40E-01	9.82E-03
f1N	1.41E-01	6.79E-04	1.70E-01	9.59E-04	1.80E-01	9.70E-04	1.61E-01	1.00E-03	1.36E-01	4.11E-04
f2N	4.79E-02	2.33E-04	4.37E-02	2.18E-04	4.23E-02	2.00E-04	4.28E-02	2.08E-04	4.25E-02	1.45E-04
f3N	6.64E-01	4.28E-03	6.70E-01	3.88E-03	6.76E-01	3.65E-03	6.96E-01	3.16E-03	7.08E-01	3.46E-03
f5N	1.06E-01	9.53E-04	8.29E-02	4.66E-04	7.28E-02	4.82E-04	8.87E-02	5.62E-04	1.17E-01	4.17E-04
CiN	2.53E+06	2.25E+04	2.11E+06	2.02E+04	1.61E+06	1.40E+04	2.09E+06	1.44E+04	2.55E+06	2.26E+04
CwN	1.85E+07	8.37E+05	2.19E+07	1.92E+06	4.44E+06	1.50E+05	3.77E+06	1.22E+05	3.59E+06	6.62E+04
CwiN	3.01E+06	9.56E+04	3.74E+06	1.38E+05	4.18E+06	1.48E+05	4.27E+06	1.57E+05	2.44E+06	5.95E+04
hwN	3.54E+02	2.85E+00	3.24E+02	3.79E+00	2.53E+02	2.98E+00	2.28E+02	3.32E+00	1.54E+02	1.87E+00
hwiN	1.34E+02	1.47E+00	1.10E+02	9.49E-01	8.71E+01	6.82E-01	8.74E+01	6.93E-01	6.63E+01	6.19E-01
infN	1.29E+02	1.77E+00	1.15E+02	1.43E+00	8.72E+01	7.75E-01	8.76E+01	5.78E-01	6.02E+01	2.97E-01
UwN	9.80E+02	4.72E+04	7.30E+02	2.96E+04	2.42E+02	2.54E+04	1.97E+02	1.79E+04	8.55E+01	1.31E+04
CfiD	9.94E+08	2.87E+07	2.03E+08	3.34E+07	3.01E+08	6.41E+07	9.92E+08	4.46E+07	9.97E+08	9.89E+06
CfiN	1.39E+08	7.13E+07	9.98E+08	8.22E+06	9.98E+08	8.29E+06	9.96E+08	1.88E+07	9.95E+08	2.44E+07
UfDN	9.51E+01	7.52E-01	7.87E+01	4.14E-01	5.68E+01	4.04E-01	7.44E+01	4.90E-01	1.71E+02	1.34E+00
Ufi	1.11E-03	1.10E-01	1.90E+03	3.14E+02	1.63E+03	3.44E+02	3.88E+02	4.79E+02	1.12E-03	1.91E-01
UfND	2.33E+02	2.23E+00	2.22E+02	1.95E+00	1.77E+02	1.65E+00	1.84E+02	2.13E+00	1.60E+02	1.15E+00

Table B.2: Grey-box model parameters for original semi-detached buildings

Parameters	SD1		SD2		SD3		SD4		SD5	
	Est.	Std.	Est.	Std.	Est.	Std.	Est.	Std.	Est.	Std.
abs1ED	2.20E-01	2.44E-02	2.85E-01	2.04E-02	3.46E-01	1.53E-02	3.22E-01	4.98E-03	1.83E-01	8.05E-03
abs1ND	1.32E+00	6.13E-02	8.24E-01	4.68E-02	3.93E-01	3.67E-02	1.61E-01	1.71E-02	1.11E-01	1.99E-02
abs1SD	4.53E-01	1.32E-02	4.91E-01	1.09E-02	4.30E-01	8.94E-03	3.52E-01	3.15E-03	2.98E-01	4.48E-03
abs1WD	4.05E-01	1.23E-02	3.86E-01	1.08E-02	2.73E-01	9.00E-03	4.02E-01	5.19E-03	1.64E-01	4.51E-03
abs2ED	9.32E-01	6.20E-02	7.64E-01	4.37E-02	7.85E-01	2.62E-02	6.72E-01	8.68E-03	4.07E-01	1.54E-02
abs2ND	8.97E-01	1.47E-01	8.49E-01	1.06E-01	5.89E-01	6.52E-02	2.31E-01	2.41E-02	2.37E-02	3.76E-02
abs2SD	7.83E-01	3.47E-02	8.61E-01	2.49E-02	7.83E-01	1.36E-02	7.12E-01	5.65E-03	5.57E-01	8.36E-03
abs2WD	1.06E+00	3.13E-02	8.79E-01	2.55E-02	6.70E-01	1.54E-02	8.36E-01	9.22E-03	4.09E-01	8.77E-03
abs3ED	5.98E-01	1.40E-01	5.17E-01	1.31E-01	2.62E-01	9.16E-02	6.44E-01	1.55E-01	2.00E-01	7.17E-02
abs3ND	1.56E-01	2.47E-01	1.29E+00	2.24E-01	1.08E+00	1.60E-01	4.67E-06	5.37E-06	7.84E-01	1.30E-01
abs3SD	1.99E-01	5.67E-02	2.71E-01	4.94E-02	2.47E-01	3.53E-02	6.33E-02	7.21E-02	1.60E-01	2.70E-02
abs3WD	8.33E-02	6.01E-02	8.61E-02	6.12E-02	2.84E-01	4.47E-02	4.29E-07	5.93E-07	3.88E-01	3.27E-02
abs4ED	6.14E-01	2.66E-02	5.80E-01	2.81E-02	5.56E-01	1.43E-02	6.34E-01	6.28E-03	4.04E-01	1.15E-02
abs4ND	7.00E-10	5.63E-08	1.08E-08	3.72E-07	4.29E-01	3.25E-02	6.26E-02	1.86E-02	6.29E-01	2.88E-02
abs4SD	4.61E-01	1.48E-02	4.96E-01	1.55E-02	5.80E-01	6.94E-03	6.97E-01	3.99E-03	7.03E-01	6.19E-03
abs4WS	5.64E-01	1.40E-02	5.46E-01	1.43E-02	4.43E-01	8.16E-03	8.20E-01	6.60E-03	4.53E-01	6.82E-03
abs5ED	2.37E-02	3.46E-02	1.43E-01	1.41E-02	1.62E-01	1.10E-02	1.70E-01	4.31E-03	1.54E-01	2.31E-02
abs5ND	5.24E-01	8.07E-02	9.03E-02	3.14E-02	1.03E-01	2.63E-02	2.99E-09	4.59E-09	7.87E-01	6.26E-02
abs5SD	1.22E-01	1.65E-02	1.80E-01	7.26E-03	1.70E-01	6.45E-03	1.71E-01	3.08E-03	3.47E-01	1.31E-02
abs5WD	6.44E-10	3.57E-08	1.34E-01	7.02E-03	8.42E-02	5.83E-03	1.83E-01	4.45E-03	1.51E-07	1.25E-06
f1D	5.59E-02	2.51E-04	5.51E-02	2.10E-04	5.69E-02	2.82E-04	6.16E-02	2.38E-04	4.80E-02	1.72E-04
f2D	1.39E-01	6.40E-04	1.21E-01	5.16E-04	1.28E-01	4.98E-04	1.26E-01	4.98E-04	1.00E-01	3.62E-04
f3D	7.26E-01	1.69E-03	7.34E-01	1.72E-03	7.20E-01	1.70E-03	7.39E-01	7.30E-03	7.26E-01	1.86E-03
f4D	8.04E-02	2.56E-04	7.98E-02	2.80E-04	8.53E-02	2.50E-04	1.16E-01	3.18E-04	1.07E-01	2.85E-04
f5D	6.31E-03	3.54E-04	2.13E-02	1.44E-04	2.41E-02	1.73E-04	3.14E-02	2.05E-04	3.79E-02	4.38E-04
CfID	4.11E+07	3.02E+06	1.74E+07	8.27E+05	7.85E+06	6.45E+04	9.52E+06	1.07E+05	5.66E+06	4.08E+04
CiD	1.78E+06	1.05E+04	1.58E+06	9.62E+03	1.63E+06	1.09E+04	2.19E+06	4.47E+04	1.68E+06	1.04E+04
CwD	2.41E+07	4.28E+05	1.30E+07	1.95E+05	1.15E+07	1.65E+05	7.26E+06	1.20E+05	4.06E+06	4.93E+04
CwiD	1.05E+07	9.71E+04	1.12E+07	1.11E+05	1.20E+07	6.91E+04	1.07E+07	6.72E+04	5.20E+06	3.63E+04
hwD	1.89E+02	6.79E-01	1.59E+02	5.47E-01	1.45E+02	5.61E-01	1.05E+02	4.46E-01	8.04E+01	3.44E-01
hfID	1.67E+02	7.71E-01	1.45E+02	6.85E-01	1.52E+02	5.00E-01	1.48E+02	5.22E-01	1.46E+02	5.51E-01
hwiD	4.09E+02	1.76E+00	3.19E+02	1.18E+00	3.16E+02	9.99E-01	2.42E+02	7.34E-01	1.92E+02	7.32E-01
infD	1.63E+02	5.70E-01	1.61E+02	4.96E-01	1.41E+02	3.65E-01	1.24E+02	1.38E+00	8.89E+01	2.22E-01
UflD	1.86E+02	1.18E+01	2.15E+02	6.63E+00	6.74E+01	7.62E-01	4.40E+01	6.59E-01	4.12E+01	4.48E-01
Uwd	4.81E+02	3.76E+04	2.12E+02	2.36E+04	1.17E+02	1.29E+04	5.41E+01	4.90E+03	2.62E+01	2.79E+03
abs1EN	1.12E-07	2.27E-06	3.45E-08	2.08E-06	1.66E-01	4.64E-02	6.13E-01	1.83E-02	2.23E-01	1.53E-02
abs1NN	8.04E-01	1.32E-01	7.03E-08	4.23E-06	4.46E-01	7.93E-02	1.34E-09	9.71E-08	9.44E-01	3.31E-02
abs1SN	6.04E-01	3.51E-02	1.52E-03	3.58E-02	6.70E-01	2.63E-02	8.45E-01	1.02E-02	7.22E-01	7.78E-03
abs1WN	8.59E-01	2.79E-02	1.09E+00	2.98E-02	7.45E-01	1.84E-02	9.82E-01	1.73E-02	4.05E-01	6.60E-03
abs2EN	1.57E+00	7.64E-02	1.29E+00	5.19E-02	8.33E-01	2.89E-02	7.20E-01	1.53E-02	6.05E-01	2.29E-02
abs2NN	8.16E-01	1.60E-01	1.21E+00	1.06E-01	5.78E-01	6.36E-02	3.55E-01	5.98E-02	3.88E-01	4.38E-02
abs2SN	1.17E+00	3.91E-02	1.46E+00	3.12E-02	8.92E-01	1.71E-02	8.52E-01	8.48E-03	9.10E-01	1.26E-02
abs2WN	6.23E-01	3.40E-02	4.97E-01	2.49E-02	4.40E-01	1.22E-02	9.55E-01	1.51E-02	6.34E-01	1.09E-02
abs3EN	5.95E-08	1.49E-06	1.12E-20	2.23E-18	1.43E-01	7.25E-02	4.86E-01	4.90E-02	2.13E-03	1.55E-02
abs3NN	8.43E-12	3.05E-09	4.87E-14	6.54E-12	2.81E-08	1.63E-05	9.65E-08	6.69E-07	1.58E-06	7.42E-06
abs3SN	5.54E-07	2.71E-05	2.23E-01	5.27E-02	9.91E-02	3.82E-02	3.45E-06	3.22E-05	1.50E-01	1.74E-02
abs3WN	2.40E-01	5.65E-02	1.52E-01	5.70E-02	2.73E-01	3.12E-02	1.32E-01	5.19E-02	2.12E-01	1.84E-02
abs5EN	3.38E-01	3.91E-02	5.03E-01	2.32E-02	5.70E-01	2.67E-02	3.62E-01	9.07E-03	2.41E-01	1.13E-02
abs5NN	1.31E-07	2.37E-06	8.12E-01	5.08E-02	7.05E-01	5.07E-02	3.72E-01	3.37E-02	4.20E-01	2.55E-02
abs5SN	2.73E-01	2.35E-02	5.91E-01	1.32E-02	6.23E-01	1.29E-02	4.20E-01	5.20E-03	3.82E-01	5.77E-03
abs5WN	2.01E-01	1.75E-02	1.87E-01	1.05E-02	2.77E-01	9.31E-03	4.58E-01	8.90E-03	2.40E-01	4.68E-03
f1N	1.05E-01	5.42E-04	1.13E-01	7.40E-04	1.28E-01	9.10E-04	1.37E-01	4.71E-04	9.86E-02	4.30E-04
f2N	1.38E-01	6.88E-04	1.32E-01	5.91E-04	1.04E-01	5.96E-04	1.37E-01	3.91E-04	1.44E-01	6.70E-04
f3N	6.80E-01	2.60E-03	6.86E-01	2.84E-03	7.01E-01	2.03E-03	6.15E-01	4.74E-03	7.07E-01	1.88E-03
f5N	4.79E-02	3.40E-04	4.89E-02	2.41E-04	6.03E-02	4.06E-04	6.39E-02	2.21E-04	5.59E-02	2.84E-04
CiN	2.42E+06	1.99E+04	1.93E+06	1.79E+04	1.55E+06	9.32E+03	1.75E+06	2.00E+04	2.38E+06	1.24E+04
CwN	3.25E+07	7.43E+05	1.70E+07	5.66E+05	6.44E+06	1.65E+05	4.78E+06	1.29E+05	6.13E+06	8.54E+04
CwiN	1.33E+07	2.72E+05	1.74E+07	5.45E+05	1.13E+07	3.16E+05	4.59E+07	9.54E+06	2.43E+07	1.04E+06
hwN	4.58E+02	2.34E+00	3.42E+02	2.60E+00	2.57E+02	2.18E+00	2.82E+02	2.21E+00	2.07E+02	1.30E+00
hwiN	5.76E+02	4.08E+00	3.90E+02	2.32E+00	2.50E+02	1.60E+00	2.73E+02	1.78E+00	2.97E+02	2.38E+00
infN	1.27E+02	1.30E+00	1.22E+02	1.07E+00	9.48E+01	4.08E-01	7.26E+01	9.28E-01	7.06E+01	1.90E-01
UwN	1.29E+03	8.55E+04	7.75E+02	4.81E+04	2.56E+02	3.02E+04	2.20E+02	3.38E+04	9.01E+01	2.07E+04
CfiD	9.92E+08	4.33E+07	9.95E+08	2.00E+07	9.95E+08	1.97E+07	9.94E+08	2.95E+07	9.96E+08	1.49E+07
CfiN	9.89E+08	7.46E+07	9.93E+08	4.40E+07	9.95E+08	2.69E+07	9.94E+08	3.04E+07	9.94E+08	2.68E+07
UfDN	7.40E+01	7.48E-01	8.05E+01	3.71E-01	8.02E+01	4.19E-01	9.23E+01	5.29E-01	1.53E+02	1.11E+00
Ufi	1.84E-03	7.72E-02	3.54E-03	1.46E+00	1.32E-03	2.76E-01	2.28E+02	3.33E+02	1.55E-03	2.91E-01
UfND	1.57E+02	1.33E+00	1.41E+02	1.21E+00	1.36E+02	1.11E+00	1.29E+02	9.39E-01	1.04E+02	7.93E-01

Table B.3: Grey-box model parameters for original terraced buildings

Parameters	T1		T2		T3		T4		T5	
	Est.	Std.	Est.	Std.	Est.	Std.	Est.	Std.	Est.	Std.
abs1ED	1.62E-01	1.24E-02	1.67E-01	3.64E-03	1.28E-01	5.38E-03	1.13E-01	4.12E-03	9.22E-02	3.48E-03
abs1ND	6.40E-01	2.79E-02	2.61E-01	1.38E-02	1.66E-01	1.19E-02	1.51E-01	1.01E-02	1.89E-02	8.49E-03
abs1SD	2.92E-01	6.04E-03	1.68E-01	1.87E-03	1.29E-01	2.78E-03	1.10E-01	2.25E-03	9.24E-02	1.93E-03
abs1WD	1.73E-01	5.92E-03	1.51E-01	3.23E-03	1.03E-01	2.86E-03	1.13E-01	2.38E-03	5.28E-02	1.96E-03
abs2ED	1.02E+00	4.44E-02	1.16E+00	1.51E-02	8.23E-01	2.27E-02	9.54E-01	2.08E-02	6.19E-01	1.44E-02
abs2ND	1.77E+00	1.13E-01	1.22E+00	5.89E-02	9.43E-01	5.68E-02	1.03E+00	5.00E-02	4.27E-01	3.56E-02
abs2SD	1.04E+00	2.46E-02	1.11E+00	8.19E-03	7.13E-01	1.14E-02	7.78E-01	1.13E-02	6.31E-01	7.97E-03
abs2WD	1.08E+00	2.52E-02	1.13E+00	1.46E-02	8.73E-01	1.29E-02	1.12E+00	1.26E-02	5.16E-01	9.04E-03
abs3ED	5.96E-01	1.15E-01	3.72E-01	1.43E-01	2.48E-01	5.30E-02	2.36E-01	5.54E-02	1.67E-01	4.53E-02
abs3ND	5.61E-01	1.90E-01	1.02E-06	2.44E-05	5.21E-01	9.83E-02	3.66E-01	9.40E-02	7.65E-01	7.89E-02
abs3SD	2.14E-01	4.29E-02	1.01E-01	7.66E-02	1.38E-01	2.12E-02	1.21E-01	2.17E-02	1.18E-01	1.78E-02
abs3WD	2.94E-01	5.25E-02	1.95E-01	1.39E-01	2.39E-01	2.56E-02	2.85E-01	2.67E-02	2.18E-01	2.35E-02
abs4ED	5.33E-01	1.62E-02	4.35E-01	5.45E-03	2.79E-01	7.29E-03	2.90E-01	6.51E-03	2.48E-01	5.27E-03
abs4ND	8.10E-10	1.30E-08	5.28E-02	1.94E-02	3.39E-01	1.83E-02	3.42E-01	1.59E-02	2.81E-01	1.30E-02
abs4SD	4.17E-01	9.07E-03	3.99E-01	2.93E-03	2.45E-01	3.75E-03	2.43E-01	3.48E-03	2.73E-01	2.82E-03
abs4WS	4.27E-01	9.55E-03	4.13E-01	5.20E-03	2.73E-01	4.23E-03	3.20E-01	3.85E-03	2.02E-01	3.12E-03
abs5ED	1.65E-01	1.13E-02	2.87E-01	5.20E-03	1.85E-01	5.60E-03	1.93E-01	5.14E-03	2.21E-01	8.88E-03
abs5ND	5.04E-11	8.66E-10	5.56E-08	1.16E-06	8.60E-26	6.54E-24	2.43E-08	8.96E-08	3.61E-01	2.19E-02
abs5SD	1.70E-01	6.75E-03	3.02E-01	2.99E-03	1.47E-01	2.93E-03	1.47E-01	2.79E-03	2.69E-01	5.05E-03
abs5WD	1.08E-01	6.98E-03	2.90E-01	4.98E-03	1.48E-01	3.05E-03	1.79E-01	2.86E-03	1.39E-01	5.47E-03
f1D	3.00E-02	1.70E-04	2.86E-02	1.46E-04	2.44E-02	1.60E-04	2.09E-02	1.45E-04	2.14E-02	1.31E-04
f2D	1.51E-01	7.43E-04	1.89E-01	6.67E-04	1.77E-01	6.92E-04	1.91E-01	8.19E-04	1.59E-01	7.04E-04
f3D	7.54E-01	2.11E-03	7.35E-01	7.05E-03	7.22E-01	1.70E-03	7.07E-01	1.76E-03	7.30E-01	1.91E-03
f4D	6.33E-02	2.93E-04	6.63E-02	2.17E-04	5.46E-02	2.19E-04	5.38E-02	2.36E-04	6.15E-02	2.54E-04
f5D	2.77E-02	2.09E-04	5.45E-02	1.57E-04	4.65E-02	1.31E-04	4.50E-02	1.40E-04	5.63E-02	3.01E-04
CflD	2.36E+07	1.49E+06	5.42E+07	8.18E+06	5.33E+06	5.69E+04	7.34E+06	7.95E+04	3.74E+06	3.02E+04
CiD	1.42E+06	1.18E+04	1.68E+06	3.61E+04	1.09E+06	8.10E+03	1.44E+06	1.02E+04	1.06E+06	7.53E+03
CwD	1.25E+07	2.44E+05	8.18E+06	1.62E+05	4.74E+06	7.10E+04	3.68E+06	4.22E+04	1.83E+06	2.80E+04
CwiD	1.26E+07	1.38E+05	2.37E+07	5.13E+05	1.92E+07	1.88E+05	3.08E+07	3.20E+05	1.04E+07	8.78E+04
hwD	9.26E+01	3.77E-01	7.51E+01	3.15E-01	6.06E+01	2.47E-01	6.28E+01	2.53E-01	3.79E+01	1.89E-01
hflD	1.26E+02	6.54E-01	1.07E+02	4.60E-01	9.58E+01	3.30E-01	1.18E+02	4.08E-01	8.76E+01	3.28E-01
hwiD	3.56E+02	1.73E+00	3.45E+02	1.48E+00	3.23E+02	1.10E+00	4.40E+02	1.43E+00	2.49E+02	9.68E-01
infD	1.45E+02	5.17E-01	1.48E+02	1.63E+00	9.93E+01	2.11E-01	9.45E+01	1.87E-01	6.93E+01	1.37E-01
UflD	2.63E+02	1.02E+01	3.54E+02	2.41E+01	6.15E+01	5.90E-01	5.84E+01	5.35E-01	3.17E+01	2.78E-01
Uwd	2.56E+02	1.66E+04	1.57E+02	1.24E+04	5.13E+01	6.13E+03	2.87E+01	4.37E+03	1.22E+01	1.08E+03
abs1EN	3.32E-08	7.93E-06	2.49E-12	1.19E-10	4.75E-09	1.62E-07	2.15E-10	1.76E-07	1.28E-01	9.50E-03
abs1NN	4.32E-01	1.03E-01	1.60E-11	6.82E-10	1.60E-08	5.46E-07	2.30E-09	1.82E-06	5.15E-01	1.99E-02
abs1SN	4.14E-01	2.79E-02	2.51E-01	5.03E-02	1.44E-01	1.46E-02	1.63E-01	1.37E-02	2.91E-01	4.82E-03
abs1WN	5.70E-01	2.19E-02	9.17E-01	1.01E-01	3.85E-01	1.25E-02	4.41E-01	1.12E-02	1.55E-01	3.80E-03
abs2EN	1.88E+00	8.00E-02	4.16E-01	2.70E-02	1.24E+00	4.80E-02	1.23E+00	4.24E-02	9.15E-01	2.97E-02
abs2NN	1.67E+00	1.62E-01	5.70E-01	6.49E-02	7.94E-01	7.48E-02	8.67E-01	6.50E-02	5.37E-01	5.67E-02
abs2SN	1.72E+00	4.01E-02	3.20E-01	1.41E-02	1.08E+00	2.75E-02	1.09E+00	2.31E-02	9.54E-01	1.60E-02
abs2WN	8.65E-01	3.93E-02	3.64E-02	6.15E-03	8.40E-01	2.04E-02	1.06E+00	1.75E-02	7.98E-01	1.31E-02
abs3EN	1.08E-08	3.10E-06	7.16E-06	5.18E-05	5.81E-02	6.82E-02	9.98E-02	5.82E-02	2.36E-02	5.48E-02
abs3NN	3.46E-13	1.76E-10	5.76E-10	1.95E-08	6.66E-10	2.76E-08	3.53E-07	9.88E-05	5.98E-07	4.00E-06
abs3SN	3.35E-07	8.17E-05	1.21E-05	1.89E-04	7.28E-02	3.63E-02	2.32E-02	3.25E-02	1.18E-01	2.42E-02
abs3WN	2.82E-01	5.91E-02	2.37E-16	1.70E-14	2.39E-01	3.20E-02	2.55E-01	2.78E-02	9.93E-02	2.44E-02
abs5EN	1.53E-01	2.39E-02	8.54E-01	5.61E-02	1.77E-01	8.53E-03	2.38E-01	9.31E-03	1.00E-01	4.68E-03
abs5NN	1.76E-08	3.92E-06	1.94E+00	1.40E-01	2.84E-01	1.87E-02	3.45E-01	2.03E-02	1.90E-01	1.03E-02
abs5SN	1.14E-01	1.55E-02	6.58E-01	2.95E-02	1.68E-01	4.68E-03	2.16E-01	5.09E-03	1.20E-01	2.46E-03
abs5WN	1.12E-01	1.14E-02	2.44E-12	1.18E-10	1.31E-01	3.59E-03	2.13E-01	4.07E-03	8.95E-02	1.85E-03
f1N	6.81E-02	5.49E-04	9.43E-02	4.23E-03	6.42E-02	5.54E-04	5.99E-02	5.20E-04	5.21E-02	2.19E-04
f2N	1.93E-01	1.16E-03	7.45E-03	2.54E-04	2.07E-01	8.95E-04	2.03E-01	8.61E-04	2.24E-01	8.06E-04
f3N	6.92E-01	2.37E-03	6.95E-01	4.58E-03	6.94E-01	1.79E-03	6.96E-01	2.15E-03	6.91E-01	2.97E-03
f5N	2.99E-02	2.85E-04	5.01E-11	1.41E-09	2.76E-02	1.42E-04	3.70E-02	1.83E-04	2.62E-02	9.99E-05
CiN	2.62E+06	1.89E+04	7.08E+05	1.02E+04	1.82E+06	1.16E+04	1.90E+06	1.60E+04	2.78E+06	3.43E+04
CwN	2.88E+07	8.10E+05	3.16E+07	5.16E+06	5.64E+06	1.50E+05	3.05E+06	7.46E+04	4.70E+06	7.34E+04
CwiN	2.32E+07	5.34E+05	6.44E+06	1.27E+05	3.57E+07	1.12E+06	4.10E+07	1.61E+06	5.67E+07	3.08E+06
hwN	3.29E+02	2.23E+00	4.63E+02	7.79E+00	1.94E+02	1.44E+00	1.82E+02	1.73E+00	1.55E+02	1.01E+00
hwiN	8.32E+02	5.91E+00	1.85E+02	2.06E+00	5.53E+02	2.51E+00	5.21E+02	2.87E+00	5.78E+02	3.76E+00
infN	1.14E+02	8.67E-01	1.54E-16	8.36E-15	7.16E+01	2.89E-01	6.24E+01	2.53E-01	5.67E+01	2.65E-01
UwN	1.35E+03	5.03E+04	7.87E+02	2.49E+04	2.16E+02	2.40E+04	1.30E+02	1.94E+04	6.45E+01	1.63E+04
CfiD	9.95E+08	2.65E+07	4.36E+07	1.45E+07	9.93E+08	4.05E+07	9.94E+08	3.57E+07	9.96E+08	2.01E+07
CfiN	2.53E+08	1.23E+08	9.95E+08	2.04E+07	9.94E+08	3.30E+07	9.95E+08	2.71E+07	9.91E+08	6.06E+07
UfDN	4.63E+01	4.92E-01	4.00E+01	4.51E-01	3.91E+01	2.26E-01	4.95E+01	3.62E-01	7.49E+01	5.38E-01
Ufi	6.99E+02	3.61E+02	9.23E+02	2.79E+02	1.04E-03	1.58E-01	8.58E-04	9.35E-02	9.48E-04	2.37E-02
UfND	9.82E+01	1.16E+00	9.61E+01	7.31E-01	6.89E+01	4.23E-01	7.85E+01	5.37E-01	5.71E+01	3.67E-01

Table B.4: Grey-box model parameters for mildly renovated detached buildings (Ref. 1)

Parameters	D1		D2		D3		D4	
	Est.	(Std.)	Est.	(Std.)	Est.	(Std.)	Est.	(Std.)
abs1ED	8.82E-01	(1.49E-01)	1.11E+00	(9.82E-02)	1.22E+00	(7.20E-02)	1.38E+00	(5.36E-02)
abs1ND	6.06E+00	(3.22E-01)	3.19E+00	(2.33E-01)	1.31E+00	(1.58E-01)	1.28E+00	(1.38E-01)
abs1SD	2.32E+00	(6.46E-02)	1.91E+00	(4.47E-02)	1.47E+00	(2.77E-02)	1.54E+00	(2.47E-02)
abs1WD	8.59E-01	(6.03E-02)	1.03E+00	(5.21E-02)	9.50E-01	(3.30E-02)	1.08E+00	(2.88E-02)
abs2ED	2.46E+00	(2.43E-01)	2.10E+00	(1.64E-01)	2.06E+00	(1.03E-01)	2.57E+00	(7.93E-02)
abs2ND	3.18E+00	(4.51E-01)	3.51E+00	(3.09E-01)	3.24E+00	(2.79E-01)	2.99E+00	(1.99E-01)
abs2SD	2.75E+00	(1.15E-01)	2.63E+00	(7.49E-02)	2.43E+00	(5.15E-02)	2.76E+00	(3.68E-02)
abs2WD	2.95E+00	(9.55E-02)	2.63E+00	(8.48E-02)	2.42E+00	(5.83E-02)	2.61E+00	(4.33E-02)
abs3ED	9.45E-01	(3.87E-01)	1.23E+00	(2.81E-01)	7.49E-01	(2.50E-01)	6.78E-01	(2.21E-01)
abs3ND	6.89E-14	(1.22E-10)	5.29E-11	(1.63E-09)	1.11E+00	(5.03E-01)	2.18E+00	(4.13E-01)
abs3SD	4.46E-01	(1.51E-01)	9.11E-01	(1.10E-01)	7.94E-01	(8.58E-02)	7.90E-01	(7.11E-02)
abs3WD	1.36E-10	(1.39E-07)	3.32E-01	(1.32E-01)	7.48E-01	(1.15E-01)	8.87E-01	(9.39E-02)
abs4ED	8.33E-01	(6.05E-02)	8.44E-01	(6.90E-02)	1.22E+00	(4.54E-02)	1.26E+00	(3.11E-02)
abs4ND	1.29E-07	(4.22E-05)	7.04E-18	(2.29E-16)	9.35E-01	(1.21E-01)	9.16E-01	(7.76E-02)
abs4SD	7.69E-01	(3.06E-02)	8.24E-01	(3.27E-02)	1.29E+00	(1.97E-02)	1.26E+00	(1.38E-02)
abs4WS	8.22E-01	(3.18E-02)	1.02E+00	(3.78E-02)	1.20E+00	(2.42E-02)	1.13E+00	(1.53E-02)
abs5ED	4.01E-01	(9.46E-02)	7.61E-01	(6.14E-02)	6.97E-01	(4.25E-02)	1.00E+00	(4.74E-02)
abs5ND	2.06E-14	(7.61E-12)	1.29E+00	(1.56E-01)	9.20E-01	(1.13E-01)	1.12E+00	(1.20E-01)
abs5SD	4.55E-01	(4.55E-02)	9.45E-01	(2.78E-02)	8.12E-01	(1.90E-02)	1.08E+00	(2.08E-02)
abs5WD	6.88E-01	(4.76E-02)	5.40E-01	(3.20E-02)	5.06E-01	(2.17E-02)	6.88E-01	(2.25E-02)
f1D	6.90E-02	(4.70E-04)	6.62E-02	(4.31E-04)	6.57E-02	(4.10E-04)	6.67E-02	(4.25E-04)
f2D	1.35E-01	(8.56E-04)	1.35E-01	(6.86E-04)	1.34E-01	(6.31E-04)	1.38E-01	(6.46E-04)
f3D	7.11E-01	(1.31E-03)	7.14E-01	(1.18E-03)	7.04E-01	(1.53E-03)	7.00E-01	(1.60E-03)
f4D	4.30E-02	(1.97E-04)	5.06E-02	(2.93E-04)	6.69E-02	(2.81E-04)	5.92E-02	(2.49E-04)
f5D	4.21E-02	(3.18E-04)	4.16E-02	(2.34E-04)	3.82E-02	(2.22E-04)	4.65E-02	(2.56E-04)
CfID	9.81E+09	(1.84E+09)	3.36E+07	(2.00E+06)	1.29E+07	(1.54E+05)	1.23E+07	(1.42E+05)
CiD	2.20E+06	(9.39E+03)	2.13E+06	(8.72E+03)	2.42E+06	(1.13E+04)	2.29E+06	(1.22E+04)
CwD	8.01E+07	(1.39E+06)	3.48E+07	(4.48E+05)	2.47E+07	(3.06E+05)	1.74E+07	(1.89E+05)
CwiD	2.43E+07	(1.94E+05)	2.27E+07	(2.10E+05)	2.24E+07	(2.30E+05)	2.42E+07	(2.35E+05)
hwD	5.35E+02	(1.59E+00)	3.98E+02	(1.42E+00)	3.10E+02	(1.21E+00)	3.02E+02	(1.19E+00)
hfID	2.23E+02	(6.49E-01)	1.97E+02	(1.07E+00)	2.20E+02	(8.43E-01)	1.94E+02	(7.03E-01)
hwiD	8.41E+02	(3.13E+00)	5.78E+02	(2.64E+00)	4.90E+02	(2.15E+00)	5.03E+02	(2.05E+00)
infD	9.91E+01	(4.49E-01)	1.03E+02	(3.00E-01)	1.08E+02	(2.51E-01)	1.11E+02	(2.41E-01)
UfID	9.80E-03	(7.72E-01)	3.23E+02	(1.08E+01)	9.98E+01	(1.21E+00)	7.75E+01	(9.34E-01)
Uwd	1.46E+03	(1.16E+05)	6.17E+02	(8.13E+04)	2.66E+02	(4.05E+04)	1.34E+02	(2.20E+04)
abs1EN	1.02E+00	(8.49E-02)	8.68E-01	(7.80E-02)	3.69E-01	(1.10E-01)	8.03E-01	(6.99E-02)
abs1NN	2.70E+00	(1.76E-01)	1.91E+00	(1.50E-01)	9.47E-01	(1.65E-01)	2.20E+00	(1.39E-01)
abs1SN	1.81E+00	(4.03E-02)	1.86E+00	(3.74E-02)	1.53E+00	(3.17E-02)	1.85E+00	(2.63E-02)
abs1WN	7.62E-01	(3.30E-02)	1.15E+00	(3.04E-02)	1.70E+00	(3.66E-02)	1.55E+00	(2.52E-02)
abs2EN	5.33E-01	(3.78E-02)	5.73E-01	(2.50E-02)	6.80E-01	(3.83E-02)	6.56E-01	(2.84E-02)
abs2NN	3.39E-01	(8.32E-02)	1.67E-20	(1.15E-17)	3.10E-01	(8.47E-02)	7.54E-02	(6.67E-02)
abs2SN	5.21E-01	(1.73E-02)	5.03E-01	(1.24E-02)	6.02E-01	(1.63E-02)	5.48E-01	(1.23E-02)
abs2WN	2.84E-01	(1.46E-02)	3.33E-01	(9.97E-03)	2.08E-01	(1.33E-02)	3.76E-01	(1.01E-02)
abs3EN	1.03E-10	(5.41E-08)	7.22E-20	(5.95E-17)	3.04E-02	(1.30E-01)	5.74E-12	(9.68E-10)
abs3NN	6.00E-12	(1.96E-09)	1.95E-07	(4.08E-05)	9.54E-19	(9.55E-16)	6.13E-17	(1.49E-14)
abs3SN	2.05E-01	(6.30E-02)	2.02E-02	(4.74E-02)	5.81E-12	(3.53E-09)	1.02E-11	(1.45E-09)
abs3WN	3.83E-01	(6.97E-02)	4.09E-01	(5.37E-02)	2.96E-01	(4.86E-02)	3.01E-01	(4.37E-02)
abs5EN	4.72E-01	(6.47E-02)	8.56E-01	(4.45E-02)	9.37E-01	(5.16E-02)	1.12E+00	(4.75E-02)
abs5NN	3.73E-10	(1.23E-07)	5.91E-01	(9.72E-02)	1.08E+00	(1.14E-01)	4.46E-01	(1.07E-01)
abs5SN	4.91E-01	(3.42E-02)	7.56E-01	(1.97E-02)	8.45E-01	(2.23E-02)	8.67E-01	(1.99E-02)
abs5WN	5.98E-01	(2.84E-02)	4.17E-01	(1.58E-02)	2.15E-01	(1.80E-02)	5.37E-01	(1.82E-02)
f1N	1.45E-01	(5.49E-04)	1.66E-01	(7.12E-04)	1.88E-01	(1.27E-03)	1.63E-01	(7.73E-04)
f2N	4.95E-02	(2.29E-04)	4.55E-02	(2.06E-04)	4.19E-02	(3.66E-04)	4.45E-02	(2.78E-04)
f3N	6.97E-01	(2.61E-03)	6.92E-01	(2.90E-03)	6.82E-01	(2.41E-03)	6.98E-01	(2.91E-03)
f5N	9.47E-02	(5.30E-04)	7.79E-02	(3.48E-04)	6.74E-02	(5.05E-04)	8.31E-02	(5.03E-04)
CiN	2.51E+06	(1.57E+04)	1.86E+06	(1.20E+04)	1.53E+06	(7.10E+03)	2.06E+06	(1.37E+04)
CwN	1.18E+07	(3.24E+05)	4.40E+06	(8.66E+04)	3.50E+06	(6.41E+04)	2.90E+06	(4.29E+04)
CwiN	2.53E+06	(4.39E+04)	4.30E+06	(1.07E+05)	5.73E+06	(2.66E+05)	5.50E+06	(2.39E+05)
hwN	2.51E+02	(2.11E+00)	2.33E+02	(2.13E+00)	2.78E+02	(2.59E+00)	2.27E+02	(2.20E+00)
hwiN	1.16E+02	(9.36E-01)	9.61E+01	(6.24E-01)	9.27E+01	(7.30E-01)	8.46E+01	(8.93E-01)
infN	4.52E+01	(3.95E-01)	3.91E+01	(3.19E-01)	3.43E+01	(2.37E-01)	4.29E+01	(2.37E-01)
UwN	1.76E+02	(2.10E+04)	1.25E+02	(2.32E+04)	1.29E+02	(2.81E+04)	8.40E+01	(2.11E+04)
CfiD	3.39E+06	(1.16E+05)	1.77E+08	(1.83E+07)	9.96E+08	(1.59E+07)	9.97E+08	(9.96E+06)
CfiN	6.89E+06	(2.57E+05)	9.99E+08	(2.56E+06)	9.95E+08	(2.10E+07)	9.92E+08	(4.33E+07)
UfDN	1.73E+02	(1.11E+00)	1.49E+02	(7.15E-01)	1.19E+02	(6.98E-01)	1.48E+02	(9.33E-01)
Ufi	2.95E+02	(6.18E+00)	7.31E+03	(6.77E+02)	6.50E+02	(4.33E+02)	2.02E-03	(4.14E-01)
UfND	1.71E+02	(1.66E+00)	1.10E+02	(1.20E+00)	9.25E+01	(1.08E+00)	8.70E+01	(2.23E+00)

Table B.5: Grey-box model parameters for mildly renovated semi-detached buildings (Ref. 1)

Parameters	SD1		SD2		SD3		SD4	
	Est.	(Std.)	Est.	(Std.)	Est.	(Std.)	Est.	(Std.)
abs1ED	4.69E-02	(2.38E-02)	1.08E-01	(1.77E-02)	1.89E-01	(1.25E-02)	1.59E-01	(7.41E-03)
abs1ND	9.43E-01	(5.24E-02)	6.36E-01	(4.01E-02)	3.17E-01	(3.72E-02)	2.96E-01	(1.98E-02)
abs1SD	2.83E-01	(1.23E-02)	2.87E-01	(8.96E-03)	2.77E-01	(8.56E-03)	2.33E-01	(4.13E-03)
abs1WD	2.15E-01	(1.06E-02)	1.81E-01	(9.61E-03)	1.44E-01	(6.67E-03)	2.05E-01	(4.46E-03)
abs2ED	3.05E-01	(5.46E-02)	3.09E-01	(3.12E-02)	3.72E-01	(2.49E-02)	3.09E-01	(1.13E-02)
abs2ND	9.73E-01	(8.53E-02)	6.21E-01	(6.80E-02)	3.80E-01	(5.67E-02)	4.20E-01	(3.05E-02)
abs2SD	4.38E-01	(2.94E-02)	3.90E-01	(1.67E-02)	4.08E-01	(1.25E-02)	3.53E-01	(6.06E-03)
abs2WD	4.67E-01	(2.29E-02)	3.90E-01	(1.89E-02)	3.46E-01	(1.25E-02)	3.96E-01	(6.90E-03)
abs3ED	4.31E-01	(8.25E-02)	3.59E-01	(7.08E-02)	2.63E-01	(7.06E-02)	2.40E-01	(6.06E-02)
abs3ND	1.74E-15	(2.16E-12)	7.19E-06	(6.29E-05)	3.55E-01	(1.39E-01)	1.65E-01	(1.10E-01)
abs3SD	6.13E-02	(3.94E-02)	1.37E-01	(3.24E-02)	1.01E-01	(2.76E-02)	8.62E-02	(2.22E-02)
abs3WD	7.47E-14	(6.38E-11)	1.49E-01	(3.80E-02)	2.72E-01	(3.58E-02)	3.88E-01	(2.98E-02)
abs4ED	2.89E-01	(2.00E-02)	2.75E-01	(1.97E-02)	3.04E-01	(1.28E-02)	3.35E-01	(9.40E-03)
abs4ND	1.23E-14	(1.23E-11)	1.99E-07	(1.64E-06)	3.50E-01	(3.27E-02)	4.48E-01	(2.45E-02)
abs4SD	2.14E-01	(1.21E-02)	2.29E-01	(1.11E-02)	3.43E-01	(7.28E-03)	4.06E-01	(5.16E-03)
abs4WS	2.83E-01	(1.03E-02)	2.68E-01	(1.15E-02)	2.53E-01	(8.27E-03)	4.20E-01	(5.67E-03)
abs5ED	6.67E-02	(1.91E-02)	1.10E-01	(2.49E-02)	1.44E-01	(2.20E-02)	1.59E-01	(1.69E-02)
abs5ND	7.95E-14	(7.14E-11)	5.76E-01	(5.54E-02)	4.84E-01	(5.88E-02)	3.59E-01	(4.38E-02)
abs5SD	6.73E-02	(1.06E-02)	1.92E-01	(1.38E-02)	2.03E-01	(1.32E-02)	1.98E-01	(9.39E-03)
abs5WD	1.01E-01	(9.96E-03)	2.53E-02	(1.29E-02)	5.80E-03	(1.17E-02)	4.61E-02	(9.00E-03)
f1D	5.66E-02	(3.18E-04)	5.72E-02	(3.09E-04)	5.94E-02	(3.11E-04)	5.46E-02	(2.05E-04)
f2D	1.16E-01	(8.31E-04)	1.18E-01	(5.54E-04)	1.20E-01	(5.50E-04)	1.06E-01	(3.43E-04)
f3D	7.17E-01	(1.28E-03)	7.17E-01	(1.36E-03)	7.07E-01	(1.62E-03)	7.08E-01	(1.56E-03)
f4D	8.07E-02	(2.89E-04)	8.16E-02	(3.29E-04)	8.60E-02	(3.14E-04)	1.04E-01	(2.56E-04)
f5D	3.35E-02	(2.97E-04)	3.48E-02	(3.83E-04)	3.75E-02	(4.29E-04)	3.98E-02	(3.88E-04)
CfID	6.68E+07	(7.19E+06)	1.09E+07	(3.22E+05)	6.76E+06	(6.88E+04)	7.37E+06	(6.34E+04)
CiD	1.72E+06	(6.79E+03)	1.50E+06	(6.82E+03)	1.60E+06	(7.91E+03)	1.73E+06	(9.24E+03)
CwD	2.60E+07	(4.69E+05)	1.20E+07	(1.54E+05)	1.04E+07	(1.35E+05)	6.04E+06	(5.68E+04)
CwiD	1.20E+07	(1.28E+05)	9.60E+06	(1.00E+05)	9.93E+06	(8.84E+04)	8.11E+06	(5.49E+04)
hwD	1.87E+02	(7.11E-01)	1.58E+02	(6.03E-01)	1.44E+02	(5.82E-01)	1.06E+02	(3.64E-01)
hfID	1.57E+02	(6.93E-01)	1.44E+02	(7.21E-01)	1.45E+02	(5.75E-01)	1.45E+02	(4.81E-01)
hwiD	3.73E+02	(2.14E+00)	2.72E+02	(1.42E+00)	2.53E+02	(1.10E+00)	1.97E+02	(6.14E-01)
infD	7.50E+01	(2.54E-01)	7.48E+01	(2.13E-01)	7.94E+01	(1.97E-01)	7.49E+01	(1.85E-01)
UfID	2.81E+02	(2.11E+01)	2.84E+02	(3.95E+00)	7.43E+01	(7.40E-01)	6.01E+01	(5.42E-01)
Uwd	5.52E+02	(3.97E+04)	2.31E+02	(2.95E+04)	1.22E+02	(1.60E+04)	4.83E+01	(8.20E+03)
abs1EN	1.43E-01	(2.71E-02)	1.69E-01	(2.60E-02)	1.66E-01	(2.83E-02)	1.77E-01	(2.09E-02)
abs1NN	1.29E+00	(5.72E-02)	8.58E-01	(5.03E-02)	4.14E-01	(5.62E-02)	7.01E-01	(4.06E-02)
abs1SN	5.47E-01	(1.43E-02)	5.62E-01	(1.47E-02)	4.94E-01	(1.54E-02)	5.44E-01	(1.18E-02)
abs1WN	2.72E-01	(1.18E-02)	2.89E-01	(1.19E-02)	4.36E-01	(1.15E-02)	5.20E-01	(8.88E-03)
abs2EN	6.21E-01	(3.19E-02)	5.88E-01	(2.41E-02)	5.35E-01	(2.43E-02)	5.30E-01	(2.33E-02)
abs2NN	5.32E-23	(2.73E-20)	3.84E-08	(1.35E-06)	2.52E-01	(5.13E-02)	7.82E-02	(4.42E-02)
abs2SN	5.05E-01	(1.74E-02)	5.35E-01	(1.57E-02)	5.57E-01	(1.31E-02)	5.59E-01	(1.31E-02)
abs2WN	4.28E-01	(1.70E-02)	4.17E-01	(1.15E-02)	2.81E-01	(9.57E-03)	5.33E-01	(9.97E-03)
abs3EN	4.79E-10	(4.25E-08)	3.41E-05	(2.71E-03)	1.10E-01	(4.60E-02)	7.32E-02	(4.04E-02)
abs3NN	3.76E-10	(3.29E-08)	1.21E-06	(8.77E-05)	3.60E-16	(1.64E-13)	1.09E-24	(1.03E-21)
abs3SN	2.24E-09	(1.98E-07)	2.24E-02	(2.19E-02)	1.06E-01	(2.32E-02)	6.78E-02	(2.16E-02)
abs3WN	1.66E-01	(2.62E-02)	2.27E-01	(2.38E-02)	1.98E-01	(1.96E-02)	2.38E-01	(1.88E-02)
abs5EN	1.02E-01	(1.81E-02)	1.59E-01	(1.11E-02)	2.37E-01	(1.17E-02)	1.95E-01	(1.06E-02)
abs5NN	2.93E-08	(2.49E-06)	1.99E-01	(2.43E-02)	3.01E-01	(2.41E-02)	1.71E-01	(2.13E-02)
abs5SN	1.06E-01	(1.03E-02)	1.59E-01	(6.27E-03)	2.45E-01	(6.71E-03)	1.93E-01	(5.75E-03)
abs5WN	1.06E-01	(8.57E-03)	9.71E-02	(4.46E-03)	1.10E-01	(4.55E-03)	1.80E-01	(4.34E-03)
f1N	1.03E-01	(4.47E-04)	1.13E-01	(7.27E-04)	1.30E-01	(8.59E-04)	1.19E-01	(6.97E-04)
f2N	1.46E-01	(7.83E-04)	1.35E-01	(8.49E-04)	1.07E-01	(7.48E-04)	1.25E-01	(7.76E-04)
f3N	6.91E-01	(1.69E-03)	6.92E-01	(1.84E-03)	6.92E-01	(1.84E-03)	6.95E-01	(1.93E-03)
f5N	4.31E-02	(2.99E-04)	4.68E-02	(2.54E-04)	5.91E-02	(3.49E-04)	5.36E-02	(2.85E-04)
CiN	2.25E+06	(1.06E+04)	1.76E+06	(9.30E+03)	1.51E+06	(7.90E+03)	2.07E+06	(1.14E+04)
CwN	3.47E+07	(6.93E+05)	1.63E+07	(3.82E+05)	7.59E+06	(1.59E+05)	5.75E+06	(9.63E+04)
CwiN	1.45E+07	(1.84E+05)	1.82E+07	(4.04E+05)	1.31E+07	(3.85E+05)	2.26E+07	(1.07E+06)
hwN	3.92E+02	(1.71E+00)	2.82E+02	(1.87E+00)	2.57E+02	(1.84E+00)	2.49E+02	(1.83E+00)
hwiN	5.46E+02	(2.52E+00)	3.71E+02	(2.08E+00)	2.63E+02	(1.74E+00)	2.72E+02	(2.58E+00)
infN	4.03E+01	(4.06E-01)	3.79E+01	(2.64E-01)	3.80E+01	(2.09E-01)	4.36E+01	(1.82E-01)
UwN	5.13E+02	(6.62E+04)	2.89E+02	(3.17E+04)	1.77E+02	(2.92E+04)	1.10E+02	(2.40E+04)
CfiD	2.53E+07	(3.06E+06)	9.97E+08	(1.65E+07)	9.97E+08	(1.17E+07)	9.97E+08	(1.20E+07)
CfiN	9.90E+08	(6.66E+07)	9.88E+08	(1.65E+08)	9.92E+08	(4.48E+07)	9.92E+08	(4.57E+07)
UfDN	1.10E+02	(7.27E-01)	1.59E+02	(9.03E-01)	1.60E+02	(9.29E-01)	1.59E+02	(8.57E-01)
Ufi	2.40E-04	(6.09E-03)	1.76E-03	(1.12E-01)	1.18E-03	(6.06E-02)	4.45E-03	(9.97E-02)
UfND	8.82E+01	(1.08E+00)	6.63E+01	(6.25E-01)	6.75E+01	(8.32E-01)	6.02E+01	(1.03E+00)

Table B.6: Grey-box model parameters for mildly renovated terraced buildings (Ref. 1)

Parameters	T1		T2		T3		T4	
	Est.	(Std.)	Est.	(Std.)	Est.	(Std.)	Est.	(Std.)
abs1ED	3.86E-02	(1.07E-02)	6.17E-02	(8.61E-03)	7.80E-02	(5.02E-03)	6.73E-02	(3.52E-03)
abs1ND	5.38E-01	(2.56E-02)	2.63E-01	(1.91E-02)	9.88E-02	(1.28E-02)	8.60E-02	(8.88E-03)
abs1SD	1.91E-01	(5.75E-03)	1.36E-01	(4.09E-03)	8.53E-02	(2.62E-03)	7.22E-02	(2.06E-03)
abs1WD	6.63E-02	(5.23E-03)	5.87E-02	(4.06E-03)	4.70E-02	(2.70E-03)	5.49E-02	(2.04E-03)
abs2ED	3.96E-01	(3.90E-02)	4.49E-01	(3.66E-02)	4.69E-01	(1.85E-02)	5.43E-01	(1.70E-02)
abs2ND	1.35E+00	(6.36E-02)	9.78E-01	(8.70E-02)	4.02E-01	(4.56E-02)	4.09E-01	(4.18E-02)
abs2SD	5.54E-01	(2.28E-02)	5.41E-01	(1.92E-02)	4.10E-01	(9.99E-03)	4.51E-01	(9.28E-03)
abs2WD	5.01E-01	(2.20E-02)	5.62E-01	(1.94E-02)	4.75E-01	(1.07E-02)	6.11E-01	(9.62E-03)
abs3ED	3.44E-01	(5.60E-02)	3.07E-01	(5.80E-02)	1.48E-01	(4.73E-02)	1.40E-01	(4.22E-02)
abs3ND	1.67E-09	(1.48E-06)	4.96E-02	(1.18E-01)	5.82E-01	(8.41E-02)	5.38E-01	(7.64E-02)
abs3SD	8.44E-02	(2.97E-02)	1.19E-01	(2.50E-02)	5.37E-02	(1.85E-02)	4.51E-02	(1.68E-02)
abs3WD	6.81E-02	(3.19E-02)	1.32E-01	(2.92E-02)	1.62E-01	(2.27E-02)	1.88E-01	(2.06E-02)
abs4ED	2.38E-01	(1.19E-02)	1.91E-01	(1.21E-02)	1.58E-01	(5.59E-03)	1.64E-01	(4.58E-03)
abs4ND	1.13E-02	(2.92E-02)	4.87E-08	(4.17E-07)	1.78E-01	(1.40E-02)	1.60E-01	(1.13E-02)
abs4SD	2.06E-01	(6.69E-03)	1.43E-01	(7.01E-03)	1.41E-01	(3.02E-03)	1.40E-01	(2.48E-03)
abs4WS	1.94E-01	(6.14E-03)	1.94E-01	(6.39E-03)	1.46E-01	(2.99E-03)	1.72E-01	(2.59E-03)
abs5ED	1.60E-01	(1.32E-02)	1.62E-01	(1.11E-02)	1.41E-01	(8.01E-03)	1.49E-01	(7.10E-03)
abs5ND	6.12E-09	(3.99E-06)	3.11E-01	(2.62E-02)	2.35E-01	(2.00E-02)	2.04E-01	(1.74E-02)
abs5SD	1.30E-01	(8.01E-03)	1.93E-01	(6.15E-03)	1.43E-01	(4.37E-03)	1.42E-01	(3.93E-03)
abs5WD	1.80E-01	(7.76E-03)	1.36E-01	(6.10E-03)	1.07E-01	(4.17E-03)	1.31E-01	(3.92E-03)
f1D	2.84E-02	(2.19E-04)	2.39E-02	(1.90E-04)	2.52E-02	(1.82E-04)	2.18E-02	(1.35E-04)
f2D	1.48E-01	(9.28E-04)	1.66E-01	(8.86E-04)	1.76E-01	(8.02E-04)	1.91E-01	(7.74E-04)
f3D	7.26E-01	(1.35E-03)	7.19E-01	(1.45E-03)	7.11E-01	(1.72E-03)	6.96E-01	(1.61E-03)
f4D	5.87E-02	(2.62E-04)	5.46E-02	(3.38E-04)	5.37E-02	(2.46E-04)	5.29E-02	(2.16E-04)
f5D	5.49E-02	(3.31E-04)	5.18E-02	(2.58E-04)	5.06E-02	(2.51E-04)	4.93E-02	(2.38E-04)
CflD	5.92E+07	(6.99E+06)	1.42E+07	(7.20E+05)	4.61E+06	(4.84E+04)	6.24E+06	(6.10E+04)
CiD	1.30E+06	(5.82E+03)	1.29E+06	(6.70E+03)	1.06E+06	(6.68E+03)	1.40E+06	(8.73E+03)
CwD	1.48E+07	(3.18E+05)	6.92E+06	(1.02E+05)	4.46E+06	(6.36E+04)	3.37E+06	(3.87E+04)
CwiD	1.40E+07	(1.79E+05)	1.91E+07	(2.78E+05)	1.71E+07	(1.92E+05)	2.66E+07	(2.91E+05)
hwD	9.16E+01	(4.15E-01)	7.71E+01	(3.44E-01)	5.91E+01	(2.78E-01)	6.08E+01	(2.76E-01)
hflD	1.22E+02	(5.84E-01)	1.17E+02	(6.34E-01)	9.14E+01	(3.48E-01)	1.12E+02	(3.79E-01)
hwiD	3.38E+02	(2.27E+00)	3.75E+02	(2.07E+00)	3.07E+02	(1.23E+00)	4.15E+02	(1.42E+00)
infD	6.89E+01	(1.81E-01)	6.86E+01	(1.68E-01)	6.68E+01	(1.45E-01)	6.23E+01	(1.21E-01)
UflD	4.66E+02	(2.72E+01)	4.95E+02	(1.09E+01)	6.80E+01	(4.63E-01)	6.40E+01	(3.65E-01)
Uwd	3.13E+02	(1.72E+04)	1.36E+02	(1.47E+04)	5.35E+01	(6.99E+03)	2.95E+01	(5.43E+03)
abs1EN	8.35E-02	(2.31E-02)	5.99E-02	(2.01E-02)	1.39E-09	(3.55E-08)	4.07E-02	(1.17E-02)
abs1NN	1.11E+00	(4.07E-02)	6.62E-01	(3.93E-02)	1.13E-01	(3.61E-02)	3.77E-01	(2.50E-02)
abs1SN	4.64E-01	(1.15E-02)	3.58E-01	(1.06E-02)	1.48E-01	(9.98E-03)	2.04E-01	(6.25E-03)
abs1WN	1.10E-01	(8.97E-03)	1.46E-01	(8.21E-03)	2.05E-01	(7.60E-03)	2.00E-01	(4.92E-03)
abs2EN	8.98E-01	(3.50E-02)	8.44E-01	(4.31E-02)	7.54E-01	(3.81E-02)	7.49E-01	(2.62E-02)
abs2NN	2.60E-06	(4.35E-05)	2.02E-10	(6.92E-09)	3.37E-01	(5.27E-02)	1.82E-01	(4.50E-02)
abs2SN	7.41E-01	(1.54E-02)	7.01E-01	(2.41E-02)	6.21E-01	(2.10E-02)	5.85E-01	(1.50E-02)
abs2WN	5.68E-01	(2.12E-02)	6.58E-01	(1.89E-02)	5.31E-01	(1.63E-02)	7.30E-01	(1.09E-02)
abs3EN	9.02E-06	(2.62E-04)	6.06E-02	(5.61E-02)	9.71E-02	(4.76E-02)	9.04E-02	(4.10E-02)
abs3NN	2.49E-06	(1.36E-04)	2.15E-06	(1.23E-04)	3.28E-11	(1.14E-09)	1.97E-08	(5.52E-08)
abs3SN	2.17E-08	(2.12E-06)	4.42E-02	(2.82E-02)	5.50E-02	(2.58E-02)	4.27E-02	(2.10E-02)
abs3WN	2.15E-01	(2.62E-02)	2.17E-01	(2.53E-02)	1.62E-01	(2.19E-02)	1.48E-01	(1.77E-02)
abs5EN	6.00E-02	(9.51E-03)	8.93E-02	(6.32E-03)	7.29E-02	(4.50E-03)	1.00E-01	(4.80E-03)
abs5NN	3.37E-09	(1.50E-07)	1.36E-01	(1.40E-02)	1.25E-01	(1.09E-02)	8.61E-02	(1.01E-02)
abs5SN	3.67E-02	(5.92E-03)	8.43E-02	(3.48E-03)	6.47E-02	(2.69E-03)	7.71E-02	(2.69E-03)
abs5WN	8.49E-02	(4.68E-03)	6.63E-02	(2.61E-03)	5.20E-02	(2.07E-03)	9.43E-02	(1.93E-03)
f1N	6.58E-02	(4.44E-04)	6.61E-02	(5.06E-04)	6.53E-02	(5.62E-04)	6.00E-02	(4.48E-04)
f2N	2.08E-01	(1.33E-03)	2.09E-01	(1.19E-03)	2.15E-01	(1.27E-03)	2.08E-01	(1.10E-03)
f3N	6.89E-01	(1.71E-03)	6.88E-01	(1.76E-03)	6.83E-01	(1.97E-03)	6.85E-01	(2.68E-03)
f5N	2.73E-02	(2.33E-04)	2.89E-02	(1.42E-04)	2.68E-02	(1.43E-04)	3.54E-02	(1.57E-04)
CiN	2.50E+06	(9.27E+03)	2.11E+06	(1.14E+04)	1.81E+06	(1.00E+04)	1.99E+06	(2.30E+04)
CwN	2.78E+07	(5.63E+05)	1.24E+07	(2.74E+05)	6.48E+06	(1.52E+05)	3.65E+06	(5.82E+04)
CwiN	2.49E+07	(4.54E+05)	4.19E+07	(1.32E+06)	3.87E+07	(1.60E+06)	5.48E+07	(3.98E+06)
hwN	2.72E+02	(1.53E+00)	1.98E+02	(1.45E+00)	1.80E+02	(1.25E+00)	1.60E+02	(1.41E+00)
hwiN	7.50E+02	(4.80E+00)	6.03E+02	(3.68E+00)	5.21E+02	(3.19E+00)	4.90E+02	(3.61E+00)
infN	3.96E+01	(2.27E-01)	3.69E+01	(1.84E-01)	3.61E+01	(1.77E-01)	3.16E+01	(1.69E-01)
UwN	4.61E+02	(3.97E+04)	2.51E+02	(2.38E+04)	1.50E+02	(2.02E+04)	7.30E+01	(1.54E+04)
CfiD	9.98E+08	(6.66E+06)	9.96E+08	(1.44E+07)	9.96E+08	(2.18E+07)	9.96E+08	(1.73E+07)
CfiN	4.44E+07	(6.18E+06)	9.89E+08	(7.36E+07)	9.89E+08	(8.23E+07)	9.89E+08	(8.14E+07)
UfDN	7.10E+01	(5.49E-01)	-1.61E+01	(6.76E+02)	7.67E+01	(5.00E-01)	9.76E+01	(6.48E-01)
Ufi	2.53E+03	(3.55E+02)	-1.74E+01	(6.65E+02)	1.24E-03	(6.23E-02)	1.21E-03	(3.11E-01)
UfND	6.41E+01	(5.66E-01)	5.11E-02	(1.61E-04)	3.26E+01	(3.30E-01)	3.96E+01	(4.02E-01)

Table B.7: Grey-box model parameters for thoroughly renovated detached buildings (Ref. 2)

Parameters	D1		D2		D3		D4	
	Est.	(Std.)	Est.	(Std.)	Est.	(Std.)	Est.	(Std.)
	Ref. 2		Ref. 2		Ref. 2		Ref. 2	
abs1ED	6.75E-01	(4.37E-02)	9.61E-01	(3.63E-02)	9.45E-01	(2.91E-02)	1.10E+00	(2.71E-02)
abs1ND	8.35E-12	(2.01E-10)	1.90E+00	(1.24E-01)	7.98E-01	(9.80E-02)	8.11E-01	(1.09E-01)
abs1SD	9.80E-01	(2.44E-02)	1.15E+00	(2.06E-02)	1.04E+00	(1.66E-02)	1.17E+00	(1.52E-02)
abs1WD	7.67E-01	(4.11E-02)	7.90E-01	(3.48E-02)	8.27E-01	(2.92E-02)	9.90E-01	(2.82E-02)
abs2ED	1.89E-01	(5.10E-02)	1.95E+00	(4.27E-02)	1.83E+00	(2.88E-02)	2.17E+00	(2.89E-02)
abs2ND	1.33E-14	(4.69E-13)	1.81E+00	(1.36E-01)	1.22E+00	(8.38E-02)	1.49E+00	(8.77E-02)
abs2SD	3.70E-01	(2.94E-02)	2.26E+00	(2.55E-02)	2.10E+00	(1.74E-02)	2.33E+00	(1.69E-02)
abs2WD	1.24E-01	(5.20E-02)	1.91E+00	(4.29E-02)	1.77E+00	(3.08E-02)	2.01E+00	(3.21E-02)
abs3ED	1.29E-06	(9.88E-06)	2.60E-01	(2.72E-01)	5.37E-01	(2.38E-01)	8.58E-01	(1.74E-01)
abs3ND	3.15E-07	(3.11E-06)	2.42E-08	(1.41E-05)	1.12E-07	(6.95E-06)	8.88E-07	(6.41E-06)
abs3SD	3.93E-07	(1.73E-06)	5.09E-01	(1.19E-01)	3.41E-01	(1.33E-01)	3.26E-01	(1.05E-01)
abs3WD	5.55E-07	(3.89E-06)	2.12E-07	(1.01E-04)	5.91E-02	(2.27E-01)	2.86E-01	(1.94E-01)
abs4ED	1.89E-10	(2.52E-09)	7.99E-01	(1.65E-02)	9.88E-01	(1.56E-02)	1.00E+00	(1.38E-02)
abs4ND	2.51E-01	(4.99E-02)	7.39E-08	(6.66E-06)	3.12E-07	(1.27E-05)	1.07E-01	(4.25E-02)
abs4SD	1.32E-15	(4.30E-14)	9.49E-01	(9.77E-03)	1.14E+00	(9.37E-03)	1.09E+00	(7.75E-03)
abs4WS	2.40E-10	(3.30E-09)	7.90E-01	(1.58E-02)	9.94E-01	(1.59E-02)	9.58E-01	(1.46E-02)
abs5ED	4.44E-10	(5.52E-09)	6.46E-01	(1.27E-02)	5.60E-01	(1.11E-02)	7.84E-01	(1.40E-02)
abs5ND	1.92E-08	(2.23E-07)	9.05E-09	(3.13E-06)	6.18E-10	(5.93E-08)	1.16E-08	(1.38E-06)
abs5SD	4.48E-11	(4.91E-10)	7.90E-01	(7.62E-03)	6.76E-01	(6.24E-03)	8.88E-01	(7.79E-03)
abs5WD	1.67E-10	(2.19E-09)	6.25E-01	(1.23E-02)	5.50E-01	(1.14E-02)	7.36E-01	(1.46E-02)
f1D	9.29E-02	(1.47E-03)	7.70E-02	(7.19E-04)	6.96E-02	(7.65E-04)	6.81E-02	(8.49E-04)
f2D	1.76E-01	(1.97E-03)	1.47E-01	(9.40E-04)	1.36E-01	(8.93E-04)	1.37E-01	(1.04E-03)
f3D	9.82E-01	(1.30E-02)	7.33E-01	(5.48E-03)	7.72E-01	(5.12E-03)	7.67E-01	(3.90E-03)
f4D	5.90E-02	(5.91E-04)	6.14E-02	(3.24E-04)	7.13E-02	(4.60E-04)	6.22E-02	(4.78E-04)
f5D	2.82E-02	(2.67E-04)	5.01E-02	(2.47E-04)	4.37E-02	(2.84E-04)	5.31E-02	(4.16E-04)
CfID	1.10E+08	(1.45E+07)	9.92E+08	(4.73E+07)	1.48E+07	(2.57E+05)	1.42E+07	(2.26E+05)
CiD	1.02E+07	(2.24E+05)	2.99E+06	(5.63E+04)	3.53E+06	(5.49E+04)	3.42E+06	(4.45E+04)
CwD	5.99E+07	(1.32E+06)	4.41E+07	(1.06E+06)	3.17E+07	(1.08E+06)	2.24E+07	(6.73E+05)
CwiD	2.63E+07	(3.85E+05)	2.63E+07	(3.70E+05)	2.50E+07	(2.50E+05)	2.81E+07	(2.59E+05)
hwD	6.73E+02	(6.88E+00)	3.81E+02	(2.57E+00)	2.79E+02	(2.52E+00)	2.62E+02	(2.85E+00)
hfID	2.71E+02	(2.41E+00)	1.74E+02	(1.14E+00)	2.19E+02	(1.30E+00)	2.04E+02	(1.35E+00)
hwiD	9.11E+02	(9.15E+00)	5.16E+02	(3.29E+00)	4.61E+02	(2.36E+00)	4.97E+02	(2.75E+00)
infD	5.05E+02	(1.14E+01)	2.54E+02	(2.98E+00)	2.72E+02	(2.13E+00)	2.74E+02	(1.32E+00)
UfID	1.48E+02	(1.22E+01)	2.54E+02	(2.50E+02)	7.62E+01	(1.42E+00)	5.89E+01	(1.25E+00)
Uwd	1.09E+03	(6.54E+04)	7.35E+02	(4.61E+04)	3.25E+02	(1.73E+04)	1.54E+02	(9.26E+03)
abs1EN	3.12E-01	(3.77E-02)	2.49E-12	(1.19E-10)	2.02E-01	(7.91E-02)	3.36E-01	(5.76E-02)
abs1NN	5.76E-06	(8.68E-05)	1.60E-11	(6.82E-10)	6.29E-07	(4.52E-05)	1.17E-14	(6.34E-12)
abs1SN	6.48E-01	(2.09E-02)	2.51E-01	(5.03E-02)	7.77E-01	(4.03E-02)	7.92E-01	(3.32E-02)
abs1WN	5.32E-01	(3.35E-02)	9.17E-01	(1.01E-01)	6.54E-01	(6.29E-02)	6.61E-01	(5.67E-02)
abs2EN	2.13E-01	(1.09E-02)	4.16E-01	(2.70E-02)	2.35E-01	(1.24E-02)	2.57E-01	(1.13E-02)
abs2NN	2.33E-01	(3.98E-02)	5.70E-01	(6.49E-02)	3.09E-01	(4.13E-02)	2.71E-01	(3.77E-02)
abs2SN	2.28E-01	(5.79E-03)	3.20E-01	(1.41E-02)	1.76E-01	(7.18E-03)	2.29E-01	(6.61E-03)
abs2WN	1.49E-01	(9.10E-03)	3.64E-02	(6.15E-03)	1.30E-01	(1.12E-02)	1.34E-01	(1.13E-02)
abs3EN	5.10E-01	(9.84E-02)	7.16E-06	(5.18E-05)	2.53E-01	(1.58E-01)	1.11E-01	(1.17E-01)
abs3NN	1.08E-05	(2.35E-04)	5.76E-10	(1.95E-08)	4.23E-12	(4.10E-10)	2.61E-11	(1.31E-08)
abs3SN	5.05E-06	(1.08E-04)	1.21E-05	(1.89E-04)	2.49E-02	(8.94E-02)	3.23E-10	(1.36E-07)
abs3WN	2.90E-01	(8.95E-02)	2.37E-16	(1.70E-14)	1.14E-01	(1.42E-01)	3.52E-02	(1.23E-01)
abs5EN	4.28E-01	(2.60E-02)	8.54E-01	(5.61E-02)	5.25E-01	(3.51E-02)	6.27E-01	(3.42E-02)
abs5NN	5.21E-06	(1.01E-04)	1.94E+00	(1.40E-01)	1.00E+00	(1.14E-01)	1.17E+00	(1.13E-01)
abs5SN	4.91E-01	(1.26E-02)	6.58E-01	(2.95E-02)	3.09E-01	(1.98E-02)	4.92E-01	(1.96E-02)
abs5WN	2.81E-01	(2.20E-02)	2.44E-12	(1.18E-10)	2.59E-01	(3.23E-02)	2.65E-01	(3.31E-02)
f1N	1.65E-01	(4.68E-04)	9.43E-02	(4.23E-03)	2.31E-01	(2.38E-03)	1.96E-01	(1.76E-03)
f2N	5.84E-02	(1.49E-04)	7.45E-03	(2.54E-04)	4.85E-02	(4.03E-04)	4.88E-02	(3.58E-04)
f3N	6.11E-01	(6.25E-03)	6.95E-01	(4.58E-03)	6.40E-01	(1.04E-02)	6.13E-01	(1.05E-02)
f5N	1.17E-01	(3.21E-04)	5.01E-11	(1.41E-09)	7.32E-02	(1.07E-03)	9.38E-02	(9.76E-04)
CiN	1.47E+06	(2.26E+04)	7.08E+05	(1.02E+04)	7.66E+05	(2.10E+04)	1.19E+06	(3.20E+04)
CwN	2.09E+08	(1.89E+07)	3.16E+07	(5.16E+06)	8.78E+06	(7.95E+05)	6.55E+06	(6.03E+05)
CwiN	4.49E+07	(4.60E+07)	6.44E+06	(1.27E+05)	1.51E+07	(4.42E+06)	1.01E+07	(1.45E+06)
hwN	2.99E+02	(1.56E+00)	4.63E+02	(7.79E+00)	2.18E+02	(4.38E+00)	1.99E+02	(5.37E+00)
hwiN	1.20E+02	(9.14E-01)	1.85E+02	(2.06E+00)	8.62E+01	(6.79E-01)	8.66E+01	(9.47E-01)
infN	6.93E+01	(2.36E+00)	1.54E-16	(8.36E-15)	5.11E+01	(1.81E+00)	6.68E+01	(1.88E+00)
UwN	9.90E+03	(2.72E+05)	7.87E+02	(2.49E+04)	3.53E+02	(1.26E+04)	2.74E+02	(9.43E+03)
CfiD	9.90E+08	(9.19E+07)	2.51E+07	(3.30E+06)	1.92E+07	(2.60E+06)	1.20E+08	(1.57E+07)
CfiN	1.13E+08	(4.87E+07)	4.22E+07	(1.33E+07)	6.51E+07	(3.32E+07)	6.30E+05	(3.35E+04)
UfDN	7.84E+01	(8.05E-01)	2.46E+02	(4.61E+00)	1.98E+02	(4.01E+00)	1.38E+02	(1.20E+00)
Ufi	5.60E-04	(6.08E-02)	3.74E-04	(1.90E-02)	3.48E-04	(3.04E-03)	7.61E+03	(1.17E+02)
UfND	2.36E+02	(1.49E+00)	3.08E+02	(6.33E+00)	2.21E+02	(3.53E+00)	3.71E+02	(5.67E+00)

Table B.8: Grey-box model parameters for thoroughly renovated semi-detached buildings (Ref. 2)

Parameters	SD1		SD2		SD3		SD4	
	Est.	(Std.)	Est.	(Std.)	Est.	(Std.)	Est.	(Std.)
abs1ED	3.65E-01	(7.88E-03)	9.61E-01	(3.63E-02)	9.45E-01	(2.91E-02)	2.99E-01	(1.17E-02)
abs1ND	5.46E-01	(3.09E-02)	1.90E+00	(1.24E-01)	7.98E-01	(9.80E-02)	3.52E-01	(2.70E-02)
abs1SD	3.74E-01	(4.50E-03)	1.15E+00	(2.06E-02)	1.04E+00	(1.66E-02)	3.74E-01	(6.07E-03)
abs1WD	3.60E-01	(7.59E-03)	7.90E-01	(3.48E-02)	8.27E-01	(2.92E-02)	3.62E-01	(6.54E-03)
abs2ED	9.80E-01	(2.03E-02)	1.95E+00	(4.27E-02)	1.83E+00	(2.88E-02)	6.75E-01	(1.79E-02)
abs2ND	6.72E-01	(7.82E-02)	1.81E+00	(1.36E-01)	1.22E+00	(8.38E-02)	5.68E-01	(4.00E-02)
abs2SD	8.80E-01	(1.13E-02)	2.26E+00	(2.55E-02)	2.10E+00	(1.74E-02)	6.93E-01	(9.19E-03)
abs2WD	9.67E-01	(2.00E-02)	1.91E+00	(4.29E-02)	1.77E+00	(3.08E-02)	7.76E-01	(1.02E-02)
abs3ED	5.30E-01	(2.74E-01)	2.60E-01	(2.72E-01)	5.37E-01	(2.38E-01)	2.30E-01	(9.56E-02)
abs3ND	4.45E-04	(8.55E-03)	2.42E-08	(1.41E-05)	1.12E-07	(6.95E-06)	6.79E-01	(1.58E-01)
abs3SD	7.99E-02	(1.53E-01)	5.09E-01	(1.19E-01)	3.41E-01	(1.33E-01)	1.87E-01	(3.60E-02)
abs3WD	5.15E-01	(2.71E-01)	2.12E-07	(1.01E-04)	5.91E-02	(2.27E-01)	4.84E-01	(4.71E-02)
abs4ED	6.07E-01	(7.18E-03)	7.99E-01	(1.65E-02)	9.88E-01	(1.56E-02)	6.16E-01	(1.22E-02)
abs4ND	7.06E-02	(2.65E-02)	7.39E-08	(6.66E-06)	3.12E-07	(1.27E-05)	5.67E-01	(3.09E-02)
abs4SD	5.61E-01	(4.25E-03)	9.49E-01	(9.77E-03)	1.14E+00	(9.37E-03)	6.88E-01	(6.88E-03)
abs4WS	5.83E-01	(7.51E-03)	7.90E-01	(1.58E-02)	9.94E-01	(1.59E-02)	7.23E-01	(7.53E-03)
abs5ED	5.77E-02	(7.74E-03)	6.46E-01	(1.27E-02)	5.60E-01	(1.11E-02)	1.73E-01	(1.15E-02)
abs5ND	2.38E-01	(3.07E-02)	9.05E-09	(3.13E-06)	6.18E-10	(5.93E-08)	1.57E-01	(2.83E-02)
abs5SD	7.76E-02	(4.21E-03)	7.90E-01	(7.62E-03)	6.76E-01	(6.24E-03)	1.81E-01	(6.08E-03)
abs5WD	3.80E-02	(7.57E-03)	6.25E-01	(1.23E-02)	5.50E-01	(1.14E-02)	1.34E-01	(6.69E-03)
f1D	6.57E-02	(1.83E-04)	7.70E-02	(7.19E-04)	6.96E-02	(7.65E-04)	5.32E-02	(2.19E-04)
f2D	1.62E-01	(4.46E-04)	1.47E-01	(9.40E-04)	1.36E-01	(8.93E-04)	1.14E-01	(4.64E-04)
f3D	7.12E-01	(1.12E-02)	7.33E-01	(5.48E-03)	7.72E-01	(5.12E-03)	7.22E-01	(2.04E-03)
f4D	9.58E-02	(1.67E-04)	6.14E-02	(3.24E-04)	7.13E-02	(4.60E-04)	1.03E-01	(2.93E-04)
f5D	6.81E-03	(1.63E-04)	5.01E-02	(2.47E-04)	4.37E-02	(2.84E-04)	2.67E-02	(1.98E-04)
CflD	2.67E+08	(1.46E+08)	9.92E+08	(4.73E+07)	1.48E+07	(2.57E+05)	8.55E+06	(6.75E+04)
CiD	2.59E+06	(7.33E+04)	2.99E+06	(5.63E+04)	3.53E+06	(5.49E+04)	1.80E+06	(1.29E+04)
CwD	3.15E+07	(6.54E+05)	4.41E+07	(1.06E+06)	3.17E+07	(1.08E+06)	6.74E+06	(7.85E+04)
CwiD	1.05E+07	(1.91E+05)	2.63E+07	(3.70E+05)	2.50E+07	(2.50E+05)	9.90E+06	(4.96E+04)
hwD	1.80E+02	(6.62E-01)	3.81E+02	(2.57E+00)	2.79E+02	(2.52E+00)	1.09E+02	(4.38E-01)
hflD	1.51E+02	(6.09E-01)	1.74E+02	(1.14E+00)	2.19E+02	(1.30E+00)	1.57E+02	(5.10E-01)
hwiD	3.13E+02	(2.01E+00)	5.16E+02	(3.29E+00)	4.61E+02	(2.36E+00)	2.59E+02	(7.65E-01)
infD	1.76E+02	(4.30E+00)	2.54E+02	(2.98E+00)	2.72E+02	(2.13E+00)	1.22E+02	(3.40E-01)
UflD	2.44E+02	(6.41E+01)	2.54E+02	(2.50E+02)	7.62E+01	(1.42E+00)	5.45E+01	(6.48E-01)
Uwd	7.09E+02	(4.12E+04)	7.35E+02	(4.61E+04)	3.25E+02	(1.73E+04)	4.63E+01	(5.52E+03)
abs1EN	5.90E-01	(2.61E-02)	2.49E-12	(1.19E-10)	2.02E-01	(7.91E-02)	4.35E-02	(4.69E-02)
abs1NN	1.40E-06	(9.08E-07)	1.60E-11	(6.82E-10)	6.29E-07	(4.52E-05)	5.64E-01	(7.68E-02)
abs1SN	6.97E-01	(1.59E-02)	2.51E-01	(5.03E-02)	7.77E-01	(4.03E-02)	6.57E-01	(2.32E-02)
abs1WN	7.66E-01	(2.60E-02)	9.17E-01	(1.01E-01)	6.54E-01	(6.29E-02)	9.73E-01	(1.78E-02)
abs2EN	1.12E+00	(3.20E-02)	4.16E-01	(2.70E-02)	2.35E-01	(1.24E-02)	8.77E-01	(3.46E-02)
abs2NN	5.27E-01	(1.22E-01)	5.70E-01	(6.49E-02)	3.09E-01	(4.13E-02)	5.05E-01	(7.05E-02)
abs2SN	9.54E-01	(1.89E-02)	3.20E-01	(1.41E-02)	1.76E-01	(7.18E-03)	1.02E+00	(1.91E-02)
abs2WN	9.57E-01	(3.06E-02)	3.64E-02	(6.15E-03)	1.30E-01	(1.12E-02)	7.47E-01	(1.45E-02)
abs3EN	8.05E-01	(9.31E-02)	7.16E-06	(5.18E-05)	2.53E-01	(1.58E-01)	1.78E-01	(6.90E-02)
abs3NN	2.24E-10	(3.59E-10)	5.76E-10	(1.95E-08)	4.23E-12	(4.10E-10)	1.24E-16	(1.98E-14)
abs3SN	4.11E-07	(3.54E-07)	1.21E-05	(1.89E-04)	2.49E-02	(8.94E-02)	2.02E-02	(3.56E-02)
abs3WN	5.24E-01	(8.68E-02)	2.37E-16	(1.70E-14)	1.14E-01	(1.42E-01)	3.53E-01	(3.18E-02)
abs5EN	3.37E-01	(1.47E-02)	8.54E-01	(5.61E-02)	5.25E-01	(3.51E-02)	4.65E-01	(2.23E-02)
abs5NN	5.56E-02	(6.21E-02)	1.94E+00	(1.40E-01)	1.00E+00	(1.14E-01)	6.37E-01	(4.47E-02)
abs5SN	3.25E-01	(7.62E-03)	6.58E-01	(2.95E-02)	3.09E-01	(1.98E-02)	5.45E-01	(1.25E-02)
abs5WN	2.93E-01	(1.38E-02)	2.44E-12	(1.18E-10)	2.59E-01	(3.23E-02)	3.73E-01	(9.46E-03)
f1N	1.19E-01	(2.57E-04)	9.43E-02	(4.23E-03)	2.31E-01	(2.38E-03)	1.19E-01	(8.89E-04)
f2N	1.63E-01	(3.16E-04)	7.45E-03	(2.54E-04)	4.85E-02	(4.03E-04)	1.20E-01	(7.20E-04)
f3N	6.55E-01	(4.00E-03)	6.95E-01	(4.58E-03)	6.40E-01	(1.04E-02)	7.05E-01	(2.05E-03)
f5N	5.50E-02	(1.31E-04)	5.01E-11	(1.41E-09)	7.32E-02	(1.07E-03)	5.62E-02	(3.95E-04)
CiN	1.76E+06	(1.69E+04)	7.08E+05	(1.02E+04)	7.66E+05	(2.10E+04)	2.10E+06	(1.06E+04)
CwN	5.33E+07	(1.55E+06)	3.16E+07	(5.16E+06)	8.78E+06	(7.95E+05)	4.73E+06	(9.05E+04)
CwiN	1.32E+07	(5.33E+05)	6.44E+06	(1.27E+05)	1.51E+07	(4.42E+06)	2.08E+07	(9.01E+05)
hwN	4.37E+02	(1.76E+00)	4.63E+02	(7.79E+00)	2.18E+02	(4.38E+00)	2.74E+02	(2.68E+00)
hwiN	5.59E+02	(2.35E+00)	1.85E+02	(2.06E+00)	8.62E+01	(6.79E-01)	2.84E+02	(2.25E+00)
infN	1.30E+02	(2.14E+00)	1.54E-16	(8.36E-15)	5.11E+01	(1.81E+00)	9.19E+01	(3.44E-01)
UwN	2.29E+03	(9.90E+04)	7.87E+02	(2.49E+04)	3.53E+02	(1.26E+04)	1.89E+02	(3.07E+04)
CfiD	9.84E+08	(1.41E+08)	2.51E+07	(3.30E+06)	1.92E+07	(2.60E+06)	9.96E+08	(1.83E+07)
CfiN	9.73E+08	(9.96E+07)	4.22E+07	(1.33E+07)	6.51E+07	(3.32E+07)	9.94E+08	(2.81E+07)
UfDN	6.31E+01	(6.51E-01)	2.46E+02	(4.61E+00)	1.98E+02	(4.01E+00)	8.64E+01	(4.44E-01)
Ufi	1.51E+02	(2.43E+02)	3.74E-04	(1.90E-02)	3.48E-04	(3.04E-03)	1.29E-03	(2.44E-01)
UfND	1.47E+02	(9.69E-01)	3.08E+02	(6.33E+00)	2.21E+02	(3.53E+00)	1.19E+02	(1.38E+00)

Table B.9: Grey-box model parameters for thoroughly renovated terraced buildings (Ref. 2)

Parameters	T1		T2		T3		T4	
	Est.	(Std.)	Est.	(Std.)	Est.	(Std.)	Est.	(Std.)
abs1ED	2.15E-01	(4.69E-03)	1.42E-01	(8.02E-03)	1.28E-01	(2.44E-03)	1.18E-01	(1.95E-03)
abs1ND	3.53E-01	(1.81E-02)	3.99E-01	(2.10E-02)	1.31E-01	(8.23E-03)	9.76E-02	(6.23E-03)
abs1SD	2.21E-01	(2.32E-03)	2.21E-01	(4.73E-03)	1.11E-01	(1.35E-03)	9.65E-02	(1.06E-03)
abs1WD	1.77E-01	(4.22E-03)	1.46E-01	(4.46E-03)	1.09E-01	(2.40E-03)	1.16E-01	(1.91E-03)
abs2ED	1.16E+00	(1.67E-02)	9.93E-01	(4.62E-02)	8.92E-01	(1.06E-02)	1.01E+00	(1.11E-02)
abs2ND	1.17E+00	(5.66E-02)	2.05E+00	(1.12E-01)	7.23E-01	(3.55E-02)	6.79E-01	(3.22E-02)
abs2SD	1.10E+00	(9.03E-03)	1.10E+00	(2.51E-02)	7.63E-01	(6.07E-03)	8.34E-01	(6.35E-03)
abs2WD	1.02E+00	(1.51E-02)	1.16E+00	(2.63E-02)	8.28E-01	(1.05E-02)	1.08E+00	(1.18E-02)
abs3ED	5.54E-01	(2.05E-01)	5.53E-01	(1.07E-01)	2.73E-01	(8.12E-02)	2.42E-01	(4.11E-02)
abs3ND	2.09E-01	(3.27E-01)	1.57E-01	(1.93E-01)	3.02E-07	(1.09E-05)	2.05E-10	(7.50E-09)
abs3SD	7.58E-02	(1.25E-01)	1.87E-01	(4.14E-02)	4.96E-02	(3.31E-02)	1.79E-06	(3.05E-05)
abs3WD	4.93E-01	(2.04E-01)	2.88E-01	(5.23E-02)	4.72E-07	(3.57E-06)	2.81E-29	(7.74E-27)
abs4ED	5.18E-01	(5.34E-03)	4.33E-01	(1.54E-02)	3.00E-01	(3.46E-03)	3.07E-01	(3.29E-03)
abs4ND	1.25E-01	(1.92E-02)	2.31E-07	(1.25E-05)	1.36E-01	(1.12E-02)	1.05E-01	(9.88E-03)
abs4SD	4.85E-01	(3.04E-03)	3.37E-01	(8.27E-03)	2.52E-01	(1.97E-03)	2.49E-01	(1.88E-03)
abs4WS	4.42E-01	(5.29E-03)	3.97E-01	(8.82E-03)	2.79E-01	(3.49E-03)	3.26E-01	(3.43E-03)
abs5ED	2.02E-01	(4.34E-03)	2.56E-01	(9.36E-03)	2.02E-01	(3.42E-03)	2.02E-01	(3.27E-03)
abs5ND	4.65E-02	(1.50E-02)	8.74E-08	(2.19E-06)	2.47E-07	(9.07E-06)	1.22E-08	(5.32E-07)
abs5SD	2.09E-01	(2.39E-03)	2.23E-01	(4.90E-03)	1.90E-01	(1.78E-03)	1.88E-01	(1.77E-03)
abs5WD	1.78E-01	(4.24E-03)	2.20E-01	(5.13E-03)	1.98E-01	(3.32E-03)	2.34E-01	(3.29E-03)
f1D	3.68E-02	(1.60E-04)	2.33E-02	(1.38E-04)	3.03E-02	(2.01E-04)	2.63E-02	(2.08E-04)
f2D	1.81E-01	(5.44E-04)	1.64E-01	(7.39E-04)	2.07E-01	(9.59E-04)	2.31E-01	(1.29E-03)
f3D	7.27E-01	(9.52E-03)	7.40E-01	(1.90E-03)	7.34E-01	(4.23E-03)	7.18E-01	(4.12E-03)
f4D	7.81E-02	(1.89E-04)	5.35E-02	(2.51E-04)	6.41E-02	(2.97E-04)	6.43E-02	(3.74E-04)
f5D	3.38E-02	(1.27E-04)	4.77E-02	(1.41E-04)	5.38E-02	(2.04E-04)	5.27E-02	(2.79E-04)
CfID	2.83E+08	(1.18E+06)	1.58E+07	(7.68E+05)	6.11E+06	(9.22E+04)	8.40E+06	(1.16E+05)
CiD	1.88E+06	(4.41E+04)	1.42E+06	(1.26E+04)	1.27E+06	(2.28E+04)	1.62E+06	(3.79E+04)
CwD	1.58E+07	(3.80E+05)	7.04E+06	(1.04E+05)	5.46E+06	(9.73E+04)	4.02E+06	(5.56E+04)
CwiD	1.36E+07	(2.59E+05)	2.08E+07	(2.77E+05)	2.20E+07	(3.03E+05)	3.73E+07	(5.22E+05)
hwD	8.94E+01	(3.69E-01)	7.75E+01	(3.27E-01)	5.67E+01	(2.73E-01)	5.91E+01	(2.82E-01)
hfID	1.17E+02	(3.99E-01)	1.19E+02	(7.23E-01)	8.87E+01	(3.89E-01)	1.11E+02	(4.84E-01)
hwiD	2.91E+02	(1.42E+00)	3.84E+02	(2.44E+00)	2.99E+02	(1.17E+00)	4.01E+02	(1.58E+00)
infD	1.50E+02	(2.43E+00)	1.45E+02	(4.15E-01)	1.00E+02	(6.19E-01)	9.38E+01	(4.57E-01)
UfID	3.07E+02	(1.95E+01)	3.92E+02	(9.40E+00)	5.29E+01	(5.76E-01)	4.90E+01	(5.02E-01)
Uwd	3.64E+02	(1.76E+04)	1.26E+02	(1.30E+04)	6.21E+01	(6.06E+03)	3.29E+01	(4.29E+03)
abs1EN	4.08E-01	(2.08E-02)	8.80E-08	(7.02E-07)	2.96E-01	(1.35E-02)	2.72E-01	(1.05E-02)
abs1NN	5.86E-07	(7.99E-05)	4.97E-08	(3.91E-07)	8.22E-07	(4.21E-06)	3.63E-07	(6.61E-07)
abs1SN	4.75E-01	(1.29E-02)	4.99E-08	(4.42E-07)	2.97E-01	(7.16E-03)	2.88E-01	(6.80E-03)
abs1WN	5.01E-01	(1.95E-02)	6.21E-01	(2.60E-02)	3.20E-01	(1.25E-02)	3.95E-01	(1.17E-02)
abs2EN	1.60E+00	(4.61E-02)	1.79E+00	(6.99E-02)	1.20E+00	(2.56E-02)	1.16E+00	(2.27E-02)
abs2NN	6.45E-01	(1.52E-01)	1.30E+00	(1.25E-01)	4.81E-01	(8.15E-02)	3.60E-01	(1.03E-01)
abs2SN	1.44E+00	(2.54E-02)	1.88E+00	(2.87E-02)	9.43E-01	(1.39E-02)	9.37E-01	(1.13E-02)
abs2WN	1.36E+00	(4.32E-02)	9.08E-01	(3.22E-02)	9.85E-01	(2.42E-02)	1.29E+00	(3.26E-02)
abs3EN	8.01E-01	(8.28E-02)	1.96E-08	(1.64E-07)	3.31E-01	(6.82E-02)	4.46E-01	(5.24E-02)
abs3NN	8.22E-09	(2.21E-06)	3.58E-08	(3.44E-07)	1.65E-06	(9.41E-06)	3.19E-06	(7.27E-06)
abs3SN	1.36E-07	(3.01E-05)	8.94E-07	(1.05E-05)	1.35E-06	(8.40E-06)	1.94E-07	(9.29E-07)
abs3WN	2.43E-01	(8.50E-02)	2.88E-01	(5.03E-02)	3.15E-02	(6.64E-02)	1.15E-06	(6.67E-06)
abs5EN	2.23E-01	(1.05E-02)	2.79E-01	(1.47E-02)	1.71E-01	(4.11E-03)	2.15E-01	(6.82E-03)
abs5NN	2.88E-07	(5.00E-05)	5.28E-01	(3.37E-02)	1.52E-01	(1.40E-02)	1.80E-01	(2.17E-02)
abs5SN	2.31E-01	(5.99E-03)	3.04E-01	(8.14E-03)	1.35E-01	(2.27E-03)	1.77E-01	(2.85E-03)
abs5WN	1.99E-01	(1.06E-02)	1.47E-01	(6.46E-03)	1.33E-01	(4.03E-03)	2.38E-01	(5.65E-03)
f1N	7.71E-02	(2.37E-04)	7.05E-02	(8.25E-04)	7.41E-02	(3.33E-04)	7.05E-02	(3.95E-04)
f2N	2.24E-01	(5.94E-04)	1.96E-01	(9.76E-04)	2.33E-01	(7.28E-04)	2.29E-01	(8.33E-04)
f3N	6.44E-01	(4.60E-03)	6.99E-01	(2.29E-03)	6.11E-01	(5.54E-03)	6.15E-01	(5.86E-03)
f5N	3.52E-02	(1.20E-04)	2.90E-02	(1.57E-04)	3.06E-02	(1.08E-04)	4.12E-02	(1.68E-04)
CiN	2.06E+06	(2.12E+04)	2.23E+06	(1.74E+04)	1.47E+06	(2.11E+04)	1.62E+06	(2.58E+04)
CwN	5.78E+07	(2.91E+06)	1.62E+07	(8.21E+05)	9.76E+06	(4.76E+05)	4.01E+06	(1.64E+05)
CwiN	2.03E+07	(9.37E+05)	4.30E+07	(1.49E+06)	3.58E+07	(1.89E+06)	4.21E+07	(3.13E+06)
hwN	3.21E+02	(1.60E+00)	2.71E+02	(3.11E+00)	1.84E+02	(1.44E+00)	1.83E+02	(1.86E+00)
hwiN	7.95E+02	(4.44E+00)	7.24E+02	(4.11E+00)	5.74E+02	(2.73E+00)	6.09E+02	(3.48E+00)
infN	1.05E+02	(2.02E+00)	1.11E+02	(6.90E-01)	4.97E+01	(1.02E+00)	4.54E+01	(7.56E-01)
UwN	2.87E+03	(6.02E+04)	8.47E+02	(2.55E+04)	2.81E+02	(1.82E+04)	1.55E+02	(1.54E+04)
CfiD	9.89E+08	(4.30E+08)	9.60E+07	(1.67E+07)	4.76E+06	(1.74E+05)	1.23E-01	(6.16E-04)
CfiN	1.13E+07	(3.19E+06)	9.98E+08	(2.03E+06)	1.11E+05	(3.66E+03)	1.89E+08	(6.24E+07)
UfDN	3.74E+01	(3.91E-01)	4.61E+01	(2.95E-01)	4.96E+01	(5.75E-01)	4.29E+01	(5.96E-01)
Ufi	2.50E+01	(3.03E+01)	1.82E+03	(2.87E+02)	3.10E+03	(1.10E+01)	5.21E+02	(1.85E+02)
UfND	9.66E+01	(9.78E-01)	1.01E+02	(7.90E-01)	6.86E+01	(1.90E+00)	1.01E+02	(6.31E-01)

Table B.10: Theoretic parameters for original detached buildings

modelparameters	D1	D2	D3	D4	D5
abs1ED	1.29E+00	1.31E+00	1.09E+00	9.80E-01	7.17E-01
abs1ND	1.49E+00	1.28E+00	9.87E-01	8.74E-01	7.89E-01
abs1SD	1.69E+00	1.71E+00	1.37E+00	1.15E+00	9.82E-01
abs1WD	1.23E+00	1.31E+00	1.17E+00	1.01E+00	5.78E-01
abs2ED	2.57E+00	2.61E+00	2.18E+00	1.96E+00	1.43E+00
abs2ND	2.99E+00	2.56E+00	1.97E+00	1.75E+00	1.58E+00
abs2SD	3.38E+00	3.42E+00	2.73E+00	2.29E+00	1.96E+00
abs2WD	2.46E+00	2.61E+00	2.34E+00	2.01E+00	1.16E+00
abs3ED	1.69E-01	2.18E-01	1.95E-01	1.80E-01	1.27E-01
abs3ND	1.96E-01	2.14E-01	1.77E-01	1.61E-01	1.40E-01
abs3SD	2.21E-01	2.86E-01	2.45E-01	2.11E-01	1.74E-01
abs3WD	1.62E-01	2.18E-01	2.10E-01	1.85E-01	1.02E-01
abs4ED	7.86E-01	9.50E-01	1.02E+00	7.87E-01	5.43E-01
abs4ND	9.13E-01	9.30E-01	9.19E-01	7.02E-01	5.98E-01
abs4SD	1.03E+00	1.24E+00	1.27E+00	9.22E-01	7.45E-01
abs4WS	7.52E-01	9.50E-01	1.09E+00	8.08E-01	4.38E-01
abs5ED	8.47E-01	8.18E-01	6.38E-01	6.78E-01	5.67E-01
abs5ND	9.84E-01	8.01E-01	5.78E-01	6.05E-01	6.24E-01
abs5SD	1.11E+00	1.07E+00	7.99E-01	7.94E-01	7.77E-01
abs5WD	8.11E-01	8.18E-01	6.85E-01	6.97E-01	4.57E-01
f1D	4.55E-02	4.43E-02	4.26E-02	4.27E-02	4.23E-02
f2D	9.09E-02	8.85E-02	8.52E-02	8.55E-02	8.46E-02
f3D	8.06E-01	8.07E-01	8.08E-01	8.08E-01	8.07E-01
f4D	2.78E-02	3.22E-02	3.97E-02	3.43E-02	3.21E-02
f5D	2.99E-02	2.77E-02	2.49E-02	2.96E-02	3.35E-02
CflD	1.49E+07	1.41E+07	1.62E+07	1.54E+07	1.21E+07
CiD	1.94E+06	1.83E+06	2.12E+06	2.01E+06	2.43E+06
CwD	8.90E+07	3.16E+07	2.85E+07	2.31E+07	2.03E+07
CwiD	3.31E+07	3.44E+07	3.10E+07	3.41E+07	2.62E+07
hwD	8.61E+02	5.56E+02	3.76E+02	5.03E+02	3.48E+02
hflD	4.27E+02	4.03E+02	4.66E+02	4.42E+02	4.70E+02
hwiD	8.76E+02	6.06E+02	5.46E+02	6.00E+02	6.94E+02
infD	2.70E+02	2.72E+02	2.34E+02	2.13E+02	1.88E+02
UflD	1.21E+02	1.14E+02	7.54E+01	6.16E+01	4.94E+01
Uwd	1.11E+03	6.31E+02	2.65E+02	1.30E+02	8.79E+01
abs1EN	1.11E+00	1.29E+00	1.22E+00	9.83E-01	6.78E-01
abs1NN	1.29E+00	1.27E+00	1.11E+00	8.76E-01	7.46E-01
abs1SN	1.46E+00	1.69E+00	1.53E+00	1.15E+00	9.28E-01
abs1WN	1.07E+00	1.29E+00	1.31E+00	1.01E+00	5.46E-01
abs2EN	4.12E-01	3.95E-01	3.21E-01	2.92E-01	2.05E-01
abs2NN	4.79E-01	3.87E-01	2.91E-01	2.61E-01	2.26E-01
abs2SN	5.41E-01	5.17E-01	4.02E-01	3.42E-01	2.81E-01
abs2WN	3.94E-01	3.95E-01	3.45E-01	3.00E-01	1.65E-01
abs3EN	7.09E-02	8.65E-02	7.54E-02	7.05E-02	4.99E-02
abs3NN	8.23E-02	8.47E-02	6.82E-02	6.29E-02	5.49E-02
abs3SN	9.30E-02	1.13E-01	9.44E-02	8.26E-02	6.83E-02
abs3WN	6.78E-02	8.65E-02	8.09E-02	7.24E-02	4.02E-02
abs5EN	8.30E-01	7.56E-01	5.75E-01	6.19E-01	5.20E-01
abs5NN	9.64E-01	7.41E-01	5.20E-01	5.52E-01	5.72E-01
abs5SN	1.09E+00	9.90E-01	7.20E-01	7.25E-01	7.12E-01
abs5WN	7.94E-01	7.56E-01	6.17E-01	6.36E-01	4.19E-01
f1N	9.18E-02	1.02E-01	1.11E-01	1.00E-01	9.33E-02
f2N	3.40E-02	3.12E-02	2.93E-02	2.98E-02	2.83E-02
f3N	8.06E-01	8.07E-01	8.07E-01	8.07E-01	8.07E-01
f5N	6.84E-02	5.97E-02	5.24E-02	6.30E-02	7.16E-02
CiN	2.09E+06	1.58E+06	1.33E+06	1.73E+06	1.47E+06
CwN	2.12E+07	7.75E+06	7.44E+06	7.32E+06	8.80E+06
CwiN	5.40E+06	5.63E+06	5.07E+06	5.57E+06	4.09E+06
hwN	5.52E+02	4.78E+02	2.08E+02	1.93E+02	5.02E+02
hwiN	1.43E+02	9.90E+01	8.92E+01	9.81E+01	1.08E+02
infN	1.76E+02	1.54E+02	1.16E+02	1.00E+02	1.08E+02
UwN	8.92E+02	8.26E+02	7.44E+02	7.29E+02	6.44E+01
CfiD	4.18E+06	2.54E+07	2.10E+07	2.78E+07	3.17E+07
CfiN	4.18E+06	2.54E+07	2.10E+07	2.78E+07	3.17E+07
UfDN	7.03E+02	6.35E+02	5.49E+02	6.96E+02	9.88E+02
Ufi	3.51E+02	3.17E+02	2.74E+02	3.48E+02	4.94E+02
UfND	7.03E+02	6.35E+02	5.49E+02	6.96E+02	9.88E+02

Table B.11: Theoretic parameters for original semi-detached buildings

modelparameters	SD1	SD2	SD3	SD4	SD5
abs1ED	5.03E-01	4.87E-01	4.98E-01	3.07E-01	2.76E-01
abs1ND	5.16E-01	4.93E-01	4.86E-01	3.60E-01	4.52E-01
abs1SD	5.23E-01	5.60E-01	5.67E-01	4.00E-01	4.69E-01
abs1WD	5.10E-01	5.00E-01	4.61E-01	4.49E-01	3.57E-01
abs2ED	1.29E+00	1.22E+00	1.23E+00	7.56E-01	6.82E-01
abs2ND	1.33E+00	1.24E+00	1.20E+00	8.88E-01	1.11E+00
abs2SD	1.35E+00	1.41E+00	1.40E+00	9.87E-01	1.16E+00
abs2WD	1.31E+00	1.26E+00	1.14E+00	1.11E+00	8.82E-01
abs3ED	9.34E-02	1.07E-01	1.08E-01	7.91E-02	1.06E-01
abs3ND	9.60E-02	1.09E-01	1.06E-01	9.28E-02	1.73E-01
abs3SD	9.72E-02	1.24E-01	1.23E-01	1.03E-01	1.80E-01
abs3WD	9.47E-02	1.10E-01	1.00E-01	1.16E-01	1.37E-01
abs4ED	6.43E-01	6.23E-01	6.45E-01	4.79E-01	4.51E-01
abs4ND	6.60E-01	6.32E-01	6.28E-01	5.63E-01	7.37E-01
abs4SD	6.69E-01	7.17E-01	7.33E-01	6.25E-01	7.65E-01
abs4WS	6.51E-01	6.40E-01	5.96E-01	7.02E-01	5.83E-01
abs5ED	6.43E-01	7.34E-01	6.00E-01	4.14E-01	4.11E-01
abs5ND	6.60E-01	7.44E-01	5.85E-01	4.86E-01	6.72E-01
abs5SD	6.69E-01	8.45E-01	6.82E-01	5.40E-01	6.97E-01
abs5WD	6.51E-01	7.54E-01	5.55E-01	6.06E-01	5.31E-01
f1D	3.17E-02	3.07E-02	3.23E-02	3.01E-02	2.87E-02
f2D	8.15E-02	7.71E-02	7.98E-02	7.43E-02	7.08E-02
f3D	8.06E-01	8.07E-01	8.07E-01	8.08E-01	8.11E-01
f4D	4.05E-02	3.92E-02	4.19E-02	4.71E-02	4.68E-02
f5D	4.05E-02	4.62E-02	3.89E-02	4.07E-02	4.27E-02
CflD	1.14E+07	9.85E+06	1.07E+07	1.15E+07	9.02E+06
CiD	1.48E+06	1.64E+06	1.77E+06	1.90E+06	1.42E+06
CwD	3.25E+07	1.26E+07	1.34E+07	8.86E+06	6.99E+06
CwiD	2.00E+07	1.98E+07	1.46E+07	1.30E+07	9.03E+06
hwD	3.14E+02	2.21E+02	1.78E+02	1.92E+02	1.20E+02
hflD	3.26E+02	2.83E+02	3.05E+02	3.29E+02	3.49E+02
hwiD	4.36E+02	3.32E+02	3.22E+02	2.87E+02	2.91E+02
infD	1.72E+02	1.83E+02	1.66E+02	1.42E+02	1.29E+02
UflD	9.26E+01	8.02E+01	4.95E+01	4.59E+01	3.71E+01
Uwd	4.03E+02	2.51E+02	1.25E+02	4.97E+01	3.03E+01
abs1EN	1.17E+00	1.14E+00	1.21E+00	7.83E-01	7.25E-01
abs1NN	1.20E+00	1.16E+00	1.18E+00	9.20E-01	1.19E+00
abs1SN	1.21E+00	1.32E+00	1.37E+00	1.02E+00	1.23E+00
abs1WN	1.18E+00	1.17E+00	1.12E+00	1.15E+00	9.38E-01
abs2EN	1.40E+00	1.28E+00	1.16E+00	8.03E-01	7.77E-01
abs2NN	1.44E+00	1.30E+00	1.13E+00	9.43E-01	1.27E+00
abs2SN	1.46E+00	1.48E+00	1.32E+00	1.05E+00	1.32E+00
abs2WN	1.42E+00	1.32E+00	1.07E+00	1.18E+00	1.00E+00
abs3EN	7.71E-02	9.55E-02	1.10E-01	7.20E-02	8.72E-02
abs3NN	7.92E-02	9.68E-02	1.07E-01	8.45E-02	1.43E-01
abs3SN	8.03E-02	1.10E-01	1.25E-01	9.39E-02	1.48E-01
abs3WN	7.82E-02	9.82E-02	1.02E-01	1.05E-01	1.13E-01
abs5EN	5.31E-01	6.53E-01	6.07E-01	3.77E-01	3.38E-01
abs5NN	5.45E-01	6.62E-01	5.92E-01	4.43E-01	5.52E-01
abs5SN	5.52E-01	7.52E-01	6.90E-01	4.92E-01	5.73E-01
abs5WN	5.38E-01	6.71E-01	5.61E-01	5.52E-01	4.37E-01
f1N	7.34E-02	7.20E-02	7.83E-02	7.70E-02	7.53E-02
f2N	8.83E-02	8.08E-02	7.51E-02	7.89E-02	8.06E-02
f3N	8.05E-01	8.06E-01	8.07E-01	8.07E-01	8.09E-01
f5N	3.34E-02	4.11E-02	3.94E-02	3.70E-02	3.51E-02
CiN	1.95E+06	1.16E+06	9.14E+05	1.34E+06	1.96E+06
CwN	4.77E+07	1.65E+07	1.43E+07	1.27E+07	1.37E+07
CwiN	2.62E+07	2.34E+07	1.36E+07	1.52E+07	1.25E+07
hwN	7.23E+02	5.09E+02	2.59E+02	2.99E+02	4.85E+02
hwiN	5.73E+02	3.91E+02	2.99E+02	3.34E+02	4.03E+02
infN	1.68E+02	1.35E+02	1.01E+02	9.42E+01	1.22E+02
UwN	1.07E+03	7.59E+02	5.64E+02	5.33E+02	7.81E+01
CfiD	2.96E+06	2.43E+07	2.04E+07	2.08E+07	2.06E+07
CfiN	2.96E+06	2.43E+07	2.04E+07	2.08E+07	2.06E+07
UfDN	4.98E+02	6.09E+02	5.33E+02	5.20E+02	6.41E+02
Ufi	2.49E+02	3.04E+02	2.66E+02	2.60E+02	3.21E+02
UfND	4.98E+02	6.09E+02	5.33E+02	5.20E+02	6.41E+02

Table B.12: Theoretic parameters for original terraced buildings

modelparameters	T1	T2	T3	T4	T5
abs1ED	3.32E-01	2.64E-01	1.95E-01	1.64E-01	1.97E-01
abs1ND	3.53E-01	2.36E-01	1.77E-01	1.57E-01	2.36E-01
abs1SD	3.41E-01	2.71E-01	1.83E-01	1.54E-01	2.17E-01
abs1WD	2.99E-01	2.64E-01	2.01E-01	2.00E-01	1.88E-01
abs2ED	1.68E+00	1.79E+00	1.36E+00	1.13E+00	1.28E+00
abs2ND	1.78E+00	1.60E+00	1.23E+00	1.07E+00	1.53E+00
abs2SD	1.72E+00	1.84E+00	1.27E+00	1.06E+00	1.41E+00
abs2WD	1.51E+00	1.79E+00	1.40E+00	1.37E+00	1.22E+00
abs3ED	1.34E-01	1.14E-01	7.83E-02	7.90E-02	1.41E-01
abs3ND	1.43E-01	1.02E-01	7.08E-02	7.53E-02	1.68E-01
abs3SD	1.38E-01	1.17E-01	7.33E-02	7.41E-02	1.55E-01
abs3WD	1.21E-01	1.14E-01	8.08E-02	9.60E-02	1.34E-01
abs4ED	6.46E-01	5.70E-01	3.98E-01	3.74E-01	4.61E-01
abs4ND	6.87E-01	5.10E-01	3.60E-01	3.57E-01	5.52E-01
abs4SD	6.62E-01	5.85E-01	3.73E-01	3.51E-01	5.09E-01
abs4WS	5.80E-01	5.70E-01	4.10E-01	4.54E-01	4.40E-01
abs5ED	6.46E-01	5.70E-01	3.98E-01	7.59E-01	4.61E-01
abs5ND	6.87E-01	5.10E-01	3.60E-01	7.24E-01	5.52E-01
abs5SD	6.62E-01	5.85E-01	3.73E-01	7.13E-01	5.09E-01
abs5WD	5.80E-01	5.70E-01	4.10E-01	9.23E-01	4.40E-01
f1D	1.93E-02	1.60E-02	1.61E-02	1.31E-02	1.55E-02
f2D	9.77E-02	1.08E-01	1.12E-01	9.00E-02	1.01E-01
f3D	8.08E-01	8.07E-01	8.06E-01	8.06E-01	8.11E-01
f4D	5.64E-02	5.17E-02	4.92E-02	4.48E-02	5.45E-02
f5D	3.76E-02	3.45E-02	3.28E-02	6.07E-02	3.64E-02
CflD	8.40E+06	8.27E+06	6.88E+06	7.01E+06	5.52E+06
CiD	1.10E+06	1.08E+06	8.97E+05	9.15E+05	8.68E+05
CwD	1.58E+07	6.25E+06	5.51E+06	3.72E+06	2.98E+06
CwiD	2.05E+07	2.91E+07	2.71E+07	2.44E+07	1.86E+07
hwD	1.53E+02	1.10E+02	7.29E+01	8.09E+01	5.12E+01
hflD	2.41E+02	2.37E+02	1.97E+02	2.01E+02	2.14E+02
hwiD	4.24E+02	4.72E+02	3.75E+02	2.62E+02	2.58E+02
infD	1.44E+02	1.41E+02	1.03E+02	9.48E+01	9.48E+01
UflD	6.84E+01	6.73E+01	3.20E+01	2.80E+01	2.25E+01
Uwd	1.96E+02	1.25E+02	5.14E+01	2.09E+01	1.29E+01
abs1EN	7.20E-01	6.74E-01	4.83E-01	4.32E-01	5.04E-01
abs1NN	7.66E-01	6.03E-01	4.37E-01	4.12E-01	6.03E-01
abs1SN	7.39E-01	6.92E-01	4.53E-01	4.05E-01	5.56E-01
abs1WN	6.47E-01	6.74E-01	4.99E-01	5.25E-01	4.80E-01
abs2EN	2.32E+00	2.23E+00	1.67E+00	1.63E+00	1.74E+00
abs2NN	2.47E+00	1.99E+00	1.51E+00	1.55E+00	2.09E+00
abs2SN	2.38E+00	2.28E+00	1.56E+00	1.53E+00	1.93E+00
abs2WN	2.09E+00	2.23E+00	1.72E+00	1.98E+00	1.66E+00
abs3EN	6.78E-02	6.77E-02	4.51E-02	4.20E-02	6.78E-02
abs3NN	7.21E-02	6.06E-02	4.08E-02	4.00E-02	8.12E-02
abs3SN	6.95E-02	6.95E-02	4.22E-02	3.94E-02	7.49E-02
abs3WN	6.09E-02	6.77E-02	4.65E-02	5.10E-02	6.46E-02
abs5EN	3.26E-01	3.38E-01	2.29E-01	4.04E-01	2.22E-01
abs5NN	3.47E-01	3.03E-01	2.07E-01	3.85E-01	2.66E-01
abs5SN	3.34E-01	3.47E-01	2.15E-01	3.79E-01	2.45E-01
abs5WN	2.93E-01	3.38E-01	2.37E-01	4.90E-01	2.12E-01
f1N	4.19E-02	4.08E-02	3.99E-02	3.45E-02	3.97E-02
f2N	1.35E-01	1.35E-01	1.38E-01	1.30E-01	1.37E-01
f3N	8.04E-01	8.04E-01	8.04E-01	8.03E-01	8.05E-01
f5N	1.90E-02	2.05E-02	1.89E-02	3.23E-02	1.75E-02
CiN	2.17E+06	1.80E+06	1.54E+06	1.86E+06	2.02E+06
CwN	3.51E+07	1.19E+07	1.07E+07	9.33E+06	9.77E+06
CwiN	4.08E+07	4.90E+07	4.69E+07	5.01E+07	3.77E+07
hwN	5.36E+02	4.06E+02	1.93E+02	2.20E+02	3.44E+02
hwiN	1.02E+03	9.54E+02	7.75E+02	7.51E+02	7.37E+02
infN	1.44E+02	1.87E+02	8.94E+01	7.69E+01	1.08E+02
UwN	7.93E+02	6.24E+02	4.12E+02	3.97E+02	5.55E+01
CfiD	2.19E+06	1.78E+07	1.42E+07	3.07E+07	1.38E+07
CfiN	2.19E+06	1.78E+07	1.42E+07	3.07E+07	1.38E+07
UfDN	3.68E+02	4.98E+02	3.70E+02	8.58E+02	4.31E+02
Ufi	1.84E+02	2.49E+02	1.85E+02	4.29E+02	2.15E+02
UfND	3.68E+02	4.98E+02	3.70E+02	8.58E+02	4.31E+02

Table B.13: Theoretic parameters for mildly renovated detached buildings (Ref. 1)

Parameters	D1	D2	D3	D4
abs1ED	6.95E-01	7.06E-01	6.66E-01	7.80E-01
abs1ND	8.08E-01	6.92E-01	6.03E-01	6.96E-01
abs1SD	9.12E-01	9.25E-01	8.34E-01	9.14E-01
abs1WD	6.65E-01	7.06E-01	7.15E-01	8.01E-01
abs2ED	1.39E+00	1.41E+00	1.33E+00	1.56E+00
abs2ND	1.62E+00	1.38E+00	1.21E+00	1.39E+00
abs2SD	1.82E+00	1.85E+00	1.67E+00	1.83E+00
abs2WD	1.33E+00	1.41E+00	1.43E+00	1.60E+00
abs3ED	9.12E-02	1.18E-01	1.19E-01	1.44E-01
abs3ND	1.06E-01	1.15E-01	1.08E-01	1.28E-01
abs3SD	1.20E-01	1.54E-01	1.49E-01	1.68E-01
abs3WD	8.73E-02	1.18E-01	1.28E-01	1.47E-01
abs4ED	4.25E-01	5.13E-01	6.20E-01	6.27E-01
abs4ND	4.93E-01	5.02E-01	5.61E-01	5.59E-01
abs4SD	5.57E-01	6.72E-01	7.76E-01	7.34E-01
abs4WS	4.06E-01	5.13E-01	6.66E-01	6.44E-01
abs5ED	4.58E-01	4.42E-01	3.90E-01	5.40E-01
abs5ND	5.31E-01	4.33E-01	3.53E-01	4.82E-01
abs5SD	6.00E-01	5.78E-01	4.88E-01	6.33E-01
abs5WD	4.38E-01	4.42E-01	4.18E-01	5.55E-01
f1D	4.55E-02	4.43E-02	4.26E-02	4.27E-02
f2D	9.09E-02	8.85E-02	8.52E-02	8.55E-02
f3D	8.06E-01	8.07E-01	8.08E-01	8.08E-01
f4D	2.78E-02	3.22E-02	3.97E-02	3.43E-02
f5D	2.99E-02	2.77E-02	2.49E-02	2.96E-02
CflD	1.49E+07	1.41E+07	1.62E+07	1.54E+07
CiD	1.94E+06	1.83E+06	2.12E+06	2.01E+06
CwD	8.90E+07	3.16E+07	2.85E+07	2.31E+07
CwiD	3.31E+07	3.44E+07	3.10E+07	3.41E+07
hwD	7.40E+02	5.56E+02	3.76E+02	5.03E+02
hflD	2.79E+02	4.03E+02	4.66E+02	4.42E+02
hwiD	5.85E+02	6.06E+02	5.46E+02	6.00E+02
infD	1.25E+02	1.26E+02	1.29E+02	1.34E+02
UflD	1.21E+02	1.14E+02	7.54E+01	6.16E+01
Uwd	1.11E+03	6.31E+02	2.65E+02	1.30E+02
abs1EN	6.02E-01	6.99E-01	7.47E-01	7.83E-01
abs1NN	6.99E-01	6.85E-01	6.76E-01	6.98E-01
abs1SN	7.90E-01	9.15E-01	9.35E-01	9.17E-01
abs1WN	5.76E-01	6.99E-01	8.02E-01	8.04E-01
abs2EN	2.23E-01	2.13E-01	1.96E-01	2.33E-01
abs2NN	2.59E-01	2.09E-01	1.77E-01	2.08E-01
abs2SN	2.92E-01	2.79E-01	2.46E-01	2.73E-01
abs2WN	2.13E-01	2.13E-01	2.10E-01	2.39E-01
abs3EN	3.83E-02	4.67E-02	4.60E-02	5.62E-02
abs3NN	4.45E-02	4.58E-02	4.16E-02	5.01E-02
abs3SN	5.02E-02	6.12E-02	5.76E-02	6.58E-02
abs3WN	3.66E-02	4.67E-02	4.94E-02	5.77E-02
abs5EN	4.48E-01	4.08E-01	3.51E-01	4.93E-01
abs5NN	5.21E-01	4.00E-01	3.18E-01	4.40E-01
abs5SN	5.88E-01	5.35E-01	4.40E-01	5.78E-01
abs5WN	4.29E-01	4.08E-01	3.77E-01	5.07E-01
f1N	4.48E-01	4.08E-01	3.51E-01	4.93E-01
f2N	5.21E-01	4.00E-01	3.18E-01	4.40E-01
f3N	5.88E-01	5.35E-01	4.40E-01	5.78E-01
f5N	4.29E-01	4.08E-01	3.77E-01	5.07E-01
CiN	2.09E+06	1.58E+06	1.33E+06	1.73E+06
CwN	2.12E+07	7.75E+06	7.44E+06	8.71E+06
CwiN	5.40E+06	5.63E+06	5.07E+06	5.57E+06
hwN	4.05E+02	1.82E+02	1.64E+02	1.72E+02
hwiN	9.56E+01	9.90E+01	8.92E+01	9.81E+01
infN	2.47E+01	5.55E+01	5.00E+01	5.36E+01
UwN	2.29E+02	1.89E+02	1.39E+02	1.06E+02
CfiD	4.18E+06	2.54E+07	2.10E+07	2.78E+07
CfiN	4.18E+06	2.54E+07	2.10E+07	2.78E+07
UfDN	5.31E+02	6.35E+02	5.49E+02	6.96E+02
Ufi	2.65E+02	3.17E+02	2.74E+02	3.48E+02
UfND	5.31E+02	6.35E+02	5.49E+02	6.96E+02

Table B.14: Theoretic parameters for mildly renovated semi-detached buildings (Ref. 1)

Parameters	SD1	SD2	SD3	SD4
abs1ED	2.72E-01	2.63E-01	3.04E-01	2.44E-01
abs1ND	2.79E-01	2.67E-01	2.96E-01	2.87E-01
abs1SD	2.83E-01	3.03E-01	3.46E-01	3.18E-01
abs1WD	2.75E-01	2.70E-01	2.81E-01	3.57E-01
abs2ED	6.99E-01	6.61E-01	7.50E-01	6.03E-01
abs2ND	7.18E-01	6.70E-01	7.32E-01	7.07E-01
abs2SD	7.28E-01	7.61E-01	8.54E-01	7.86E-01
abs2WD	7.09E-01	6.80E-01	6.94E-01	8.82E-01
abs3ED	5.05E-02	5.80E-02	6.62E-02	6.30E-02
abs3ND	5.18E-02	5.88E-02	6.45E-02	7.39E-02
abs3SD	5.25E-02	6.67E-02	7.53E-02	8.21E-02
abs3WD	5.11E-02	5.96E-02	6.12E-02	9.22E-02
abs4ED	3.47E-01	3.37E-01	3.93E-01	3.82E-01
abs4ND	3.57E-01	3.41E-01	3.84E-01	4.48E-01
abs4SD	3.61E-01	3.87E-01	4.48E-01	4.98E-01
abs4WS	3.52E-01	3.46E-01	3.64E-01	5.59E-01
abs5ED	3.47E-01	3.96E-01	3.66E-01	3.30E-01
abs5ND	3.57E-01	4.02E-01	3.57E-01	3.87E-01
abs5SD	3.61E-01	4.56E-01	4.16E-01	4.30E-01
abs5WD	3.52E-01	4.07E-01	3.39E-01	4.83E-01
f1D	4.75E-02	4.60E-02	4.85E-02	4.52E-02
f2D	1.22E-01	1.16E-01	1.20E-01	1.11E-01
f3D	7.09E-01	7.10E-01	7.11E-01	7.12E-01
f4D	6.07E-02	5.89E-02	6.28E-02	7.07E-02
f5D	6.07E-02	6.93E-02	5.84E-02	6.10E-02
CflD	1.14E+07	9.85E+06	1.07E+07	1.15E+07
CiD	1.48E+06	1.64E+06	1.77E+06	1.90E+06
CwD	3.25E+07	1.26E+07	1.34E+07	8.86E+06
CwiD	9.99E+06	9.92E+06	7.32E+06	6.52E+06
hwD	2.11E+02	1.58E+02	1.37E+02	1.41E+02
hflD	2.13E+02	1.85E+02	2.00E+02	2.15E+02
hwiD	2.85E+02	2.23E+02	1.80E+02	1.99E+02
infD	8.75E+01	9.13E+01	9.65E+01	9.19E+01
UflD	1.15E+02	9.77E+01	2.55E+01	2.06E+01
Uwd	4.03E+02	2.51E+02	1.25E+02	4.97E+01
abs1EN	5.70E-01	5.82E-01	7.36E-01	5.52E-01
abs1NN	5.86E-01	5.90E-01	7.18E-01	6.48E-01
abs1SN	5.93E-01	6.69E-01	8.37E-01	7.21E-01
abs1WN	5.78E-01	5.98E-01	6.81E-01	8.09E-01
abs2EN	8.48E-01	7.53E-01	7.06E-01	7.53E-01
abs2NN	8.71E-01	7.63E-01	6.89E-01	8.83E-01
abs2SN	8.83E-01	8.67E-01	8.03E-01	9.82E-01
abs2WN	8.60E-01	7.74E-01	6.53E-01	1.10E+00
abs3EN	3.77E-02	4.86E-02	6.70E-02	5.07E-02
abs3NN	3.88E-02	4.93E-02	6.53E-02	5.96E-02
abs3SN	3.93E-02	5.59E-02	7.62E-02	6.62E-02
abs3WN	3.82E-02	4.99E-02	6.20E-02	7.43E-02
abs5EN	2.60E-01	3.32E-01	3.70E-01	2.66E-01
abs5NN	2.67E-01	3.37E-01	3.61E-01	3.12E-01
abs5SN	2.70E-01	3.82E-01	4.21E-01	3.47E-01
abs5WN	2.63E-01	3.41E-01	3.43E-01	3.89E-01
f1N	2.60E-01	3.32E-01	3.70E-01	2.66E-01
f2N	2.67E-01	3.37E-01	3.61E-01	3.12E-01
f3N	2.70E-01	3.82E-01	4.21E-01	3.47E-01
f5N	2.63E-01	3.41E-01	3.43E-01	3.89E-01
CiN	1.95E+06	1.16E+06	9.14E+05	1.34E+06
CwN	4.77E+07	1.65E+07	1.43E+07	1.36E+07
CwiN	2.81E+07	3.07E+07	1.36E+07	2.98E+07
hwN	3.40E+02	2.92E+02	2.35E+02	2.71E+02
hwiN	4.32E+02	2.96E+02	1.67E+02	2.98E+02
infN	5.61E+01	5.00E+01	4.85E+01	5.13E+01
UwN	5.93E+02	2.76E+02	1.55E+02	1.10E+02
CfiD	2.96E+06	2.43E+07	2.04E+07	2.08E+07
CfiN	2.96E+06	2.43E+07	2.04E+07	2.08E+07
UfDN	3.76E+02	4.39E+02	3.81E+02	3.74E+02
Ufi	1.88E+02	2.19E+02	1.91E+02	1.87E+02
UfND	3.76E+02	4.39E+02	3.81E+02	3.74E+02

Table B.15: Theoretic parameters for mildly renovated terraced buildings (Ref. 1)

Parameters	T1	T2	T3	T4
abs1ED	1.80E-01	1.43E-01	1.19E-01	1.00E-01
abs1ND	1.91E-01	1.28E-01	1.08E-01	9.56E-02
abs1SD	1.84E-01	1.46E-01	1.12E-01	9.41E-02
abs1WD	1.61E-01	1.43E-01	1.23E-01	1.22E-01
abs2ED	9.07E-01	9.66E-01	8.28E-01	6.87E-01
abs2ND	9.64E-01	8.65E-01	7.49E-01	6.56E-01
abs2SD	9.30E-01	9.92E-01	7.75E-01	6.45E-01
abs2WD	8.15E-01	9.66E-01	8.54E-01	8.35E-01
abs3ED	7.26E-02	6.15E-02	4.78E-02	4.82E-02
abs3ND	7.72E-02	5.51E-02	4.32E-02	4.60E-02
abs3SD	7.44E-02	6.32E-02	4.47E-02	4.52E-02
abs3WD	6.52E-02	6.15E-02	4.93E-02	5.86E-02
abs4ED	3.49E-01	3.08E-01	2.43E-01	2.28E-01
abs4ND	3.71E-01	2.75E-01	2.20E-01	2.18E-01
abs4SD	3.58E-01	3.16E-01	2.27E-01	2.14E-01
abs4WS	3.14E-01	3.08E-01	2.51E-01	2.77E-01
abs5ED	3.49E-01	3.08E-01	2.43E-01	4.64E-01
abs5ND	3.71E-01	2.75E-01	2.20E-01	4.42E-01
abs5SD	3.58E-01	3.16E-01	2.27E-01	4.35E-01
abs5WD	3.14E-01	3.08E-01	2.51E-01	5.63E-01
f1D	2.90E-02	2.40E-02	1.61E-02	1.97E-02
f2D	1.47E-01	1.62E-01	1.12E-01	1.35E-01
f3D	7.12E-01	7.10E-01	8.06E-01	7.09E-01
f4D	5.64E-02	5.17E-02	4.92E-02	4.48E-02
f5D	5.64E-02	5.17E-02	3.28E-02	9.10E-02
CflD	8.40E+06	8.27E+06	6.88E+06	7.01E+06
CiD	1.10E+06	1.08E+06	8.97E+05	9.15E+05
CwD	1.58E+07	6.25E+06	5.51E+06	3.72E+06
CwiD	1.03E+07	1.46E+07	2.71E+07	1.22E+07
hwD	1.53E+02	7.87E+01	7.29E+01	5.93E+01
hflD	2.41E+02	2.37E+02	1.97E+02	1.31E+02
hwiD	2.75E+02	3.11E+02	3.75E+02	2.34E+02
infD	8.08E+01	7.91E+01	7.50E+01	6.88E+01
UflD	2.36E+02	8.64E+01	3.20E+01	5.04E+01
Uwd	1.96E+02	1.25E+02	5.14E+01	2.09E+01
abs1EN	3.89E-01	3.64E-01	2.95E-01	2.63E-01
abs1NN	4.14E-01	3.26E-01	2.67E-01	2.51E-01
abs1SN	3.99E-01	3.74E-01	2.76E-01	2.47E-01
abs1WN	3.50E-01	3.64E-01	3.04E-01	3.20E-01
abs2EN	1.25E+00	1.20E+00	1.02E+00	9.92E-01
abs2NN	1.33E+00	1.08E+00	9.21E-01	9.46E-01
abs2SN	1.29E+00	1.23E+00	9.53E-01	9.31E-01
abs2WN	1.13E+00	1.20E+00	1.05E+00	1.21E+00
abs3EN	3.66E-02	3.66E-02	2.75E-02	2.56E-02
abs3NN	3.90E-02	3.27E-02	2.49E-02	2.44E-02
abs3SN	3.76E-02	3.75E-02	2.58E-02	2.40E-02
abs3WN	3.29E-02	3.66E-02	2.84E-02	3.11E-02
abs5EN	1.76E-01	1.83E-01	1.40E-01	2.46E-01
abs5NN	1.87E-01	1.64E-01	1.27E-01	2.35E-01
abs5SN	1.81E-01	1.88E-01	1.31E-01	2.31E-01
abs5WN	1.58E-01	1.83E-01	1.44E-01	2.99E-01
f1N	1.76E-01	1.83E-01	1.40E-01	2.46E-01
f2N	1.87E-01	1.64E-01	1.27E-01	2.35E-01
f3N	1.81E-01	1.88E-01	1.31E-01	2.31E-01
f5N	1.58E-01	1.83E-01	1.44E-01	2.99E-01
CiN	2.17E+06	1.80E+06	1.54E+06	1.86E+06
CwN	3.51E+07	1.19E+07	1.07E+07	1.00E+07
CwiN	4.50E+07	7.24E+07	4.69E+07	8.07E+07
hwN	2.50E+02	1.80E+02	1.73E+02	1.62E+02
hwiN	6.82E+02	6.19E+02	7.75E+02	6.26E+02
infN	5.78E+01	5.25E+01	5.03E+01	4.48E+01
UwN	4.37E+02	2.05E+02	1.33E+02	8.48E+01
CfiD	2.19E+06	1.78E+07	1.42E+07	3.07E+07
CfiN	2.19E+06	1.78E+07	1.42E+07	3.07E+07
UfDN	2.78E+02	2.98E+02	3.70E+02	5.94E+02
Ufi	1.39E+02	1.49E+02	1.85E+02	2.97E+02
UfND	2.78E+02	2.98E+02	3.70E+02	5.94E+02

Table B.16: Theoretic parameters for thoroughly renovated detached buildings (Ref. 2)

Parameters	D1	D2	D3	D4
abs1ED	6.95E-01	7.06E-01	6.66E-01	7.80E-01
abs1ND	8.08E-01	6.92E-01	6.03E-01	6.96E-01
abs1SD	9.12E-01	9.25E-01	8.34E-01	9.14E-01
abs1WD	6.65E-01	7.06E-01	7.15E-01	8.01E-01
abs2ED	1.39E+00	1.41E+00	1.33E+00	1.56E+00
abs2ND	1.62E+00	1.38E+00	1.21E+00	1.39E+00
abs2SD	1.82E+00	1.85E+00	1.67E+00	1.83E+00
abs2WD	1.33E+00	1.41E+00	1.43E+00	1.60E+00
abs3ED	9.12E-02	1.18E-01	1.19E-01	1.44E-01
abs3ND	1.06E-01	1.15E-01	1.08E-01	1.28E-01
abs3SD	1.20E-01	1.54E-01	1.49E-01	1.68E-01
abs3WD	8.73E-02	1.18E-01	1.28E-01	1.47E-01
abs4ED	4.25E-01	5.13E-01	6.20E-01	6.27E-01
abs4ND	4.93E-01	5.02E-01	5.61E-01	5.59E-01
abs4SD	5.57E-01	6.72E-01	7.76E-01	7.34E-01
abs4WS	4.06E-01	5.13E-01	6.66E-01	6.44E-01
abs5ED	4.58E-01	4.42E-01	3.90E-01	5.40E-01
abs5ND	5.31E-01	4.33E-01	3.53E-01	4.82E-01
abs5SD	6.00E-01	5.78E-01	4.88E-01	6.33E-01
abs5WD	4.38E-01	4.42E-01	4.18E-01	5.55E-01
f1D	6.82E-02	4.43E-02	4.26E-02	4.27E-02
f2D	1.36E-01	8.85E-02	8.52E-02	8.55E-02
f3D	7.09E-01	8.07E-01	8.08E-01	8.08E-01
f4D	4.16E-02	3.22E-02	3.97E-02	3.43E-02
f5D	4.49E-02	2.77E-02	2.49E-02	2.96E-02
CflD	1.49E+07	1.41E+07	1.62E+07	1.54E+07
CiD	1.94E+06	1.83E+06	2.12E+06	2.01E+06
CwD	8.90E+07	3.16E+07	2.85E+07	2.31E+07
CwiD	1.65E+07	3.44E+07	3.10E+07	3.41E+07
hwD	4.31E+02	5.56E+02	3.76E+02	5.03E+02
hflD	2.79E+02	4.03E+02	4.66E+02	4.42E+02
hwiD	5.85E+02	6.06E+02	5.46E+02	6.00E+02
infD	1.25E+02	1.26E+02	1.29E+02	9.41E+01
UflD	3.60E+01	2.76E+01	3.64E+01	4.25E+01
Uwd	7.37E+01	5.58E+01	5.74E+01	7.20E+01
abs1EN	6.02E-01	6.99E-01	7.47E-01	7.83E-01
abs1NN	6.99E-01	6.85E-01	6.76E-01	6.98E-01
abs1SN	7.90E-01	9.15E-01	9.35E-01	9.17E-01
abs1WN	5.76E-01	6.99E-01	8.02E-01	8.04E-01
abs2EN	2.23E-01	2.13E-01	1.96E-01	2.33E-01
abs2NN	2.59E-01	2.09E-01	1.77E-01	2.08E-01
abs2SN	2.92E-01	2.79E-01	2.46E-01	2.73E-01
abs2WN	2.13E-01	2.13E-01	2.10E-01	2.39E-01
abs3EN	3.83E-02	4.67E-02	4.60E-02	5.62E-02
abs3NN	4.45E-02	4.58E-02	4.16E-02	5.01E-02
abs3SN	5.02E-02	6.12E-02	5.76E-02	6.58E-02
abs3WN	3.66E-02	4.67E-02	4.94E-02	5.77E-02
abs5EN	4.48E-01	4.08E-01	3.51E-01	4.93E-01
abs5NN	5.21E-01	4.00E-01	3.18E-01	4.40E-01
abs5SN	5.88E-01	5.35E-01	4.40E-01	5.78E-01
abs5WN	4.29E-01	4.08E-01	3.77E-01	5.07E-01
f1N	4.48E-01	4.08E-01	3.51E-01	4.93E-01
f2N	5.21E-01	4.00E-01	3.18E-01	4.40E-01
f3N	5.88E-01	5.35E-01	4.40E-01	5.78E-01
f5N	4.29E-01	4.08E-01	3.77E-01	5.07E-01
CiN	2.09E+06	1.58E+06	1.33E+06	1.73E+06
CwN	2.12E+07	7.75E+06	7.44E+06	8.71E+06
CwiN	2.70E+06	5.63E+06	5.07E+06	5.57E+06
hwN	3.81E+02	1.82E+02	1.64E+02	1.72E+02
hwiN	9.56E+01	9.90E+01	8.92E+01	9.81E+01
infN	2.47E+01	5.55E+01	5.00E+01	5.36E+01
UwN	6.04E+01	9.53E+01	1.05E+02	9.63E+01
CfiD	4.18E+06	2.54E+07	2.10E+07	2.78E+07
CfiN	4.18E+06	2.54E+07	2.10E+07	2.78E+07
UfDN	5.31E+02	6.35E+02	5.49E+02	5.01E+02
Ufi	2.65E+02	3.17E+02	2.74E+02	2.51E+02
UfND	5.31E+02	6.35E+02	5.49E+02	5.01E+02

Table B.17: Theoretic parameters for thoroughly renovated semi-detached buildings (Ref. 2)

Parameters	SD1	SD2	SD3	SD4
abs1ED	2.72E-01	2.63E-01	3.04E-01	2.44E-01
abs1ND	2.79E-01	2.67E-01	2.96E-01	2.87E-01
abs1SD	2.83E-01	3.03E-01	3.46E-01	3.18E-01
abs1WD	2.75E-01	2.70E-01	2.81E-01	3.57E-01
abs2ED	6.99E-01	6.61E-01	7.50E-01	6.03E-01
abs2ND	7.18E-01	6.70E-01	7.32E-01	7.07E-01
abs2SD	7.28E-01	7.61E-01	8.54E-01	7.86E-01
abs2WD	7.09E-01	6.80E-01	6.94E-01	8.82E-01
abs3ED	5.05E-02	5.80E-02	6.62E-02	6.30E-02
abs3ND	5.18E-02	5.88E-02	6.45E-02	7.39E-02
abs3SD	5.25E-02	6.67E-02	7.53E-02	8.21E-02
abs3WD	5.11E-02	5.96E-02	6.12E-02	9.22E-02
abs4ED	3.47E-01	3.37E-01	3.93E-01	3.82E-01
abs4ND	3.57E-01	3.41E-01	3.84E-01	4.48E-01
abs4SD	3.61E-01	3.87E-01	4.48E-01	4.98E-01
abs4WS	3.52E-01	3.46E-01	3.64E-01	5.59E-01
abs5ED	3.47E-01	3.96E-01	3.66E-01	3.30E-01
abs5ND	3.57E-01	4.02E-01	3.57E-01	3.87E-01
abs5SD	3.61E-01	4.56E-01	4.16E-01	4.30E-01
abs5WD	3.52E-01	4.07E-01	3.39E-01	4.83E-01
f1D	4.75E-02	4.60E-02	4.85E-02	4.52E-02
f2D	1.22E-01	1.16E-01	1.20E-01	1.11E-01
f3D	7.09E-01	7.10E-01	7.11E-01	7.12E-01
f4D	6.07E-02	5.89E-02	6.28E-02	7.07E-02
f5D	6.07E-02	6.93E-02	5.84E-02	6.10E-02
CflD	1.14E+07	9.85E+06	1.07E+07	1.15E+07
CiD	1.48E+06	1.64E+06	1.77E+06	1.90E+06
CwD	3.25E+07	1.26E+07	1.34E+07	8.86E+06
CwiD	6.03E+06	9.92E+06	7.32E+06	6.52E+06
hwD	2.08E+02	1.58E+02	1.37E+02	1.41E+02
hflD	3.26E+02	1.85E+02	2.00E+02	2.15E+02
hwiD	2.85E+02	2.23E+02	2.23E+02	1.99E+02
infD	8.75E+01	9.13E+01	9.65E+01	9.19E+01
UflD	2.75E+01	8.55E+00	1.04E+01	1.03E+01
Uwd	2.69E+01	2.22E+01	2.71E+01	2.76E+01
abs1EN	5.70E-01	5.82E-01	7.36E-01	5.52E-01
abs1NN	5.86E-01	5.90E-01	7.18E-01	6.48E-01
abs1SN	5.93E-01	6.69E-01	8.37E-01	7.21E-01
abs1WN	5.78E-01	5.98E-01	6.81E-01	8.09E-01
abs2EN	8.48E-01	7.53E-01	7.06E-01	7.53E-01
abs2NN	8.71E-01	7.63E-01	6.89E-01	8.83E-01
abs2SN	8.83E-01	8.67E-01	8.03E-01	9.82E-01
abs2WN	8.60E-01	7.74E-01	6.53E-01	1.10E+00
abs3EN	3.77E-02	4.86E-02	6.70E-02	5.07E-02
abs3NN	3.88E-02	4.93E-02	6.53E-02	5.96E-02
abs3SN	3.93E-02	5.59E-02	7.62E-02	6.62E-02
abs3WN	3.82E-02	4.99E-02	6.20E-02	7.43E-02
abs5EN	2.60E-01	3.32E-01	3.70E-01	2.66E-01
abs5NN	2.67E-01	3.37E-01	3.61E-01	3.12E-01
abs5SN	2.70E-01	3.82E-01	4.21E-01	3.47E-01
abs5WN	2.63E-01	3.41E-01	3.43E-01	3.89E-01
f1N	2.60E-01	3.32E-01	3.70E-01	2.66E-01
f2N	2.67E-01	3.37E-01	3.61E-01	3.12E-01
f3N	2.70E-01	3.82E-01	4.21E-01	3.47E-01
f5N	2.63E-01	3.41E-01	3.43E-01	3.89E-01
CiN	1.95E+06	1.16E+06	9.14E+05	1.34E+06
CwN	4.77E+07	1.72E+07	1.43E+07	1.36E+07
CwiN	1.77E+07	1.54E+07	6.81E+06	1.49E+07
hwN	5.84E+02	2.41E+02	1.88E+02	2.21E+02
hwiN	4.32E+02	2.96E+02	2.08E+02	2.98E+02
infN	6.09E+01	5.00E+01	4.85E+01	5.13E+01
UwN	7.18E+01	8.13E+01	8.65E+01	8.89E+01
CfiD	2.96E+06	2.43E+07	2.04E+07	2.08E+07
CfiN	2.96E+06	2.43E+07	2.04E+07	2.08E+07
UfDN	3.76E+02	4.39E+02	3.81E+02	3.74E+02
Ufi	1.88E+02	2.19E+02	1.91E+02	1.87E+02
UfND	3.76E+02	4.39E+02	3.81E+02	3.74E+02

Table B.18: Theoretic parameters for thoroughly renovated terraced buildings (Ref. 2)

Parameters	T1	T2	T3	T4
abs1ED	1.80E-01	1.43E-01	1.19E-01	1.00E-01
abs1ND	1.91E-01	1.28E-01	1.08E-01	9.56E-02
abs1SD	1.84E-01	1.46E-01	1.12E-01	9.41E-02
abs1WD	1.61E-01	1.43E-01	1.23E-01	1.22E-01
abs2ED	9.07E-01	9.66E-01	8.28E-01	6.87E-01
abs2ND	9.64E-01	8.65E-01	7.49E-01	6.56E-01
abs2SD	9.30E-01	9.92E-01	7.75E-01	6.45E-01
abs2WD	8.15E-01	9.66E-01	8.54E-01	8.35E-01
abs3ED	7.26E-02	6.15E-02	4.78E-02	4.82E-02
abs3ND	7.72E-02	5.51E-02	4.32E-02	4.60E-02
abs3SD	7.44E-02	6.32E-02	4.47E-02	4.52E-02
abs3WD	6.52E-02	6.15E-02	4.93E-02	5.86E-02
abs4ED	3.49E-01	3.08E-01	2.43E-01	2.28E-01
abs4ND	3.71E-01	2.75E-01	2.20E-01	2.18E-01
abs4SD	3.58E-01	3.16E-01	2.27E-01	2.14E-01
abs4WS	3.14E-01	3.08E-01	2.51E-01	2.77E-01
abs5ED	3.49E-01	3.08E-01	2.43E-01	4.64E-01
abs5ND	3.71E-01	2.75E-01	2.20E-01	4.42E-01
abs5SD	3.58E-01	3.16E-01	2.27E-01	4.35E-01
abs5WD	3.14E-01	3.08E-01	2.51E-01	5.63E-01
f1D	2.90E-02	1.60E-02	2.41E-02	1.97E-02
f2D	1.47E-01	1.08E-01	1.68E-01	1.35E-01
f3D	7.12E-01	8.07E-01	7.10E-01	7.09E-01
f4D	5.64E-02	5.17E-02	4.92E-02	4.48E-02
f5D	5.64E-02	3.45E-02	4.92E-02	9.10E-02
CflD	8.40E+06	8.27E+06	6.88E+06	7.01E+06
CiD	1.10E+06	1.08E+06	8.97E+05	9.15E+05
CwD	1.58E+07	6.25E+06	5.51E+06	3.72E+06
CwiD	1.03E+07	2.91E+07	1.35E+07	1.22E+07
hwD	1.01E+02	1.10E+02	5.61E+01	8.09E+01
hflD	2.41E+02	4.47E+02	1.29E+02	2.01E+02
hwiD	2.75E+02	4.72E+02	2.60E+02	1.90E+02
infD	8.05E+01	7.91E+01	7.50E+01	6.88E+01
UflD	2.03E+01	1.62E+01	2.05E+01	6.76E+00
Uwd	1.31E+01	1.10E+01	1.11E+01	1.16E+01
abs1EN	3.89E-01	3.64E-01	2.95E-01	2.63E-01
abs1NN	4.14E-01	3.26E-01	2.67E-01	2.51E-01
abs1SN	3.99E-01	3.74E-01	2.76E-01	2.47E-01
abs1WN	3.50E-01	3.64E-01	3.04E-01	3.20E-01
abs2EN	1.25E+00	1.20E+00	1.02E+00	9.92E-01
abs2NN	1.33E+00	1.08E+00	9.21E-01	9.46E-01
abs2SN	1.29E+00	1.23E+00	9.53E-01	9.31E-01
abs2WN	1.13E+00	1.20E+00	1.05E+00	1.21E+00
abs3EN	3.66E-02	3.66E-02	2.75E-02	2.56E-02
abs3NN	3.90E-02	3.27E-02	2.49E-02	2.44E-02
abs3SN	3.76E-02	3.75E-02	2.58E-02	2.40E-02
abs3WN	3.29E-02	3.66E-02	2.84E-02	3.11E-02
abs5EN	1.76E-01	1.83E-01	1.40E-01	2.46E-01
abs5NN	1.87E-01	1.64E-01	1.27E-01	2.35E-01
abs5SN	1.81E-01	1.88E-01	1.31E-01	2.31E-01
abs5WN	1.58E-01	1.83E-01	1.44E-01	2.99E-01
f1N	1.76E-01	1.83E-01	1.40E-01	2.46E-01
f2N	1.87E-01	1.64E-01	1.27E-01	2.35E-01
f3N	1.81E-01	1.88E-01	1.31E-01	2.31E-01
f5N	1.58E-01	1.83E-01	1.44E-01	2.99E-01
CiN	2.17E+06	1.80E+06	1.54E+06	1.86E+06
CwN	3.51E+07	1.19E+07	1.07E+07	1.00E+07
CwiN	4.50E+07	4.86E+07	6.67E+07	8.00E+07
hwN	4.34E+02	2.11E+02	1.73E+02	2.09E+02
hwiN	6.82E+02	9.32E+02	5.40E+02	5.23E+02
infN	5.78E+01	5.25E+01	5.03E+01	4.48E+01
UwN	5.23E+01	4.26E+02	6.35E+01	6.58E+01
CfiD	2.19E+06	1.73E+07	1.42E+07	2.99E+07
CfiN	2.19E+06	1.73E+07	1.42E+07	2.99E+07
UfDN	2.78E+02	4.34E+02	2.65E+02	5.38E+02
Ufi	1.39E+02	2.17E+02	1.32E+02	2.69E+02
UfND	2.78E+02	4.34E+02	2.65E+02	5.38E+02

Bibliography

[1] T. B. Johansson and W. Turkenburg, "Policies for renewable energy in the European Union and its member states: an overview," *Energy for Sustainable Development*, vol. 8, no. 1, pp. 5–24, 2012.

[2] O. Edenhofer, R. Pichs-Madruga, Y. Sokona, K. Seyboth, M. Patrick, S. Kadner, T. Zwickel, P. Eickemeier, G. Hansen, S. Schlömer, and C. von Steckow, "IPCC Special Report on Renewable Energy Sources and Climate Change Mitigation," tech. rep., Intergovernmental Panel on Climate Change, 2011.

[3] R. Baetens, R. De Coninck, J. Van Roy, B. Verbruggen, J. Driesen, L. Helsen, and D. Saelens, "Assessing electrical bottlenecks at feeder level for residential net zero-energy buildings by integrated system simulation," *Applied Energy*, vol. 96, pp. 74–83, Aug. 2012.

[4] H. Lund, A. Marszal, and P. Heiselberg, "Zero energy buildings and mismatch compensation factors," *Energy and Buildings*, vol. 43, pp. 1646–1654, July 2011.

[5] J. Widén, E. Wäckelgå rd, and P. D. Lund, "Options for improving the load matching capability of distributed photovoltaics: Methodology and application to high-latitude data," *Solar Energy*, vol. 83, pp. 1953–1966, Nov. 2009.

[6] P. Torcellini, S. Pless, M. Deru, and D. Crawley, "Zero Energy Buildings: A Critical Look at the Definition," in *2006 ACEEE Summer Study on Energy Efficiency in Buildings*, (Pacific Grove, California), 2006.

[7] A. Marszal, P. Heiselberg, J. Bourrelle, E. Musall, K. Voss, I. Sartori, and A. Napolitano, "Zero Energy Building – A review of definitions and calculation methodologies," *Energy and Buildings*, vol. 43, pp. 971–979, Apr. 2011.

[8] A. a. Bayod-Rújula, "Future development of the electricity systems with distributed generation," *Energy*, vol. 34, pp. 377–383, Mar. 2009.

[9] G. Pepermans, J. Driesen, D. Haeseldonckx, R. Belmans, and W. D'haeseleer, "Distributed generation: definition, benefits and issues," *Energy Policy*, vol. 33, pp. 787–798, Apr. 2005.

[10] J. P. Lopes, N. Hatziargyriou, J. Mutale, P. Djapic, and N. Jenkins, "Integrating distributed generation into electric power systems: A review of drivers, challenges and opportunities," *Electric Power Systems Research*, vol. 77, pp. 1189–1203, July 2007.

[11] ELIA, "Grid data," 2014.

[12] International Energy Agency, "Technology Roadmap Energy-efficient Buildings: Heating and Cooling Equipment," tech. rep., 2011.

[13] The European Parliament, "Directive 2010/31/EU of the European Parliament and of the Council on the energy performance of buildings (recast)," tech. rep., 2010.

[14] A. Orioli and A. Di Gangi, “Load mismatch of grid-connected photovoltaic systems: Review of the effects and analysis in an urban context,” *Renewable and Sustainable Energy Reviews*, vol. 21, pp. 13–28, May 2013.

[15] G. Reynders, T. Nuytten, and D. Saelens, “Potential of structural thermal mass for demand-side management in dwellings,” *Building and Environment*, vol. 64, pp. 187–199, Mar. 2013.

[16] IEA, *Harnessing variable renewables: A guide to the balancing challenge*. 2011.

[17] G. Strbac, “Demand side management: Benefits and challenges,” *Energy Policy*, vol. 36, pp. 4419–4426, Dec. 2008.

[18] B. Biegel, L. H. Hansen, J. Stoustrup, P. Andersen, and S. Harbo, “Value of flexible consumption in the electricity markets,” *Energy*, vol. 66, pp. 354–362, Mar. 2014.

[19] R. P. Hamalainen, J. Mantysaari, J. Ruusunen, and P.-o. Pineau, “Cooperative consumers in a deregulated electricity market — dynamic consumption strategies and price coordination,” *Energy*, vol. 25, pp. 857–875, 2000.

[20] M. Anda and J. Temmen, “Smart metering for residential energy efficiency: The use of community based social marketing for behavioural change and smart grid introduction,” *Renewable Energy*, vol. 67, pp. 119–127, Dec. 2013.

[21] H. Lund, S. Werner, R. Wiltshire, S. Svendsen, J. E. Thorsen, F. Hvelplund, and B. V. Mathiesen, “4th Generation District Heating (4GDH). Integrating smart thermal grids into future sustainable energy systems.,” Mar. 2014.

[22] P. D. Lund, J. Lindgren, J. Mikkola, and J. Salpakari, “Review of energy system flexibility measures to enable high levels of variable renewable electricity,” *Renewable and Sustainable Energy Reviews*, vol. 45, pp. 785–807, 2015.

[23] M. Muratori, B.-A. Schuelke-Leech, and G. Rizzoni, “Role of residential demand response in modern electricity markets,” *Renewable and Sustainable Energy Reviews*, vol. 33, pp. 546–553, May 2014.

[24] J. Torriti, “A review of time use models of residential electricity demand,” *Renewable and Sustainable Energy Reviews*, vol. 37, pp. 265–272, Sept. 2014.

[25] P. Siano, “Demand response and smart grids - A survey,” *Renewable and Sustainable Energy Reviews*, vol. 30, pp. 461–478, 2014.

[26] D. Kirschen and Chua-Liang Su, “Quantifying the Effect of Demand Response on Electricity Markets,” *IEEE Transactions on Power Systems*, vol. 24, no. 3, pp. 1199–1207, 2009.

[27] M. H. Albadi and E. F. El-Saadany, “A summary of demand response in electricity markets,” *Electric Power Systems Research*, vol. 78, pp. 1989–1996, 2008.

[28] L. Gelazanskas and K. a.a. Gamage, “Demand side management in smart grid: A review and proposals for future direction,” *Sustainable Cities and Society*, vol. 11, pp. 22–30, 2014.

[29] P. Bradley, M. Leach, and J. Torriti, “A review of the costs and benefits of demand response for electricity in the UK,” *Energy Policy*, vol. 52, pp. 312–327, 2013.

[30] R. De Coninck, R. Baetens, D. Saelens, A. Woyte, and L. Helsen, “Rule-based demand-side management of domestic hot water production with heat pumps in zero energy neighbourhoods,” *Journal of Building Performance Simulation*, vol. 7, pp. 271–288, July 2014.

[31] D. Vanhoudt, D. Geysen, B. Claessens, F. Leemans, L. Jespers, and J. Van Bael, “An actively controlled residential heat pump: Potential on peak shaving and maximization of self-consumption of renewable energy,” *Renewable Energy*, vol. 63, pp. 531–543, Mar. 2014.

[32] K. Roth, J. Dieckmann, and J. Brodrick, “Using Off-Peak Precooling,” *ASHRAE Journal*, pp. 80–83, 2009.

[33] D. Patteeuw, G. Reynders, K. Bruninx, C. Protopapadaki, E. Delarue, W. D’haeseleer, D. Saelens, and L. Helsen, “CO2-abatement cost of residential heat pumps with active demand response: demand- and supply-side effects,” *Applied Energy*, vol. 156, pp. 490–501, Oct. 2015.

[34] Y. Sun, S. Wang, F. Xiao, and D. Gao, “Peak load shifting control using different cold thermal energy storage facilities in commercial buildings: A review,” *Energy Conversion and Management*, vol. 71, pp. 101–114, July 2013.

[35] J. F. Nicol and M. A. Humphreys, “Adaptive thermal comfort and sustainable thermal standards for buildings,” *Energy and Buildings*, vol. 34, pp. 563–572, 2002.

[36] G. Brager and R. de Dear, “Thermal adaptation in the built environment: a literature review,” *Energy and buildings*, vol. 27, no. 1, pp. 83–96, 1998.

[37] S. Sabihuddin, A. Kiprakis, and M. Mueller, “A Numerical and Graphical Review of Energy Storage Technologies,” *Energies*, vol. 8, no. 1, pp. 172–216, 2014.

[38] W. a. Qureshi, N.-K. C. Nair, and M. M. Farid, “Impact of energy storage in buildings on electricity demand side management,” *Energy Conversion and Management*, vol. 52, pp. 2110–2120, May 2011.

[39] F. Oldewurtel, A. Parisio, C. N. Jones, D. Gyalistras, M. Gwerder, V. Stauch, B. Lehmann, and M. Morari, “Use of model predictive control and weather forecasts for energy efficient building climate control,” *Energy and Buildings*, vol. 45, pp. 15–27, Feb. 2012.

[40] M. Morari and J. H. Lee, “Model predictive control : past, present and future,” *Computers and Chemical Engineering*, vol. 23, pp. 667–682, 1999.

[41] L. Schibuola, M. Scarpa, and C. Tambani, “Demand response management by means of heat pumps controlled via real time pricing,” *Energy and Buildings*, vol. 90, pp. 15–28, 2015.

[42] G. P. Henze, C. Felsmann, and G. Knabe, “Evaluation of optimal control for active and passive building thermal storage,” *International Journal of Thermal Sciences*, vol. 43, pp. 173–183, Feb. 2004.

[43] J. Braun, K. Montgomery, and N. Chaturvedi, “Evaluating the performance of building thermal mass control strategies,” *HVAC&R Research*, vol. 7, no. 4, pp. 403–428, 2001.

[44] J. Široký, F. Oldewurtel, J. Cigler, and S. Prívara, “Experimental analysis of model predictive control for an energy efficient building heating system,” *Applied Energy*, vol. 88, pp. 3079–3087, Sept. 2011.

[45] M. Kintner-Meyer and A. Emery, “Optimal control of an HVAC system using cold storage and building thermal capacitance,” *Energy and Buildings*, vol. 23, pp. 19–31, Oct. 1995.

[46] M. Kummert, P. André, and J. Nicolas, “Optimal heating control in a passive solar commercial building,” *Solar Energy*, vol. 69, pp. 103–116, July 2001.

[47] G. P. Henze, T. H. Le, A. R. Florita, and C. Felsmann, “Sensitivity Analysis of Optimal Building Thermal Mass Control,” 2007.

[48] S. Prívara, J. Široký, L. Ferkl, and J. Cigler, “Model predictive control of a building heating system: The first experience,” *Energy and Buildings*, vol. 43, pp. 564–572, Feb. 2011.

[49] S. Liu and G. Henze, “Impact of Modeling Accuracy on Predictive Optimal Control of Active and Passive Building Thermal Storage Inventory.,” *ASHRAE transactions*, vol. 110, 2004.

[50] J. Cigler, “Beyond theory : the challenge of implementing Model Predictive Control in buildings,” in *Proceedings of 11th Rehva World Congress, Clima*, 2013.

[51] S. Prívara, J. Cigler, Z. Váňa, F. Oldewurtel, C. Sagerschnig, and E. Žáčeková, "Building modeling as a crucial part for building predictive control," *Energy and Buildings*, vol. 56, pp. 8–22, 2013.

[52] KU Leuven, VITO, and BBRI, "SuFiQuad - Sustainability, Financial and Quality evaluation of Dwelling Types, BELSPO," tech. rep., 2001.

[53] M. Packer and L. Glicksman, "An assessment of thermal energy storage in conjunction with heat pumps for residential heating and cooling," *Energy*, vol. 4, pp. 393–399, 1979.

[54] C. Balaras, "The role of thermal mass on the cooling load of buildings. An overview of computational methods," *Energy and Buildings*, vol. 24, pp. 1–10, Jan. 1996.

[55] G. Zhou, M. Krarti, and G. P. Henze, "Parametric Analysis of Active and Passive Building Thermal Storage Utilization," 2005.

[56] J. E. Braun, "Load Control Using Building Thermal Mass," *Journal of Solar Energy Engineering*, vol. 125, no. 3, p. 292, 2003.

[57] K. Bettgenhäuser, M. Offermann, T. Boemans, M. Bosquet, J. Grözinger, B. von Manteuffel, and N. Surmeli, "Heat Pump Implementation Scenarios until 2030 An analysis of the technology ' s potential in the building," tech. rep., 2013.

[58] R. De Coninck, *Grey-Box Based Optimal Control for Thermal Systems in Buildings - Unlocking Energy Efficiency and Flexibility*. Phd. thesis, KU Leuven, 2015.

[59] C. Verhelst, F. Logist, J. Van Impe, and L. Helsen, "Study of the optimal control problem formulation for modulating air-to-water heat pumps connected to a residential floor heating system," *Energy and Buildings*, vol. 45, pp. 43–53, 2012.

[60] R. De Coninck, R. Baetens, B. Verbruggen, J. Driesen, D. Saelens, and L. Helsen, "Modelling and simulation of a grid connected photovoltaic heat pump system with thermal energy storage using Modelica," in *8th International Conference on System Simulation in Buildings*, no. June, pp. 1–21, 2010.

[61] A. Afram and F. Janabi-Sharifi, "Theory and applications of HVAC control systems – A review of model predictive control (MPC)," *Building and Environment*, vol. 72, pp. 343–355, Feb. 2014.

[62] J. Erlandsson, P. Fahlén, and T. Lindholm, "Improvements of heat pump efficiency by adding a storage tank – monitoring experiences from a single family house," in *Proceedings of the 10th REHVA World Congress "Sustainable Energy use in Buildings", Antalya, 9-12 may*, 2010.

[63] H. Chappells and E. Shove, "Debating the future of comfort: environmental sustainability, energy consumption and the indoor environment," *Building Research & Information*, vol. 33, pp. 32–40, Jan. 2005.

[64] R.-L. Hwang, M.-J. Cheng, T.-P. Lin, and M.-C. Ho, "Thermal perceptions, general adaptation methods and occupant's idea about the trade-off between thermal comfort and energy saving in hot–humid regions," *Building and Environment*, vol. 44, pp. 1128–1134, June 2009.

[65] P. Morales-Valdés, A. Flores-Tlacuahuac, and V. M. Zavala, "Analyzing the effects of comfort relaxation on energy demand flexibility of buildings: A multiobjective optimization approach," *Energy and Buildings*, vol. 85, pp. 416–426, Dec. 2014.

[66] S. Banfi, M. Farsi, M. Filippini, and M. Jakob, "Willingness to pay for energy-saving measures in residential buildings," *Energy Economics*, vol. 30, no. 2, pp. 503–516, 2008.

[67] M. Castilla, J. Álvarez, M. Berenguel, F. Rodríguez, J. Guzmán, and M. Pérez, "A comparison of thermal comfort predictive control strategies," *Energy and Buildings*, vol. 43, pp. 2737–2746, Oct. 2011.

[68] M. C. Mozer, L. Vidmar, and R. H. Dodier, "The neurothermostat: Predictive optimal control of residential heating systems," *Advances in Neural Information Processing Systems 9*, vol. 9, pp. 953–959, 1997.

[69] P. Fanger, *Thermal comfort: analysis and applications in environmental Engineering*. United States: McGraw-Hill Book Company, 1970.

[70] ISO, "ISO 7730 - Ergonomics of the thermal environment – Analytical determination and interpretation of thermal comfort using the PMV and PPD indices and local thermal comfort criteria.," 2005.

[71] EN15251, "Indoor Environmental Input Parameters for Design and Assessment of Energy Performance of Buildings – Addressing Indoor air Quality, Thermal Environment, Lighting and Acoustics," 2007.

[72] L. Peeters, R. de Dear, J. Hensen, and W. D'Haeseleer, "Thermal comfort in residential buildings: Comfort values and scales for building energy simulation," *Applied Energy*, vol. 86, pp. 772–780, May 2009.

[73] R. de Dear and G. Brager, "Towards an adaptive model of thermal comfort and preference.," *ASHRAE Transactions*, vol. 104, no. 1, pp. 145–167, 1998.

[74] ANSI/ASHRAE 55-2004., "Thermal environmental conditions for human occupancy. American Society of Heating, Refrigerating and Air-conditioning Engineers Inc., Atlanta, USA, 2004.," tech. rep., 2004.

[75] R. De Coninck and L. Helsen, "Bottom-up quantification of the flexibility potential of buildings," in *13th Conference of International Building Physics Performance Simulation Association*, (Chambery, France), 2013.

[76] F. Oldewurtel, D. Sturzenegger, G. Andersson, M. Morari, and R. S. Smith, "Towards a standardized building assessment for demand response," *Proceedings of the IEEE Conference on Decision and Control*, pp. 7083–7088, 2013.

[77] D. B. Crawley, J. W. Hand, M. Kummert, and B. T. Griffith, "Contrasting the capabilities of building energy performance simulation programs," *Building and Environment*, vol. 43, pp. 661–673, Apr. 2008.

[78] S. Leenknegt, R. Wagemakers, W. Bosschaerts, and D. Saelens, "Numerical study of convection during night cooling and the implications for convection modeling in Building Energy Simulation models," *Energy and Buildings*, vol. 64, pp. 41–52, May 2013.

[79] E. Djunaedy, J. L. M. Hensen, and M. G. Loomans, "Towards External Coupling of Building Energy and Air Flow Towards External Coupling of Building Energy and Air Flow," *ASHRAE Transactions*, vol. 109, pp. 771–787, 2003.

[80] R. Baetens, *On the impact of Nearly-Zero Energy Dwellings on the Electricity Distribution Grid*. Phd. thesis, KU Leuven, 2015.

[81] The Modelica Association, "https://www.modelica.org/."

[82] R. Baetens, R. De Coninck, F. Jorissen, D. Picard, L. Helsen, and D. Saelens, "OpenIDEAS - An Open Framework for Integrated District Energy Assessments," in *Proceedings of the 14th IBPSA Conference - Building Simulation 2015*, (Hyderabad, India), 2015.

[83] M. Sourbron, *Dynamic thermal behaviour of buildings with concrete core activation*. PhD thesis, KU Leuven, 2012.

[84] G. Masy, *Definition and Validation of a Simplified Multizone Dynamic Building Model Connected to Heating System and HVAC Unit*. PhD thesis, 2008.

[85] A. Kennelly, "Equivalence of triangles and three-pointed stars in conducting networks," *Electrical World and Engineer*, vol. 34, pp. 413–414, 1899.

[86] R. J. Liesen and C. Pedersen, "An evaluation of inside surface heat balance models for cooling load calculations.," *ASHRAE Transactions*, vol. 103, no. 2, pp. 485–502, 1997.

[87] A. Khalifa, “Natural convective heat transfer coefficient–a review: II. Surfaces in two-and three-dimensional enclosures,” *Energy Conversion and Management*, vol. 42, pp. 505–517, 2001.

[88] H. B. Awbi and a. Hatton, “Mixed convection from heated room surfaces,” *Energy and Buildings*, vol. 32, no. 2, pp. 153–166, 2000.

[89] T. Defraeye, B. Blocken, and J. Carmeliet, “Convective heat transfer coefficients for exterior building surfaces: Existing correlations and CFD modelling,” *Energy Conversion and Management*, vol. 52, no. 1, pp. 512–522, 2011.

[90] D. C. Hamilton and W. R. Morgan, “Radiant-interchange configuration factors,” tech. rep., National Advisory Comittee for Aeronautics, Washington, 1952.

[91] E. U. Finlayson, D. K. Arasteh, C. Huizenga, M. D. Rubin, and M. S. Reilly, “WINDOW 4.0: Documentation of calculation procedures,” 1993.

[92] D. K. Arasteh, J. Hartmann, and M. Rubin, “Experimental verification of a model of heat transfer through windows,” *ASHRAE Transactions*, vol. 93, no. 1, pp. 1425–1431, 1986.

[93] R. A. Furler, P. Williams, and F. K. Kneubühl, “Experimental and theoretical studies on the energy balance of windows - NEFF Project report 177.1,” tech. rep., 1988.

[94] Meteotest, “METEONORM Version 6.1 - Edition 2009,” 2008.

[95] R. Baetens and D. Saelens, “Modelling uncertainty in district energy simulations by stochastic residential occupant behaviour,” *Journal of Building Performance Simulation*, vol. submitted, 2015.

[96] Dassault Systèmes, “Dymola - Multi-engineering Modeling and Simulation,” 2015.

[97] IEA EBC, “ANNEX 58: Reliable building energy performance characterisation based on full scale dynamic measurement.”

[98] H. Janssen, B. Blocken, and J. Carmeliet, “Conservative modelling of the moisture and heat transfer in building components under atmospheric excitation,” *International Journal of Heat and Mass Transfer*, vol. 50, no. 5-6, pp. 1128–1140, 2007.

[99] M. C. Kersken, I. Heusler, and P. Strachan, “Full scale empirical validation for building energy simulation programs,” in *9th International Conference on System Simulation in Buildings (SSB2014)*, (Liege, Belgium), 2014.

[100] G. Reynders, R. Baetens, C. Protopapadaki, M. Deurinck, and D. Saelens, “Report : Empirical whole model validation IEA ECB Annex 58 subtask 4,” tech. rep., KU Leuven - Building Physics Section, 2014.

[101] G. Reynders and D. Saelens, “Report : Empirical whole model validation Experiment 2 IEA ECB Annex 58 subtask 4,” tech. rep., KU Leuven - Building Physics Section, 2014.

[102] E. M. Greensfelder, G. P. Henze, C. Felsmann, and P. Taylor, “An investigation of optimal control of passive building thermal storage with real time pricing,” *Journal of Building Performance Simulation*, vol. 4, pp. 91–104, June 2011.

[103] M. Kavgic, A. Mavrogianni, D. Mumovic, A. Summerfield, Z. Stevanovic, and M. Djurovic-Petrovic, “A review of bottom-up building stock models for energy consumption in the residential sector,” *Building and Environment*, vol. 45, no. 7, pp. 1683–1697, 2010.

[104] H. C. Gils, “Assessment of the theoretical demand response potential in Europe,” *Energy*, vol. 67, pp. 1–18, 2014.

[105] M. P. Moghaddam, a. Abdollahi, and M. Rashidinejad, “Flexible demand response programs modeling in competitive electricity markets,” *Applied Energy*, vol. 88, no. 9, pp. 3257–3269, 2011.

[106] K. Bruninx, D. Patteeuw, E. Delarue, L. Helsen, and W. D'haeseleer, "Short-term demand response of flexible electric heating systems: The need for integrated simulations," in *2013 10th International Conference on the European Energy Market (EEM)*, no. May, pp. 1–10, IEEE, May 2013.

[107] J. Salom, J. Widén, J. Candanedo, and K. B. Lindberg, "Analysis of grid interaction indicators in net zero-energy buildings with sub-hourly collected data," *Advances in Building Energy Research*, vol. 136, pp. 1–18, 2014.

[108] H. Ibrahim, A. Ilinca, and J. Perr, "Energy storage systems -Characteristics and comparisons," *Renewable and Sustainable Energy Reviews*, vol. 12, pp. 1221–1250, June 2008.

[109] J. M. Grothoff, "Battery storage for renewables: market status and technology outlook," Tech. Rep. January, International Renewable Energy Agency (IRENA), 2015.

[110] F. Oldewurtel, T. Borsche, M. Bucher, P. Fortenbacher, M. Gonz, T. Haring, J. L. Mathieu, M. Olivier, and E. Vrettos, "A Framework for and Assessment of Demand Response and Energy Storage in Power Systems a," in *2013 IREP Symposium-Bul Power System Dynamics and Control*, pp. 1–24, 2013.

[111] K. Heussen, S. Koch, A. Ulbig, and G. Andersson, "Unified System-Level Modeling of Intermittent Renewable Energy Sources and Energy Storage for Power System Operation," *IEEE Systems Journal*, vol. 6, pp. 140–151, Mar. 2012.

[112] M. Geidl, G. Koeppel, P. Favre-Perrod, B. Klöckl, G. Andersson, and K. Fröhlich, "Energy hubs for the future," *IEEE Power and Energy Magazine*, vol. 5, no. february, pp. 24–30, 2007.

[113] P. Ahcin and M. Sikic, "Simulating demand response and energy storage in energy distribution systems," *Power System Technology (POWERCON), 2010 International Conference on*, 2010.

[114] F. Brahman, M. Honarmand, and S. Jadid, "Optimal electrical and thermal energy management of a residential energy hub, integrating demand response and energy storage system," *Energy and Buildings*, vol. 90, pp. 65–75, 2015.

[115] F. Kienzle, P. Ahcin, and G. Anderson, "Valuing investments in multi-energy conversion, storage, and demand-side management systems under uncertainty," *IEEE Transactions on Sustainable Energy*, vol. 2, no. 2, pp. 194–202, 2011.

[116] A. Ulbig and G. Andersson, "On operational flexibility in power systems," in *IEEE Power and Energy Society General Meeting*, 2012.

[117] W. Cyx, N. Renders, V. H. M., and S. Verbeke, "IEE TABULA - Typology Approach for Building Stock Energy Assessment," Tech. Rep. August, 2011.

[118] K. Allacker, *Sustainable building: the development of an evaluation method*. Phd thesis, KU Leuven, 2010.

[119] E. Georges, S. Gendebien, S. Bertagnolio, and V. Lemort, "Modeling and simulation of the domestic energy use in Belgium following a bottom-up approach," in *Proceedings of the CLIMA 2013 11th REHVA World Congress & 8th International Conference on IAQVEC*, (Prague (Czech Republic)), 2013.

[120] CEN, "EN 12831 Heating systems in buildings - Method for calculation of the design heat load," 2003.

[121] ISO, "ISO 6946:2007 Building components and building elements - Thermal resistance and thermal transmittance - Calculation Method," 2007.

[122] H. Akaike, "A new look at the statistical model identification," *IEEE Transactions on Automatic Control*, vol. 19, pp. 716–723, Dec. 1974.

[123] M. Sourbron, C. Verhelst, and L. Helsen, "Building models for model predictive control of office buildings with concrete core activation," *Journal of Building Performance Simulation*, vol. 6, pp. 175–198, May 2013.

[124] R. H. Henninger, M. J. Witte, and D. B. Crawley, “Analytical and comparative testing of EnergyPlus using IEA HVAC BESTEST E100-E200 test suite,” *Energy and Buildings*, vol. 36, no. January 2002, pp. 855–863, 2004.

[125] T. S. Nouidui, K. Phalak, W. Zuo, and M. Wetter, “Validation and Application of the Room Model of the Modelica Buildings Library,” in *9th International Modelica Conference*, 2012.

[126] S. r. O. s. Jensen, “Validation of building energy simulation programs: a methodology,” *Energy and Buildings*, vol. 22, pp. 133–144, Jan. 1995.

[127] B. Coffey, F. Haghighat, E. Morofsky, and E. Kutrowski, “A software framework for model predictive control with GenOpt,” *Energy and Buildings*, vol. 42, no. 7, pp. 1084–1092, 2010.

[128] K. Zhang, N. R. E, H. Quintana, and M. Kummert, “Assessing simplified and detailed models for predictive control of space heating in homes,” in *9th International Conference on System Simulation in Buildings*, vol. 1, (Liege, Belgium), pp. 1–20, 2014.

[129] S. Prívara, Z. Váňa, E. Žáčeková, and J. Cigler, “Building modeling: Selection of the most appropriate model for predictive control,” *Energy and Buildings*, vol. 55, pp. 341–350, 2012.

[130] M. Gouda, S. Danaher, and C. Underwood, “Low-order model for the simulation of a building and its heating system,” *Building Services Engineering Research and Technology*, vol. 21, pp. 199–208, Jan. 2000.

[131] M. Kummert, P. Andre, and J. Nicolas, “Development of simplified models for solar buildings optimal control,” in *Proceedings of ISES Eurosun*, no. 1, pp. 1055–1061, 1996.

[132] K. Deng, P. Barooah, P. G. Mehta, and S. P. Meyn, “Building Thermal Model Reduction via Aggregation of States,” pp. 5118–5123, 2010.

[133] S. Goyal and P. Barooah, “A method for model-reduction of non-linear thermal dynamics of multi-zone buildings,” *Energy and Buildings*, vol. 47, pp. 332–340, 2012.

[134] W. H. A. Schilders, H. A. V. D. Vorst, and J. Rommes, *Model Order Reduction: Theory, Research Aspects and Applications*, vol. 13. Springer, 2008.

[135] J. Singh, N. Singh, and J. K. Sharma, “Fuzzy modeling and control of HVAC systems – A review,” *Journal of Scientific and Industrial Research (JSIR)*, vol. 65, no. June, pp. 470–476, 2006.

[136] H. Zhang, A. Davigny, F. Colas, Y. Poste, and B. Robyns, “Fuzzy logic based energy management strategy for commercial buildings integrating photovoltaic and storage systems,” *Energy and Buildings*, vol. 54, pp. 196–206, Nov. 2012.

[137] M. Killian, B. Mayer, and M. Kozek, “Effective Fuzzy Black-Box Modeling for Building Heating Dynamics,” *Energy and Buildings*, 2015.

[138] T. Takagi and M. Sugeno, “Fuzzy identification of systems and its applications to modeling and control,” *Systems, Man and Cybernetics, IEEE Transactions on*, vol. SMC-15, no. 1, pp. 116–132, 1985.

[139] F. Ruelens, B. Claessens, B. Vandael, R. De Schutter, R. Babuska, and R. Belmans, “Demand Response Applications Using Batch Reinforcement Learning,” *IEEE Transactions on Smart Grid*, no. 1, pp. 1–9, 2015.

[140] S. Liu and G. Henze, “Experimental analysis of simulated reinforcement learning control for active and passive building thermal storage inventoryPart 2: Results and analysis,” *Energy and Buildings*, vol. 38, pp. 148–161, Feb. 2006.

[141] S. Kalogirou, “Artificial neural networks for the prediction of the energy consumption of a passive solar building,” *Energy*, vol. 25, pp. 479–491, May 2000.

[142] Y. Yoru, T. H. Karakoc, and M. Z. Sogut, “Artificial Neural Network (ANN) Applications on the Mechanical Systems of Buildings in 2010 and Beyond,” *Sciences-New York*, 2010.

[143] S. L. Wong, K. K. W. Wan, and T. N. T. Lam, “Artificial neural networks for energy analysis of office buildings with daylighting,” *Applied Energy*, vol. 87, no. 2, pp. 551–557, 2010.

[144] A. a. Argiriou, I. Bellas-Velidis, M. Kummert, and P. André, “A neural network controller for hydronic heating systems of solar buildings.,” *Neural networks : the official journal of the International Neural Network Society*, vol. 17, pp. 427–40, Apr. 2004.

[145] S. Li, J. Joe, J. Hu, and P. Karava, “System identification and model-predictive control of office buildings with integrated photovoltaic-thermal collectors, radiant floor heating and active thermal storage,” *Solar Energy*, vol. 113, pp. 139–157, 2015.

[146] M. Jiménez and H. Madsen, “Models for describing the thermal characteristics of building components,” *Building and Environment*, vol. 43, pp. 152–162, Feb. 2008.

[147] L. Ferkl, “Ceiling radiant cooling: Comparison of ARMAX and subspace identification modelling methods,” *Building and Environment*, vol. 45, pp. 205–212, Jan. 2010.

[148] T. Y. Chen, “Application of adaptive predictive control to a ¯ oor heating system with a large thermal lag,” vol. 34, pp. 45–51, 2002.

[149] I. M. Yassin, M. N. Taib, and R. Adnan, “Recent Advancements & Methodologies in System Identification : A Review,” vol. 1, no. 1, pp. 14–33, 2013.

[150] T. Bohlin, “A case study of grey box identification,” *Automatica*, vol. 30, no. 2, pp. 307–318, 1994.

[151] H. Melgaard, *Identication of Physical Models*. PhD thesis, DTU - Denmark, 1994.

[152] J. N. Nielsen, H. Madsen, and P. C. Young, “Parameter estimation in stochastic differential equations: An overview,” *Annual Reviews in Control*, vol. 24, pp. 83–94, 2000.

[153] N. R. Kristensen, H. Madsen, and S. B. Jø rgensen, “A method for systematic improvement of stochastic grey-box models,” *Computers and Chemical Engineering*, vol. 28, pp. 1431–1449, 2004.

[154] P. Bacher and H. Madsen, “Identifying suitable models for the heat dynamics of buildings,” *Energy and Buildings*, vol. 43, pp. 1511–1522, July 2011.

[155] A. Rabl, “Parameter estimation in buildings: methods for dynamic analysis of measured energy use,” *Journal of Solar Energy Engineering*, 1988.

[156] T. Berthou, P. Stabat, R. Salvazet, and D. Marchio, “Development and validation of a gray box model to predict thermal behavior of occupied office buildings,” *Energy and Buildings*, vol. 74, pp. 91–100, 2014.

[157] A. Afram and F. Janabi-Sharifi, “Gray-box modeling and validation of residential HVAC system for control system design,” *Applied Energy*, vol. 137, pp. 134–150, Jan. 2015.

[158] M. J. Jiménez, H. Madsen, and K. K. Andersen, “Estimation of the main thermal characteristics of building components using parametric models in MATLAB,” in *DYNASTEE 2005 - Dynamic Analysis, Simulation and Testing applied to the Energy and Environmental Performance of Buildings*, pp. 1–17, 2005.

[159] M. J. Jiménez, B. Porcar, and M. R. Heras, “Estimation of building component UA and gA from outdoor tests in warm and moderate weather conditions,” *Solar Energy*, vol. 82, no. 7, pp. 573–587, 2008.

[160] I. Naveros, P. Bacher, D. P. Ruiz, M. J. Jiménez, and H. Madsen, “Setting up and validating a complex model for a simple homogeneous wall,” *Energy and Buildings*, vol. 70, pp. 303–317, 2014.

[161] P. D. Andersen, M. J. Jiménez, H. Madsen, and C. Rode, “Characterization of heat dynamics of an arctic low-energy house with floor heating,” *Building Simulation*, pp. 595–614, 2014.

[162] H. Madsen, *Time Series Analysis*. Chapman & Hall/CRC, 2008.

[163] N. R. Kristensen, H. Madsen, and S. B. Jø rgensen, “Parameter estimation in stochastic grey-box models,” *Automatica*, vol. 40, pp. 225–237, Feb. 2004.

[164] K. Letherman, C. Palin, and P. Park, “The measurement of dynamic thermal response in rooms using pseudo-random binary sequences,” *Building and Environment*, vol. 17, pp. 11–16, Jan. 1982.

[165] G. Lethé, P. Steskens, G. Flamant, and B. Meurisse, “An adapted co - heating test and experimental infrastructure for thermal dynamic response and performance identification of residential buildings,” pp. 1–24.

[166] P. Steskens, “The prediction of building thermal dynamics based on a modified co-heating test and grey-box modelling,”

[167] G. Bauwens and S. Roels, “Co-heating test: A state-of-the-art,” *Energy and Buildings*, vol. 82, pp. 163–172, Oct. 2014.

[168] L. Ljung and T. Glad, “On Global Identifiability for Arbitrary Model Parametrizations,” *Automatica*, vol. 30, no. 2, pp. 265–276, 1994.

[169] P. Bacher and H. Madsen, “Identifying suitable models for the heat dynamics of buildings,” *Energy and Buildings*, vol. 43, pp. 1511–1522, July 2011.

[170] R. Perez, P. Ineichen, R. Seals, J. Michalsky, and R. Stewart, “Modeling daylight availability and irradiance components from direct and global irradiance,” *Solar Energy*, vol. 44, no. 5, pp. 271–289, 1990.

[171] L. Mei, D. Infield, U. Eicker, and V. Fux, “Thermal modelling of a building with an integrated ventilated PV façade,” *Energy and buildings*, vol. 35, pp. 605–617, 2003.

[172] G. Reynders, J. Diriken, and D. Saelens, “Quality of grey-box models and identified parameters as function of the accuracy of input and observation signals,” *Energy and Buildings*, vol. 82, pp. 263–274, Oct. 2014.

[173] K. Antonopoulos and E. Koronaki, “Apparent and effective thermal capacitance of buildings,” *Energy*, vol. 23, pp. 183–192, Mar. 1998.

[174] L. G. Swan and V. I. Ugursal, “Modeling of end-use energy consumption in the residential sector: A review of modeling techniques,” *Renewable and Sustainable Energy Reviews*, vol. 13, pp. 1819–1835, Oct. 2009.

[175] G. Verbeeck, *Optimisation of extremely low energy residential buildings*. phd-thesis, K.U.Leuven, 2007.

[176] T. Loga, C. Balaras, E. Dascalaki, and M. Zavrl, *Use of Building Typologies for Energy Performance Assessment of National Building Stocks: Existent Experiences in European Countries and Common*. No. June 2009, Institut Wohnen und Umwelt GmbH, 2010.

[177] K. Heylen, M. Le Roy, S. Vanden Broucke, B. Vandekerckhove, and S. Winters, “Wonen in Vlaanderen: De resultaten van de Woonsurvey 2005 en de Uitwendige Woningschouwing 2005, Ministerie van de Vlaamse Gemeenschap, Depar- tement RWO – Woonbeleid, 2007.,” tech. rep., 2005.

[178] NIS, “General Socio-economic Survey, National Institute of Statistics,” tech. rep., 2001.

[179] H. Hens and B. Verdonck, “Living, heating: energy, emissions, CO2-project Electrabel- SPE,” tech. rep., 1997.

[180] C. Protopapadaki, G. Reynders, and D. Saelens, “Bottom-up modelling of the Belgian residential building stock: impact of building stock descriptions,” in *SSB 2014 (Liège)*, 2014.

[181] J. Babiak, B. W. Olesen, and D. Petras, *Low temperature heating and high temperature cooling : embedded water based surface heating and cooling systems*. Brussels: Rehva, 2nd rev. e ed., 2009.

[182] D. Aerts, J. Minnen, I. Glorieux, I. Wouters, and F. Descamps, “A method for the identification and modelling of realistic domestic occupancy sequences for building energy demand simulations and peer comparison,” *Building and Environment*, Feb. 2014.

[183] D. Patteeuw, K. Bruninx, A. Arteconi, E. Delarue, W. D'haeseleer, and L. Helsen, "Integrated modeling of active demand response with electric heating systems," *Accepted in Applied Energy*, 2015.

[184] E. Heylen, R. Jordens, D. Patteeuw, and L. Helsen, "The Potential of Air-Water Heat Pumps in a {B}elgian Residential Retrofit Context In Relation To Future Electricity Prices," in *9th International Conference on System Simulation in Buildings*, (Liège, Belgium), Dec. 2014.

[185] K. Bettgenhäuser, M. Offermann, T. Boermans, M. Bosquet, J. Grözinger, B. von Manteuffel, and N. Surmeli, "Heat Pump Implementation Scenarios until 2030, appendix," tech. rep., Ecofys, 2013.

[186] D. Patteeuw and L. Helsen, "Residential buildings with heat pumps, a verified bottom-up model for demand side management studies," in *International Conference on System Simulation in Buildings Edition 9*, (Liège, Belgium), Dec. 2014.

[187] IEA and NEA, "Projected Costs of Generating Electricity, 2010 Edition," tech. rep., IEA and NEA, 2010.

[188] J. Smeds and M. Wall, "Enhanced energy conservation in houses through high performance design," *Energy and Buildings*, vol. 39, no. 3, pp. 273–278, 2007.

[189] F. Oldewurtel, D. Sturzenegger, M. Morari, and R. S. Smith, "Towards a Standardized Building Assessment for Demand Response,"

[190] Linear-consortium, "LINEAR - Demand Response for Families," tech. rep., EnergyVille, Genk, 2014.

Curriculum

GLENN REYNDERS

Building Physics Section
Department of Civil Engineering, KU Leuven
Kasteelpark Arenberg 40 box 2447| BE-3001 Heverlee | Belgium
Tel. + 32 (0)16 32 25 70 | Fax. + 32 (0)16 32 19 80
glenn.reynders@bwk.kuleuven.be | www.kuleuven.be/bwf

Education

Sint-Jozefscollege, Beringen

2001-2005 General Secondary Education
Option: Science & Mathematics (8h)

University of Leuven – KU Leuven, Leuven

2005-2008 Bachelor in Science and Engineering
Faculty of Engineering Science

2008-2010 Master in Science and Engineering: Civil Engineering
Faculty of Engineering Science
Department of Civil Engineering
Option: Building technology
Master thesis: "Evaluation of ventilation in laboratories"

2010-2015 Phd in Engineering Science: Civil Engineering
"Quantifying the impact of building design on the potential of structural storage for active demand response in residential buildings"
Financed by: VITO – Flemish institute for technologic research

Scientific Experiences

2010-2015 Phd in Engineering Science: Civil Engineering
"Quantifying the impact of building design on the potential of structural storage for active demand response in residential buildings"

2011-2015 IEA EBC Annex 58-project:
"Reliable building energy performance characterization based on full scale dynamic measurements"

2014-2015 IEA EBC Annex 67-project:
"Energy Flexible Buildings"

List of publications

Publications in international journals

- Patteeuw, D., Reynders, G., Bruninx, K., Protopapadaki, C., Delarue, E., William, D., Helsen, L. and Saelens, D. "CO_2-abatement cost of residential heat pumps with Active Demand Response : demand- and supply-side effects", *Applied Energy*, vol 156, pp 490-501, 2015.
- Reynders, G., Diriken, J., Saelens, D., "Quality of grey-box models and identified parameters as function of the accuracy of input and observation signals," *Energy and Buildings*, vol 82, pp 263–274, 2014.
- Reynders, G., Nuytten, T., Saelens, D., "Potential of structural thermal mass for demand-side management in dwellings," *Building and Environment*, vol 64, pp 187–199, 2013.

Publications at international conferences

- Reynders, G., Diriken, J. and Saelens, D., "A generic quantification method for the active demand response potential of structural storage in buildings," *Accepted for the 14^{th} international conference of the International Building Performance Simulation Association, Building Simulation 2015*, Hyderabad, India, 2015
- Reynders, G., Diriken, J. and Saelens, D., "Impact of the heat emission system on the identification of grey-box models for residential buildings," *Proceedings of the 6^{th} international Building Physics Conference, IPBC 2015*, Turin, Italy, June 2015
- Reynders, G., Diriken, J. and Saelens, D., "Bottom-up modelling of the Belgian residential building stock: influence of model complexity," *Proceedings of the 9th international conference on System Simulation in Buildings, SSB 2014*, Liège, Belgium, December 2014
- Protopapadaki, C., Reynders, G. and Saelens, D., "Bottom-up modelling of the Belgian residential building stock: impact of building stock descriptions," *Proceedings of the 9th international conference on System Simulation in Buildings, SSB 2014*, Liège, Belgium, December 2014
- Reynders, G., Nuytten, T. and Saelens, D., "Robustness of reduced-order models for prediction and simulation of the thermal behavior of dwellings," *Proceedings of the 13^{th} international conference of the International Building Performance Simulation Association, Building Simulation 2013*. Chambery, France, 2013

- Reynders, G., Baetens, R. and Saelens, D., “Using thermal mass to counter decreasing overall heating system efficiencies in low-energy dwellings,” *Proceedings of the 5^{th} international Building Physics Conference, IBPC 2013*, Kyoto, Japan, 2013
- Reynders, G., Baetens, R. and Saelens, D., “Identifying opportunities of passive thermal storage in residential buildings for electrical grid measures,” *Proceedings of CISBAT 2011*, Lausanne, Switzerland, 2011
- Reynders, G. and Saelens, D., “Numerical and experimental evaluation of ventilation in laboratories: a case study.” *Proceedings of the 12^{th} international conference on air distribution in rooms, Roomvent 2011*, Trondheim, Norway, 2011